Expression, Purification and Characterisation of Tryptophan Hydroxylases

Windahl, Michael Skovbo; Christensen, Hans Erik Mølager; Harris, Pernille

Publication date:
2007

Expression, Purification and Characterisation of Tryptophan Hydroxylases

Dissertation by

Michael Skovbo Nielsen

Submitted in partial fulfilment
of the requirements for the degree of
Doctor of Philosophy in Bioinorganic Chemistry

Department of Chemistry
Technical University of Denmark
Kgs. Lyngby

2007

Preface and acknowledgements

This dissertation, entitled "Expression, Purification and Characterisation of Tryptophan Hydroxylases," is in partial fulfilment of the requirements for the degree of Doctor of Philosophy at the Technical University of Denmark (DTU). The Ph.D.-scholarship that made it possible was funded in part by DTU and in part by the Graduate School on Metal Ions in Biological Systems. Performed at the Department of Chemistry at DTU, the project was supervised by Associate Professors Hans E. M. Christensen and Pernille Harris, both from the Department of Chemistry.

This project would probably not have been initiated without Professor Ulstrup's course in bioinorganic chemistry (autumn 2000), which triggered my interest in tryptophan hydroxylase, an iron-containing enzyme responsible for the biosynthesis of serotonin. At the time I was fascinated by the neurotransmitter serotonin and its implications in neuropsychiatric disorders, which inspired me to look for possibilities of combining bioinorganic-chemistry research with research on serotonin. As the most obvious combination of this was tryptophan hydroxylase, it became the subject of the report I wrote for Professor Ulstrup's bioinorganic chemistry course. During the writing process, I received help from Associate Professor Hans E. M. Christensen. He not only helped me to procure relevant scholarly literature unavailable at DTU, but also assisted me in clarifying confusing aspects of protein chemistry. This proved to be the beginning of mutually beneficial collaboration; Hans became so interested in tryptophan hydroxylase that he launched it as a new project in his research group which I later joined. Tryptophan hydroxylase became the subject of my Master's Thesis (2004) as well as the subject of this Dissertation.

First of all I would like to thank my supervisors Associate Professors Hans E. M. Christensen and Pernille Harris for their help and guidance during the project. Also thanks to the Technical University of Denmark and the Graduate School on Metal Ions in Biological Systems who provided me with the financial means to complete this project.

Many students and laboratory technicians have been involved in the tryptophan hydroxylase project since its start and their work have inevitably contributed to the results presented in this dissertation. I would like to thank: Per Gervin Nielsen, Kristian M. Fischer, Hildur Gudmundsdottir, Astrid Munch, Maja Martic, Jane Boesen, Mads-Jacob K. Klitgaard, Charlotte Rode Petersen, Trine V. Vendelboe, Majbritt Nielsen, Morten Storgaard, Anne Louise Damgaard, Hajnalka Jankovics, Mark Nygaard, Sabine Fantoni, Ivalo Linnebjerg, Astrid N. Jørgensen, Karen M. D. Jørgensen, Lærke T. Haahr, Pernille E. Karlsen, Lise-Lotte Jespersen and Stefani Boy.

Additionally, I would like to thank Anders Raffalt for readily assisting me in statistical matters.

Last but not least, I would like to express my sincere gratitude to all members of the Analytical and Bioinorganic Chemistry Group for providing a pleasant and friendly atmosphere. Special thanks also to Lise-Lotte Jespersen for taking such a good care of us all.

Michael Skovbo Nielsen
Kgs. Lyngby, 15th of August 2007.

Abstract

Expression, Purification and Characterisation of Tryptophan Hydroxylases

Tryptophan hydroxylase (TPH) catalyses the first and rate-limiting step in the biosynthesis of the neurotransmitter and hormone serotonin (5-hydroxytryptamine). Although serotonin has many physiological functions, it is mainly known as a neurotransmitter. Abnormalities in the serotonergic neurons are implicated in a wide range of neuropsychiatric disorders such as depression, obsessive-compulsive disorder and schizophrenia.

TPH is a mononuclear non-heme iron enzyme which catalyses the reaction between tryptophan, O_2 and tetrahydrobiopterin to produce 5-hydroxytryptophan and 4a-hydroxy-tetrahydrobiopterin. TPH is a homotetrameric three domain enzyme; its three domains are an N-terminal regulatory domain, a catalytic domain and a small C-terminal tetramerisation domain. Two isoforms of TPH exist: while isoform 1 (TPH1) is primarily found in the mast cells, pineal gland and enterochromaffin cells, isoform 2 (TPH2) appears mostly in the serotonergic neurons of the brain and gut.

This study concerns the chicken TPH1 and the human TPH2 and 17 different variants of these two enzymes have been expressed in *Escherichia coli*. Three of these variants could be purified to homogeneity using only two simple chromatographic steps. These variants were the catalytic domain of chicken TPH1, the catalytic domain of human TPH2 and the catalytic and tetramerisation domain of human TPH2. The expression and purification of the three variants yielded 11-60 mg purified TPH/L culture; the specific activities of these three variants ranged from 0.6 to 5.9 µmol/min/mg.

The TPH variants that could not be purified all contain the regulatory domain. This indicates that the regulatory domains of TPH1 and TPH2 when expressed in *Escherichia coli* are responsible for aggregation. This aggregation obstructs the purification.

For all three variants that could be purified the K_m and V_{max} values were determined for all three substrates. Large differences were observed between some of the K_m values of isoform 1 and 2: the $K_{m,tetrahydrobiopterin}$ of the catalytic domain of chicken TPH1 is 324±10 µM, while for its counterpart the catalytic domain of human TPH2 it is 26.5±1.3 µM; the respective $K_{m,O2}$ values of the catalytic domains of chicken TPH1 and human TPH2 are 39±2 µM and 273±9 µM. While substrate inhibition by tryptophan is observed with a $K_{i,tryptophan}$ of 164±24 µM for the catalytic domain of chicken TPH1, no such inhibition is observed for the variants of human TPH2.

Having investigated the kinetic mechanism of the catalytic domain of human TPH2, I have found that the mechanism is sequential, that is, all three substrates must be bound in the enzyme before the enzymatic reaction proceeds. The results also ascertained the

order of substrate addition: tryptophan binds as the first substrate, followed by a random addition of tetrahydrobiopterin and O_2.
The extensive screenings of crystallisation conditions performed for all three variants revealed crystallisation conditions for the catalytic domain of chicken TPH1. A data set was collected to 3 Å and the structure was solved by molecular replacement. The subsequent trials to optimise the crystallisation have currently not resulted in a better data set. The structure was refined to an R_{free} of 32.8% and the overall structure is compared to the overall structure of the catalytic domain of human TPH1 co-crystallised with dihydrobiopterin. This structure is the only other structure of TPH. Rather large conformational changes are seen upon binding of substrate analogue dihydrobiopterin. Furthermore, the structure of the C-terminal end of the catalytic domain is visible, which is not seen in the structure of the catalytic domain of human TPH1.

Dansk resumé

Ekspression, oprensning og karakterisering af tryptophanhydroxylaser

Tryptophanhydroxylase (TPH) katalyserer det første og hastighedsbestemmende trin i biosyntesen af serotonin (5-hydroxytryptamin). Serotonin har mange fysiologiske funktioner, men er hovedsagelig kendt for sin funktion som signalstof i hjernen. Unormalheder i de serotoninholdige neuroner menes at spille en rolle i flere psykiatriske lidelser såsom depression, obsessiv-kompulsiv lidelse (OCD) og skizofreni.

TPH er et jern-holdigt enzym, som katalyserer reaktionen mellem tryptophan, O_2 og tetrahydrobiopterin under dannelsen af produkterne 5-hydroxytryptophan og 4a-hydroxytetrahydrobiopterin. TPH er en homotetramer, hvor hver monomer består af tre domæner. De tre domæner er et N-terminalt regulatorisk domæne, et katalytisk domæne og et mindre C-terminalt tetrameriseringsdomæne.

Der findes to isoformer af TPH, hvor isoform 1 (TPH1) hovedsagligt findes i mastcellerne, pinealkirtelen og i de enterochromaffine celler og isoform 2 (TPH2) findes i de serotoninholdige neuroner i hjernen og tarmen.

I dette projekt er kylling TPH1 og human TPH2 blevet studeret. Sytten forskellige varianter af disse to enzymer er blevet udtrykt i *Escherichia coli*. Tre af disse varianter kan oprenses ved brug af to simple kromatografiske trin. De tre varianter er det katalytiske domæne af kylling TPH1, det katalytiske domæne af human TPH2 samt det katalytiske domæne sammen med det efterfølgende tetrameriseringsdomæne af human TPH2. Ekspressionen af de tre varianter gav et udbytte på 11-60 mg oprenset TPH/L kultur. De opnåede specifikke aktiviteter for disse tre varianter er 0,6-5,9 µmol/min/mg.

De varianter af TPH, som ikke kunne oprenses, indeholder alle det regulatoriske domæne. Dette indikerer, at de regulatoriske domæner af TPH1 og TPH2 er ansvarlige for aggregeringen af TPH ved ekspression i *Escherichia coli*.

For de tre varianter der kunne oprenses blev K_m- og V_{max}-værdierne bestemt for alle tre substrater. Der er store forskelle mellem K_m-værdier for isoform 1 og 2. For det katalytiske domæne af kylling TPH1 er $K_{m,tetrahydrobiopterin}$ 324±10 µM, mens den er 26,5±1,3 µM for det katalytiske domæne af human TPH2. $K_{m,O2}$ for det katalytiske domæne af kylling TPH1 er 39±2 µM, mens den er 273±9 µM for det katalytiske domæne af human TPH2. Derudover blev der observeret substrat-inihibering af tryptophan for det katalytiske domæne af kylling TPH1 med en $K_{i,tryptophan}$ på 164±24 µM. Substrat-inhibering blev ikke observeret for de to humane TPH2 varianter.

Enzymkinetikmekanismen for det katalytiske domæne af human TPH2 blev ligeledes undersøgt. Det blev vist, at den er sekventiel, dvs. at alle tre substrater skal være

bundet, før den enzymatiske reaktion kan forløbe. Resultaterne viser derudover, at tryptophan bindes som det første substrat fulgt af en tilfældig bindingsrækkefølge af tetrahydrobiopterin og O_2.
Der er udført omfattende screeningsforsøg for at finde krystallisationsbetingelser for alle tre varianter. Krystallisationsbetingelser er fundet for det katalytiske domæne af kylling TPH1. Et datasæt til 3 Å er opsamlet, og strukturen er løst. Forsøg på at optimere krystallisationen har foreløbig ikke resulteret i et forbedret datasæt. Den overordnede struktur af det katalytiske domæne af kylling TPH1 er sammenlignet med den overordnede struktur af den eneste anden struktur af TPH, nemlig det katalytiske domæne af human TPH1. Der ses forskelle i substratbindingsregionen samt i et fleksibelt loop. Desuden ses strukturen af den C-terminale ende af det katalytiske domæne, som ikke er synlig i strukturen af det katalytiske domæne af human TPH1.

List of abbreviations

$6MePH_4$	6-methyl-5,6,7,8-tetrahydropterin
AAAH	Aromatic amino acid hydroxylases
A. aeolicus	*Aquifex aeolicus*
ADHD	Attention deficit hyperactivity disorder
BICINE	*N,N*-Bis(2-hydroxyethyl)glycine
BH_4	(6R)-5,6,7,8-tetrahydro-L-biopterin
BH_2	(6R)-7,8-dihydro-L-biopterin
$C_{12}E_6$	Hexaethylene glycol monododecyl ether
$C_{12}E_8$	Octaethylene glycol monododecyl ether
Cam	Chloramphenicol
c*g*TPH1	Catalytic domain of *g*TPH1
CHES	2-(Cyclohexylamino)ethanesulfonic acid
c*h*TPH1	Catalytic domain of *h*TPH1
c*h*TPH2	Catalytic domain of *h*TPH2
ct*h*TPH2	Catalytic and tetramerisation domain of *h*TPH2
cTPH1	Catalytic domain of TPH1
CAPS	3-(Cyclohexylamino)-1-propanesulfonic acid
CV	Column volume
Cv	*Chromobacterium violaceum*
Cp	*Colwellia psychrerythraea*
DF	Degrees of freedom
$DMPH_4$	6,7-dimethyl-5,6,7,8-tetrahydropterin
Dopa	3,4-dihydroxyphenylalanine
E. coli	*Escherichia coli*
EDTA	ethylenediamine tetraacetate
ESRF	European synchrotron radiation facility
GST	Glutathione-S-transferase
*g*TPH1	Chicken (*Gallus gallus*) tryptophan hydroxylase isoform 1
HEPES	4-(2-hydroxyethyl)-piperazine-1-ethanesulfonic acid
*h*TPH1	Human tryptophan hydroxylase isoform 1
*h*TPH2	Human tryptophan hydroxylase isoform 2
IMAC	Immobilised metal affinity chromatography
IPTG	Isopropyl-β-D-thiogalactopyranoside
Kan	Kanamycin sulphate
LB	Luria Bertani
MBP	Maltose-binding protein
MES	2-(N-morpholino)ethanesulfonic acid

MIB	Malonate imidazole borate buffer
MM	Michaelis-Menten
MMT	Malic acid, MES and Tris buffer system
MPD	2-methyl-2,4-pentanediol
MPEG	Polyethylene glycol monomethyl ether
mRNA	Messenger ribonucleic acid
NIH	National Institutes of Health
NusA	N-utilization substance A
OCD	Obsessive-compulsive disorder
PAH	Phenylalanine hydroxylase
PEG	Polyethylene glycol
PCB	Propionate, cacodylate and Bis-Tris propane buffer system
PDB	Protein data bank
PIPES	1,4-Piperazinediethanesulfonic acid
PMT	Photomultiplicator tube
qBH_2	Quinonoid-7,8-dihydro-L-biopterin
rc*g*TPH1	Regulatory and catalytic domain of *g*TPH1
rc*h*TPH2	Regulatory and catalytic domain of *h*TPH2
r*h*TPH2	Regulatory domain of *h*TPH2
rpm	Revolutions per minute
SDS-PAGE	Sodium dodecyl sulphate polyamide gel electrophoresis
SET	Solubility-enhancement tag
SET3-*h*TPH2	Fusion protein of SET variant 3 to *h*TPH2
SET3-rc*h*TPH2	Fusion protein of SET variant 3 to rc*h*TPH2
SPG	Succinic acid, sodium dihydrogen phosphate, glycine buffer system
SS	Sum of squares
SUMO	Small ubiquitin-related modifier
TH	Tyrosine hydroxylase
TMAO	Trimethylamine N-oxide
Tris	Tris(hydroxymethyl)-aminomethane
Trx	Thioredoxin
TPH	Tryptophan hydroxylase
TPH1	Tryptophan hydroxylase isoform 1
TPH2	Tryptophan hydroxylase isoform 2
u*g*TPH1	Fusion protein of ubiquitin and *g*TPH1
u*h*TPH2	Fusion protein of ubiquitin *h*TPH2
urc*g*TPH1	Fusion protein of ubiquitin and rc*g*TPH1
urc*h*TPH2	Fusion protein of ubiquitin and rc*h*TPH2
ur*h*TPH2	Fusion protein of ubiquitin and r*h*TPH2
xc*h*TPH2	Core of the catalytic domain of *h*TPH2 variant x
yc*h*TPH2	Core of the catalytic domain of *h*TPH2 variant y

Contents

CHAPTER ONE

1 Introduction

This dissertation deals with the important iron containing enzyme tryptophan hydroxylase (TPH) which catalyses the first and rate limiting step in the biosynthesis of serotonin [1]. The TPH catalysed reaction is furthermore the first step in biosynthesis of the indoleamines shown in figure 1.1 with the hormone melatonin as the final compound [2,3]. Since 1948, when Rapport *et al.* first isolated and identified the vasoconstrictor from serum as 5-hydroxytryptamine (serotonin), the biosynthesis of serotonin has been in constant focus by many researchers [4,5,6]. It was found that serotonin had many important physiological functions but most importantly it was found to be a neurotransmitter. The interest in tryptophan hydroxylase further increased as serotonin was hypothesised to be implicated in a wide range of neuropsychiatric disorders such as depression and obsessive-compulsive disorder [7]. Even though TPH has been studied for many years several issues still remain to be resolved. The three-dimensional structure of the whole protein is for example unknown and the mechanism of enzyme regulation has not been determined.

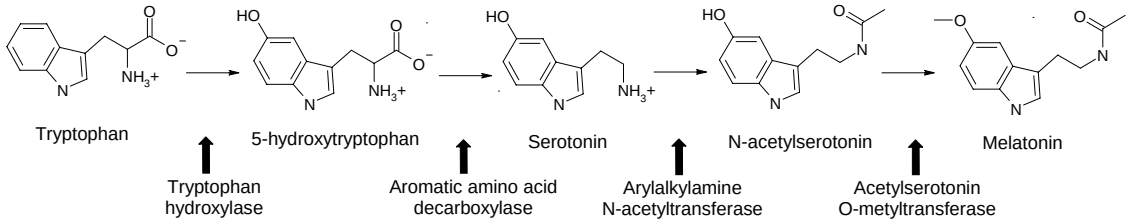

Figure 1.1 The biosynthesis of the indoleamines 5-hydroxytryptophan, serotonin, N-acetylserotonin and melatonin. Tryptophan hydroxylase is the rate limiting enzyme in the biosynthesis of serotonin [2,3].

The initial work on TPH in the Bioinorganic Research Group at DTU was done with chicken (*Gallus gallus*) TPH (*g*TPH1) [8]. TPH contains three domains being an N-terminal regulatory domain (r), a catalytic domain (c) and a small C-terminal tetramerisation domain (t). Truncated versions of *g*TPH1 were made and expressed in *Escherichia coli* [8,9]. During my master thesis I worked on two truncated versions, one containing the catalytic domain (c*g*TPH1) and one containing the regulatory and catalytic domain (rc*g*TPH1) [10]. Different versions of *g*TPH1 were further studied by students in the Bioinorganic Research Group [11,12,13].
Just before I started my Ph.D. study, the identification of a second gene for TPH in human was reported [14]. This human TPH isoform 2 (*h*TPH2) was the brain specific isoform while the isoform 1 was expressed in peripheral parts of the body. Reports on purification of TPH from natural sources had earlier claimed the presence of two

isoforms of TPH but because of the instability and low concentrations of TPH in natural sources the existence of two isoforms were never proven.
Since *h*TPH2 had not been expressed recombinantly and characterised thoroughly we decided to focus on this isoform. My initial goal of this project was to express recombinant *h*TPH2 in *Escherichia coli* (*E. coli*), purify it and characterise it. The main methods chosen for characterisation were enzyme kinetic studies and X-ray crystallography.
Enzyme kinetics study how the reaction rate is affected by different factors. These factors are typically the substrate concentrations. From enzyme kinetic studies one determines the K_m and V_{max} parameters for the enzyme. One may also determine the kinetic mechanism of the enzyme.
X-ray crystallography is used to determine the three-dimensional structures of proteins. The structure of a protein holds much information of its function. For example, the architecture of the active site is very useful when studying the kinetic and enzymatic mechanisms. The structure may also elucidate mechanism of allosteric regulation or mechanism of cooperativity in multimeric enzymes. Furthermore, the structure can be used in designing molecules that will interact with the enzyme and regulate its activity.
In my Ph.D. study I therefore set forth to characterise *h*TPH2 by enzyme kinetics and to crystallise it for X-ray crystallographic characterisation. As the project developed it became evident that *h*TPH2 was difficult to express in *E. coli* in a form that could be purified. Subsequently, truncated versions of *h*TPH2 were made of which two could be purified. In addition to these variants the c*g*TPH1 could also be purified. These three TPH variants were subjected to enzymatic characterisation and crystallisation experiments. Conditions for crystallising c*g*TPH1 were found by C. R. Petersen [15] and I continued the crystallisation when she finished her M. Sc. project.

1.1 Outline of the dissertation

In chapter 2 an introduction to the properties of TPH will be given. The important functions of serotonin will be introduced as well as disorders related to serotonin.
Chapter 3 starts with a small introduction of proteonomics tools used to analyse the TPH sequences. Then ubiquitin and the solubility-enhancement tag are introduced as these are used as fusion proteins in the expression of some TPH variants. This is followed by a presentation of the 17 different *E. coli* expression constructs of *g*TPH1 and *h*TPH2 tested in this project. The procedure for expression and protein solubility tests are presented and followed by the results.
In chapter 4 the expression of three TPH variants are described. The first variant is catalytic domain of *g*TPH1 (c*g*TPH1). The second variant is the catalytic domain of *h*TPH2 (c*h*TPH2), and the third variant holds the catalytic and tetramerisation domain of *h*TPH2 (ct*h*TPH2). The purification procedures for these proteins are presented followed by the results of expression and purification.
Chapter 5 gives an introduction to selected topics of enzyme kinetics. TPH catalyses the reaction between three substrates. Such a reaction may follow different kinetic mechanisms and these will be presented as will the corresponding rate equations. A method for studying the kinetic mechanisms will be presented.
Chapter 6 describes the assay used to measure the formation of 5-hydroxytryptophan, followed by the procedure used for measuring the initial rates. For the three variants c*g*TPH1, c*h*TPH2 and ct*h*TPH2 the initial rates were measured in experiments where

the substrate concentrations were varied one at a time. From these initial rates the K_m and V_{max} parameters are determined and discussed.
In chapter 7 the kinetic mechanism of the catalytic domain of *h*TPH2 is investigated by the method presented in chapter 5. The data are analysed graphically and by global curve fitting. The results are presented and discussed.
Chapter 8 serves a short introduction to the crystallisation of proteins. Chapter 9 deals with the trials to crystallise the three TPH variants purified in chapter 4. Results of data collection on c*g*TPH1 crystals are described as well as the overall structure of c*g*TPH1.
Chapter 10 is the final chapter giving a short status.

CHAPTER TWO

2 Tryptophan hydroxylase

This chapter serves as an introduction to TPH and summarises the most important properties of TPH. A short introduction to the co-substrate tetrahydrobiopterin and related pterins are given, as it will be useful in the further reading. Serotonin will also be introduced as well as disorders related to the serotonin functions. The possible roles of TPH in these disorders are presented. The enzymes phenylalanine hydroxylase and tyrosine hydroxylase are closely related to TPH. These enzymes are characterised to a greater extent than TPH. Knowledge obtained from these enzymes will therefore be presented here in order to fill some of the gaps in the knowledge of TPH.

2.1 The aromatic amino acid hydroxylases

Tryptophan hydroxylase (TPH) (tryptophan 5-monooxygenase, EC 1.14.16.4) catalyses the reaction between tryptophan, 5,6,7,8-tetrahydrobiopterin (BH_4) and O_2 to give 5-hydroxytryptophan and 4a-hydroxy-tetrahydrobiopterin (4a-hydroxy-BH_4) as shown in scheme 2.1 [16,17,18].

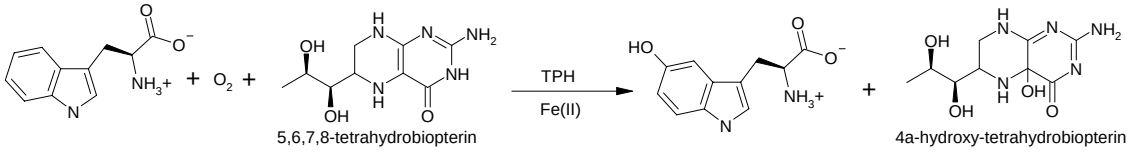

5,6,7,8-tetrahydrobiopterin

4a-hydroxy-tetrahydrobiopterin

Scheme 2.1

Together with phenylalanine hydroxylase (EC 1.14.16.1) and tyrosine hydroxylase (EC 1.14.16.2), TPH form the small enzyme family of aromatic amino acid hydroxylases (AAAH) [18]. These enzymes all contain iron and use BH_4 as a co-substrate in the hydroxylation of their respective aromatic amino acids [1,19,20]. Additionally all mammalian AAAH form homotetramers and each monomer consists of three domains. These domains are the N-terminal regulatory domain (100-150 residues), the catalytic domain (approximately 315 residues) and the C-terminal tetramerisation domain (approximately 30-40 residues) [21,22,23,24].

2.1.1 Phenylalanine hydroxylase and tyrosine hydroxylase

Phenylalanine hydroxylase (PAH) is found in the liver where it catalyses the hydroxylation of phenylalanine to tyrosine. This is the first step in the oxidative degradation of phenylalanine [25]. Mutations in PAH, which lead to a decrease in enzyme activity result in the disease phenylketonuria, where phenylalanine is conver-

ted to phenylpyruvate. Phenylpyruvate is toxic and leads to mental retardation, but this can generally be avoided through a low phenylalanine diet [26]. PAH is also found in some bacteria, but only PAH from the bacteria *Chromobacterium violaceum* and *Colwellia psychrerythraea* have been characterised [27,28,29]. The bacterial PAHs are monomeric and do not contain a regulatory domain [28,29]. Therefore, all the AAAH are believed to have evolved from common ancestor containing only the catalytic domain [21].
Tyrosine hydroxylase (TH) is found in the brain and in the adrenal gland where it catalyses the conversion of tyrosine to 3,4-dihydroxyphenylalanine (dopa) [30]. This is the first and rate limiting step in the biosynthesis of the catecholamines dopamine, norepinephrine and epinephrine as illustrated in figure 2.1 [31]. Deficiency in TH has been observed in dopa responsive dystonia and juvenile parkinsonism. A reduced 3,4-dihydroxyphenylalanine production is also observed in Parkinson's disease [31].

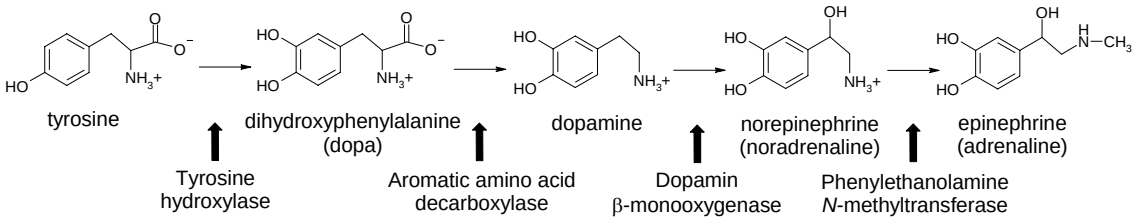

Figure 2.1 The biosynthetic pathway of the catecholamines dihydroxyphenylalanine (dopa), dopamine, norepinephrine and epinephrine [32].

2.2 The two isoforms of tryptophan hydroxylase

TPH exists in two isoforms called TPH isoform 1 (TPH1) and TPH isoform 2 (TPH2) [14]. The existence of two isoforms was observed when TPH was purified and characterised from different tissues [33,34,35,36,37]. The gene encoding for rabbit TPH1 was identified in 1987 by Grenett *et al.*[21] and a few years later the human gene for TPH1 was identified on chromosome 11 [38,39]. The gene for isoform 2 was identified in 2003 by Walther *et al.* and the human gene is located on chromosome 12 [14].
The two isoforms are expressed in different tissues. TPH2 is mainly expressed in serotonergic neurons of the brain and gut [14,40,41,42,43]. TPH1 is expressed in other parts of the body such as the pineal gland [1,40], skin cells [44], mast cells [16], intestinal mucosa and enterochromaffin cells [45] and in cancer cells [46,47]. The most pronounced difference between the two isoforms is that the N-terminal is extended by 46 residues in TPH2 (see sequence alignment in figure 2.2) [48].
No isoforms are reported of PAH and non-primate TH, while four isoforms of human TH exist. Only one human TH gene exists and the isoforms are the result of alternative mRNA splicing. The differences between the four isoforms are found in the regulatory domain [49].

2.3 Sequence alignment of the aromatic amino acid hydroxylases

The sequence alignment of *g*TPH1 [50], *h*TPH1 [38], *h*TPH2 [14], human PAH [51] and human TH isoform 4 [52] is shown in figure 2.2. The sequence identities are listed in table 2.1.

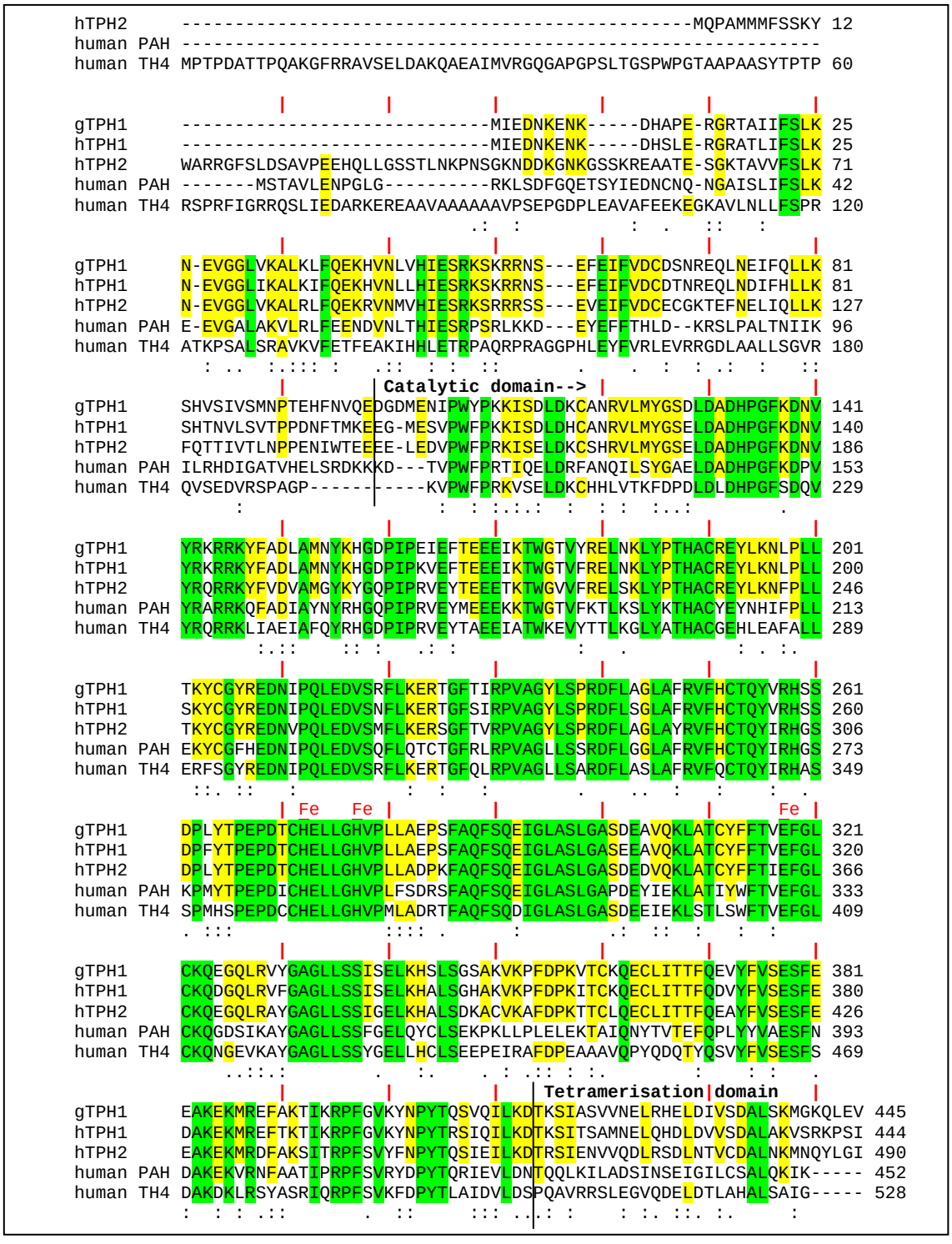

Figure 2.2. Alignment of sequences of *g*TPH1, *h*TPH1, *h*TPH2, human PAH and human TH isoform 4. The sequences are obtained from the ExPASy server [53] with the primary accession numbers P70080 (*g*TPH1), P17752 (*h*TPH1), Q8IWU9 (*h*TPH2), P00439 (human PAH) and P07101 (human TH4). The alignment was done using ClustalW 1.83 [54]. Green background indicates conserved residues in all sequences. Yellow background indicates conserved residues in at least all TPHs. ":" means that conserved substitutions have been observed within the groups (AVFPMILW), (DE), (RHK), (STYHCNGQ). "." means that semi conserved substitutions are observed. The domain boundaries as used in this project are marked by a black vertical line.

Table 2.1 Sequence identities between the *g*TPH1, *h*TPH1, *h*TPH2, human PAH and human TH isoform 4. The numbers in parenthesis are the sequence identities for the catalytic domains of the respective enzymes. The sequence identity calculation was done using ClustalW 1.83 [54].

	Sequence identity in %			
Protein	*h*TPH1	*h*TPH2	human PAH	human TH isoform 4
*g*TPH1	86 (91)	74 (82)	54 (63)	46 (60)
*h*TPH1		70 (81)	53 (64)	47 (59)
*h*TPH2			54 (64)	44 (62)
human PAH				48 (62)

2.4 Pterins

Pterins got their name from the greek word *pteron* meaning wing, because the first pterins were originally isolated as pigments from butterfly wings [55]. The structures of pterin and the derivatives (6*R*,1′*R*,2′*S*)-6-(1′,2′-dihydroxypropyl)-5,6,7,8-tetrahydropterin (tetrahydrobiopterin, BH_4), 7,8-dihydro-L-biopterin (BH_2), quinonoid-7,8-dihydro-L-biopterin (qBH_2), 6-methyl-5,6,7,8-tetrahydropterin ($6MePH_4$) and 6,7-dimethyl-5,6,7,8-tetrahydropterin ($DMPH_4$) relevant to AAAH are shown in figure 2.3 [55,56].

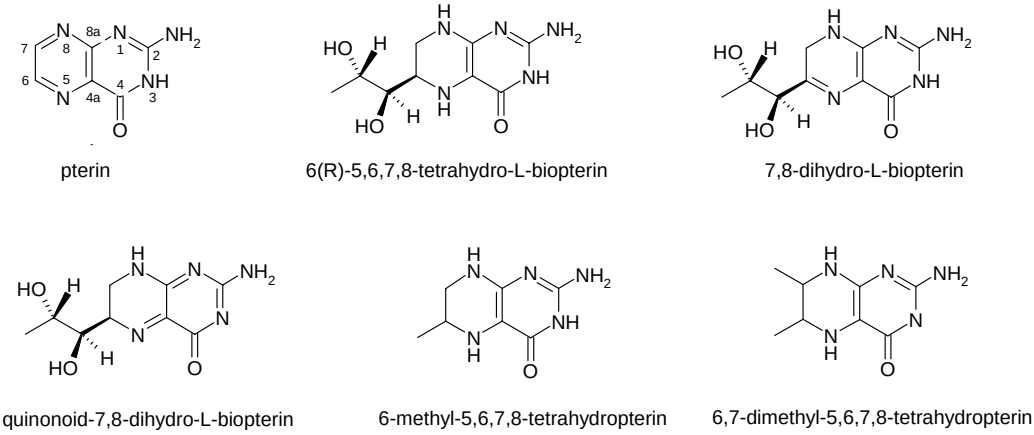

Figure 2.3 Structures of pterin, 6(R)-5,6,7,8-tetrahydro-L-biopterin (BH_4), 7,8-dihydro-L-biopterin (BH_2), quinonoid-7,8-dihydro-L-biopterin (qBH_2), 6-methyl-5,6,7,8-tetrahydropterin ($6MePH_4$), and 6,7-dimethyl-5,6,7,8-tetrahydropterin ($DMPH_4$) [55,56].

BH_4 is the naturally occurring co-substrate for the AAAH [1,57], glyceryl-ether monooxygenase (EC 1.14.16.5) [58] and nitric oxide synthase (EC 1.14.13.39) [59]. At neutral pH BH_4 is prone to oxidation by O_2 [60,61]. The initial step in this oxidation is a slow electron transfer from BH_4 to O_2, producing the free $O_2^-\cdot$ radical as shown in equation 2.1 [62].

$$BH_4 + O_2 \rightarrow BH_4^+\cdot + O_2^-\cdot \tag{2.1}$$

This reaction initiates a chain reaction involving several intermediates yielding BH_2 as the final oxidation product. Equation 2.2 summarises the overall auto oxidation reaction of BH_4 in the presence of catalase. For details on the chain reaction see Kirsch *et al.* [62].

$$2BH_4 + O_2 \rightarrow 2BH_2 + 2H_2O \tag{2.2}$$

At acidic pH BH_4 is protonated at N5 (pK_a 5.6) and at N1 (pK_a 1.3). The protonation of N5 increases the stability of BH_4 toward the autooxidation [55].
In the reaction catalysed by TPH BH_4 is converted to 4a-hydroxy-BH_4 also called BH_4-carbinolamine. *In vivo* 4a-hydroxy-BH_4 is then regenerated by the enzymes pterin-4a-carbinolamin dehydratase and dihydrobiopteridine reductase at the expense of NADH [63] This is schematically shown in figure 2.4. *In vitro* 4a-hydroxy-BH_4 spontaneously decomposes to qBH_2 [61].

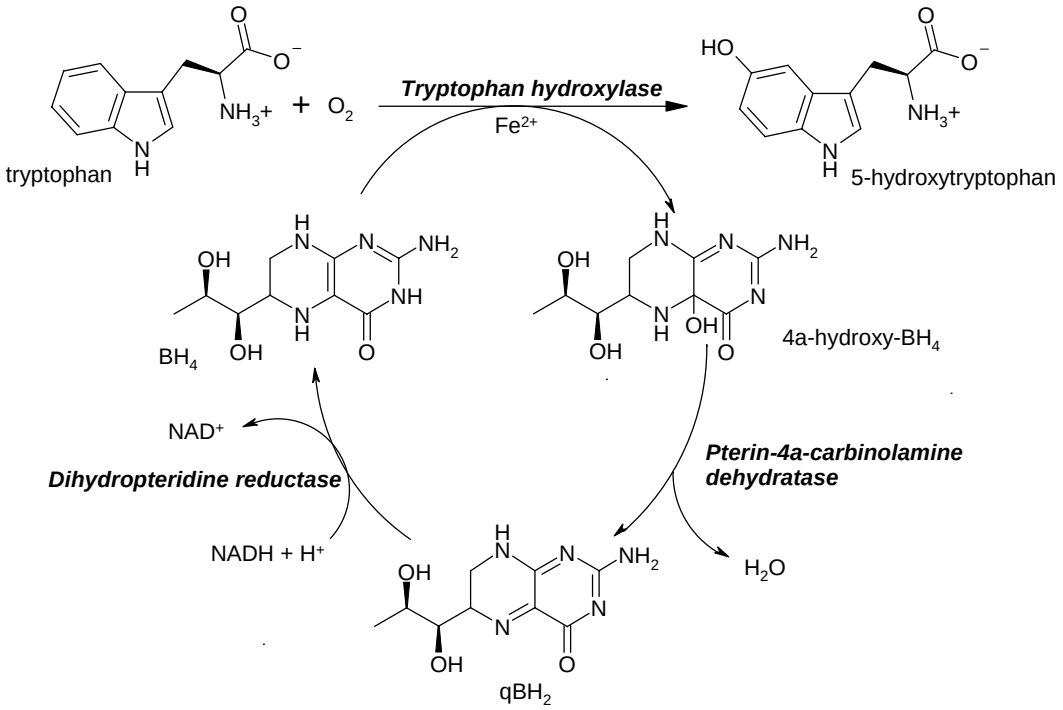

Figure 2.4 The TPH catalysed reaction and regeneration of BH_4. TPH uses BH_4 as an electron donor in reduction of O_2 and hydroxylation of tryptophan. The 4a-hydroxy-BH_4 is converted by the enzyme pterin-4a-carbinolamine dehydratase to qBH_2. qBH2 is then reduced to BH_4 by dihydrobiopteridine reductase at the expense of NADH [63].

2.5 The three-dimensional structure of tryptophan hydroxylase

As described in section 2.1 TPH consists of a regulatory, a catalytic and a tetramerisation domain [21,22,23]. The X-ray crystal structure of the catalytic domain of *h*TPH1 (c*h*TPH1) is the only structure that has been determined for any TPH. It was determined by Wang *et al.* to a 1.7 Å resolution and refined to an R_{free} of 23.1 % [64]. The overall structure is illustrated in figure 2.5A. It is similar to the catalytic domains of PAH and TH with a root mean square deviation of 1.0 Å for PAH (PDB entry 1PAH) and 0.9 Å for TH (PDB entry 1TOH) [64]. The structure of TPH was solved with ferric iron, while the active form is ferrous iron [64,65]. The iron is octahedrally coordinated by His272, His277, Glu317 on one face and three water molecules on the other (see figure 2.5B) [64]. The coordination of the iron by 2 histidines and a glutamate is also seen in PAH and TH [66,67,68,69]. This coordination of iron by two histidines and glutamate/ aspartate motif is also called the facial triad and is seen in many iron enzymes involved mainly in O_2 activation [70,71].
In c*h*TPH1 the iron is found in a cavity being 9 Å deep and 10 Å wide which is accessible for substrates. The BH_2 bound in the active site is sandwiched between

Tyr235 and Phe241 (see figure 2.5B). Furthermore, BH_2 is hydrogen bonded to the backbone of Gly234 and Leu236 (not shown in figure 2.5) and through bridging water molecules to Glu273 and Glu317 [64].

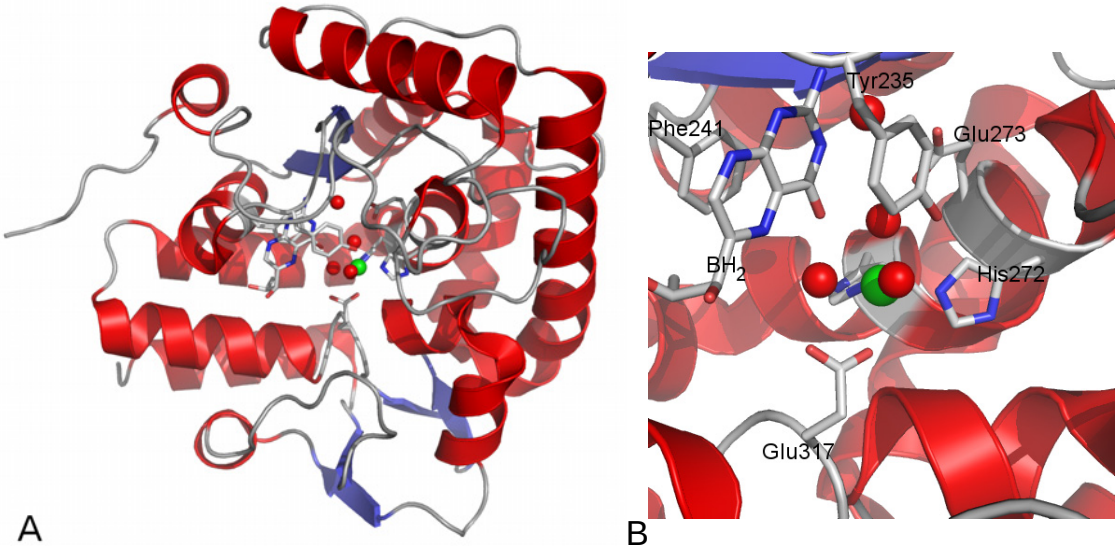

Figure 2.5 **(A)** The overall structure of the catalytic domain of *h*TPH1 (Protein data bank (PDB) entry 1MLW). **(B)** The catalytic site with the iron in green coordinated by His 272, His 277, Glu317 and three water molecules (red). The BH_2 is bound by π-stacking interactions with Tyr235 and Phe241 [64]. The figures were made using Pymol [72].

The structures of the regulatory and tetramerisation domains of TPH are not known, but are believed to be similar to that of PAH and TH [73]. All new structural information of TPH will be useful in a better understanding of this enzyme. Information about the structures of the N-terminals of TPH1 and TPH2 would especially be interesting, since this is where the largest sequence differences are seen. Some structural properties of PAH and TH are presented in the next section.

2.5.1 Structures of tyrosine hydroxylase and phenylalanine hydroxylase

TH and especially PAH have been more extensively characterised structurally than TPH. The crystal structures that have been determined for TH and PAH are summarised in table 2.2. The structure of a full length enzyme has not yet been determined. Truncated versions of TH and PAH containing the catalytic and tetramerisation domain have been crystallised as tetramers [68,69] and the structure of PAH (PDB entry 2PAH) is shown in figure 2.6. The tetramerisation domains interact through hydrophobic interactions in a coiled-coil motif [68].
The structure of the regulatory and catalytic domains of rat PAH has been determined (see figure 2.7) [74]. The first 18 residues are not visible in the structure. Residues 19-33 extends across the catalytic domain partially blocking the entrance to the active site (see figure 2.7). Movement of this N-terminal part of the regulatory domain is believed to be involved in the regulation of PAH [74].
All three AAAH have been crystallised with BH_2 and Fe(III). It has not been possible to obtain crystals with bound aromatic amino acids, but PAH-Fe(II) has been crystallised with BH_4 and thienylalanine (PDB entry 1MMK)[75]. Comparison of this structure with the structure without thinenylalanine (PDB entry 1J8U) reveals large structural changes

upon thienylalanine binding. The loop containing Tyr138 moves from a surface position to a buried position as shown in figure 2.8 [75]. This loop flexibility has also been reported for TH [76,77], but has not been studied for TPH.

Table 2.2 Three-dimensional structures of TH and PAH determined by X-ray crystallography. *Cv* is *Chromobacterium violaceum* and *Cp* is *Colwellia psychrerythraea.*

PDB entry	Organism	Domains	Resolution	Comments	Ref.
Tyrosine hydroxylase					
1TOH	Rat	ct 156-177, 200-498	2.3 Å	Fe(III)	[68]
2TOH	Rat	ct 160-182, 186-498	2.3 Å	Fe(III), BH_2	[78]
Phenylalanine hydroxylase					
1PAH	Human	c 117-424	2.0 Å	Fe(III)	[69,79]
2PAH	Human	ct 118-136, 143-452	3.1 Å	Fe(III)	[80]
3PAH	Human	c 117-424	2.0 Å	Fe(III), adrenaline	[81]
4PAH	Human	c 117-424	2.0 Å	Fe(III), noradrenaline	[81]
5PAH	Human	c 117-424	2.1 Å	Fe(III), dopamine	[81]
6PAH	Human	c 117-424	2.15 Å	Fe(III), dopa	[81]
2PHM	Rat	rc 19-136, 143-427	2.6Å	Fe(III), dephosphorylated	[74]
1PHZ	Rat	rc 19-136, 143-427	2.2 Å	Fe(III), phosphorylated	[74]
1DMW	Human	c 118-424	2.0 Å	Fe(III), BH_2	[82]
1KW0	Human	c 118-424	2.5 Å	Fe(II), BH_4, thienylalanine	[83]
1MMK	Human	c 117-425	2.0 Å	Fe(II), BH_4, thienylalanine	[75]
1MMT	Human	c 117-424	2.0 Å	Fe(II), BH_4, norleucine	[75]
1J8T	Human	c 118-424	1.7 Å	Fe(II)	[84]
1J8U	Human	c 118-424	1.5 Å	Fe(II), BH_4	[84]
1TDW	Human	c 117-424	2.1 Å	Fe(III), A313T	[85]
1TG2	Human	c 117-424	2.2 Å	Fe(III), BH_2, A313T	[85]
1LRM	Human	c 118-424	2.1 Å	Fe(III), BH_2	
1LTU	*Cv*	2-285	1.74 Å		[86]
1LTV	*Cv*	9-283	2.0 Å	Fe(III)	[86]
1LTZ	*Cv*	7-253, 257-284	1.4 Å	Fe(III), BH_2	[86]
2V27	*Cp*	4-267	1.5 Å	Fe(III)	[29]
2V28	*Cp*	7-267	1.95 Å		[29]

2.6 Substrate specificities of TPH, TH and PAH

TPH can hydroxylate tryptophan, phenylalanine and tyrosine with efficiencies in this order [87]. PAH can hydroxylate phenylalanine and tryptophan, but not tyrosine [88,89]. TH can hydroxylate tyrosine, phenylalanine and tryptophan with efficiencies in this order [90].

The substrate specificity is mainly governed by the catalytic domains of the respective enzymes. The Phe313 (in *h*TPH1) located in active site cavity is conserved in all TPHs and is important for the substrate specificity [91,92]. In PAH the equivalent residue is Trp326 and in TH Trp372. By mutating Phe313 in *h*TPH1 to a tryptophan, *h*TPH1 no longer showed a preference of tryptophan over phenylalanine. Mutating the equivalent Trp372 in TH and Trp326 in PAH to a phenylalanine, resulted in a decrease in the affinity of their respective natural substrates [91,92]. For TH the Asp425 has been reported as very important for tyrosine hydroxylation. A mutation of the Asp425 to valine, which is found in PAH, drastically decreased the affinity for tyrosine and improved the ability of hydroxylating phenylalanine [93].

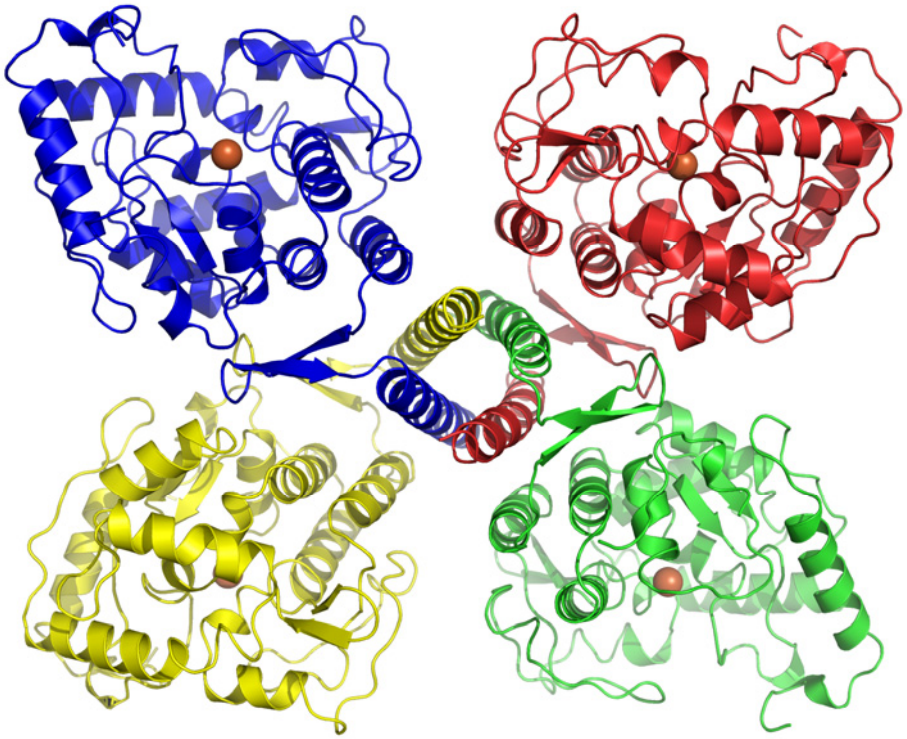

Figure 2.6 The crystal structure of the catalytic and tetramerisation domains of tetrameric PAH (PDB entry 2PAH) [80]. The coiled-coil motif is seen in the centre of the structure. The figure was made using Pymol [72].

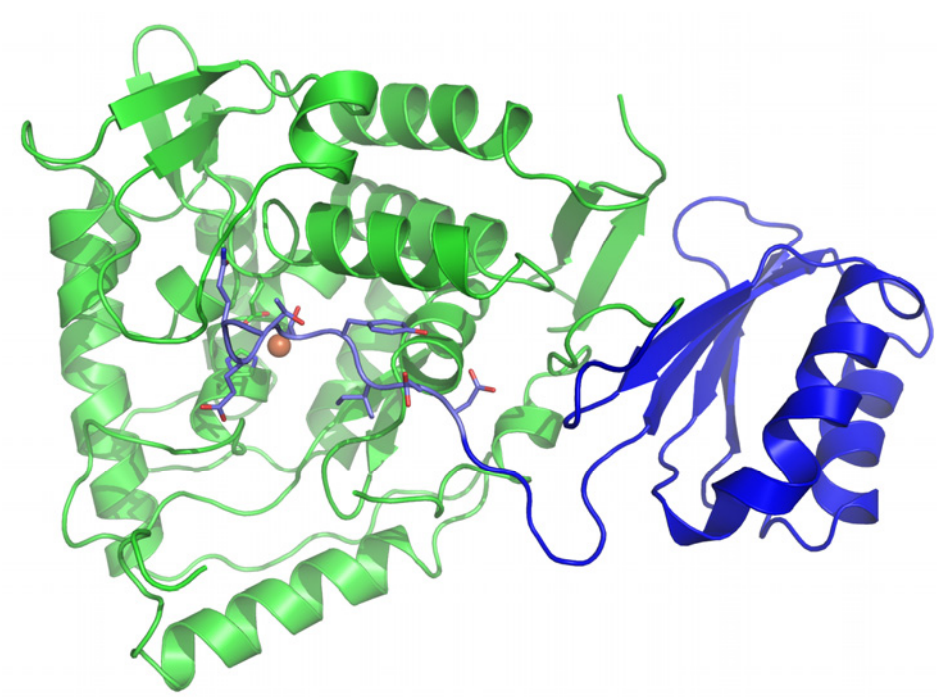

Figure 2.7 The crystal structure of the regulatory and catalytic domain of rat PAH residues 19-427(PDB entry 1PHZ) [74]. The catalytic domain is shown in green with iron as a red-brown sphere. The regulatory domain is shown in blue with the side chains shown for residue Gly19-Asp27. Gly19-Asp27 partially blocks the entrance to the active site. The figure was made using Pymol [72].

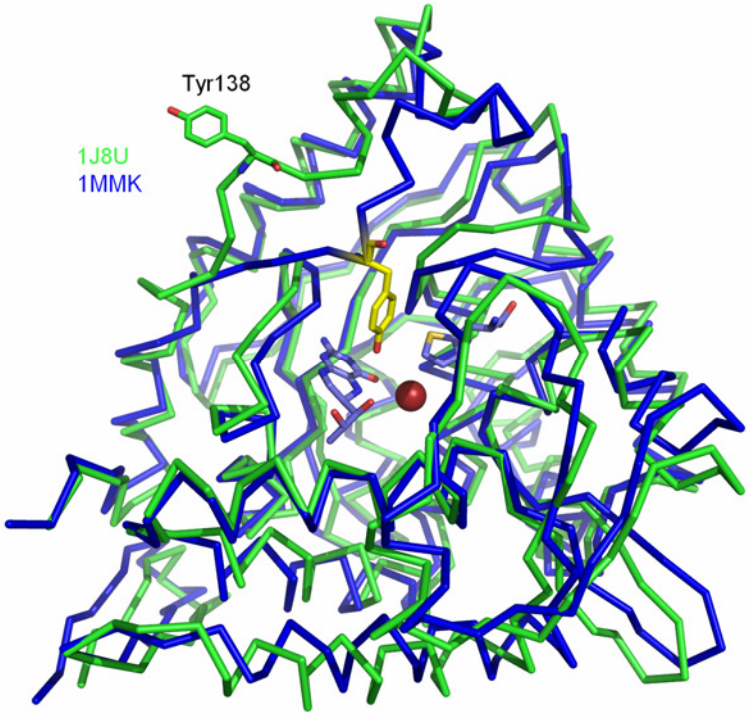

Figure 2.8 Structural alignment of the catalytic domain of PAH-Fe(II)-BH_4 (green backbone, PDB entry 1J8U) with PAH-Fe(II)-BH_4-thienylalanine (blue backbone, PDB entry 1MMK). The largest differences are seen for Tyr138 which moves from a surface position (shown in green) to a buried position (shown in yellow) close to the active site. Tyr138, BH_4 (1MMK) and thienylalanine are shown as sticks. The iron of 1MMK is shown as a red sphere. The structural alignment was done with Coot [94] and the figure was made using Pymol [72].

2.7 Order of substrate binding

No enzyme kinetic investigations of TPH have been carried out to determine the order of substrate binding. This is probably due to the limited availability and the instability of TPH. The kinetic mechanisms of rat TH and *Chromobacterium violaceum* PAH (*Cv*PAH) have been investigated [95,96,97]. All three reports agree upon a sequential mechanism, *i. e.* all three substrates must be bound before a chemical reaction can occur. However, the three disagree on the binding order of the substrates.
For rat TH the binding order is $6MePH_4$ first, followed by O_2 and then tyrosine [95]. For *Cv*PAH Pember *et al.* report that O_2 binds first, followed by random binding of $DMPH_4$ and phenylalanine [96]. It should be noted that Pember *et al.* at the time believed that *Cv*PAH was a Cu-dependent enzyme and the assay conditions were therefore not supplemented with iron, which might have affected the outcome of the investigation [27,28,98,99]. Volner *et al.* have reported an ordered binding for *Cv*PAH of $DMPH_4$, phenylalanine and O_2 in this order [97].
Substrate inhibition by the respective amino acids has been observed for the three AAAH [87,95,97,100,101], which is usually a sign of the amino acid not being the first substrate to bind (see section 5.3). As mentioned in section 2.5.1 all three AAAH have been crystallised with BH_2 or BH_4, but not with any of the respective amino acids. This indicates that binding of BH_4 occurs before the amino acid.

2.8 Mechanism of the enzymatic reaction

Because of the high homology between the catalytic domains of TPH, TH and PAH it is generally believed that they share a common catalytic mechanism [102,103]. It has been shown that the source of the oxygen incorporated into phenylalanine by PAH is molecular oxygen [104], while the other oxygen atom is incorporated into the $6MePH_4/BH_4$ [105]. All three AAAH can be inhibited by catechols which chelate the iron [106,107,108]. The active form of the iron is the ferrous state, and ferric iron can be reduced to ferrous iron by BH_4 [109,110,111].
The catalytic mechanism can be separated in two partial reactions, where the first is the formation of the hydroxylating intermediate and the second is the oxygen transfer to tryptophan [102]. No intermediates have been trapped for direct detection for any of the AAAH [102].

2.8.1 Mechanism of oxygen activation

Different hydroxylating intermediates have been proposed. One of these is a peroxo-BH_4 species seen in figure 2.9 (compound **I)** [112]. The formation and the following reaction of this species does not include the function of iron, and as the hydroxylation of the amino acid does not occur without the presence of iron, the peroxo-BH_4 species is not a likely candidate.
An Fe(II) μ-peroxy-BH_4 species (compound **II**) has been proposed as the hydroxylating species [105]. If this is the hydroxylating species the cleavage of the O-O bond should be concerted with the oxygen addition to the amino acid [102]. Subsequently the amount of hydroxylated amino acid should equal the amount of produced 4a-hydroxy-BH_4. This is not always the case. When tyrosine is the substrate in TPH or PAH the enzymes primarily function as a BH_4 oxidase without hydroxylating tyrosine [113,114,115]. This suggests that the Fe μ-peroxy-BH_4 is not the hydroxylating species [102].

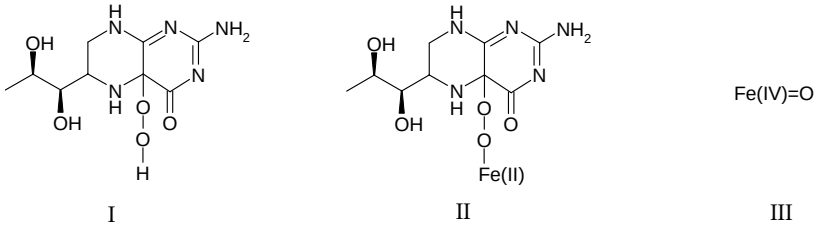

I II III

Figure 2.9 Proposed hydroxylating species of the aromatic amino acid hydroxylases. **I** is the peroxo-BH_4 species, **II** the Fe μ-peroxy-BH_4 species and **III** the ferryl oxo species [102].

A ferryl oxo species (compound **III**) was proposed based on the observation that PAH was able to hydroxylate an aliphatic carbon in norleucine to ε-hydroxynorleucine [116]. Theoretical investigations show that the ferryl oxo species is a likely candidate for the hydroxylating intermediate in the AAAH [117,118]. The ferryl oxo species has been detected as an intermediate in the catalytic mechanisms of taurine/α-ketoglutarate dioxygenase [119,120,121,122] and of prolyl-4-hydroxylase [123]. In both of these enzymes the iron is coordinated in the 2 histidine-carboxylate facial triad. The ferryl oxo species is expected to be an intermediate in several mononuclear iron enzymes with facial triad coordination [124]. Currently no report has been published on the detection of the ferryl oxo species in any AAAH.

In the AAAH the ferryl oxo species is believed to be formed from the Fe μ-peroxy-BH_4 by cleavage of the O-O bond. Whether O_2 binds to Fe(II) or to BH_4 in the initial step is uncertain. Theoretical investigations suggest that O_2 initially binds to iron and then the Fe-O-O^{2-} species attacks the C4a of BH_4 [117,118]. An Fe-O-O species has recently been structurally characterised in the oxidative ring cleavage of 4-nitrocatechol by homo-protocatechuate 2,3-dioxygenase also containing iron coordinated by the 2 histidine-carboxylate facial triad [125].

2.8.2 Mechanism of hydroxylation

The first step in the hydroxylation of the aromatic amino acid is believed to be an electrophilic attack of the Fe(IV)=O on the aromatic C atom (see scheme 2.2) making an arenium cation intermediate [102]. This mechanism is different from that of the α-ketoglutarate dependent oxygenases, where the initial step in the hydroxylation is H atom abstraction from the substrate and subsequent OH transfer [124]. The cationic intermediate is consistent with the observation that when [5-^{3}H]-tryptophan is hydroxylated by TPH, tritium is shifted to position 4 [126]. This is called the NIH- shift and is also observed in the hydroxylations by PAH and TH [127,128,129]. The believed electrophilic attack of the Fe(IV)=O is furthermore supported by theoretical investigations [130,131].
The generally accepted mechanism of the enzymatic reaction is summarised in scheme 2.2 [102].

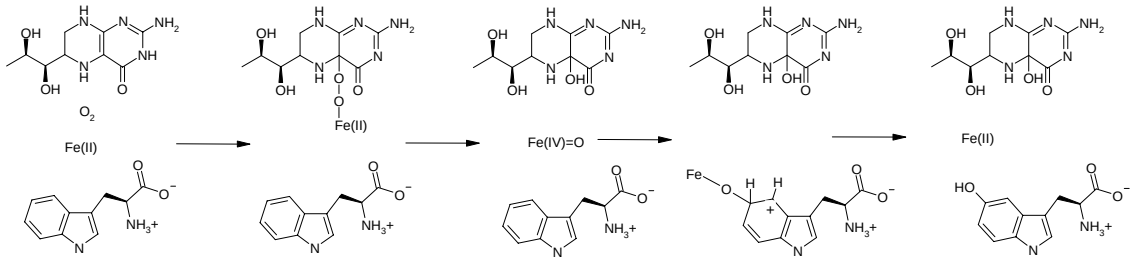

Scheme 2.2

The hydroxylation step of tryptophan is the rate limiting step in the enzymatic turnover by TPH [87, 103,113,132], while the oxygen activation step is believed to be the rate limiting step of TH and PAH (when BH_4 is used) [95,133,134]. This difference is believed to occur because the hydroxylation of tryptophan is slower than hydroxylation of phenylalanine and tyrosine [113].

2.9 Expression of recombinant tryptophan hydroxylases

TPH has been expressed in *E.coli*, *Pichia pastoris*, insect cells and mammalian cell cultures. A list summarising selected reports is shown in table 2.3.
Not surprisingly *E. coli* dominates in expression of recombinant TPH, since it is well studied as an expression host and offers rapid and inexpensive production of recombinant proteins [135,136]. Unfortunately, some proteins expressed in *E. coli* do not fold properly and subsequently form insoluble aggregates called inclusion bodies [137].
When TPH is expressed in *E. coli*, insolubility and instability have been reported to be a general problem [21,138,139,140,141,142]. In a few cases these problems seem to have been overcome [143,144], but detailed explanations on how this was done is lacking.

Table 2.3 A summary of selected reports on expression of recombinant TPH variants. Abbreviations for fusion proteins are: 6 histidine tag (6His), maltose binding protein (MBP), thioredoxin (Trx), glutathione transferase (GST) and N-utilization substance A (NusA). COS7 cells are the African green monkey SV40-transfected kidney fibroblast cell line.

Organism and isoform	Domains	Fusion protein	Expression host	Expression temp. / time	Ref.
Human TPH1	Full length	6His-TPH MBP-TPH 6His-Trx-TPH	*E. coli* BL21 Star (DE3)	37˚C/4 h or 27˚C/18 h	[138]
Human TPH1	Full length	None	*Pichia pastoris* KM21	30˚C/24 h	[138]
Human TPH1	Full length	None	*E.coli* BL21(DE3)	Room temp./ overnight	[143]
Human TPH1	Full length ct, 92-444 c, 92-425	MBP-TPH	*E. coli* DH5	Not reported	[139]
Human TPH1	ct, 91-444	6His-Trx-TPH	*E.coli* TOP10	37˚C/>3 h	[92]
Human TPH1	c, 103-401	TPH-6His	*E.coli* BL21(DE3)	25˚C/15 h	[64]
Human and Rabbit TPH1	Full length		*E.coli* BL21(DE3), pLysS	37˚C/2 h	[140]
Rabbit TPH1	Full length	6His-TPH	*Spodoptera frugiperda* 21	27˚C/72 h	[145]
Rabbit TPH1	c, 102-416	None	*E.coli* BL21 (DE)	20˚C/7.5 h	[87]
Rat TPH1	Full length ct, 99-444	GST-TPH	*E. coli* BL21	30˚C/2 h	[146]
Rat TPH1	Full length	None	Human fibroblast cell line GM4429	37˚C/48 h	[147]
Mouse TPH1	Full length	None	*E. coli* MC 1061	Not rep. /15 h	[148]
Schistosoma mansoni	Full length	6His-TPH	*E.coli* BL21(DE3), pLysS	30˚C/2.5 h	[149]
Human TPH2	Full length	6His-TPH Trx-6His-TPH 6His-GST-TPH 6His-MBP-TPH NusA-6His-TPH	*E.coli* BL21(DE3), pLysS	27˚C/6 h	[141]
Human TPH2	Full length ct, 151-490 c, 151-466	6His-TPH	*E. coli* BL21-CodonPlus(DE3)-RIL	15˚C/45 h	[21]
Human TPH2	Full length 45-490 1-473	None	COS7 cells	37˚C/48 h	[150]
Mouse TPH2	Full length	GST-TPH	*E. coli*	Probably 30˚C/2 h	[144]

Truncated versions of TPH have been expressed in *E. coli* more successfully, yielding protein suitable for characterisation. These truncated versions contain either the catalytic domain alone or the catalytic-tetramerisation domains [64,87,92].
If expression of a protein in *E. coli* fails, expression in eukaryotic cell cultures is sometimes tried [151,152]. TPH has been expressed in yeast [138], insect cells [145] and mammalian cell cultures [147,150]. The results in these reports do not indicate that eukaryotic expression of TPH is superior to expression in *E. coli*.

In summary none of the expression reports listed in table 2.3 is superior to the others, so no method can be singled out as the one to use.

2.10 Purification of tryptophan hydroxylases

Several different strategies have been applied in the purification of recombinant TPH and TPH from natural sources. Generally these can be divided into three groups, one using hydroxyapatite chromatography in combination with other methods, another using affinity chromatography with immobilised $DMPH_4$ and a third method using the properties of fusion proteins or tags for affinity chromatography.
A combination of $(NH_4)_2SO_4$ fractionation and hydroxyapatite chromatography have been used by several groups [87,153,154], most successfully by Moran *et al.* purifying the catalytic domain of rabbit TPH [87]. This procedure consists of an initial anion exchange on a Q Sepharose column, followed by $(NH_4)_2SO_4$ precipitation. The redissolved pellet was then applied to a hydroxyapatite column and the fractions containing TPH was concentrated through another $(NH_4)_2SO_4$ fractionation. From 1 L of cell culture this procedure gave 10 mg TPH with a specific activity of 0.6 µmol/min/mg [87].
The use of $DMPH_4$ as an adsorbent was initially reported in the purification of PAH [155] and was later applied to TPH [34,36,37,143,156,157,158]. The report by Nakata and Fujisawa is most noteworthy of these, since TPH was highly purified in one step only, with a 48% yield and a specific activity of 5.28 µmol/min/mg [36]. The elution of TPH from a $DMPH_4$ column was in most cases done with a $NaHCO_3$/NaOH buffer pH 10.8, while Nakata and Fujisawa used a Tris/acetate buffer pH 7.6 containing 50% ethylene glycol [36]. Additionally Cash has reported that TPH can be eluted by 5 mM tryptophan in a 50 mM glycine buffer pH 8.0 [157].
Most of the more recent reports on purification of TPH have used immobilised metal affinity chromatography (IMAC) [21,64,92,138,141] or affinity chromatography using either glutathione agarose as an adsorbent for glutathione S-transferase (GST) [144,146] or an amylose resin as the adsorbent for the maltose binding protein (MBP) [138,139,141]. Attempts to cleave the fusion protein have proven difficult in several cases leading to unstable TPH and incomplete cleaving [21,138,139,141]. The C-terminally His-tagged c*h*TPH1 was purified using IMAC (twice) and anion exchange chromatography and subsequently crystallised with the His-tag. The His-tag and the C-terminal end of c*h*TPH1 were not visible in the X-ray crystal structure [64].

2.11 Regulation of tryptophan hydroxylases

The regulation of TPH1 and TPH2 is not well understood [18]. TH and PAH are activated by phophorylation of serines in the regulatory domain [18]. PAH is furthermore allosterically activated by binding of phenylalanine in the regulatory domain which induces a conformational change [159,160]. This activating conformational change in PAH can also be induced by phospholips such as lysolechitin and by sulfhydryl modifications [161,162,163]. The extent of the conformational change has not been determined, but is likely to involve movement of the N-terminal end which blocks the entrance to the active site (see figure 2.7) [74,164]. TH is, in addition to regulation by phosphorylation, feedback inhibited by the catecholamines dopamine, norepinephrine and epinephrine [165].
The differences in the regulatory domains of TPH1 and TPH2 may allow for differentiated regulations, but this still has to be proven [48]. Phosphorylation is

believed to be important in the regulation of both isoforms [48]. TPH1 has been reported to be phosphorylated at Ser58 by protein kinase A [141,166]. TPH2 is also phosphorylated by protein kinase A [141,167] and by calmodulin-dependent phosphorylation [168,169]. Phosphorylated TPH and TH have been reported to interact with 14-3-3 protein [170,171]. The 14-3-3 protein is believed to bind to the regulatory domain of TPH and TH increasing the enzyme activity and prevent dephosphorylation [145,172]. In humans 7 isoforms exist of the 14-3-3 protein. All isoforms are acidic dimeric proteins which have been found to interact with more than 100 different proteins with various functions [173,174]. It has been hypothesised that the 14-3-3 protein binding has a function in stabilising the phosphorylated TPH [145]. This is further supported by reports showing that phosphorylated TPH is degraded faster in the cells than nonphosphorylated TPH [175]. The degradation of TPH in rat basophilic leukaemia cells (RBL2H3) and in mouse mastocytoma cells has been reported to be rapid with half-life times of 11-15 min in RBL2H3 cells and 40-60 min in the mastocytoma cells [176,177]. The rapid turnover of TPH also indicates that regulation at the transcriptional level is important for the immediate TPH activity [175,178].

2.12 Serotonin

Serotonin is a hormone and a neurotransmitter [179,180]. Serotonin functions as a neurotransmitter in the serotonergic neurons of the brain and gut [7]. In the rest of the body serotonin is involved in a wide range of physiological functions such as: mediating liver regeneration [180], immune system [181], peristaltic function of the gut [182], cardiac function [183], cardio vascular regulation, body temperature regulation and appetite [7]. In the pineal gland serotonin serves as a precursor for melatonin which is a hormone involved in circadian rhythm control [3]. Arylalkylamine N-acetyltransferase catalyses the rate-limiting step in the biosynthesis of melatonin [3,184].

2.12.1 Disorders related to serotonin

Serotonin has been implicated in a wide range of disorders [179]. In the pheripheral part of the body serotonin is believed to play a role in ulcerative colitis and in irritable bowel syndrome [43]. Dysfunction of the central serotonergic system is found in psychiatric disorders like obsessive-compulsive disorder (OCD), depression, anxiety disorders, attention deficit hyperactivity disorder (ADHD), anorexia nervosa and schizophrenia [7,185]. Behaviours such as substance abuse, gambling, aggression and suicide attempts may also have been associated with altered serotonin function [7]. Furthermore, dysfunction of the central serotonergic system is also believed to be implicated in sudden infant death syndrome [186].
Neuropsychiatric disorders like those mentioned above are very complex diseases. These may be caused by gene polymorphisms influencing a multitude of biochemical pathways. Environmental influences further add to this complexity.
In the case of depression it has been hypothesised that major depression is caused by a deficiency of available serotonin in the brain [187]. Selective serotonin re-uptake inhibitors (SSRI) are commonly used in the treatment of depression, OCD and anxiety disorders [179]. This medicine increases the serotonin concentration in the synapse by inhibiting the serotonin transporter [188].
Since TPH is the rate limiting step in the biosynthesis of serotonin many studies have been performed on the possible correlations between genetic variation in the TPH

genes and the occurrence of some of the above mentioned disorders [189]. Correlation between the TPH1 and suicide attempts have been reported, but the two polymorphisms are found on introns and their effect is not understood [190]. Even though TPH1 is not expressed in the developed brain evidence suggests that TPH1 has a function in the late developmental stage of the brain [191]. Serotonin synthesis is important during the development of the brain and TPH1 may therefore still have a role in psychiatric disorders [192]. Correlations have been reported between the TPH2 gene and OCD [193], ADHD [185,194] and depression [195,196]. Zhang *et al.* reported a single nucleotide polymorphism correlated with depression, which results in a mutation in TPH2 of Arg441 to a histidine [196]. Zhang *et al*. have also reported a single nucleotide polymorphism, not necessarily correlated to depression, which causes a mutation of Pro449 to an arginine [42]. These two mutations are believed to decrease stability or activity of the mouse TPH2 and *h*TPH2 [144,196,197].

2.13 The perspectives of tryptophan hydroxylase research

TPH is centrally positioned in the regulation of serotonin synthesis. Serotonin is involved in a wide range of important physiological and neurobiological functions. A full understanding of the biochemistry of TPH1 and TPH2 is a necessary foundation in understanding the complex functions of serotonin. Knowledge about the three-dimensional structure of the full-length enzymes and their regulatory mechanisms may also lead to the identification of compounds that modulate the activity of TPH. The differences in the regulatory domains of TPH1 and TPH2 may also allow isoform specific modulation of activity.

CHAPTER THREE

3 Sequence analysis and expression of different TPH constructs

This chapter starts with an introduction to selected protein sequence analysis tools which are later applied to the sequences of *g*TPH1 and *h*TPH2. During this project I have tested 17 different constructs of TPH in order to obtain soluble TPH that can be purified. These constructs and the fusion proteins used will be presented. This is followed by experimental, result and discussion sections for these constructs.

3.1 Theoretical methods for predicting protein properties

Many proteonomics tools are available for predicting the properties of proteins based upon their amino acid sequences. Some of these predict for example glycosylation sites, phosphorylation sites or helical content of the protein. Predictions can be useful but one should not blindly trust these predictions, since proteins are complicated molecules making it difficult to predict anything for sure. Therefore, predictions should always be treated with some scepticism. I will present some prediction tools, which I have used to analyse the TPH sequences.

3.1.1 Protein instability index

The protein instability index was developed by Guruprasad *et al.* [198] and is implemented in the ProtParam tool of the ExPASy proteonomics server [53]. The instability index predicts the *in vivo* stability of a protein from its primary sequence. In a statistical analysis of 12 unstable and 32 stable proteins Guruprasad *et al.* found that certain dipeptide sequences were more frequent in the unstable proteins than in the stable proteins. For each possible dipeptide they calculated a dipeptide instability weight value. When a protein sequence is analysed all the dipeptide instability weight values are calculated and from these values an instability index for the protein is calculated. A protein is predicted to be stable when the instability index is below 40.

3.1.2 Solubility of protein expressed in *Escherichia coli*

A model for predicting the solubility of proteins expressed in *E. coli* was developed by Wilkinson and Harrison [199]. This model was later modified, since it was realised that only two of the original five parameters were critical in predicting soluble versus insoluble protein expression in *E. coli* [200]. A canonical variable (cv) is calculated from the two critical parameters as shown in equation 3.1.

$$cv = 15.43\left(\frac{N+G+P+S}{n}\right) - 29.56\left(\left|\frac{(R+K)-(D+E)}{n} - 0.03\right|\right) \quad (3.1)$$

N, G, P, S, R, K, D and E represent the number of the respective amino acids in the protein and n is the total number of residues in the protein. When cv < 1.71 the protein is predicted to be soluble. This means that a protein is more likely to be expressed in a soluble form if it is highly charged, preferably negatively charged. The fewer of the turn forming residues asparagine, glycine, proline the more likely is soluble expression. For the probability calculation based on the cv see Davis *et al.* [200]. The probability can be calculated on www.biotech.ou.edu [201].

3.1.3 Prediction of intrinsic disorder in proteins

Some proteins or regions of some proteins exist naturally in a disordered state [202]. This is also called intrinsic disorder. If a protein contains disordered regions it might lead to problems with recombinant expression, protein purification and crystallisation [203]. It is sometimes necessary to truncate a multi-domain protein in order to obtain a domain suitable for crystallographic characterisation. Being able to predict disordered regions can be useful when deciding on where in the amino acid sequence to make such truncations [203].

Several computer programs have been developed to predict intrinsic disorder of a protein from its primary sequence. I will briefly introduce the 8 programs used later and which criteria they use for detection.

Disopred uses a support vector machine which is trained on proteins with disordered regions found in the PDB [204]. *FoldIndex* uses an algorithm based on average residue hydrophobicity and net charge of the protein [205,206]. *FoldUnfold* calculates the expected average number of close residue contacts computed from the amino acid sequence [207]. *Globplot* calculates a tendency for disorder based on the propensity for a given amino acid to be in a random coil or in an ordered secondary structure [208]. *IUPred* makes an estimate on the potential of the amino acids to form stabilising inter-residue interactions [209]. *PONDR VL3* uses a neural network trained on a data set consisting mostly of proteins from the PDB [210]. *Prelink* calculates a probability of a given sequence fragment of being in a structured or unstructured region based on known amino acid distributions in structured and unstructured regions. Furthermore, this is combined with the distance of a given region to the nearest hydrophobic cluster [211]. *RONN* uses a neural network trained on the amino acid sequences which were not visible in the electron density maps obtained by X-ray crystallography [212]. Links to all these programs can be found on www.disprot.org [213].

The amino acid sequences of *g*TPH1 and *h*TPH2 have been tested using these 8 programs and the predicted disordered regions are shown in figure 3.1.

*g*TPH1 is generally predicted to be a structured protein with possible dynamic turns, since no region is predicted disordered by all programs. The N-terminal end is identified by 6 programs as disordered and this may be similar to PAH where the first 19 residues of the N-terminal are not visible in the crystal structure [74].

For *h*TPH2 a region in the regulatory domain is predicted disordered by all programs with a consensus from amino acid 42-55. Little is known about the regulatory domain of *h*TPH2 but it might very well be that it contains a region with no structure. This region could also extend over the active site opening or be important in amino acid

binding or enzyme regulator binding for example of the 14-3-3 proteins (see section 2.11)[214].

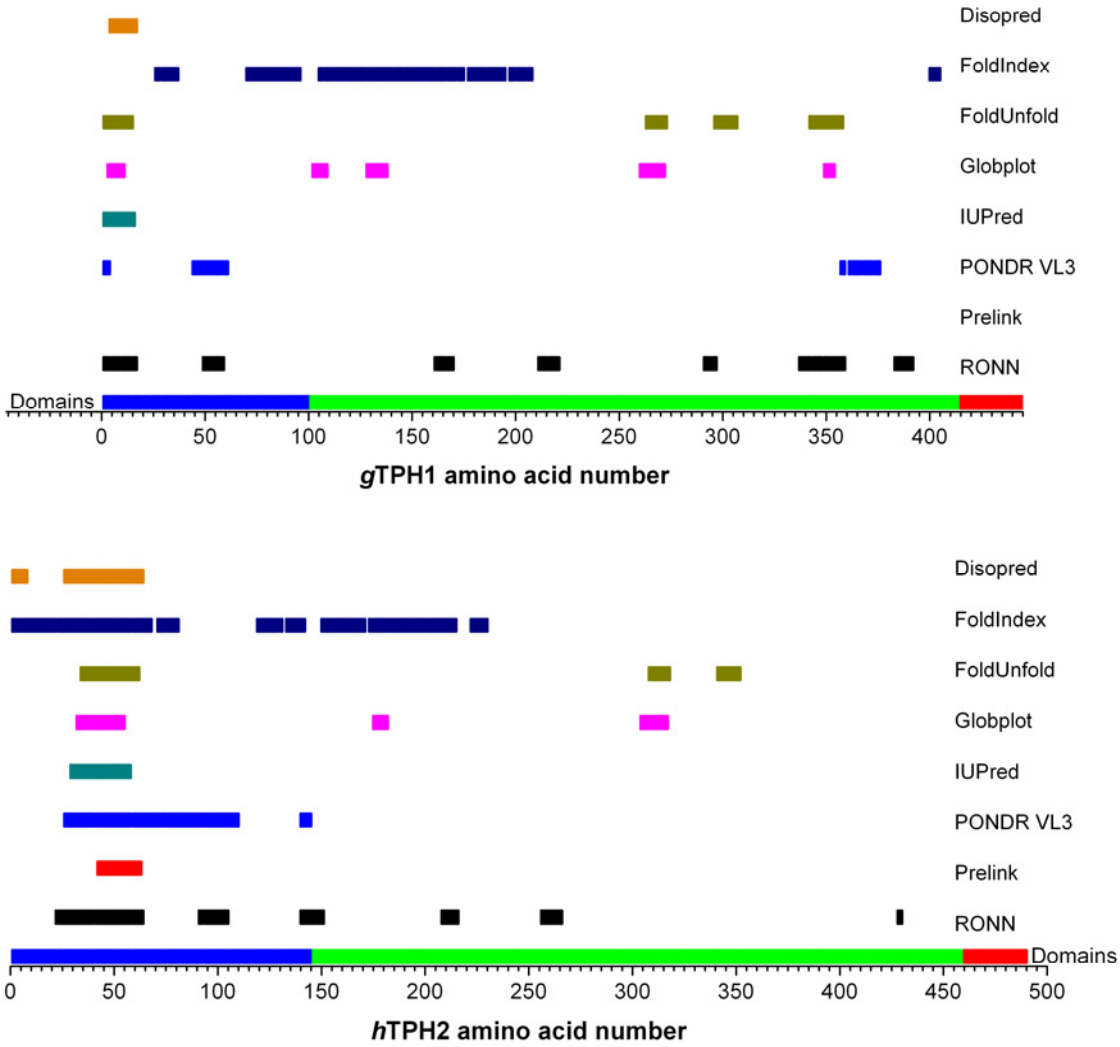

Figure 3.1 The predicted disordered regions of *g*TPH1 (top) and *h*TPH2 (bottom) are shown by the coloured bars. The prediction programs used are listed to the right of the prediction. The domains of *g*TPH1 and *h*TPH2 are shown as the blue-green-red bar just above the amino acid numbers. Blue is the regulatory domain, green is the catalytic domain and red is the tetramerisation domain.

3.1.4 Similarities of the regulatory domains of TPH with other proteins

BLAST search for protein sequences that are homologues to the regulatory domain of *h*TPH2 (r*h*TPH2) was performed [215]. Different TPH variants obviously appear followed by PAH variants. Following PAH, sequences of the bifunctional enzyme chorismate mutase - prephenate dehydratase, also called the P-protein, from different bacteria appears. The enzyme from the hyperthermophilic bacteria *Aquifex aeolicus (A. aeolicus)* shows the highest identity with 25 out of 60 amino acids being identical to r*h*TPH2. The P-protein consists of three domains: a chorismate mutase domain (N-

terminal), a prephenate dehydratase domain (middle) and a regulatory domain (C-terminal). The chorismate mutase catalyses the conversion of chorismate to prephenate, which is the first committed step in the biosynthesis of phenylalanine and tyrosine [216]. Prephenate is then decarboxylated and dehydrated to phenylpyruvate by the prephenate dehydratase domain [217]. These reactions are allosterically controlled by feedback inhibition by phenylalanine, which binds to the C-terminal regulatory domain [218]. It is this C-terminal domain of the P-protein which is homologues to residues 59-146 in *h*TPH2 and also to the corresponding sequence of *g*TPH1. A sequence alignment of the regulatory domains of *g*TPH1 and *h*TPH2 with the C-terminal domain of the *A. aeolicus* P-protein is shown in figure 3.2. Through a mutational study on the P-protein from *E. coli* the phenylalanine binding sequence was identified to be GALV and ESRP [218]. The equivalent sequences (GGLV/GALY, ESRK) are coloured blue in figure 3.2.

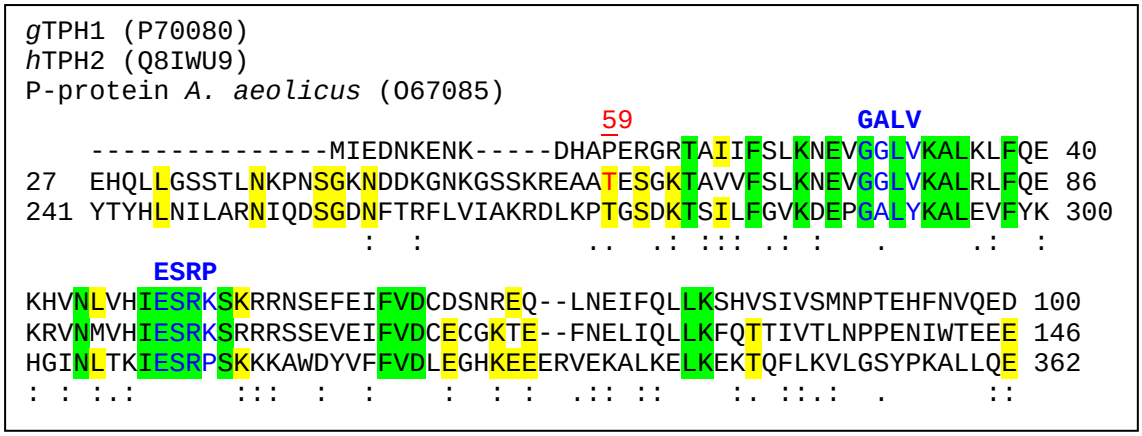

Figure 3.2 Sequence alignment of the regulatory domain of *g*TPH1, regulatory domain of *h*TPH2, and the P-protein from *A. aeolicus*. For the sequences shown the identities of the P-protein with *g*TPH1 and *h*TPH2 are 23% and 24%, respectively. The primary accession numbers in the ExPASy database are shown in parenthesis. Residues with green background are conserved in all three enzymes. Residues with yellow background are conserved between one of the TPHs and P-protein. ":" means that conserved substitutions have been observed within the groups (AVFPMILW), (DE), (RHK), (STYHCNGQ). "." means that semi-conserved substitutions are observed. The proposed phenylalanine binding sequences are shown in blue. Thr59 in *h*TPH2 is shown in red. The alignment was done with ClustalW [54].

Domains that are homologues to the regulatory domain of TPH and C-terminal domain of the P-protein are observed in many different enzymes [219,220,221]. This domain type is named the ACT domain after aspartokinase, chorismate mutase and TyrA (prephenate dehydrogenase) [219]. It has been shown that the ACT domains of many enzymes are responsible for allosteric regulation of the enzymes upon binding of an amino acid, for example phenylalanine in the P-protein and serine in D-3-phosphoglycerate dehydrogenase [220]. Therefore, speculations have been that the observed stimulating effect of phenylalanine on PAH is due to the binding in the regulatory domain [162]. For TPH very little is known about the function of the regulatory domain. However, tryptophan is likely to have the same function as phenylalaine in PAH [220].

3.2 Fusion proteins

Expression of recombinant protein fused to a tag or another protein is widely used to obtain soluble protein expressed in *E. coli* [222]. The most widely fusion proteins are the *E. coli* maltose binding protein (MBP), *E. coli* N-utilization substance A (NusA) [200], *E. coli* thioredoxin (Trx) and *Schistosoma japonicum* glutathione-S-transferase (GST)[222]. Other interesting fusion proteins or peptide tags are ubiquitin [223], small ubiquitin-related modifier (SUMO) [224] and solubility-enhancement tag (SET) [225]. Ubiquitin and SET will be further described since these have been used as fusion proteins/tags in this project. Expression of TPH fused to MBP, NusA, Trx, and GST respectively, have been tried by others with non-satisfactory results [138,141]. These fusion proteins have therefore not been tested in this project.

3.2.1 Ubiquitin as a fusion protein

Ubiquitin is a 76 amino acid protein found in eukaryotic cells where it functions in the degradation pathway of proteins [226]. Ubiquitin is highly resistant to proteolytic degradation and has a long half-life when expressed in *E. coli* [227]. Ubiquitin is used as a fusion protein for expression in *E. coli* where the ubiquitin fusion gives increased expression and solubility of the target protein [223,228]. An ubiquitin specific protease is often co-expressed with the fusion protein. This protease cleaves the fusion protein at the C-terminal end of ubiquitin [229,230]. The ubiquitin fusion protein/ubiquitin specific protease system has with success been used extensively in the Bioinorganic Chemistry Group at DTU [231].

3.2.2 The solubility-enhancement tag

Fusion proteins are used extensively in recombinant protein expression to increase expression and solubility of the target protein. The solubility-enhancement tag (SET) is small (43 amino acids) compared to fusion proteins like GST and MBP and has been reported to improve the solubility and stability of fusion products significantly [232]. SETs with different charges have been developed [225] and are available from Stratagene [233]. It is suggested that the negatively charged peptide extensions indirectly promote folding by increasing the electrostatic repulsion between nascent protein chains. This repulsion might provide more time for the protein to fold in a correct and stable conformation [225].

3.3 Constructs of TPH expressed in *Escherichia coli*

Several expression constructs for different variants of *g*TPH1 and *h*TPH2 have been made. A list with composition of constructs, molecular weight, pI and abbreviation is shown in figure 3.3. An introduction to the variants xc*h*TPH2 and yc*h*TPH2 and results of these variants will be presented separately in section 3.5.3.

3.4 Experimental

The cloning and preparation of expression strains were done by laboratory technicians or other students in the Bioinorganic Research Group. All constructs were expressed in *E. coli* BL21(DE3) cells. In some cases the expression and solubility tests were done by other students in the group. The gene for chicken (*Gallus gallus*) TPH1 were donated by Prof. J. S. Takahashi, Northwestern University, USA [50].

Chicken TPH1

Fusion protein of ubiquitin and chicken (*Gallus gallus*)
tryptophan hydroxylase isoform 1, amino acids 1-445, 59.7 kDa, pI 6.4

u*g*TPH1

Fusion protein of ubiquitin with regulatory and catalytic domains of chicken
(*Gallus gallus*) tryptophan hydroxylase isoform 1, amino acids 1-414, 56.3 kDa, pI 6.4

urc*g*TPH1

Chicken (*Gallus gallus*) tryptophan hydroxylase isoform 1
Amino acids 1-445, 51.1 kDa, pI 6.3

*g*TPH1

Regulatory and catalytic domain of chicken (*Gallus gallus*)
tryptophan hydroxylase isoform 1, amino acids 1-414, 47.7 kDa, pI 6.4

rc*g*TPH1

Catalytic domain of chicken (*Gallus gallus*) tryptophan hydroxylase isoform 1
Amino acids 101-414, 36.1 kDa, pI 6.5

c*g*TPH1

Human TPH2

Fusion protein of ubiquitin and human tryptophan hydroxylase isoform 2
Amino acids 1-490, 64.6 kDa, pI 6.1

u*h*TPH2

Fusion protein of ubiquitin with regulatory and catalytic domains of human
tryptophan hydroxylase isoform 2, amino acids 1-459, 61.1 kDa, pI 6.2

urc*h*TPH2

Fusion protein of solubility-enhancement tag 3 and human
tryptophan hydroxylase isoform 2, amino acids 1-490, 61.0 kDa, pI 5.2

SET3-*h*TPH2

Fusion protein of solubility-enhancement tag 3 with regulatory and catalytic domains
of human tryptophan hydroxylase isoform 2, amino acids 1-459, 57.5 kDa, pI 5.2

SET3-rc*h*TPH2

Full length human tryptophan hydroxylase isoform 2
Amino acids 1-490, 56.1 kDa, pI 6.0

*h*TPH2

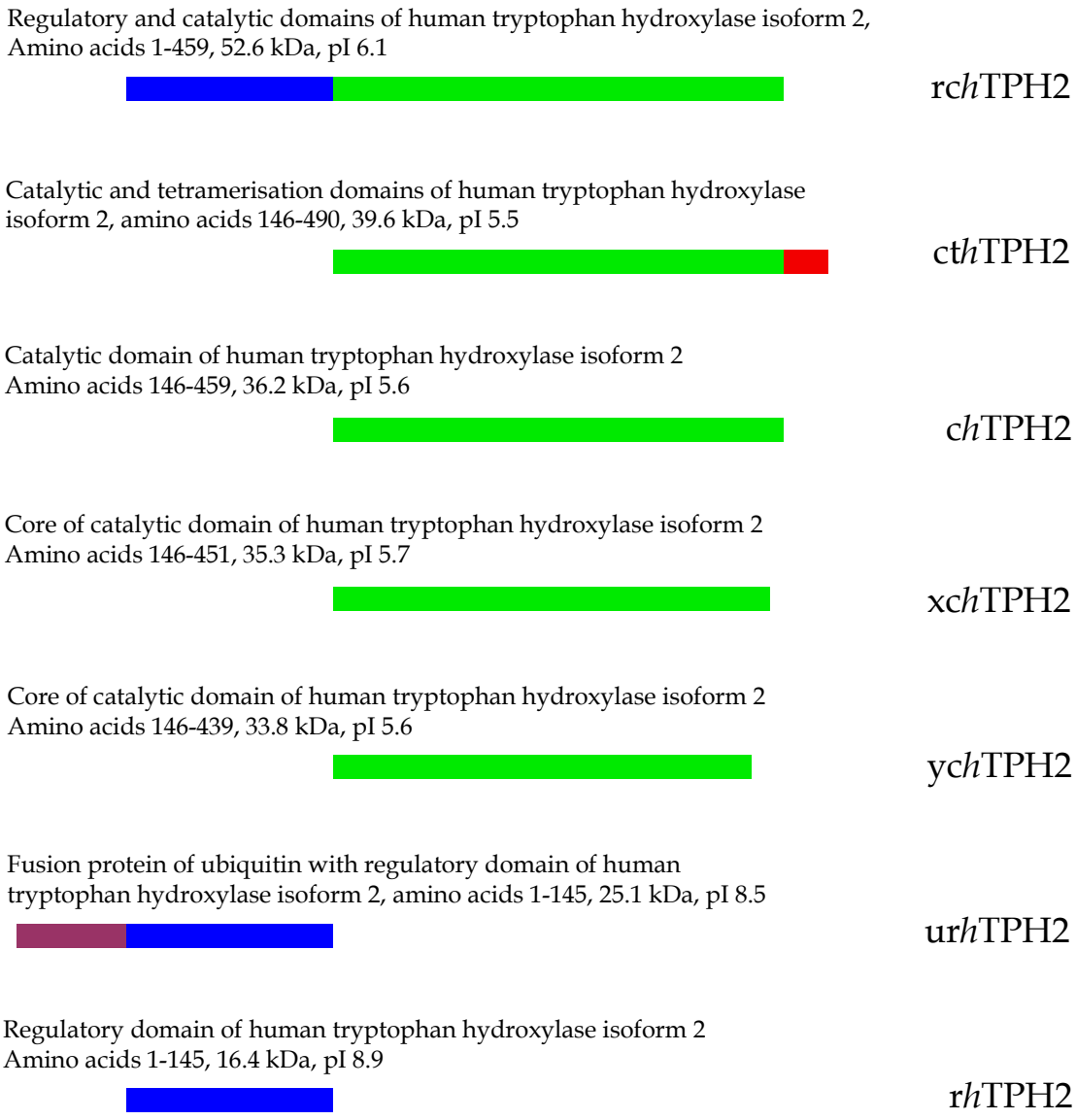

Figure 3.3 Schematic representation of constructs of TPH which have been produced in this project. For each variant the number of amino acids is listed together with the molecular weight and theoretical pI. To the right for each construct is the abbreviation for each variant. The regulatory domain is shown in blue, the catalytic domain in green and the tetramerisation domain in red. Fusion proteins are shown in maroon for ubiquitin and orange for the solubility-enhancement tag. The molecular weight and pI were calculated from the sequences using the ProtParam tool on ExPASy [53,234].

The gene for ubiquitin and the plasmid containing the ubiquitin-specific protease were donated by Prof. C. E. Cameron, Pennsylvania State University, USA [230]. An *E. coli* codon optimised version of the human TPH2 gene (gi:27497158) was obtained from Genscript, USA.

The following experimental procedures comply with general protocols used in the Bioinorganic Research Group, but small variations have in some cases been tested.

Luria Bertani (LB) media and all chemicals used were analytical grade obtained from Sigma-Aldrich. All solutions were prepared using 18.2 MΩ cm water from a Milli-Q synthesis A10 Q-Gard system (Millipore).

3.4.1 Expression of TPH variants

From a frozen stock the *E. coli* BL21(DE3) strain containing the TPH expression plasmids was plated on a Luria Bertani (LB) agar plate containing 30 µg/mL kanamycin sulphate (30 Kan) and 20 µg/mL chloramphenicol (20 Cam). 30 Kan was used to select for cells harbouring the TPH plasmids and 20 Cam was used to select for cells harbouring the ubiquitin-specific protease plasmid. The plate was incubated overnight at 37˚C. A single colony was used to inoculate 50 mL LB 30 Kan/20 Cam media and incubated at 37˚C in a 250 mL shake flask at 250 rpm. This pre-culture was incubated for approximately 4 hours until an optical density at 600 nm (OD_{600}) of 0.6-1.0 was reached. The cells were then sedimented by centrifugation at 4˚C and 1800 × g for 10 min. The cells were resuspended in 50 mL fresh LB 30 Kan/20 Cam media. 6.5 mL cell resuspension was used to inoculate 650 mL LB 30 Kan/20 Cam media in a 2 L triple baffled shake flask. The culture was incubated at 30˚C and 250 rpm for approximately 5 hours. When an OD_{600} of 0.4 - 0.6 was attained the TPH expression was induced by adding isopropyl-β-D-thiogalactopyranoside (IPTG) to a final concentration of 0.1 mM. After incubation at 30˚C and 250 rpm for 4 hours the cells were harvested by centrifugation at 4˚C, 3000 × g for 15 min. The cells from 650 mL were resuspended in 25 mL 4˚C 20 mM Tris/HCl pH 8.2 and transferred to 50 mL polypropylene tubes. The cells were again centrifuged at 4˚C, 3000 × g for 15 min. The supernatant was discarded and the cells stored at -80˚C until further use.
For some variants expression was also tested at 10˚C or 20˚C. The same procedure as just described was used, except that the time of expression was extended.

3.4.2 Solubility test for the TPH variants

Cells from 650 mL culture containing the TPH variant were resuspended in 40 mL 20 mM Tris/HCl pH 8.2. The cells were lysed on ice by sonication for 3 × 30 s using a Satorius Labsonic P at 80% amplitude. The cell extract was centrifuged (Eppendorf 5810R) at 4˚C and 18000 × g for 20 min. The supernatant was collected. Samples for sodium dodecyl sulphate polyacrylamide gel electrophoresis (SDS-PAGE) analysis were taken from the raw extract from the cells, the supernatant and from resuspended pellet. Addition of glycerol, sucrose and/or tryptophan to the lysis buffer was tested for some of the TPH variants. For x*ch*TPH2 and y*ch*TPH2 cells were lysed in 20 mM Bis Tris Propane/HCl, 5% glycerol, pH 7.2.
If the SDS-PAGE analysis showed TPH in the supernatant an initial purification test was done as described in the following. The supernatant was diluted with cold water to a conductivity below 1 mS/cm. The supernatant was then loaded onto a Q Sepharose Fast Flow 16/10 column equilibrated with 20 mM Tris/HCl pH 8.2 and the flow-through was collected. The column was washed with 1.5 column volume (CV) 20 mM Tris/HCl pH 8.2. A linear gradient 0-100% 20 mM Tris/NaOH, 0.8 M $(NH_4)_2SO_4$, pH 8.2 over 5 CV was applied to the column. Samples for SDS-PAGE analysis were taken from the flow through and the collected fractions.
In a few cases 0.45 µm filtered (GHP Acrodisc GF syringe filters from Pall) flow-through from the anion exchange was applied on a Superdex 200 26/60 prep grade column equilibrated in 20 mM Tris/NaOH, 200 mM $(NH_4)_2SO_4$, pH 8.2.

Cation exchange was tested for some of the variants that did not bind to the anion exchange. In those cases the procedure was similar to that of the anion exchange described above, except that the cells were lysed in 20 mM MES/NaOH pH 6.0 and the supernatant was filtered through a 0.45 µm filter before applied to a Source 30 S 16/10 column. The buffers used in the cation exchange were 20 mM MES/NaOH pH 6.0 and 20 mM MES/NaOH 0.4 M $(NH_4)_2SO_4$, pH 6.0.
TPH enzyme activity was done by monitoring the formation of 5-hydroxytryptophan by fluorescence spectrophotometry essentially as described by Moran *et al.* [235]. A detailed description of the TPH activity assay is presented in section 6.1.

3.4.3 SDS-PAGE analysis

SDS-PAGE was done using either 7.5% or 12% Tris-HCl precast gels from Bio-Rad. Unstained SDS-PAGE low range standard was from Bio-Rad. The SDS-PAGE experiments were carried out as recommended by Bio-Rad and protein was stained using Coomassie Blue G-250.

3.5 Results and discussion of expression and solubility tests of TPH variants

All constructs were expressed in *E. coli*. The SDS-PAGEs will only be shown for selected variants. The solubility of the TPH variants will be described using three terms: soluble, partly soluble and insoluble protein. These terms are defined in the following. Soluble protein is detected in the supernatant, and can be purified. Partly soluble protein is found in the supernatant and in the flow-through from the anion exchange column. The insoluble protein is only found in the pellet.

Table 3.1 The expressed variants of TPH with instability index, probability of solubility and the actual solubility detected from expression in *E. coli* at 30˚C.

	Theoretical		Experimental
Protein	Instability index*	Probability of solubility	Solubility
c*g*TPH1	40.9	41.2	Soluble
ct*h*TPH2	44.3	60.1	Soluble
c*h*TPH2	41.3	61.0	Soluble
u*g*TPH1	42.1	43.0	Partly soluble
*g*TPH1	44.1	43.7	Partly soluble
urc*g*TPH1	42.8	41.7	Partly soluble
rc*g*TPH1	45.1	42.2	Partly soluble
SET3-rc*h*TPH2	51.5	61.6	Partly soluble
u*h*TPH2	48.4	41.9	Insoluble
SET3-*h*TPH2	52.8	61.0	Insoluble
*h*TPH2	51.2	42.3	Insoluble
urc*h*TPH2	46.9	41.3	Insoluble
rc*h*TPH2	49.6	41.7	Insoluble
xc*h*TPH2	38.5	58.5	Insoluble
yc*h*TPH2	39.0	63.7	Insoluble
ur*h*TPH2	54.5	20.5	Insoluble
r*h*TPH2	65.2	10.5	Insoluble

* instability index < 40 is considered stable

The results of the solubility tests are summarised in table 3.1 with the calculated instability index and probability of solubility for each variant. The three variants c*g*TPH1, c*h*TPH2 and ct*h*TPH2 were found in a soluble form and the expression and purification of these variants are presented in chapter 4.
All the constructs of *g*TPH1 containing the regulatory domain were to some extent found in the partly soluble form which could be filtered through a 0.45 µm filter. The partly soluble *g*TPH1 variants did not interact with either Q Sepharose FF or Source 30 S media and were therefore found in the flow-through from the columns. Partly soluble *g*TPH1 variants eluted early in the gel filtration, equivalent to proteins with a mass of approximately 1000 kDa. Glycerol, sucrose, tryptophan and dithiothreitol were tested in the lysis buffer, but none of the tested additives yielded *g*TPH1 that could be purified. Lowering the expression temperature to 10˚C seemed to yield small amounts of *g*TPH1 variants that might bind to an anion exchange column, but the amount was so small that it was not a viable method. The partly soluble *g*TPH1 generally showed enzyme activity.
The SET3-rc*h*TPH2 was found in a partly soluble form and in the pellet. The partly soluble SET3-rc*h*TPH2 showed enzyme activity. The remaining variants of *h*TPH2 were found only in the pellet as the insoluble form.
The *h*TPH2 variant was expressed as a fusion protein to ubiquitin with the co-expression of the ubiquitin specific protease. The cleavage of the fusion protein was incomplete and a 1:1 mixture of u*h*TPH2 and *h*TPH2 was observed. When the expression temperature was lowered to 10˚C the cleavage of ubiquitin-*h*TPH2 was increased to almost 100%. The lowered expression temperature also resulted in *h*TPH2 being present in the partly soluble form and not only in the insoluble form.

3.5.1 The partly soluble variants of *g*TPH1

The partly soluble *g*TPH1 variants are believed to be small aggregates of variable sizes, small enough to be filtered through a 0.45 µm filter. These aggregates do not bind to ion exchange media. The reason for this may be that either the aggregates have no effective charge or the aggregates are larger than the exclusion limit of the ion exchange media and will therefore not have the possibility of binding.
Since *g*TPH1 variants without the tetramerisation domain did not change the solubility properties compared to full length, it is very likely that the regulatory domain is responsible for the formation of some soluble aggregates. Since the partly soluble *g*TPH1 generally shows enzyme activity the catalytic domain must be correctly folded, while the regulatory domain may be in an improper conformation or disordered. Such a regulatory domain could be responsible for unspecific interactions with other regulatory domains causing aggregation. Partly soluble aggregates have been reported for proteins fused to MBP [236,237,238] and proteins fused to the SET tag [225].

3.5.2 The insoluble variants of *h*TPH2

Expression at 30˚C of *h*TPH2 variants containing the regulatory domain yielded only protein in the insoluble form, commonly called inclusion bodies [239]. The cleavage of ubiquitin-*h*TPH2 was increased to almost 100% when the expression temperature was lowered to 10˚C. This can be explained by a lower expression rate of u*h*TPH2 yielding a lower concentration of over-expressed protein in the cells. This might increase the time where u*h*TPH2 is soluble in the cells. It is likely that only soluble u*h*TPH2 is the substrate for the ubiquitin specific protease, since proteins in the inclusion body state

are generally known to be inert to protease degradation [240]. The lower rate of expression of u*h*TPH2 may also allow *h*TPH2 longer time to fold correctly which may explain the *h*TPH2 found in the partly soluble form when expressed at 10˚C. Inclusion bodies can be isolated from the cell pellet and solubilised in strong denaturants and in some cases subsequently refolded upon removal of the denaturant [240]. This was also tried with *h*TPH2 inclusion bodies, but primarily u*h*TPH2 was used since large amounts of homogeneous inclusion bodies could be isolated of this variant. Additionally, the ubiquitin might be beneficial in the folding process of the protein. Many different kinds of refolding experiments were carried out but none yielded a satisfactory product. The refolding experiments will not be further described.
Since the c*h*TPH2 and ct*h*TPH2 can be expressed in a soluble form and can be purified, it is likely that the regulatory domain is responsible for the insolubility of *h*TPH2 when expressed in *E. coli*. The same observations have recently been published by Carkaci-Salli *et al.* [22].
The partly soluble forms of *g*TPH1 can be interpreted as an intermediate between the insoluble inclusion bodies and a soluble monodisperse form. If this is the case, one will think of *g*TPH1 as being slightly more soluble than *h*TPH2. This is if the term solubility is thought of as the propensity of the protein to be produced in a correctly folded conformation in *E. coli*. McKinney *et al.* have reported that *h*TPH2 is more soluble than *h*TPH1, both of which were expressed as fusion proteins to MBP [141]. The criterion for solubility is not defined and no documentation for the differences in solubility is presented [141]. It might therefore be difficult to compare the observation of McKinney *et al.* with those observed in this project.
The main difference between r*g*TPH1 and r*h*TPH2 is that r*h*TPH2 is elongated in the N-terminal by 46 residues. It is seen in figure 3.2 that from Thr59 in r*h*TPH2 numbering the three sequences are highly homologous indicating a similar structured domain. Since intrinsic disorder is predicted for the amino acids 42-55 in *h*TPH2, a new variant of *h*TPH2 containing amino acids 59- 490 might form a structured protein that could be purified. The instability index and chance of solubility in *E. coli* for such a protein are 51.7 and 55.9%, respectively, where the chance of solubility is much better than the predictions for the full length enzyme. Such a variant will probably not give information about the regulatory mechanism, but will give information on inter-domain structure and possible amino acid binding in the regulatory domain of which very little is known.
Expression of human intracellular multi-domain proteins in *E. coli* is known to be difficult and some estimates suggest that at the time being as little as 20% of human proteins can be expressed in *E. coli* in a soluble form [241,242,243]. Expression in eukaryotic cell cultures is more difficult and time consuming but eukaryotic cells contain the cellular machinery (*i. e.* folding chaperones and post translational modify-cation enzymes)[244], which might be necessary to obtain soluble *h*TPH2.

3.5.3 Truncating the C-terminal of the c*h*TPH2

The expression construct of the crystallised c*h*TPH1 (PDB entry 1MLW) contains amino acids equivalent to 148-448 in *h*TPH2 and is followed by a 6His-tag [64]. The last amino acid with visible electron density for this crystal structure is equivalent to Ile439 in *h*TPH2 indicating that the residues 440-448 and the His-tag are disordered [64]. c*h*TPH2 was the initial variant made of the catalytic domain in this project. c*h*TPH2 contain residues 146-459 and therefore contains 11 residues more in the C-terminal compared

to the crystallised *ch*TPH1 variant. Later I suspected that the C-terminal end of *ch*TPH2 was floppy and could prevent crystal formation. Subsequently two new versions of the catalytic domain of *h*TPH2 were made, namely xc*h*TPH2 (146-439) and yc*h*TPH2 (146-451). The extents of the yc*h*TPH2, xc*h*TPH2 and c*h*TPH2 are indicated in the structure of the catalytic domain of PAH [69] in figure 3.4 and are seen in the sequence alignment of the C-terminals of: visible residues of c*h*TPH1, yc*h*TPH2, xc*h*TPH2 and c*h*TPH2 and human PAH in figure 3.5. The structure of the catalytic domain of PAH contains the β-sheet (coloured magenta) which links the catalytic domain and the tetramerisation domain in the PAH [80] and TH [68] (see figure 2.6).

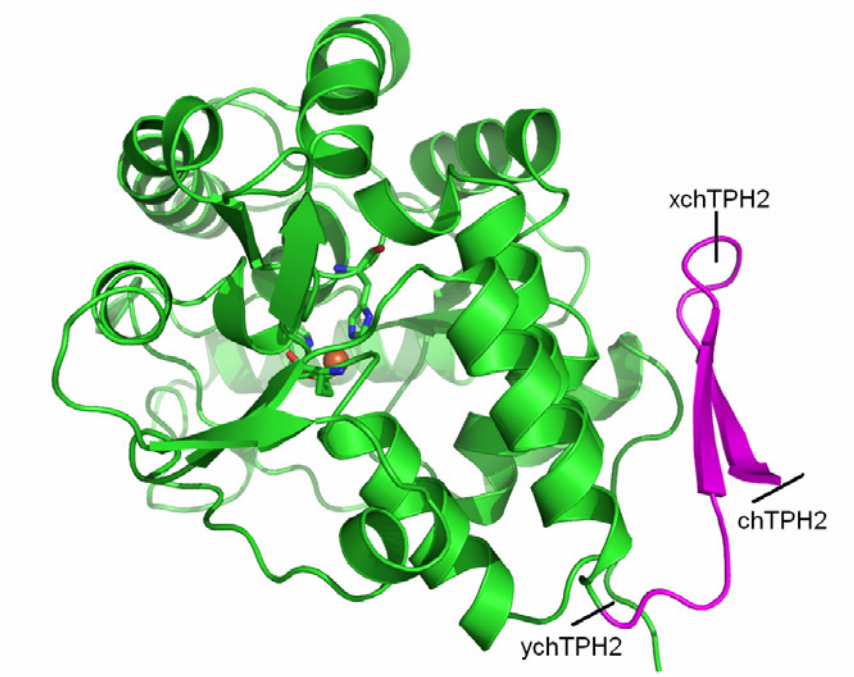

Figure 3.4 The structure of the catalytic domain of human PAH (PDB entry 1PAH) [69]. The crystal structures of the catalytic domains of human TPH1 (PDB entry 1MLW) and PAH are very similar except that the C-terminal β-sheet shown in magenta, is not present in the 1MLW structure. The c*h*TPH2 expressed in this project has the same length as the catalytic domain of PAH shown here. The figure was made using Pymol [72].

```
1MLW     387 REFTKTI 393
ychTPH2  433 RDFAKSI 439
xchTPH2  433 RDFAKSITRPFSVYFNPYT 451
chTPH2   433 RDFAKSITRPFSVYFNPYTQSIEILKD 459
hPAH     400 RNFAATIPRPFSVRYDPYTQRIEVLDNTQQLKILADSINSEIGILCSALQKIK 452
S. struc.    HHHHHHHcccSSSSSSSSSSSSSSSccHHHHHHHHHHHHHHHHHHHHHHHHH
Domains      catalytic domain-----------tetramerisation domain---
```

Figure 3.5 Sequence alignment the C-terminals of the c*h*TPH1 visible in the 1MLW structure [64], yc*h*TPH2, xc*h*TPH2, c*h*TPH2 and human PAH. The secondary structure of PAH is shown as determined in the structure of tetrameric PAH (PDB entry 2PAH) [80] H is α-helices, S is β-sheets and c is coil. The domain size as used in figure 3.3 is listed in bottom line.

3.5.3.1 Results of truncating the C-terminal of c*h*TPH2

Both xc*h*TPH2 and yc*h*TPH2 were expressed in an insoluble form as shown by the SDS-PAGEs in figure 3.6. No enzyme activity could be measured of any fractions of the yc*h*TPH2.

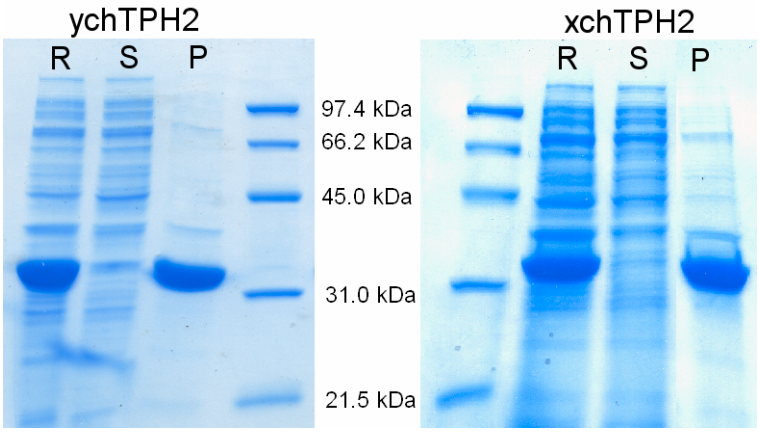

Figure 3.6 SDS-PAGE of yc*h*TPH2 and xc*h*TPH2. R is raw extracts of the cells, S is the soluble fraction, P is resuspended pellet. The molecular weight standard is shown in the lanes towards the middle. The cells were lysed in 20 mM Bis Tris Propane/HCl, 5% glycerol, pH 7.2.

3.5.3.2 Discussion of the effect of the linking β-sheet of c*h*TPH2

The expression of xc*h*TPH2 and yc*h*TPH2 in an insoluble form indicates that the linking β-sheet is important in the formation, stabilisation or solubilisation of the catalytic domain. Since no enzyme activity could be detected for yc*h*TPH2 it has probably lost its structure. The importance of the linking β-sheet to the catalytic domain will be studied further in the Bioinorganic Group through truncation and mutational studies.

3.6 Conclusion

The three variants, c*g*TPH1, c*h*TPH2 and ct*h*TPH2, were expressed in a soluble form that can be purified. Expression and purification of these variants are described in the following chapter. Variants of *g*TPH1 and *h*TPH2 containing the regulatory domain have proven difficult to express in a soluble form in *E. coli*. A partly soluble form of the *g*TPH1 variants was detected in the supernatant of centrifuged cell extract. This partly soluble form could not be purified. The *h*TPH2 variants containing the regulatory domain were only found in the cell pellet when expressed at 30˚C. When the expression temperature was lowered to 10˚C small amounts of the *h*TPH2 variants were found in the partly soluble form. A new expression construct of *h*TPH2 containing residues 59-490 is suggested.

CHAPTER FOUR

4 Expression and purification of tryptophan hydroxylase variants

In Chapter 3 the constructed expression variants of *g*TPH1 and *h*TPH2 were presented. Three variants can be expressed in a soluble form that can be purified. The three variants are c*g*TPH1, c*h*TPH2, and ct*h*TPH2. In this chapter I will describe how these three variants were expressed and purified.

4.1 Experimental

UltraPure™ glycerol was obtained from Invitrogen. (6R)-5,6,7,8-tetrahydro-L-biopterin dihydrochloride (BH_4) was from Schircks Laboratories, Jona, Switzerland. LB media and all other chemicals used were analytical grade obtained from Sigma-Aldrich. All solutions were prepared using 18.2 MΩ cm water from a Milli-Q synthesis A10 Q-Gard system (Millipore).

4.1.1 Expression of tryptophan hydroxylase variants

4.1.1.1 Expression of c*g*TPH1

The c*g*TPH1 was expressed as a fusion protein with ubiquitin. The ubiquitin-specific protease, which cleaves the polypeptide chain at the C-terminus of ubiquitin, was co-expressed together with ubiquitin-c*g*TPH1.
From a frozen stock, the *E. coli* BL21(DE3) strain containing the c*g*TPH1 expression plasmid and ubiquitin-specific protease expression plasmid was plated on a LB 30 Kan/20 Cam agar plate. The plate was incubated overnight at 37˚C. A single colony was used to inoculate 50 mL LB 30 Kan/20 Cam media and incubated at 37˚C in a 250 mL shake flask at 250 rpm. This pre-culture was incubated for approximately 4 hours until an optical density at 600 nm (OD_{600}) of 0.6-1.0 was reached. The cells were then sedimented by centrifugation at 4˚C and 1800 × g for 10 min. The cells were resuspended in 50 mL fresh LB 30 Kan/20 Cam media. 6.5 mL cell resuspension was used to inoculate 650 mL LB 30 Kan/20 Cam media in a 2 L triple baffled shake flask. The culture was incubated at 30˚C and 250 rpm for 3½ hour. The incubator temperature was then set to 20˚C and incubation continued for approximately 1½ hour. When an OD_{600} of 0.4 - 0.6 was attained the c*g*TPH1 expression was induced by adding IPTG to a final concentration of 0.1 mM. After incubation at 20˚C and 250 rpm for 14 hours the cells were harvested by centrifugation at 4˚C, 3000 × g for 15 min. Cells from

650 mL culture were resuspended in ice cold 25 mL 20 mM Tris/HCl pH 8.5 and transferred to 50 mL polypropylene tubes. The cells were again centrifuged at 4˚C, 3000 × g for 15 min. The supernatant was discarded and the cells stored at -80˚C until further use.

4.1.1.2 Expression of c*h*TPH2

The c*h*TPH2 was expressed as a non-fusion protein (see section 3.3). The cell culture step and expression were performed as described for c*g*TPH1 in section 4.1.1.1, except that Cam was not added to the media and cells were washed with 20 mM Bis Tris Propane/HCl, 5% (w/v) glycerol, pH 7.2 in the last step.

4.1.1.3 Expression of ct*h*TPH2

The ct*h*TPH2 was expressed as a non-fusion protein (see section 3.3). The cell cultures were grown and ct*h*TPH2 expressed as described for c*g*TPH1 in section 4.1.1.1, except that Cam was not added to the media and cells were washed with 20 mM Tris/HCl pH 8.2 in the last step.

4.1.2 Purification of tryptophan hydroxylase variants

The purification protocols for the three TPH variants, described in the following sections, were developed from a common starting protocol. In summary the common protocol consisted of an initial anion exchange done at pH 8.2 using Tris buffers and a gel filtration done in Tris, 200 mM $(NH_4)_2SO_4$, pH 8.2. From this protocol the purification parameters were optimised. Only the final procedures will be presented.
The use of argon flushed buffers and addition of sodium dithionite were done to keep the TPH iron in the ferrous state during the anion exchange purification step.
During the purifications the solutions containing TPH were kept on ice or at 4˚C except during the chromatographic steps which were carried out at room temperature. High Performance Liquid Chromatography was done using columns and an Äkta Purifier from GE Healthcare. Protein concentrations were determined using a HP 8453 diode array spectrophotometer.

4.1.2.1 Purification of c*g*TPH1

Cells from 3 × 650 mL culture, containing c*g*TPH1 (section 4.1.1.1), were resuspended in 3 × 40 mL 20 mM Tris/HCl pH 8.5. Sodium dithionite was added to a final concentration of 2 mM. The cells were lysed on ice by sonication for 3 × 30 s using a Satorius Labsonic P at 80% amplitude. The cell extract was centrifuged (Eppendorf 5810R) at 4˚C and 18000 × g for 20 min. The supernatant was collected and filtered through 0.45 µm GHP Acrodisc GF syringe filters from Pall. Water flushed with argon (on ice) was used to dilute the supernatant to a conductivity of approximately 1 mS/cm. The supernatant was loaded onto a Q Sepharose High Performance 26/10 column, which was equilibrated in 20 mM Tris/HCl pH 8.5, 2 mM sodium dithionite. Prior to equilibration this buffer and the salt buffer 20 mM Tris/NaOH, 0.8 M $(NH_4)_2SO_4$, pH 8.5 were flushed with argon for one hour per L buffer. The column was washed with 1.5 CV of 20 mM Tris/HCl pH 8.5, 2 mM sodium dithionite. A linear gradient of 0-15% buffer B over 6 CV was applied to the column. The fractions containing ferrous-c*g*TPH1 were collected and pooled. 20 mM Tris/NaOH, 2 M

$(NH_4)_2SO_4$ pH 8.5 was added to the collected fractions to reach an $(NH_4)_2SO_4$ concentration of 0.1 M. The collected fractions were then concentrated by ultrafiltration in an Amicon stirred pressure cell with an Ultracel PL-3 membrane. Approximately 7 mL of concentrated c*g*TPH1 solution was then filtered through a 0.45 µm filter and loaded onto a HiLoad Superdex 75 26/60 prep grade column. Prior to loading, the column was equilibrated in 20 mM Tris/NaOH, 100 mM $(NH_4)_2SO_4$, pH 8.5. Fractions containing c*g*TPH1 were collected. The c*g*TPH1 concentration was determined using the theoretical absorption coefficient [245] of $\varepsilon_{280} = 37820\ M^{-1}\ cm^{-1}$.
To the solution of purified c*g*TPH1, glycerol and 2 M $(NH_4)_2SO_4$, 20 mM Tris/NaOH, pH 8.5 was added to a concentration of 10% (w/v) glycerol and 100 mM $(NH_4)_2SO_4$. Samples for enzyme kinetic experiments were stored in aliquots of 1 mL at -80˚C. c*g*TPH1 for crystallisation experiments was concentrated by ultrafiltration in an Amicon stirred pressure cell and subsequently stored at -80˚C in aliquots of 100 µL.

4.1.2.2 Purification of c*h*TPH2

Cells from 3 × 650 mL culture containing c*h*TPH2 (see section 4.1.1.2) were resuspended in 3 × 40 mL 20 mM Bis Tris Propane/HCl, 5%(w/v) glycerol, pH 7.2. Sodium dithionite was added to a final concentration of 2 mM. The cells were lysed on ice by sonication for 3 × 30 s using a Satorius Labsonic P at 80% amplitude. The cell extract was centrifuged at 4˚C and 18000 × g for 20 min. The supernatant was collected and filtered through 0.45 µm GHP Acrodisc GF syringe filters. The supernatant was loaded onto a Q Sepharose High Performance 26/10 column which was equilibrated in buffer A: 20 mM Bis Tris Propane/HCl, 5%(w/v) glycerol, pH 7.2, 2 mM sodium dithionite. Buffer A and buffer B: 20 mM Bis Tris Propane/HCl, 5% (w/v) glycerol, 0.8 M $(NH_4)_2SO_4$, pH 7.2, were flushed with argon for one hour per L buffer prior to column equilibration. The column was washed with 1.5 CV of buffer A. A linear gradient of 0-4% buffer B (0-32 mM $(NH_4)_2SO_4$) over one CV was applied to the column followed by a gradient from 4-12% buffer B (32-96 mM $(NH_4)_2SO_4$) over 5 CV. The selected fractions containing c*h*TPH2 were collected and pooled. The collected fractions were then concentrated by ultrafiltration in an Amicon stirred pressure cell with an Ultracel PL-3 membrane. Approximately 7 mL of concentrated c*h*TPH2 solution was then filtered through a 0.45 µm filter and loaded onto a HiLoad Superdex 75 26/60 prep grade column. Prior to loading the column was equilibrated in 20 mM HEPES/NaOH, 100 mM $(NH_4)_2SO_4$, 5%(w/v) glycerol, pH 7.2. Fractions containing c*h*TPH2 were collected. The c*h*TPH2 concentration was determined using the theoretical absorption coefficient [245] of $\varepsilon_{280} = 39310\ M^{-1}\ cm^{-1}$.
Samples for enzyme kinetic experiments were stored in aliquots of 500 µL at -80˚C. c*h*TPH2 for crystallisation experiments was concentrated by ultrafiltration in an Amicon stirred pressure cell and subsequently stored at -80˚C in aliquots of 100 µL.

4.1.2.3 Purification of ct*h*TPH2

Cells containing ct*h*TPH2 (see section 4.1.1.3) from 3 × 650 mL culture were resuspended in 3 × 40 mL 20 mM Tris/HCl, 10% (w/v) glycerol, pH 8.2. Sodium dithionite was added to a final concentration of 2 mM. The cells were lysed on ice by sonication for 3 × 30 s using a Satorius Labsonic P at 80% amplitude. The cell extract was centrifuged at 4˚C and 18000 × g for 20 min. The supernatant was collected and filtered through 0.45 µm GHP Acrodisc GF syringe filters. The supernatant was loaded onto a Q Sepharose High Performance 26/10 column, which was equilibrated in buffer

A: 20 mM Tris/HCl, 10%(w/v) glycerol, pH 8.2, 2 mM sodium dithionite. Prior to equilibration, buffer A and buffer B: 20 mM Tris/NaOH, 0.8 M $(NH_4)_2SO_4$, 10%(w/v) glycerol, pH 8.2 was flushed with argon for one hour per L buffer. The column was washed with 1.5 CV of 97% buffer A and 3 % buffer B. A linear gradient from 3-10% buffer B (24-80 mM $(NH_4)_2SO_4$) was applied over 0.8 CV followed by a linear gradient from 10-24% buffer B (80 - 190 mM $(NH_4)_2SO_4$) over 5 CV. The selected fractions containing ct*h*TPH2 were collected and pooled. The collected fractions were then concentrated by ultrafiltration in an Amicon stirred pressure cell with an Ultracel PL-3 membrane. Approximately 7 mL of concentrated ct*h*TPH2 solution was then filtered through a 0.45 µm filter and loaded onto HiLoad Superdex 200 26/60 prep grade column. Prior to loading the column was equilibrated in 20 mM Tris/NaOH, 200 mM $(NH_4)_2SO_4$, 10%(w/v) glycerol, pH 8.2. Fractions containing ct*h*TPH2 were collected. The ct*h*TPH2 concentration was determined using the theoretical absorption coefficient [245] of $\varepsilon_{280} = 40800\ M^{-1}\ cm^{-1}$.
Samples for enzyme kinetic experiments were stored in aliquots of 500 µL at -80˚C. ct*h*TPH2 for crystallisation experiments was concentrated by ultrafiltration in an Amicon stirred pressure cell and subsequently stored at -80˚C in aliquots of 100 µL.

4.1.3 Activity measurements

The purification was followed by TPH activity measurements of samples from the supernatant and collected fractions from the anion exchange and the gel filtration. Each sample of 200 µL was mixed with 200 µL 60 mM HEPES/NaOH, 15 % w/v glycerol, 300 mM $(NH_4)_2SO_4$, 4 mM DTT, 0.1 g/L catalase, 1.25 mM tryptophan, pH 7.0. The mixture was stored in eppendorf tubes and closed under an argon flow. The activity measurements were done as described in sections 6.1-6.3, using 70 µM tryptophan, 300 µM BH_4 and 500 µM O_2. The activity measurements were done directly after the purification.

4.1.4 SDS-PAGE and Western blot analysis

SDS-PAGE was done using 12% Tris-HCl gels as described in section 3.4.3. Western blot analysis was done using PVDF membranes and chemicals (Immun-blot kit 170-6461) from Bio-Rad. The primary antibody was the murine monoclonal PH8 antibody against TPH, TH and PAH, from Chemicon, Victoria, Australia. 50 µL PH8 antibody was added to 5 mL 20 mM Tris, 500 mM NaCl, 0.05% (v/v) Tween-20, 1% (w/v) gelatine, pH 7.5. The secondary antibody was the goat anti-mouse alkaline phophatase (GAM-AP). 3.3 µL GAM-AP were added to 10 mL 20 mM Tris, 500 mM NaCl, 0.05%(v/v) Tween-20, 1%(w/v) gelatine, pH 7.5. Treatment of the membrane and colour development were done as described in the instructions manual for the Immun-blot kit [246].

4.2 Results and discussion of expression and purification of TPH variants

4.2.1 Expression and purification of c*g*TPH1

c*g*TPH1 was expressed in large amounts (see figure 4.1A, lane 2) as a soluble and active enzyme. The expression of c*g*TPH1 was verified by SDS-PAGE and Western blot analysis shown in figure 4.1.

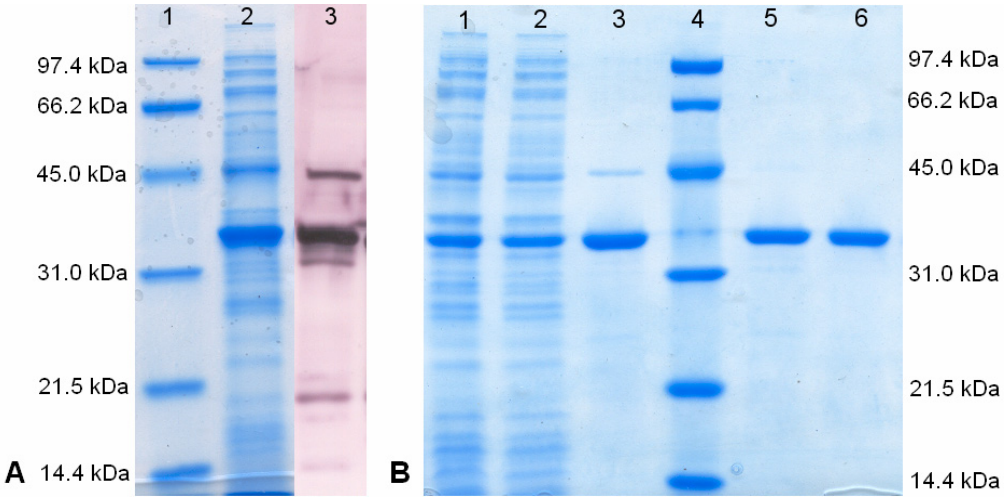

Figure 4.1 **(A)** SDS-PAGE and Western blot of c*g*TPH1. Lane 1 is the marker. Lane 2 is supernatant from cells containing c*g*TPH1 expressed at 30˚C. Lane 3 is Western blot of same sample as in lane 2. **(B)** SDS-PAGE from purification of c*g*TPH1 expressed at 20˚C. Lane 1 is 2 µL raw extract from the cells. Lane 2 is the supernatant. Lane 3 is collected fractions from anion exchange (see figure 4.2). Lane 4 is the molecular weight standard. Lane 5 is fractions C6-C8 from gel filtration (see figure 4.3). Lane 6 is fractions C9-C12 from the gel filtration.

The c*g*TPH1 is expressed as a fusion protein with ubiquitin. A small amount of the uncleaved fusion protein is present in the cells upon harvesting. The amount of ubiquitin-c*g*TPH1 was larger at 30˚C expression for 4 hours than at 20˚C expression for 14 hours and the latter was therefore chosen [15]. The presence of ubiquitin-cTPH1 from a 30˚C expression is shown in figure 4.1A by SDS-PAGE and Western blot. c*g*TPH1 could be purified without ubiquitin-c*g*TPH1 contamination. In addition to ubiquitin-c*g*TPH1 (44.6 kDa) and c*g*TPH1 (36.1 kDa) some c*g*TPH1 degradation products are also visible in the Western blot (figure 4.1A lane 3). Results presented later indicate that these degradation products do not seem to be a problem in the further purification.

A chromatogram for the anion exchange of c*g*TPH1 is shown in figure 4.2. The c*g*TPH1 eluted at 7 mS/cm and fractions C7-D3 were collected. Two other major peaks are seen in the chromatogram eluting at 5 and at 10 mS/cm respectively. These two peaks also contain minor amounts of c*g*TPH1 [15]. The c*g*TPH1 eluted in these fractions must have a different charge to surface ratios compared to the one eluting at 7 mS/cm. Experiments testing the effect of reducing conditions (dithionite and argon flushed buffers) and the effect of ethylenediamine tetraacetate (EDTA) showed that the reducing conditions lead to more c*g*TPH1 eluting at 7 mS/cm, compared to non-reducing conditions. Adding EDTA gave more c*g*TPH1 eluting at 10 mS/cm [15]. Therefore different charges are ascribed to the presence of iron or the oxidation state of the iron. The c*g*TPH1 eluting at 5 mS/cm is assigned to contain Fe^{3+}, c*g*TPH1 eluting at 7 mS/cm is assigned to contain Fe^{2+} and c*g*TPH1 eluting at 10 mS/cm is assigned to be the apoenzyme.

A chromatogram for the gel filtration of c*g*TPH1 is shown in figure 4.3. By omitting the first fractions in the c*g*TPH1 peak at 150 mL from the gel filtration, the ubiqutin-c*g*TPH1 impurity can be avoided in the final sample (data not shown). Fractions C6-C12 were collected from the gel filtration. Judging by the SDS-PAGE in figure 4.1B (lane 5 and 6) the purity of the c*g*TPH1 in fractions from the gel filtration is high and

suitable for crystallisation experiments. The c*g*TPH1 purification followed by activity measurements is summarised in table 4.1.

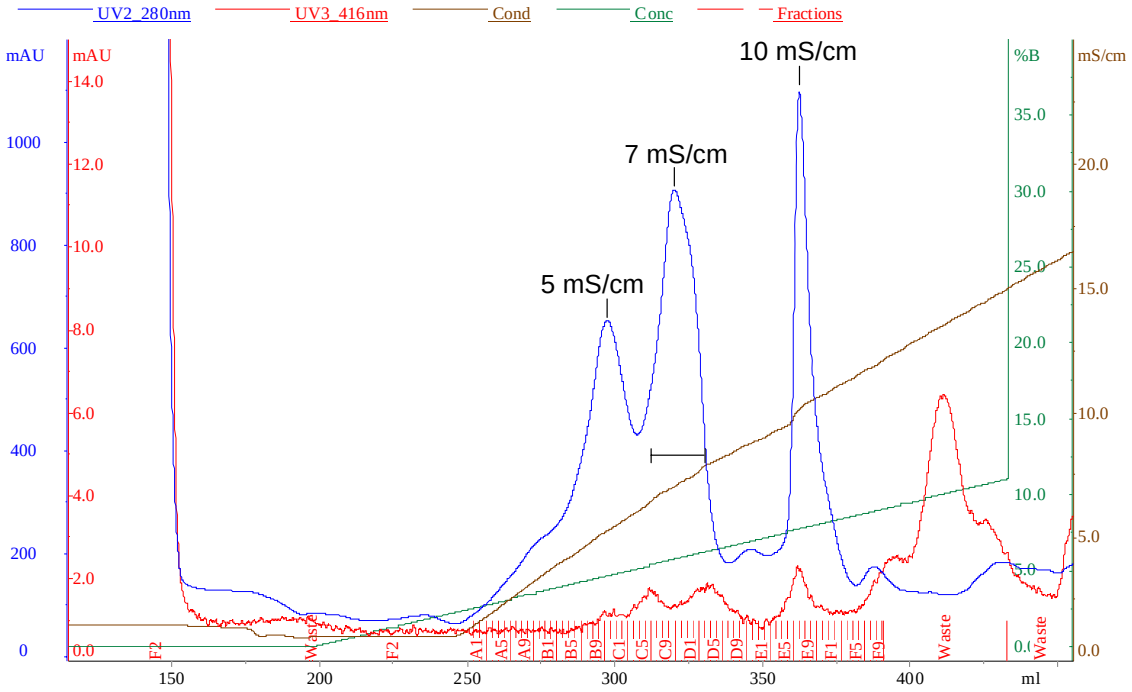

Figure 4.2 Anion exchange chromatogram of c*g*TPH1 on a Q Sepharose HP 26/10 column. Buffers were A: 20 mM Tris/HCl pH 8.5, 2 mM sodium dithionite, B: 20 mM Tris/NaOH, 0.8 M $(NH_4)_2SO_4$, pH 8.5. Fractions C7-D3 were collected.

The cTPH1 from rabbit is reported to be unstable at low ionic strength [87]. This is also the case for c*g*TPH1, but c*g*TPH1 is stable in cell lysate prior to the anion exchange. If c*g*TPH1 solution collected from the gel filtration is diluted to 1 mS/cm as in the initial cell lysate, significant amount of c*g*TPH1 is lost. Therefore a high resolution anion exchange following the gel filtration is not possible. This is compensated for by using a medium resolution anion exchange (Sepharose HP) in the first purification step. Thereby high purity is achieved without a third purification step.
The c*g*TPH1 for crystallisation experiments was concentrated to 12-15 mg/mL and above this concentration a tendency for precipitation is observed.
The yield of c*g*TPH1 per L culture is 10.9 mg, with a specific activity of 0.60 µM 5-hydroxytryptophan per min per mg c*g*TPH1. These values are similar to those reported on rabbit cTPH1 [87]. The published procedure for purification of rabbit cTPH1 consists of four steps. The first step is an anion exchange on a Q Sepharose column at pH 8. This is followed by $(NH_4)_2SO_4$ fractionation. The rabbit cTPH1 was then redissolved in a MES buffer pH 7 and loaded onto a hydroxyapatite column and eluted with 150-200 mM phosphate [87]. The rabbit cTPH1 was then again precipitated with $(NH_4)_2SO_4$ and redissolved in the final buffer 50 mM MES, 200 mM $(NH_4)_2SO_4$, 10% glycerol, 2 mM DTT, pH 7.0. The purification of c*g*TPH1 consists of only 3 steps (anion exchange, ultrafiltration and gel filtration) and is therefore more simple and faster than the purification of rabbit cTPH1.

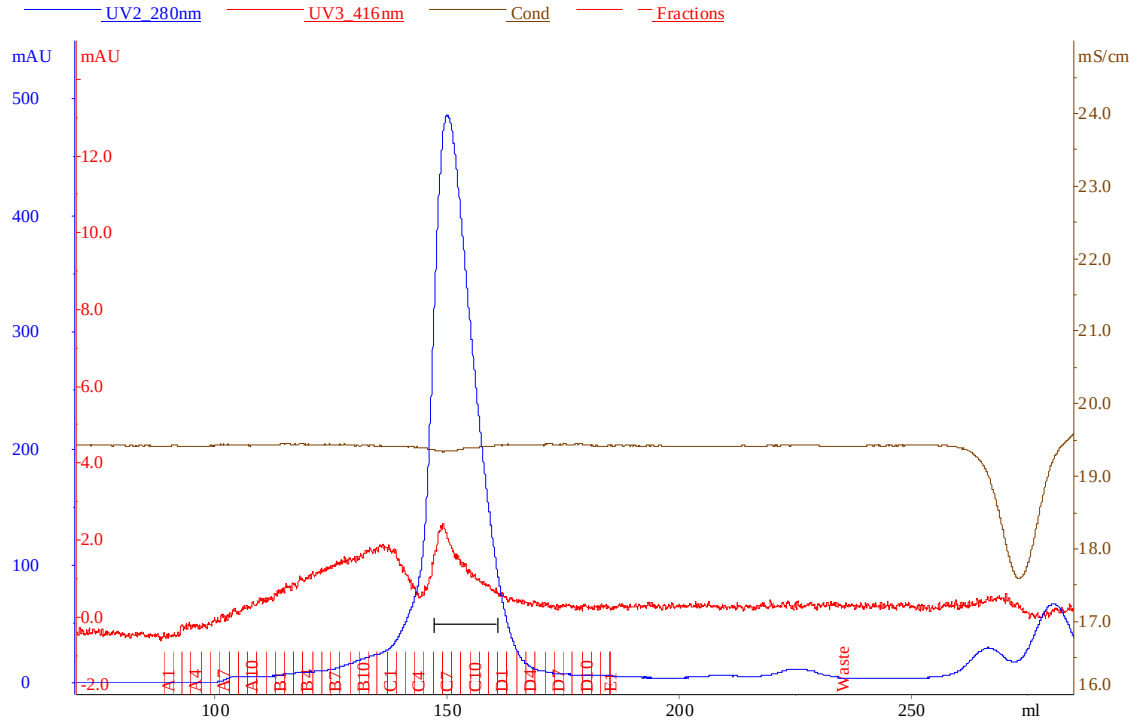

Figure 4.3 Gel filtration chromatogram of c*g*TPH1 on a Superdex 75 26/60 column. The buffer used was 20 mM Tris/NaOH, 100 mM $(NH_4)_2SO_4$, pH 8.5. Fractions C6-C12 were collected.

Table 4.1 c*g*TPH1 activity measured on samples from the different purification steps, purified from cells from 1.95 L culture. Measurements were done as described in section 4.1.3.

Purification step	Units* of enzyme	Yield (%)	c*g*TPH1 (mg)**	Specific activity (Units/mg)
Supernatant	63.4	100		
From anion exchange	24.8	39.1		
From gel filtration	12.8	20.2	21.4	0.60

* One unit is defined as the amount of enzyme that produces 1 µmole product/min.
** Determined using ε_{280} = 37820 M^{-1} cm^{-1}.

As seen in table 4.1 approximately 50% of the enzyme units are lost during ultrafiltration and gel filtration. This may either be caused by a loss of c*g*TPH1 or by a decrease in the specific activity. This loss is larger than the ones observed for c*h*TPH2 and ct*h*TPH2 (tables 4.2 and 4.3). Small aggregates of c*g*TPH1 could form during the ultrafiltration and be caught in the subsequent filtration. Since no visible aggregation was observed in the solution from the ultrafiltration, the observed loss of enzyme units is more likely to be caused by a decrease in the specific activity. In either case this indicates that c*g*TPH1 is not as stabilised in its buffer solution as c*h*TPH2 and ct*h*TPH2 are in their respective buffer solutions. Addition of different concentrated buffer solutions to the collected fractions from the anion exchange should be tried. The gel filtration should subsequently be done in the new equivalent buffer solution. I would start by trying a gel filtration buffer of 20 mM HEPES, 200 mM $(NH_4)_2SO_4$, 10%(w/v) glycerol, pH 7-7.5.

4.2.2 Expression and purification of *ch*TPH2

The expression of *ch*TPH2 is verified by SDS-PAGE shown in figure 4.4. By comparing the intensities of the *ch*TPH2 band in the raw extract and the supernatant in figure 4.4 (lane 1 and 2) approximately 90% of the *ch*TPH2 is in the soluble fraction. If one compares the intensities of the raw extract of *cg*TPH1 expressing cells (figure 4.1B lane 1) to the intensities of the raw extract *ch*TPH2 expressing cells (figure 4.4 lane 1), it is clear that the expression of *ch*TPH2 is significantly stronger than that of *cg*TPH1. A reason for this could be that the gene sequence for *ch*TPH2 is codon optimised for *E.coli* expression while the *cg*TPH1 is the gene sequence isolated from chicken. It could also be caused by increased mRNA stability for the *ch*TPH2 sequence. In the anion exchange in figure 4.5 *ch*TPH2 elutes at 9.5 mS/cm and fractions C4-C12 were collected for further purification. This is the only major peak in the chromatogram, while three peaks are seen in the *cg*TPH1 ion exchange chromatogram (figure 4.2). This is probably due to the change in pH causing fewer proteins bind to anion exchange media at pH 7.2 than at pH 8.5. A chromatogram for the gel filtration of *ch*TPH2 is shown in figure 4.6., in which *ch*TPH2 eluted at approximately 137 mL and fractions B7-C1 were collected. The *ch*TPH2 purification followed by enzyme activity measurements is summarised in table 4.2.
The *ch*TPH2 purification was originally done at pH 8.2, but the purified *ch*TPH2 was not stable in the final solution. Different additives and buffers with different pH were tested on purified *ch*TPH2. Buffers with pH 7.2 and pH 6.5 were found to improve the stability of *ch*TPH2 significantly. Purification at pH 7.2 was subsequently tested and proved to be successful.
The *ch*TPH2 for crystallisation is concentrated to 20-32 mg/mL by ultrafiltration without any signs of precipitation.

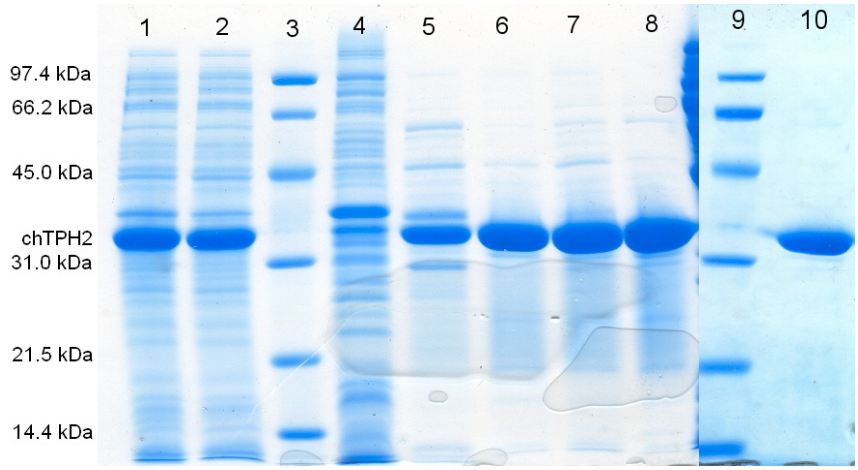

Figure 4.4 SDS-PAGE from *ch*TPH2 purification. Lane 1 is 2 µL raw extract. Lane 2 is 2 µL supernatant of raw extract. Lane 3 is the molecular weight standard. Lane 4 is 20 µL flow-through from the anion exchange column. Lane 5 is 2 µL of fraction C4 from the anion exchange chromatogram. Lane 6 is fraction C9. Lane 7 is 2 µL of pooled fractions C4-C12 from the anion exchange. Lane 8 is 2 µL from fractions B7-C1 from the gel filtration. Lane 9 is the molecular weight standard. Lane 10 is purified *ch*TPH2 from another purification batch and this *ch*TPH2 was used for crystallisation experiments.

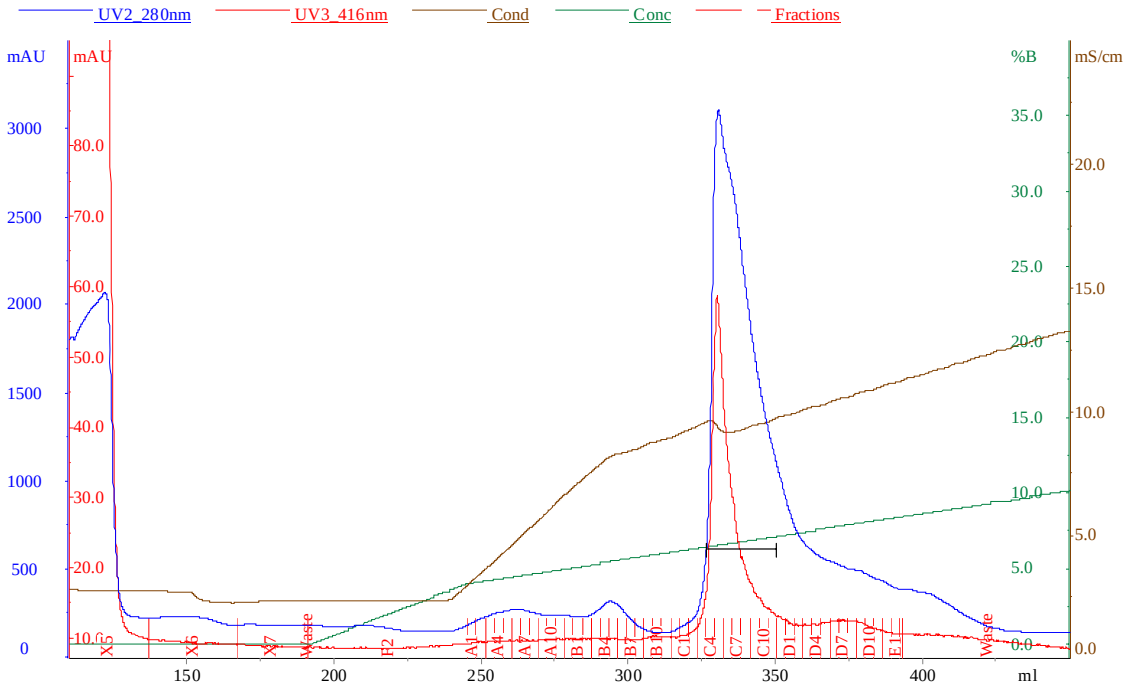

Figure 4.5 Anion exchange chromatogram of *ch*TPH2 on a Q Sepharose HP 26/10 column. Buffers were A: 20 mM Bis Tris Propane/HCl, 5% glycerol, pH 7.2, 2 mM sodium dithionite, B: 20 mM Bis Tris Propane/HCl, 5% glycerol, 0.8 M $(NH_4)_2SO_4$, pH 7.2. Fractions C4-C12 were collected.

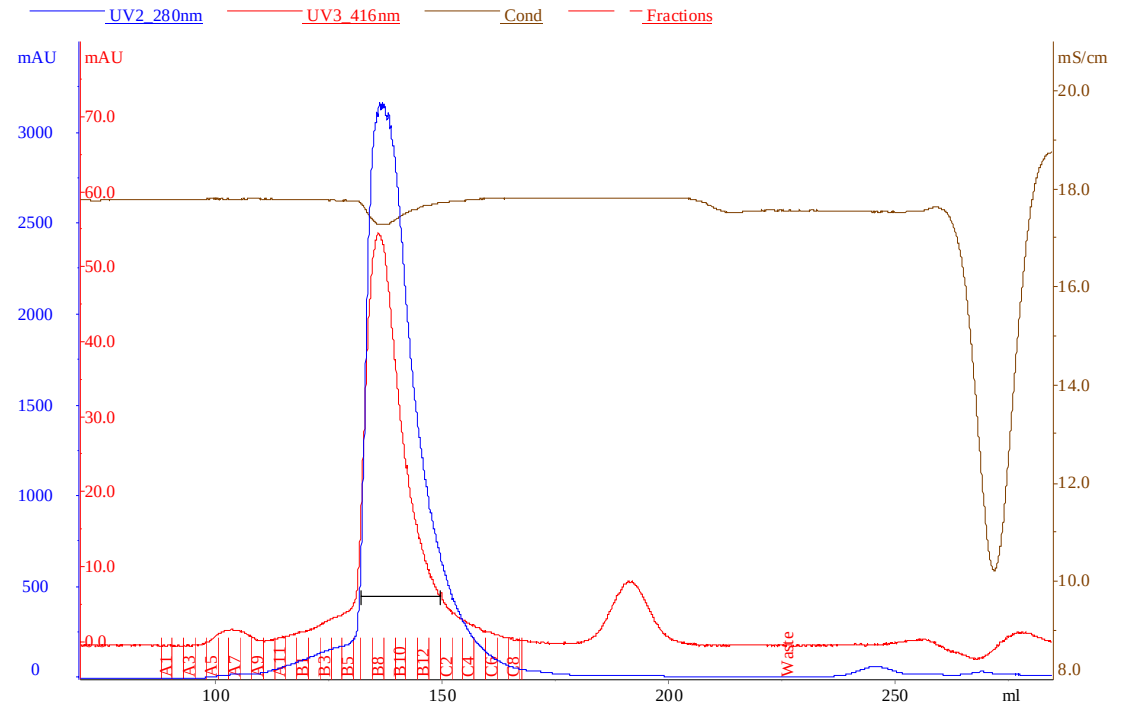

Figure 4.6 Gel filtration chromatogram of *ch*TPH2 on a Superdex 75 26/60 prep grade column. The buffer used was 20 mM HEPES/NaOH, 5% glycerol, 100 mM $(NH_4)_2SO_4$, pH 7.2. Fractions B7-C1 were collected.

Table 4.2 c*h*TPH2 activity measured on samples from the different purification steps, purified from cells from 1.95 L culture. The activity measurements were done as describe in section 4.1.3.

Step	Units* of enzyme	Yield (%)	c*h*TPH2 (mg)**	Specific activity (units/mg enzyme)
Supernatant	2235	100	-	-
From anion exchange	1168	52	-	-
From gel filtration	796	36	135	5.90

* One unit is defined as the amount of enzyme that produces 1 µmole product/min.
** Determined using ε_{280} = 39310 M^{-1} cm^{-1}.

The strong expression of c*h*TPH2 combined with a good purification yield (36%) give 69 mg purified protein per L culture. This makes it possible to produce large amounts of enzyme for crystallographic and comprehensive enzymatic characterisation. Judged from the SDS-PAGE (figure 4.4 lane 8 and 10) the purity of c*h*TPH2 is higher and suitable for crystallisation experiments. The purity can be optimised by collecting fractions in a narrower interval of the anion exchange.
The specific activity for c*h*TPH2 of 5.90 µmole 5-hydroxytryptophan/min/mg is almost a factor 10 higher than that of 0.60 µmole/min/mg for c*g*TPH1 and rabbit cTPH1 [87]. A specific activity of 5 µmole/min/mg is reported on TPH1 purified from mouse mastocytoma P815 cells by Hasegawa and Ichiyama [158], and 5.28 µmole/min/mg is reported by Nakata and Fujisawa also on TPH1 from mouse mastocytoma P815 [36]. There is only one report on expression of the c*h*TPH2 (residues 151-466) and they do not report the specific activity. Instead the $V_{max,tryptophan}$ of 0.242±0.0219 µmol/min/mg is given [22], which is even lower than the specific activity for c*g*TPH1 in this study.

4.2.3 Expression and Purification of ct*h*TPH2

Expression of ct*h*TPH2 was done at 20˚C for 14 hours to get high amounts of soluble ct*h*TPH2. Judging from the intensities of the c*h*TPH2 and ct*h*TPH2 SDS-PAGE bands for raw extract in figure 4.4 lane 1 and figure 4.7 lane 1, respectively, the expression level of these two variants is approximately the same.
A chromatogram for the anion exchange of ct*h*TPH2 is shown in figure 4.8. ct*h*TPH2 elutes at 18 mS/cm and fractions E5-F5 were collected. A chromatogram for the gel filtration of ct*h*TPH2 is shown in figure 4.9. ct*h*TPH2 elutes at 172 mL and fractions C3-C8 were collected. According to the column specifications this elution volume is approximately equal to a protein size of 150 kDa which indicates that ct*h*TPH2 elutes as a tetramer. This is in accordance with the report by Carkaci-Salli *et al.* on ct*h*TPH2 (residues 151-490) [22]. The ct*h*TPH2 purification is followed by SDS-PAGE in figure 4.7 and by enzyme activity measurements summarised in table 4.3.
The ct*h*TPH2 for enzyme kinetics measurements was stored at -80˚C in aliquots of 500 µL. The ct*h*TPH2 for crystallisation was concentrated by ultrafiltration to 39-44 mg/mL with no sign of precipitation, and was stored at -80˚C in aliquots of 100 µL.
The UV-Vis spectrum of 12 µM and 270 µM ct*h*TPH2 in 20 mM Tris/NaOH, 200 mM $(NH_4)_2SO_4$, 10% glycerol, pH 8.2 is shown in figure 4.10. The UV-Vis spectrum of concentrated ct*h*TPH2 shows a broad shoulder from the ordinary 280 nm absorption toward 450 nm. This yellowish colour is also seen in concentrated solution of c*h*TPH2,

but not in c*g*TPH1. This difference between the *h*TPH2s and c*g*TPH1 is also visible by inspecting the 416 nm absorption in the chromatograms. The reason for this colour difference has not been identified. Iron is believed to be bound in the active site of all three variants. The colour may be due to subtle changes in the active site structure or binding of a coloured compound somewhere in the c*h*TPH2/ct*h*TPH2 structures.

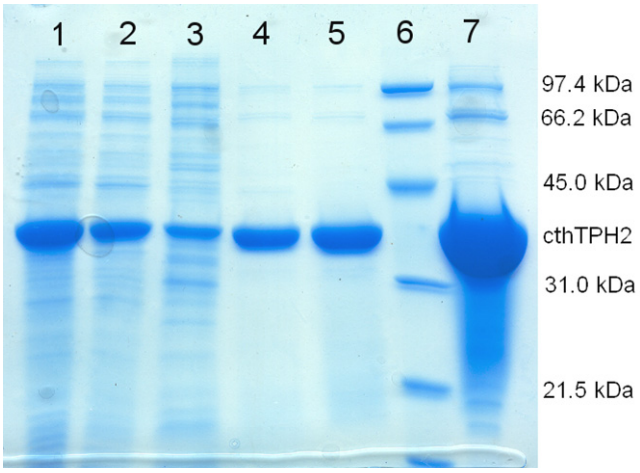

Figure 4.7 SDS-PAGE of samples from the purification of ct*h*TPH2. Lane 1 is 2 µL raw extract from the cells. Lane 2 is 2 µL unfiltered supernatant of the raw extract. Lane 3 is 20 µL flow-through when the supernatant was applied to the column. Lane 4 is 2 µL of fractions E5-F5 from the anion exchange. Lane 5 is 2 µL from fractions C3-C8 of the gel filtration. Lane 6 is the molecular weight standard. Lane 7 is 2 µL from the concentrated sample for crystallisation.

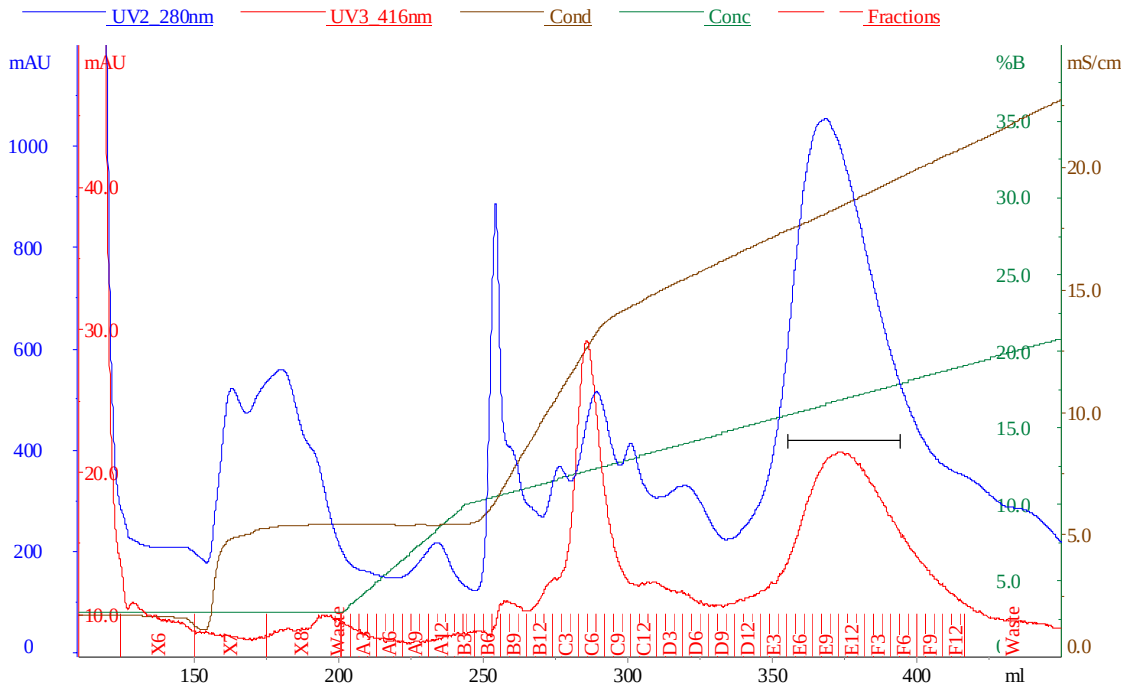

Figure 4.8 Anion exchange chromatogram of ct*h*TPH2 on a Q sepharose HP 26/10 column. Buffers used were A: 20 mM Tris/HCl, 10 % (w/v) glycerol, pH 8.2, 2 mM sodium dithionite, B: 20 mM Tris/NaOH, 0.8 M $(NH_4)_2SO_4$, 10% glycerol, pH 8.2. Fractions E5-F5 were collected.

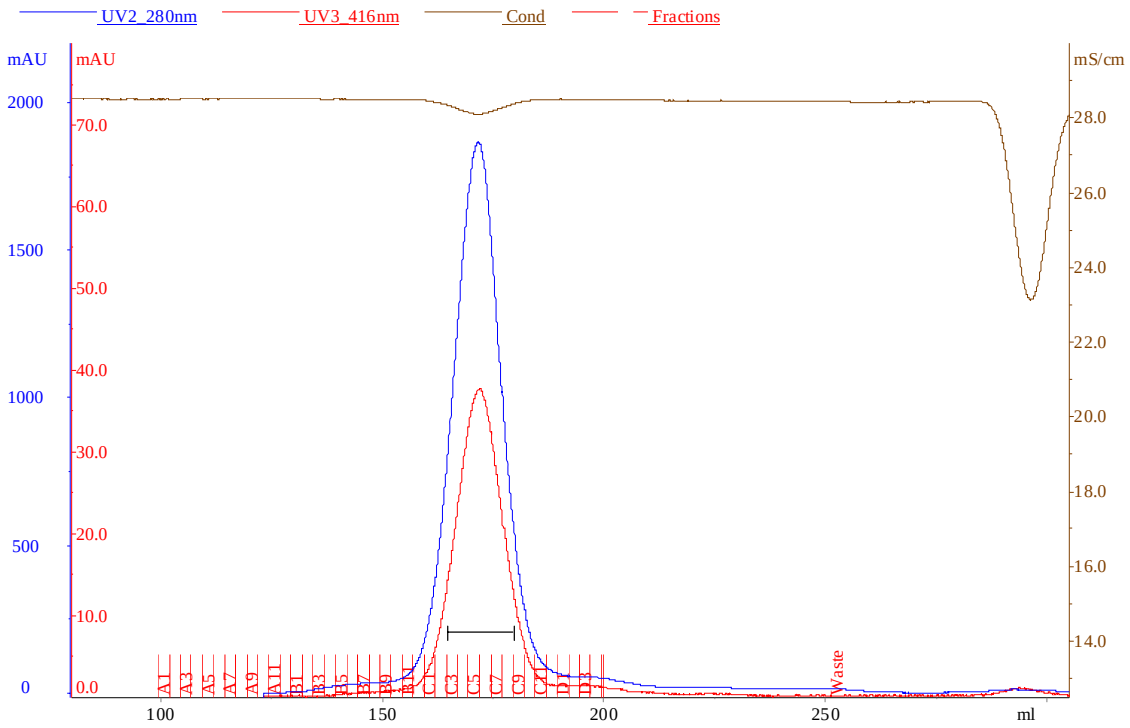

Figure 4.9 Gel filtration chromatogram of ct*h*TPH2 on a Superdex 200 26/60 column. The buffer was 20 mM Tris/NaOH, 10 % (w/v) glycerol, 200 mM $(NH_4)_2SO_4$, pH 8.2. Fractions C3-C8 were collected.

Table 4.3 ct*h*TPH2 activity measured on samples from the different purification steps, purified from cells from 1.95 L culture. Measurements were done as described in section 4.1.3.

Sample	Units* of enzyme	Yield (%)	ct*h*TPH2 (mg)**	Specific activity (units/mg enzyme)
Supernatant	1115	100		
From anion exchange	404	36		
From gel filtration	256	23	74.7	3.42

* One unit is defined as the amount of enzyme that produces 1 µmole product/min.
** Determined using ε_{280} = 40800 M^{-1} cm^{-1}.

As seen in the SDS-PAGE in figure 4.11A, a few impurities are visible when a very large quantity of ct*h*TPH2 was loaded on the gels. The Western blot in figure 4.11B shows that some of the high molecular weight impurities are TPH, probably oligomers of ct*h*TPH2, which were not separated properly into monomers by SDS. Minor amounts of degradation products are also seen in the western blot. The ct*h*TPH2 protein sample is still believed to be pure enough for crystallisation trials.
The specific activity of ct*h*TPH2 is 3.42 µmole/min/mg which is a bit lower than the 5.90 µmole/min/mg for c*h*TPH2. Still this is much higher than the $V_{max,BH4}$ of 0.1236±0.0223 µmol/min/mg reported by Carkaci-Salli *et al.* for ct*h*TPH2 (residues 151-490) [22].
Judging from the raw extracts the amount of expressed ct*h*TPH2 (see figure 4.7 lane 1) is similar to that of c*h*TPH2 (see figure 4.4 lane 1), but the amount of soluble TPH is different (lane 2, respectively). Almost no change is observed in the intensity of

*ch*TPH2 between raw extract and supernatant, while there is an obvious decrease from ct*h*TPH2 raw extract to supernatant. It is also seen that some ct*h*TPH2 is found in the flow-through from the column. This is also reflected in the yield after the anion exchange where 52% is obtained for *ch*TPH2 (see table 4.2) while only 36% for ct*h*TPH2 (see table 4.3). The reason for some of the ct*h*TPH2 not to bind to the column is likely to be caused by incorrectly folded ct*h*TPH2, which form aggregates that can be filtered through 0.45 µm filter. These aggregates do not bind to the column caused either by having no charge or by being larger than the exclusion limit of the column. The recovery of ct*h*TPH2 is lower than that of *ch*TPH2, but the 38 mg of purified ct*h*TPH2 per L culture is still better than that obtained in the c*g*TPH1 purification.

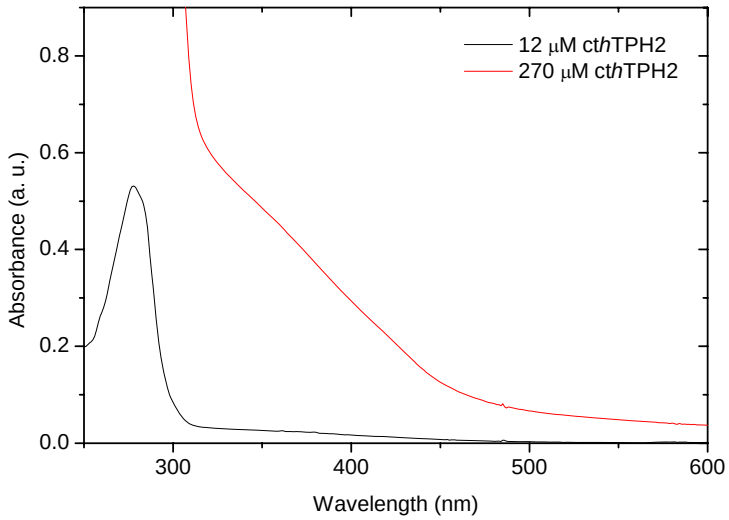

Figure 4.10 The UV-Vis spectrum of 12 µM (black) and 270 µM (red) ct*h*TPH2 in 20 mM Tris/NaOH, 200 mM $(NH_4)_2SO_4$, 10% glycerol, pH 8.2.

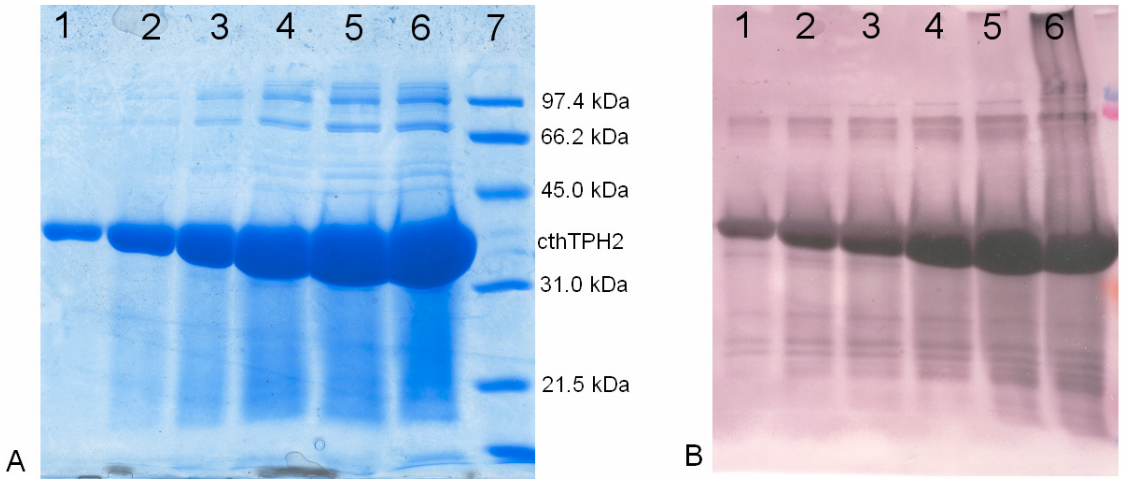

Figure 4.11 **(A)** SDS-PAGE and **(B)** Western blot of same samples of purified ct*h*TPH2. The loaded amount of purified ct*h*TPH2 in µg is as follows, lane 1-6: 4.2, 12.5, 20.9, 41.7, 62.6, 83.4. Lane 7 is the molecular weight standard.

Prior to the anion exchange purification the supernatant was filtered through 0.45 µm syringe filters. The volume that could be filtered before the filter was clogged was quite

low and 12 filters were needed for 120 mL supernatant. Protein aggregates that could not be precipitated by centrifugation are probably caught in the filters. The SDS-PAGE in figure 4.7 lane 3 shows that ct*h*TPH2 is present in the flow-through from the column when the supernatant was loaded onto the column. This indicates that some of the ct*h*TPH2 is in the partly soluble form discussed in section 3.4.2 and 3.5.1. When c*g*TPH1 and c*h*TPH2 supernatants were filtered less than half the number of filters were used compared to filtration of ct*h*TPH2. This also suggests that a higher portion of ct*h*TPH2 is in an aggregated form, than in the case of c*g*TPH1 and c*h*TPH2. When comparing the intensity of ct*h*TPH2 band for raw extract and supernatant in figure 4.7 it is also visible that a portion of ct*h*TPH2 is not in a soluble form.
During the optimisation of the c*h*TPH2 purification it was observed that the supernatant produced at pH 8.2 also clogged the filters very quickly, but changing the pH to 7.2 significantly reduced the clogging of filters. This suggests that c*h*TPH2 had a tendency to aggregate at pH 8.2 but not at pH 7.2. This might also be the case for ct*h*TPH2. An anion exchange of ct*h*TPH2 at pH 7.2 should be possible since ct*h*TPH2 elutes at relatively high conductivity (18 mS/cm) at pH 8.2. It is unlikely that dramatic changes in ct*h*TPH2 would be observed by this pH change and I would suggest the change in pH to be tested in future purifications of ct*h*TPH2.

4.3 Conclusion

Three variants of TPH: c*g*TPH1, c*h*TPH2 and ct*h*TPH2 have been expressed and purified to homogeneity. c*g*TPH1 gave a yield of 10.9 mg/L, while c*h*TPH2 and ct*h*TPH2 gave 69 mg/L and 38 mg/L, respectively. All three proteins seemed stable in the respective solutions. The specific activities of all three enzymes were high compared to other published results, especially the specific activity of 5.90 µmole/min/mg for c*h*TPH2.

CHAPTER FIVE

5 Enzyme kinetics

Enzyme kinetics deal with the factors affecting the rate of the enzyme-catalysed reaction. From studying the enzyme kinetics of an enzyme it is possible to deduce the kinetic mechanism of the enzyme. The kinetic mechanism is the order of which substrates add to the enzyme and products leave the enzyme [247]. Knowing the kinetic mechanism of an enzyme is useful in studying the molecular reaction mechanism, *i.e.* which chemical steps are involved in the enzymatic reaction [248]. The kinetic parameters (K_m, K_i and V_{max}) obtained through enzyme kinetics give information on the likely substrate concentrations *in vivo* and the possibility to differentiate isoenzymes from different tissues of the same organism [247]. In this chapter selected aspects of enzyme kinetics will be presented, which will be useful when proceeding to the following chapters dealing with enzyme kinetics of TPH.

5.1 Definitions and nomenclature for enzyme catalysed reactions

Various expressions and definitions are used to describe the reactions catalysed by enzymes. The nomenclature of Cleland [249] will be used in this and the following chapters.

Substrates will be designated A, B, and C. Products will be designated P, Q and R. The enzyme forms will be designated E, F, and G, where E is the least complex or free form of the enzyme. The number of substrates and products are described by the use of syllables uni, bi, ter and quad. A reaction like that of TPH with three substrates and two products is therefore described as a ter bi reaction [249].

The kinetic mechanism can be described in various terms. Two or more substrates can add to the enzyme in various ways. If all the binding and dissociation steps of the substrates are much faster than the catalytic reaction, then all forms of the enzyme are in a rapid equilibrium and the reaction is said to follow a rapid equilibrium mechanism. If the catalytic reaction is not the rate limiting step, all forms of the enzyme reaches a steady-state concentration shortly after the mixing of enzyme and substrates. This is then called a steady-state reaction. A steady-state reaction can follow either a sequential mechanism or a ping pong mechanism [250]. In a sequential mechanism all substrates must add before a reaction happens and products are released. A sequential reaction can further be classified as ordered if the substrates add to the enzyme in an obligatory order and random if the substrates bind in a random order. In the ping pong mechanism one or more products leave the enzyme before all substrates have added to the enzyme [249].

5.2 Determining K_m and V_{max} for terreactant enzymes

In multi-substrate enzymes the true V_{max} is the maximum reaction rate of the enzyme when saturated with all substrates. The true K_m is the substrate concentration at the true $V_{max}/2$. In practise it might not be possible to saturate the enzyme ([S]>100 K_m) with all substrates and often apparent K_m and apparent V_{max} values are determined instead, using more accessible substrate concentrations. Usually the apparent K_m and V_{max} values are quite dependent on the concentration of the fixed substrates, which makes it difficult to compare different published K_m and V_{max} values determined at different concentrations of the fixed substrates [251].
The determination of K_m and V_{max} is done most accurately by fitting the Michaelis-Menten equation (equation 5.1) to the measured initial rates (V_i) using non-linear regression instead of using for example the linear double reciprocal (equation 5.2) Lineweaver-Burk plot [251]. The double reciprocal plot can be useful in the presentation of series of measurements or in detection of patterns for different mechanisms and inhibition types, but should not be used for determination of K_m and V_{max} because the data points will be weighted differently [251].

$$V_i = \frac{V_{max}[S]}{K_m + [S]} \tag{5.1}$$

$$\frac{1}{V_i} = \frac{K_m}{V_{max}} \cdot \frac{1}{[S]} + \frac{1}{V_{max}} \tag{5.2}$$

5.3 Substrate inhibition

At high concentrations substrates will often function as dead-end inhibitors. This inhibition does usually not occur at physiological concentrations of the substrates and therefore gives information on the upper limits of substrate concentrations *in vivo* [252]. Substrate inhibition is also a good diagnostic tool when studying the kinetic mechanism. Different types of substrates inhibition are usually observed for different kinetic mechanisms. Competitive substrate inhibition shown in scheme 5.1 is characteristic of a ping pong mechanism. In this mechanism the substrate B can combine with enzyme E to form a dead-end complex EB [252].

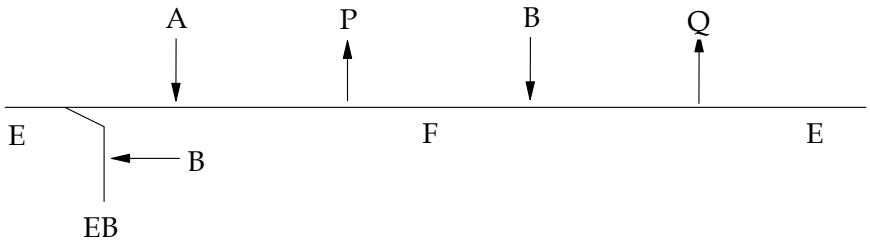

Scheme 5.1

For the ordered sequential mechanism, uncompetitive substrate inhibition is the expected inhibition type. For the uncompetitive inhibition the substrate B combines with the EQ complex to form a dead-end complex as shown in scheme 5.2.
When the inhibitory substrate resulting in a dead-end complex is varied at fixed concentrations of the other substrates equation 5.1 does no longer apply. Instead the extended form in equation 5.3 applies, where K_i is the inhibition constant for the inhibitory substrate and [S]=[B].

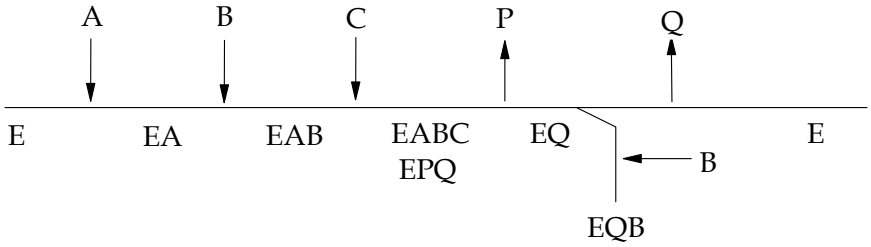

Scheme 5.2

$$V_i = \frac{V_{max}[S]}{K_m + [S] + \frac{[S]^2}{K_i}} \tag{5.3}$$

One can usually determine whether competitive or non-competitive substrate inhibition is observed from inspecting the effect of varying the concentration of a non-inhibitory substrate at different inhibitory levels of the inhibitory substrate [252].

5.4 Ter bi kinetic mechanisms

The reaction catalysed by TPH is a ter bi reaction. The possible ter bi mechanisms will be described and illustrated in schemes using the Cleland nomenclature [249] already seen in scheme 5.1-5.2.
The ordered mechanism with A, B and C added in this order, is illustrated in scheme 5.3.

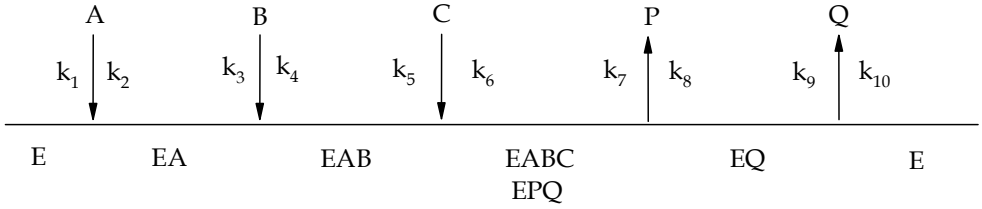

Scheme 5.3

The ordered addition of substrates in a steady-state fashion is called the ordered mechanism, while the ordered addition in an ordered equilibrium fashion is called rapid equilibrium ordered.
The bi uni uni uni ping pong ter bi mechanism is shown in scheme 5.4. In this mechanism substrates A and B bind to the enzyme, a reaction occurs and product P leaves. Substrate C then binds and reacts with the modified enzyme and Q is produced and released [256].

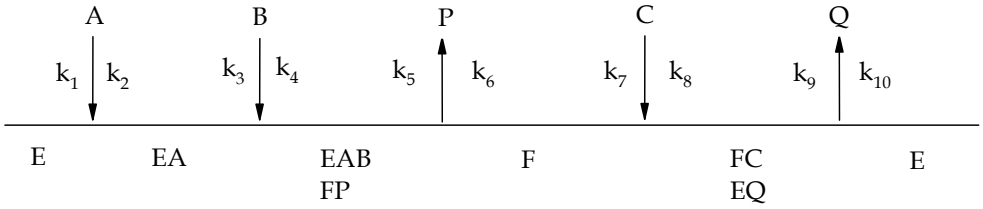

Scheme 5.4

Then there is a random A-B ordered C ter bi mechanism where A and B can add in any order in the rapid equilibrium or steady-state fashion. C then adds in the steady-state fashion.

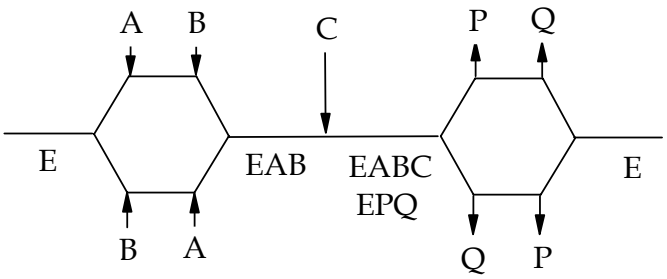

Scheme 5.5

In a similar way A can add in the steady-state followed by random addition of B and C in either steady-state or rapid equilibrium as shown in scheme 6.6. This is called the ordered A random B-C ter bi mechanism [256].

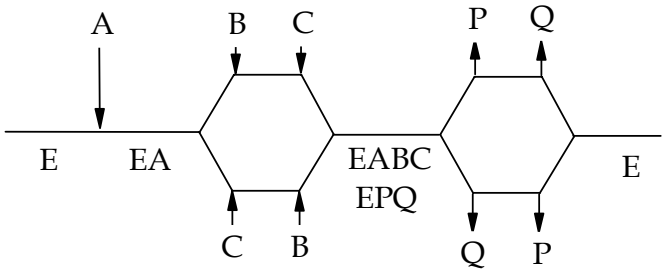

Scheme 5.6

Finally all three substrates can add randomly in rapid equilibrium as shown in scheme 5.7. This is called the rapid equilibrium random ter bi mechanism [257].

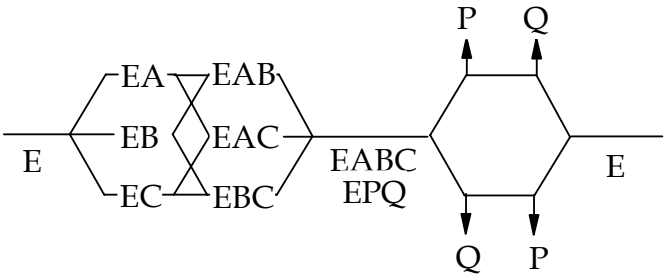

Scheme 5.7

The rate equations for these different kinetic mechanisms are presented in the following section.

5.4.1 The rate equations of ter bi reactions

Generally the rate equation for multisubstrate enzymes can be constructed using the method of King and Altman [253]. The general rate equation of a terreactant mechanism without the presence of products and assuming Michaelis-Menten kinetics is shown in equation 5.4 [250,254]. The rate equations of different mechanisms have different terms of the general rate equation present. The methods used to determine the kinetic mechanism (see section 5.5) will establish the presence or absence of different terms of the general rate equation [250]. The constant and coefficients (Coef) will consist of different mechanism dependent combinations of individual rate constants [255].

$$V_i = \frac{V_{max}[A][B][C]}{constant + Coef_A[A] + Coef_B[B] + Coef_C[C] + K_{m_C}[A][B] + K_{m_B}[A][C] + K_{m_A}[B][C] + [A][B][C]} \quad (5.4)$$

The rate equation (equation 5.4) can be expanded to contain product terms, but since the rate equations will only be used for initial rate studies on reactions in the forward direction, only the rate equations in the absence of products will be presented. The following rate equations for the different ter bi mechanisms are from Segel's book [256].

The rate equation for the ordered mechanism in scheme 5.3 is equation 5.5.

$$V_i = \frac{V_{max}[A][B][C]}{K_{ia}K_{ib}K_{m_C} + K_{ib}K_{m_C}[A] + K_{ia}K_{m_B}[C] + K_{m_C}[A][B] + K_{m_B}[A][C] + K_{m_A}[B][C] + [A][B][C]} \quad (5.5)$$

K_{ma}, K_{mb} and K_{mc} are the Michaelis constants for substrate A, B and C respecttively. K_{ia} and K_{ib} are the inhibition constant for substrates A and B respectively. In this case K_{ia} is also equal to the dissociation constant of substrate A, with $K_{ia} = k_2/k_1$, and likewise $K_{ib} = k_4/k_3$ and $K_{ic} = k_6/k_5$.

The rate equation for the rapid equilibrium ordered ter bi mechanism is equation 5.6.

$$V_i = \frac{V_{max}[A][B][C]}{K_{ia}K_{m_B}K_{m_C} + K_{ib}K_{m_C}[A] + K_{ia}K_{m_B}[C] + K_{m_C}[A][B] + K_{m_B}[A][C] + [A][B][C]} \quad (5.6)$$

The rate equation for the bi uni uni uni ping pong ter bi mechanism is equation 5.7.

$$V_i = \frac{V_{max}[A][B][C]}{K_{ia}K_{m_B}[C] + K_{m_C}[A][B] + K_{m_B}[A][C] + K_{m_A}[B][C] + [A][B][C]} \quad (5.7)$$

Random sequences in fully steady-state mechanism introduce squared concentration terms in the rate equation. Theoretically this should give non-linear double reciprocal plots. In the case of the random A-B ordered C and the ordered A random B-C mechanisms, linear plots are still expected even though the enzyme forms might not be at equilibrium [256]. The rate equation for the random A-B ordered C mechanism is equation 5.8, and the rate equation for the ordered A random B-C mechanism is equation 5.9.

$$V_i = \frac{V_{max}[A][B][C]}{K_{ia}K_{mb}K_{ic} + K_{m_B}K_{ic}[A] + K_{m_A}K_{ic}[B] + K_{ia}K_{m_B}[C] + K_{m_C}[A][B] + K_{m_B}[A][C] + K_{m_A}[B][C] + [A][B][C]} \quad (5.8)$$

$$V_i = \frac{V_{max}[A][B][C]}{K_{ia}K_{m_B}K_{ic} + K_{ic}K_{m_B}[A] + K_{m_C}[A][B] + K_{m_B}[A][C] + K_{m_A}[B][C] + [A][B][C]} \quad (5.9)$$

The rate equation for the rapid equilibrium random mechanism [257] is equation 5.10.

$$V_i = \frac{\frac{[A][B][C]}{\alpha\beta\gamma K_A K_B K_C}}{1 + \frac{[A]}{K_A} + \frac{[B]}{K_B} + \frac{[C]}{K_C} + \frac{[A][B]}{\gamma K_A K_B} + \frac{[A][C]}{\beta K_A K_C} + \frac{[B][C]}{\alpha K_B K_C} + \frac{[A][B][C]}{\alpha\beta\gamma K_A K_B K_C}} \quad (5.10)$$

The interaction factors α, β and γ are factors by which the dissociation constant of a given substrate changes when other substrates are bound [257].

5.5 Methods for investigating terreactant mechanisms

Several graphical methods have been developed for investigating the kinetic mechanisms of terreactant reactions. In the method by Dalziel the concentrations of all substrates are varied simultaneously [258]. This method demands a high degree of accuracy and might therefore be less attractive. In the method of Viola and Cleland one substrate is held at saturation (>100K_m) while the other two substrates are varied [255]. This method demands that the enzyme can be saturated with the three substrates, which might not always be possible because of substrate inhibition or limitations in the substrate solubility. High concentrations of substrates might also interfere with the sensitivity of the assay method used. In the method of Rudolph and Fromm the concentration of one substrate is varied at different fixed concentrations of the two others, maintaining a constant ratio between these two [259,260]. The concentration of each substrate is then varied, leading to three sets of experiments. The method of Rudolph and Fromm is chosen for the steady-state investigation of TPH, since it would be difficult to saturate with the different substrates and high accuracy might be difficult to obtain. The Rudolph and Fromm method will therefore be described in greater detail in the following section.

5.5.1 The method of Rudolph and Fromm

The graphical method of Rudolph and Fromm makes it possible to discriminate between different kinetic mechanisms. First of all the ping pong mechanism will give parallel lines in one or more of the double reciprocal plots of the initial rate data, while the sequential mechanism will exhibit intersecting lines in all reciprocal plots [260]. The point of intersection can either be on the y-axis or to the left of the y-axis [260]. The intercepts with the y-axis and the slopes of the lines in the double reciprocal plot can be plotted against the different reciprocal concentrations of one of the fixed substrates. The shapes of these replots depend upon the mechanism. The rate equation for the ordered mechanism (equation 5.5) is used as an example and is rewritten to the double reciprocal form when [C] is varied in equation 5.11.

$$\frac{1}{V_i} = \frac{K_{m_C}}{V_{max}}\left(1+\frac{K_{ia}K_{ib}}{[A][B]}+\frac{K_{ib}}{[B]}\right)\frac{1}{[C]}+\frac{1}{V_{max}}\left(1+\frac{K_{ia}K_{m_B}}{[A][B]}+\frac{K_{m_B}}{[B]}+\frac{K_{m_A}}{[A]}\right) \tag{5.11}$$

If the concentration of substrate C is varied at concentrations [A] = x[B] the slope in the double reciprocal plot will be given by equation 5.12.

$$\text{Slope}_{1/C} = \frac{K_{ib}K_{m_C}}{V_{max}}\left(1+\frac{K_{ia}}{x[B]}\right)\frac{1}{[B]}+\frac{K_{m_C}}{V_{max}} \tag{5.12}$$

In this case the concentration of the fixed substrates A or B will appear as a squared term giving a parabolic replot [256]. The shapes of the slope and intercept replots will allow differentiation between different kinetic mechanisms. The predicted shapes of the replots for the different mechanisms are listed in table 5.1 below.

5.5.2 Fitting rate equations to data

The graphical methods for investigating terreactant mechanisms were developed at a time where the access to computational calculations was limited. Since then it has become an easy task to fit the different rate equations to the initial rate data, by global

curve fitting. This method is widely used and is considered a more robust method than the graphical methods [261,262,263,264].

Table 5.1 The shapes of the different replots for terreactant mechanisms when one substrate is varied at different fixed concentrations of the other two, maintained in a constant ratio [260,265]. Abbreviations used: N refers to nonlinear replots with nonzero intercepts on the y-axis, NO refers to nonlinear replots that intersect the origin, L refers to linear replots with nonzero intercepts on the y-axis, A refers to a case in which the reciprocal plot intersects on the axis, pp refers to ping pong.

Varied substrate	Substrate A		Substrate B		Substrate C	
Mechanism	Slope	Intercept	Slope	Intercept	Slope	Intercept
Rapid equilibrium random	N	N	N	N	N	N
Ordered	N	N	N	L	N	N
Random AC	N	N	NO	L	N	N
Random A	N	N	NO	N	N	L
Random (no EAC)	N	N	NO	N	N	N
Random AB	NO	N	NO	N	N	A
Random BC, rapid equilibrium A	NO	N	N	L	N	L
Random BC, steady-state A	N	N	N	L	N	L
Rapid equilibrium ordered	NO	N	NO	L	N	A
Hexa uni pp	L	L	L	L	L	L
Ordered bi uni uni bi pp	L	L	L	L	L	N
Ordered bi uni uni bi pp	L	N	L	L	L	L
Random bi uni uni bi pp	L	L	L	L	L	N
Random uni uni bi bi pp	L	N	L	L	L	L

CHAPTER SIX

6 Determination of enzyme kinetic parameters of TPH variants

Tryptophan hydroxylase catalyses the reaction tryptophan + BH_4 + O_2 to give 5-hydroxytryptophan and 4a-hydroxy-BH_4. In order to study this reaction and enzymatic properties of the enzyme, one needs to measure the initial rates of 5-hydroxy-tryptophan formation (or substrate consumption). The initial rates are measured at different concentrations of all three substrates. Controlling the concentration of tryptophan and BH_4 is straight forward since the concentration in stock solutions can be determined using UV-Vis spectrophotometry. Controlling the concentration of O_2 is on the other hand not so easy. The O_2 concentration in an aqueous solution is dependent on several factors. Most important factors are temperature, the ionic strength and the partial pressure of O_2 above the solution. In this chapter I will describe the assay and procedure used to measure the initial rates at controlled concentrations of all three substrates and the determination of the apparent enzyme kinetic parameters for c*g*TPH1, c*h*TPH2 and ct*h*TPH2 will be presented.

6.1 The tryptophan hydroxylase assay

The formation of 5-hydroxytryptophan can be monitored using fluorescence spectro-photometry [266]. This is based on different spectral properties of tryptophan and 5-hydroxytryptophan shown in figure 6.1.

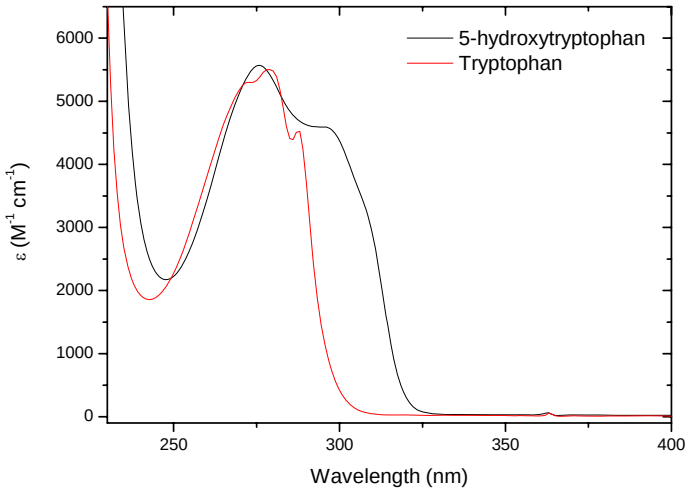

Figure 6.1 Absorbance spectra of tryptophan (black) and 5-hydroxytryptophan (red) in 10 mM HCl.

By using an excitation wavelength of 300 nm 5-hydroxytryptophan is almost selectively excited. The emission is measured at 330 nm. A continuous assay for TPH based on fluorescence spectrophotometry was developed by Moran and Fitzpatrick [235] and this assay is used in this study. The assay will be described in the following sections, while the procedures for controlling the O_2 concentration and measuring the initial rates are described in section 6.2 and 6.3, respectively.

6.1.1 Composition of the assay solution

(6R)-5,6,7,8-tetrahydro-L-biopterin dihydrochloride (BH_4) was from Schircks Laboratories, Jona, Switzerland. All other chemicals used were analytical grade obtained from Sigma-Aldrich. All solutions were prepared using 18.2 MΩ cm water from a Milli-Q synthesis A10 Q-Gard system (Millipore).
The assay volume was 2500 µL and contained 200 mM $(NH_4)_2SO_4$, 50 mM HEPES/NaOH, pH 7.0, 7 mM dithiothreitol (DTT), 25 µg/mL catalase, 25 µM $(NH_4)_2Fe(SO_4)_2$, and standard substrate concentrations were 70 µM tryptophan, 300 µM BH_4 and 500 µM O_2. All measurements were done at 15˚C. Stock solutions of the different components were prepared as seen in table 6.1. Tryptophan, BH_4, DTT and $(NH_4)_2Fe(SO_4)_2$ were prepared freshly prior to each measuring session. Catalase was dissolved in water in a larger batch and frozen (-20˚C) in aliquots of 1.2 mL until use. Tryptophan, DTT and $(NH_4)_2Fe(SO_4)_2$ were dissolved in water, while BH_4 was dissolved in 10 mM HCl in order to protonate N5 and prevent autooxidation [235] (see section 2.4). The DTT and BH_4 solutions were kept on ice. A stock solution mixture was usually made from the stock solutions of DTT and $(NH_4)_2Fe(SO_4)_2$.

Table 6.1 Concentration of compounds in the stock solutions and concentrations used in the assay.

Compound	Concentration in assay
500 mM $(NH_4)_2SO_4$ 125 mM HEPES/NaOH pH 7.0	200 mM 50 mM
175 mM DTT	7 mM
1.27 mM $(NH_4)_2Fe(SO_4)_2$	25 µM
1.25 mg/mL catalase	25 µg/mL
3.0 mM tryptophan	70 µM
15 mM BH_4	300 µM

The tryptophan concentration was determined in 10 mM HCl using ε_{278} = 5500 $M^{-1}cm^{-1}$. The concentration of BH_4 was determined in 2 M HCl using ε_{266} = 18,000 M^{-1} cm^{-1} [235].
The components in the assay have the following functions: the $(NH_4)_2SO_4$ stabilises TPH, $(NH_4)_2Fe(SO_4)_2$ is a source of Fe^{2+} required by TPH for activity, catalase removes any peroxide that could be formed for example from autooxidation of BH_4 and DTT is a reductant which keeps the iron in ferrous state and it also reduces qBH_2 to BH_4. qBH_2 is a product of the decomposition of 4a-hydroxy-BH_4 (see section 2.4) and from the autooxidation of BH_4. Accumulation of qBH_2 is unwanted because it disturbs the fluorescence signal from 5-hydroxytryptophan having a higher absorbance at 330 nm than BH_4, as seen in figure 6.2 [235].

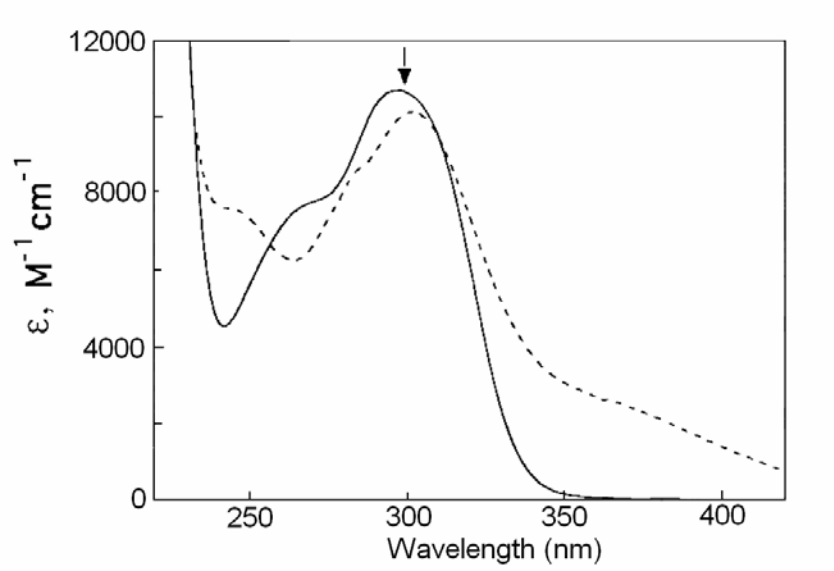

Figure 6.2 The absorption spectra of BH_4 at pH 7 (full line) and qBH_2 (dashed line) [235].

6.1.2 Standard curves for 5-hydroxytryptophan

The absorption spectrum for BH_4 at pH 7.0 is shown in figure 6.2. At pH 7.0 BH_4 absorbs at 300 nm which is used as the excitation wavelength. The fluorescence signal from 5-hydroxytryptophan is therefore reduced by the attenuation of the incoming light. Consequently it is necessary to make 5-hydroxytryptophan standard curves for all the BH_4 concentrations used.
The fluorescence of 5-hydroxytryptophan for the standard curves, at concentration from 0.4 to 20 µM 5-hydroxytryptophan, was measured in 50 mM HEPES/NaOH, 200 mM $(NH_4)_2SO_4$, pH 7.0. The standard curves can be seen in appendix 1. The concentration of 5-hydroxytryptophan was determined in 10 mM HCl using ε_{278} = 5500 M^{-1} cm^{-1} [235].

6.1.3 Instrument and instrument settings

Measurements were done on a Varian Cary Eclipse fluorescence spectrophotometer. The excitation wavelength was 300 nm and emission was measured at 330 nm. Excitation and emission slits were 5 nm. The photomultiplier tube (PMT) voltage was 650 V for most measurements. A few measurements were done at 585 V when low BH_4 concentrations were used in combination with high tryptophan and O_2 concentrations. The measurements were done in 10.00 mm × 10.00 mm QS quartz cuvettes from Hellma. The fluorescence spectrophotometer was equipped with a temperature controlled four cuvette holder with magnetic stirring. All measurements were done at 15˚C.

6.2 Controlling the O_2 concentration

The O_2 concentration in solutions saturated with O_2 can be found in reference works. The solubility of O_2 in water at 15˚C is 1528 µM at an O_2 partial pressure of 101.325 kPa [267]. In all the following measurements the value of 1528 µM will be used as equal to 100 % O_2. This is an approximation since the measurements were done in 50 mM HEPES/NaOH, 200 mM $(NH_4)_2SO_4$, pH 7.0 and not in pure water.

Another complication in the controlling the O_2 concentration is that the assay mixture contains 7 mM DTT which reacts with O_2 [268]. The reaction at pH 7.0 between DTT and O_2 is not fast, but it is faster than the diffusion of O_2 from the gas above the solution and fast enough to disturb the oxygen concentration in the assay mixture.
To solve this problem it was necessary to use an O_2 sensing electrode so that the O_2 concentration could be measured at the time of the reaction. It was impractical having the O_2 electrode in the cuvette where the measurements were done (due to protein binding to the electrode membrane, bigger chance of polluting the samples and slower mixing when adding substrates). Therefore two cuvettes, one reaction cuvette and a reference cuvette, were used for each measurement. The reference cuvette contained the same solution as the reaction cuvette except that enzyme and BH_4 was not added to the reference cuvette. The O_2 concentration was measured in the reference cuvette.

6.2.1 Mixtures of O_2 and N_2

To obtain the desired O_2 concentration in the reaction solution, the solutions in the reaction and reference cuvettes were flushed with different N_2/O_2 mixtures. The desired N_2/O_2 ratios were produced using Mass Flow controllers model 5850 TR from Brooks Instruments B.V. Veenendaal, Holland. These were calibrated for N_2 and O_2 respectively. The flow controllers were operated through a monitor model 0152 from Brooks Instruments.

6.2.2 The O_2 electrode

The O_2 concentration was determined using a MI-730 Oxygen electrode and OM-4 Oxygen Meter from Microelectrodes, Inc., Londonderry, NH, USA. The electrode was calibrated in 50 mM HEPES/NaOH, 200 mM $(NH_4)_2SO_4$, pH 7.0, in a cuvette at 15˚C. The zero set point was obtained by flushing the solution with N_2 until saturation. The 100% O_2 set point (equal to 1528 µM in water at 15˚C, P_{O2} = 101.325 kPa [267]) was obtained by flushing with O_2 until saturation. The flushing tube was lifted out of the solution but still keeping 100% O_2 above the solution surface and after a few minutes the oxygen meter was set to 100% O_2. This was done to ensure that the solution was not supersaturated with O_2. Corrections were not made for fluctuations in the ambient air pressure.

6.3 Procedure for measuring the initial rate of 5-hydroxytryptophan formation

From stock solutions HEPES $(NH_4)_2SO_4$ pH 7.0, DTT, $(NH_4)_2Fe(SO_4)_2$, tryptophan (see table 6.1) and water were added to the cuvettes containing cylindrical magnetic stir bars. Lids with holes for gas tubes, O_2 electrode and enzyme/substrate addition were sealed to the cuvettes with parafilm. The cuvettes with gas tubes and O_2 electrode were placed in temperature controlled cuvette holder in the fluorescence spectrophotometer and flushed with a desired gas mixture of O_2 and N_2 with magnetic stirring. Care was taken to ensure the same gas flow from the two tubes. The oxygen concentration was monitored and at a desired O_2 concentration the tubes were pulled up still keeping constant gas mixture above the solutions. Flushing time was dependent on the desired O_2 concentration and usually varied from 2-12 min.
Catalase and TPH (both kept on ice) were then added to the reaction cuvette and an equal volume of water (kept on ice) was added to the reference cuvette. BH_4 was added

to reaction cuvette to initiate the reaction and the equal volume of 10 mM HCl was added to the reference cuvette.
The initial rate slope (intensity/min) was determined using the fluorescence spectrophotometer software. The software performs linear regression on an interval of the progression curve. The selection of the interval was done manually usually with an interval of minimum 0.04 min. The initial rate was converted to µM 5-hydroxytryptophan/min from standard curves for 5-hydroxytryptophan at different concentrations of BH_4 (appendix 1). When the initial rates had been measured the appropriate equation was fitted to the data using OriginPro 7.5 from OriginLab Corp. For each fit to the presented in the following sections a SS/DoF is presented. This is the sum of squares divided by the number of degrees of freedom. The closer SS/DoF is to zero the better. The coefficient of determination (R^2) is also presented in the figures showing the data points and fitted equation [269].

6.4 Activity measurements of c*g*TPH1

The enzyme activity measurements on c*g*TPH1 were done using the assay described in section 6.1 and the procedure in section 6.3. The enzyme solution was prepared as follows: Stocks of c*g*TPH1 stored at -80˚C were thawed and 1700 µL was mixed with 680 µL 140 mM HEPES/NaOH, 450 mM $(NH_4)_2SO_4$, 10% glycerol, pH 7.0, 7 mM DTT, 46 µM tryptophan, 0.1 g/L catalase. The mixture was stored in 3 eppendorf tubes closed under an argon flow. This was done to prevent loss of activity. The c*g*TPH1 concentration in the assay was 1.7 µM. The standard substrate concentrations were 70 µM tryptophan, 300 µM BH_4 and 500 µM O_2. An extra experiment was carried out with varied BH_4 concentration at 10 µM tryptophan and 133 µM O_2. All data points were measured twice. V_{max}, K_m and K_i for the substrates were determined by fitting equations to the direct initial rates. The kinetic data for varied concentrations of BH_4 and O_2 were fitted to the Michaelis-Menten equation 5.1. Data for varied tryptophan concentrations were fitted to equation 5.3 taking substrate dead-end inhibition into account.

6.4.1 Results of activity measurements of c*g*TPH1

The measured initial rates of c*g*TPH1 with varied tryptophan concentrations are shown in figure 6.3A, varied BH_4 concentration in figure 6.3B, varied O_2 concentration in figure 6.3C and varied BH_4 concentration with 10 µM tryptophan 133 µM O_2 in figure 6.4. The fitted curve is shown in red. The enzyme kinetic parameters are also summarised in table 6.2. From the results here the specific activity of c*g*TPH1 is 0.58 µmol/mg/min.

Table 6.2 Summary of enzyme kinetic parameters for c*g*TPH1 determined at 15˚C with 70 µM tryptophan, 300 µM BH_4 and 500 µM O_2 except for the measurements with varied concentration of BH_4 with 10 µM tryptophan and 133 µM O_2.

Varied substrate	V_{max}, (min^{-1})	K_m (µM)	K_i (µM)	k_{cat} (min^{-1})
Tryptophan	54.9±2.4	7.7±0.7	164±24	32.3
BH_4	73.4±1.5	324±10	-	43.2
O_2	38.7±0.4	39±2	-	22.8
BH_4 (10 µM tryptophan)	33.3±0.5	71±3	-	19.6

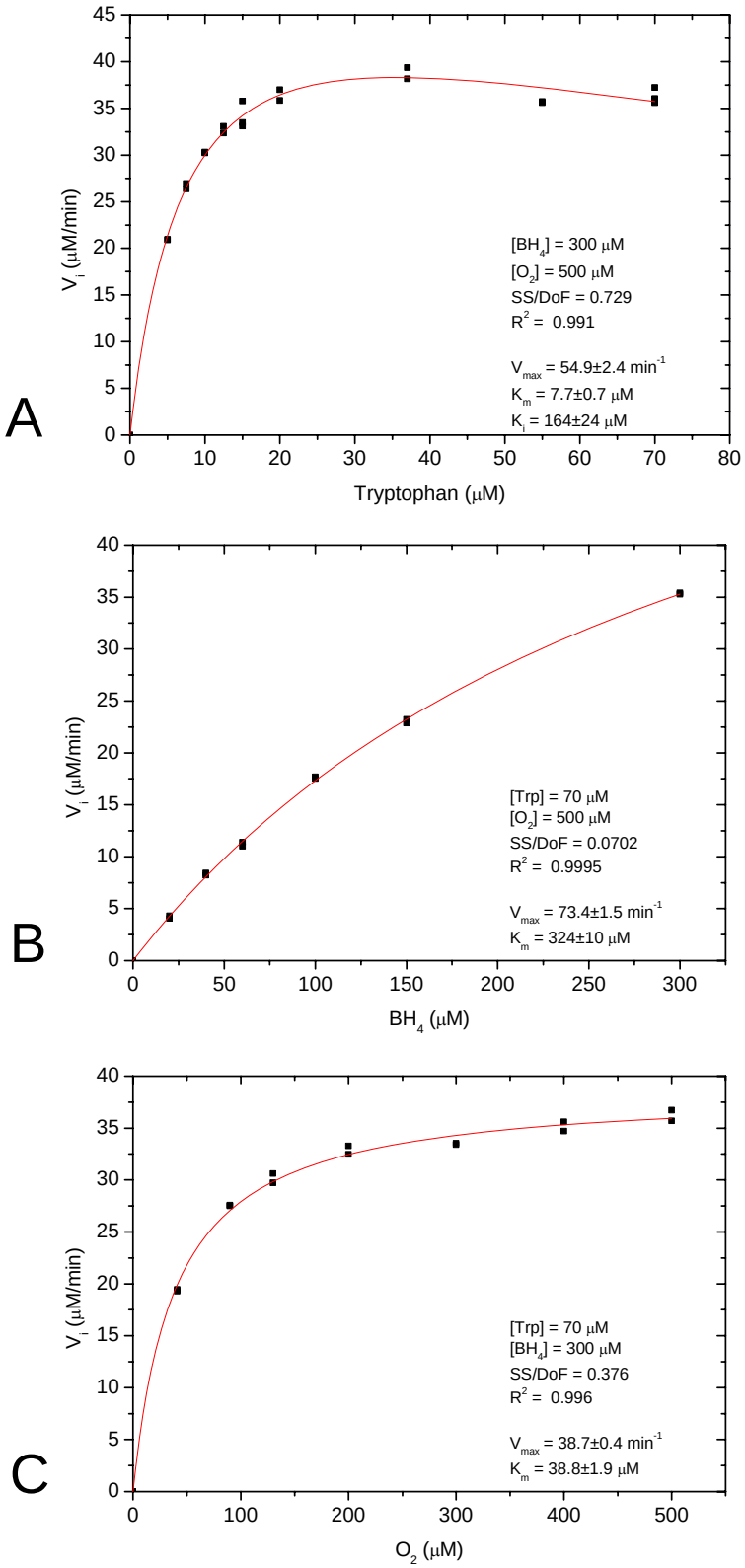

Figure 6.3 Initial rate as a function of substrate concentrations of *cg*TPH1. **(A)** Varied concentration of tryptophan. **(B)** Varied concentration of BH_4. **(C)** Varied concentration of O_2. Equation 5.3 was fitted to the data for varied tryptophan concentration. Equation 5.1 was fitted to the data from varied BH_4 and O_2 concentrations. The fitted equations are shown in red. The kinetic parameters obtained from fitting equation 5.1 and 5.2 are listed in table 6.2.

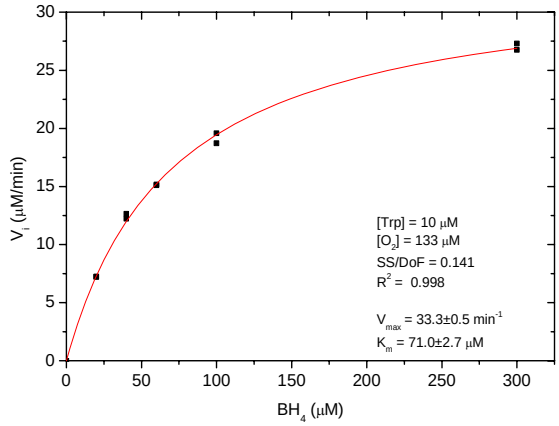

Figure 6.4 Initial rates at varied BH_4 concentrations for c*g*TPH1, with 10 µM tryptophan and 133 µM O_2. Equation 5.1 was fitted to data and is shown as the red curve.

6.4.2 Discussion of the c*g*TPH1 kinetic parameters

Since this is the first characterisation of c*g*TPH1 it is not possible to compare the kinetic constants obtained in this study with other published data of this enzyme. The rabbit cTPH1 [87] and c*h*TPH1 [64] have been characterised with determined kinetic constants. In the case of c*h*TPH1 the assay conditions are not described and data points not shown which makes it difficult to judge the validity of the data. In the case of rabbit cTPH1 the parameters were determined at 15˚C, air saturated (≈ 300 µM O_2) 50 mM MES, 100 mM $(NH_4)_2SO_4$, 50 µM $(NH_4)_2Fe(SO_4)_2$ 25 µg/mL catalase, pH 7.0, 150 µM BH_4 (for tryptophan variation), 200 µM tryptophan (for BH_4 variation). $K_{m,tryptophan}$ determined here is 7.7±0.7 µM versus 7.8±2.2 µM for c*h*TPH1 and 47.9±4.2 µM for rabbit cTPH1. The differences between the $K_{m,tryptophan}$ values of c*g*TPH1 and rabbit cTPH1 are significant and can not likely be ascribed to the differences in BH_4 concentration, since the lower BH_4 concentration used with rabbit cTPH1 should yield a lower $K_{m,tryptophan}$.

For c*g*TPH1 substrate inhibition by tryptophan is observed above 15 µM, which is lower than that of >70 µM reported for c*h*TPH1 (a $K_{i,tryptophan}$ was not reported)[64]. The $K_{i,tryptophan}$ of 146±14 µM for rabbit cTPH1 [87] is comparable to the $K_{i,tryptophan}$ of 163±24 µM determined here.

The $K_{m,BH4}$ value of 324±10 µM is quite high compared to $K_{m,BH4}$ of 135±16 µM determined at 200 µM tryptophan for rabbit cTPH1 and very high compared to 26.5±2 µM of c*h*TPH1. Substrate inhibition by tryptophan is probably one reason for the high $K_{m,BH4}$ value, but this can not be the only explanation since the $K_{m,BH4}$ for rabbit cTPH1 was measured at 200 µM tryptophan and was also influenced by tryptophan inhibition [87]. When the $K_{m,BH4}$ was determined at 10 µM tryptophan and 133 µM O_2 the $K_{m,BH4}$ should not be influenced by tryptophan inhibition. At these conditions $K_{m,BH4}$ is 71±3 µM which is significantly lower than the 324±10 µM. The $K_{m,BH4}$ for c*h*TPH2 at 10 µM tryptophan, 133 µM O_2 has been measured to 20.5±1.7 µM (figure 7.7C) which also is significantly lower than the 71±3 µM. This indicates that there may be some structural differences in the BH_4 binding site which can explain the lower affinity of c*g*TPH1 toward BH_4 compared to c*h*TPH2.

The $K_{m,O2}$ value of 39±2 µM is low compared to the oxygen concentration in pure water at equilibrium with atmospheric air, which is approximately 300 µM. It is difficult to determine the *in vivo* O_2 concentration where TPH is found. In the brain the average

P_{O2} value is 20 -30 torr, which is equal to 30-40 µM [270]. This value is similar to the $K_{m,O2}$ of c*g*TPH1. In three studies $K_{m,O2}$ has been determined for TPH partially purified from natural sources. A $K_{m,O2}$ of 2.5% at 37˚C (approximately 27 µM) was determined using TPH (probably isoform 2) from rabbit hindbrain [266]. $K_{m,O2}$ of TPH (probably isoform 1) partially purified from human carcinoid tumor was determined to 1.2% at 37˚C (approximately 13 µM) using $6MePH_4$ and 7.1% (approximately 78 µM) when $DMPH_4$ was used [47]. $K_{m,O2}$ of TPH (probably TPH1) from neoplastic murine mast cells was determined to 6.5% at 37˚C (approximately 70 µM) [153]. These values are in the same range as those determined for c*g*TPH1.
As mentioned in section 2.7 the kinetic mechanism for the aromatic amino acid hydroxylases is believed to be an ordered sequential mechanism. The expected inhibition pattern for this mechanism is uncompetitive substrate inhibition where the second substrate can add to the enzyme complex EQ (*e.g.* TPH-4a-hydroxy-BH_4) to form a dead-end complex EQB (see section 5.3, scheme 5.2). Tryptophan is generally believed to be the second substrate to bind in TPH prior to the reaction [97], which supports the uncompetitive inhibition mechanism. Two other mechanisms of tryptophan inhibition can be envisioned. Tryptophan could bind to the free enzyme hindering the binding of substrate A (*e.g.* BH_4) (similar to scheme 5.1). Another possibility is that tryptophan is the first substrate to bind (substrate A) and binding of a second tryptophan, hinders the binding of substrate B (*e.g.* BH_4). The $K_{m,BH4}$ is lowered significantly (from 324 to 71 µM) by lowering the tryptophan concentration. The greatest effect on $K_{m,BH4}$ by lowering the tryptophan concentration is likely to be seen in the inhibition mechanism where tryptophan binds to the free enzyme. Further experiments have to be done to verify the order of substrate binding and mechanism of substrate inhibition for c*g*TPH1.

6.5 Activity measurements of c*h*TPH2

The enzyme activity measurements of c*h*TPH2 were done using the assay described in section 6.1 and the procedure in section 6.3. The enzyme solution was prepared as follows: Stocks of c*h*TPH2 stored at -80˚C were thawed. The c*h*TPH2 was diluted with the gel filtration buffer (20 mM HEPES/NaOH, 100 mM $(NH_4)_2SO_4$, 5% (w/v) glycerol, pH 7.2) to give a concentration of 125 µM. Equal volumes of the c*h*TPH2 solution and 1.2 mM tryptophan, 4 mM DTT, 0.1 g/L catalase in 60 mM HEPES/NaOH, 15%(w/v) glycerol, 300 mM $(NH_4)_2SO_4$, pH 7.0 were mixed. The mixture was stored in 3-6 eppendorf tubes closed under an argon flow. The purpose of diluting the c*h*TPH2 sample with buffer solution containing tryptophan, DTT, catalase, extra $(NH_4)_2SO_4$, extra glycerol was to prevent loss of activity. If c*h*TPH2 was just stored in the gel filtration buffer loss of activity was observed during the measurements. In all the experiments 0.256 units (measured at 60 µM tryptophan, 300 µM BH_4 and 300 µM O_2) of c*h*TPH2 was used which in average was equal to 0.50±0.05 µM. The standard substrate concentrations were 70 µM tryptophan, 500 µM O_2 and 300 µM BH_4. All data points were measured in triplicate. V_{max}, and K_m for the substrates were determined by fitting the Michaelis-Menten equation (equation 5.1) to the initial rates.

6.5.1 Results of activity measurements of c*h*TPH2

The initial rates measured at varied tryptophan, BH_4 and O_2 concentrations are shown in figure 6.5A, B and C respectively. A summary of the enzyme kinetic parameters are listed in table 6.3. The specific activity of c*h*TPH2 is calculated to 6.87 µmol/mg/min.

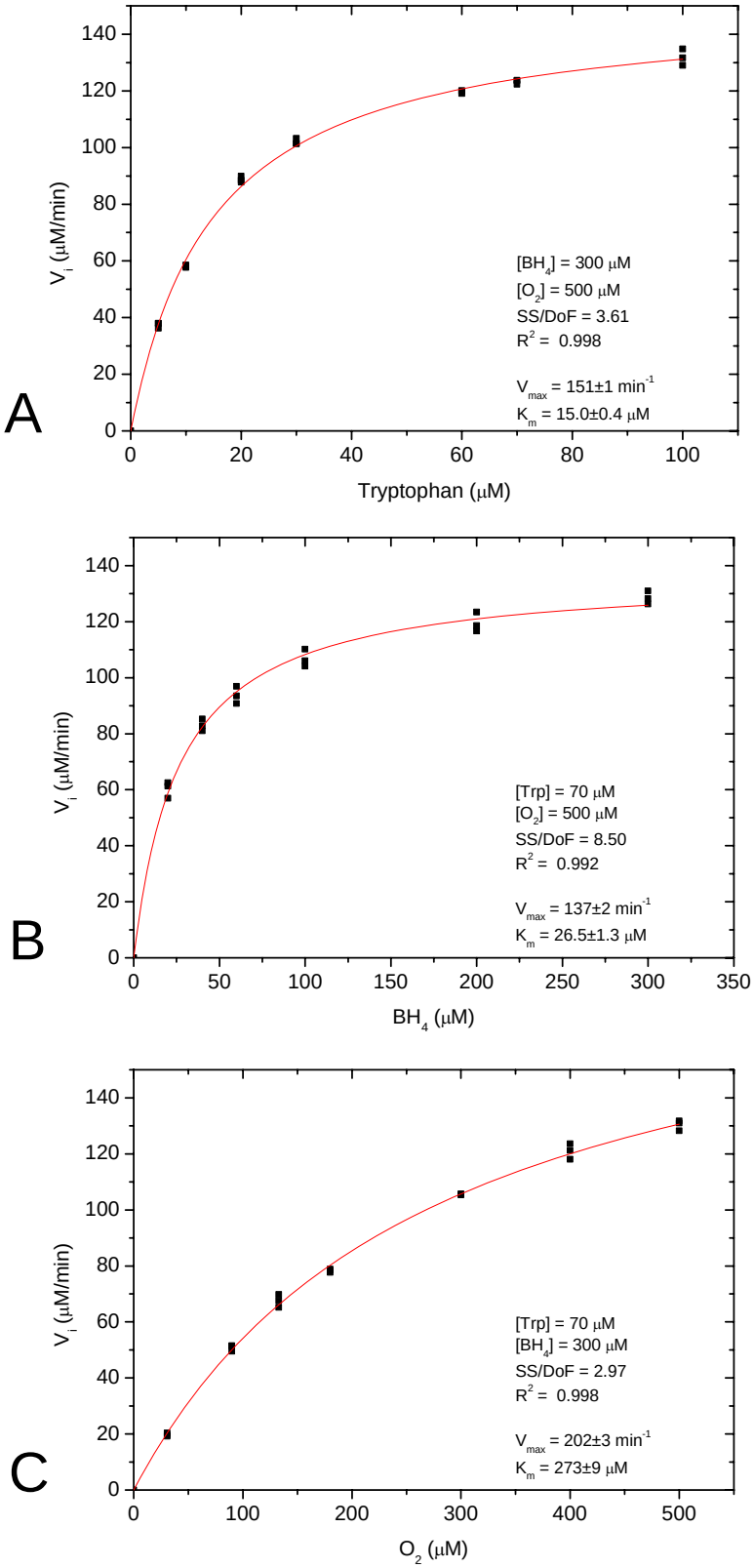

Figure 6.5 Initial rates measured at varied substrate concentrations using *ch*TPH2. **(A)** Varied tryptophan concentration. **(B)** Varied BH_4 concentration. **(C)** Varied O_2 concentration. Equation 5.1 was fitted to the data and the fitted equations are shown in red. The non-varied substrate concentrations were 70 µM tryptophan, 300 µM BH_4 and 500 µM O_2.

Table 6.3 A summary of enzyme kinetic parameters for c*h*TPH2. These were determined at 15˚C and the concentrations of the non-varied substrates were 70 µM tryptophan, 300 µM BH_4 and 500 µM O_2.

Substrate	V_{max} (min^{-1})	K_m (µM)	k_{cat} (min^{-1})
Tryptophan	151±1	15.0±0.4	302
BH_4	137±2	26.5±1.3	274
O_2	202±3	273±9	404

6.5.2 Discussion of the c*h*TPH2 enzyme kinetic parameters

The initial rate data for c*h*TPH2 follows Michaelis-Menten kinetics as seen in figures 6.5A-C. The kinetic parameters for c*h*TPH2 have been determined from fitting equation 5.1 to the data. Kinetic parameters of c*h*TPH2 have been published recently by Carkaci-Salli *et al.* [22]. The c*h*TPH2 used by Carkaci-Salli *et al.* contained amino acids 151-466 with an N-terminal 6His tag. The assay used was a radioenzymatic ^3H_2O release assay and conditions were not described in detail except that 50 µM tryptophan was used for $K_{m,BH4}$ determination and 50 µM BH_4 was used for $K_{m,tryptophan}$ determination [22]. In this study $K_{m,tryptophan}$ has been determined to 15.0±0.4 µM which is higher than the 7.7±0.7 µM of c*g*TPH1 but lower than the 41.79±3.12 µM by Carkaci-Salli *et al.* [22].
The $K_{m,BH4}$ was determined to 26.5±1.3 µM which is significantly lower than the 324±10 µM of c*g*TPH1, but higher than the 6.22±1.4 µM by Carkaci-Salli *et al.* [22]. The $K_{m,O2}$ was here determined to 273±9 µM which is in the range of the O_2 concentration in pure water in equilibrium with atmospheric air. This differs from the 39±2 µM determined for c*g*TPH1 and from the approximate O_2 concentration in brain of 30-40 µM [270]. Substrate inhibition by tryptophan was not observed but concentrations higher than 100 µM were not tested. It is possible that substrate inhibition will be observed at concentrations above 100 µM tryptophan.

6.6 Activity measurements of ct*h*TPH2

The enzyme activity measurements on ct*h*TPH2 were done using the assay described in section 6.1 and the procedure in section 6.3. The enzyme solution was prepared as follows: Stocks of ct*h*TPH2 stored at -80˚C were thawed. Equal volume of the ct*h*TPH2 solution was mixed with 1.2 mM tryptophan, 4 mM DTT, 0.1 g/L catalase in 60 mM HEPES/NaOH, 10%(w/v) glycerol, 200 mM $(NH_4)_2SO_4$, pH 7.0. The mixture was stored in 3 eppendorf tubes closed under an argon flow. The dilution with buffer containing tryptophan, DTT and catalase was done to prevent loss of activity. In all the experiments 0.179 units (measured at 70 µM tryptophan, 300 µM BH_4 and 500 µM O_2) of c*h*TPH2 was used which was equal to 0.50±0.01 µM ct*h*TPH2. The standard substrate concentrations were 70 µM tryptophan, 500 µM O_2 and 300 µM BH_4. All data points were measured twice. V_{max}, and K_m for the substrates were determined by fitting the Michaelis-Menten equation (equation 5.1) to the initial rates.

6.6.1 Results of activity measurements of ct*h*TPH2

The initial rates measured at varied tryptophan, BH_4 and O_2 concentrations are shown in figure 6.8A, B and C respectively. A summary of the enzyme kinetic parameters are listed in table 6.4. The specific activity of ct*h*TPH2 is calculated to 3.60 µmol/mg/min.

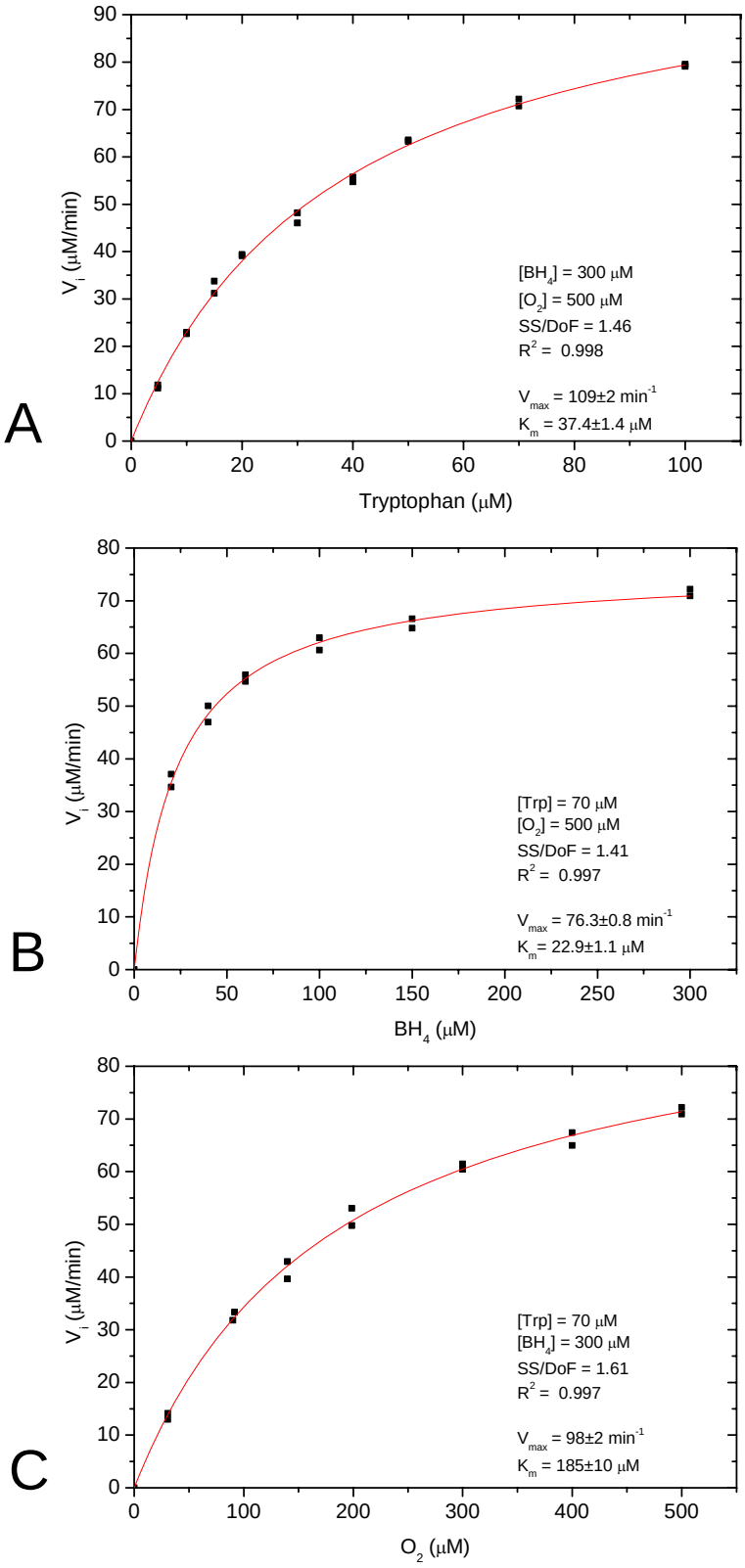

Figure 6.6 Initial rates measured at varied substrate concentration using ct*h*TPH2. **(A)** Varied tryptophan concentration. **(B)** Varied BH_4 concentration. **(C)** Varied O_2 concentration. The Michaelis-Menten equation (equation 5.1) was fitted to the data and is shown in red. The non-varied substrate concentrations were 70 µM tryptophan, 300 µM BH_4 and 500 µM O_2.

Table 6.4 A summary of enzyme kinetic parameters of ct*h*TPH2. The non-varied substrate concentrations were 70 µM tryptophan, 300 µM BH_4 and 500 µM O_2. The parameters were determined at 15˚C.

Substrate	V_{max} (min^{-1})	K_m (µM)	k_{cat} (min^{-1})
Tryptophan	109±2	37.4 ±1.4	218
BH_4	76.3±0.8	22.9 ±1.1	153
O_2	98±2	185±10	196

6.6.2 Discussion of the enzyme kinetic parameters of ct*h*TPH2

The Michaelis-Menten equation (equation 5.1) was fitted to the initial rates giving the parameters in table 6.4. Kinetic parameters have been determined for ct*h*TPH2 by Carkaci-Salli *et al.* (residues 151-490) with assay conditions described in 6.5.2 [22] and for ct*h*TPH1 (residues 91-444 with N-terminal His-tag) McKinney *et al.* [92]. Assay conditions used by McKinney *et al.* were 40 mM HEPES pH 7.0, 0.05 mg/mL catalase, 10 µM $(NH_4)_2Fe(SO_4)_2$, 2.5 mM DTT, 50 µM tryptophan and 250 µM BH_4, done at 30˚C [92]. The $K_{m,tryptophan}$ value determined here is 37.4±1.4 µM which is in the same range as the 20.1±3.4 µM by Carkaci-Salli *et al.* [22], and close to the 33±4.5 determined for ct*h*TPH1 [92]. The $K_{m,BH4}$ was determined to 22.9±1.1 µM which is close to the 16.88±3.9 µM determined by Carkaci-Salli *et al.* [22]. The $K_{m,BH4}$ of 50.8±16 µM determined for ct*h*TPH1 is a bit higher but not significantly [92]. The $K_{m,O2}$ was determined to 185±10 µM which is a bit lower than the one determined for the catalytic domain alone.

6.7 Overall summary and discussion

The kinetic parameters are determined using the same assay conditions for all three variants. This makes it possible to compare the kinetic data without taking the different assay conditions into account.

The $K_{m,tryptophan}$ values for c*h*TPH2 is a factor two higher than the $K_{m,tryptophan}$ for c*g*TPH1 indicating that c*g*TPH1 has a higher affinity for tryptophan than c*h*TPH2. In the same way $K_{m,tryptophan}$ for ct*h*TPH2 is a factor two higher than that of the c*h*TPH2, indicating that the tetramerisation domain has an influence on the affinity for tryptophan.

Table 6.5 Summary of K_m and k_{cat} values for the TPH variants determined using 70 µM tryptophan, 300 µM BH_4 and 500 µM O_2, at 15˚C.

Enzyme	Substrate	K_m (µM)	k_{cat} (min^{-1})
c*g*TPH1	Tryptophan	7.7±0.7	32.3
c*h*TPH2	Tryptophan	15.0±0.4	302
ct*h*TPH2	Tryptophan	37.6 ±1.4	218
c*g*TPH1	BH_4	324±10	43.2
c*h*TPH2	BH_4	26.5±1.3	274
ct*h*TPH2	BH_4	22.9 ±1.1	153
c*g*TPH1	O_2	39±2	22.8
c*h*TPH2	O_2	273±9	404
ct*h*TPH2	O_2	185±10	196

The $K_{m,BH4}$ values for the TPH2 variants are similar while the $K_{m,BH4}$ for c*g*TPH1 is more than a factor 10 higher. This difference is likely to be caused by both the substrate inhibition by tryptophan and a lower affinity of c*g*TPH1 for BH_4. The 3-dimensional structure of c*g*TPH1 and c*h*TPH2 will possibly give a structural explanation of these different properties. The $K_{m,O2}$ values of c*h*TPH2 and ct*h*TPH2 are in the same range while the $K_{m,O2}$ for c*g*TPH1 is lower. It is possible that the low $K_{m,O2}$ of c*g*TPH1 is a result of the tryptophan inhibition or that c*g*TPH1 simply has a much higher affinity for O_2 than c*h*TPH2 and ct*h*TPH2. From the brain oxygen concentration of 30-40 µM one would have expected the $K_{m,O2}$ for c*h*TPH2 and ct*h*TPH2 to be in this range. Possibly the regulatory domain of *h*TPH2 can affect the affinity for O_2.
The specific activities were calculated from the initial rates at 70 µM tryptophan, 300 µM BH_4 and 500 µM O_2. These were calculated for comparison to the specific activities obtained from the variants directly after purification (see chapter 4) to check if activity was lost by freezing and thawing. The specific activity of c*g*TPH1 was 0.60 µmol/min/mg before freezing and 0.58 µmol/min/mg after thawing. The specific activity of c*h*TPH2 was 5.90 µmol/min/mg before freezing and 6.87 µmol/min/mg after thawing and for ct*h*TPH2 it was 3.42 µmol/min/mg before freezing and 3.60 µmol/min/mg after thawing. The specific activities of c*g*TPH1 and ct*h*TPH2 are not significantly changed by freezing. The specific activity of c*h*TPH2 actually increases, which I currently have no explanation for, but it can be concluded that c*h*TPH2 as well as c*g*TPH1 and ct*h*TPH2 can be frozen and thawed without significant loss of activity.
From the k_{cat} values it can be concluded that c*h*TPH2 is a more effective enzyme than ct*h*TPH2 and much more effective than c*g*TPH1. The large difference in k_{cat} between c*g*TPH1 and c*h*TPH2 is likely to be due to the substrate inhibition by tryptophan. The substrate inhibition may again be due to small structural differences in the active sites of these enzymes. The difference in k_{cat} between c*h*TPH2 and ct*h*TPH2 may be due to a slightly restrained structure of the catalytic domain upon tetramerisation.

6.8 Conclusion

The apparent kinetic parameters K_m and V_{max} have successfully been determined for three TPH variants: c*g*TPH1, c*h*TPH2 and ct*h*TPH2. This is the first time any kinetic parameters have been determined for c*g*TPH1 and to my knowledge it is also the first time the $K_{m,O2}$ values have been determined for any fully purified recombinant TPH.

CHAPTER SEVEN

7 Steady-state kinetics of c*h*TPH2

In chapter 5 enzyme kinetics for ter reactant enzymes were introduced and the method of Ruldolph and Fromm was presented. In this chapter I will explain how experiments with c*h*TPH2 were done using the method of Rudolph and Fromm and present the results of these experiments. The assay and the procedure for measuring the initial rates are described in chapter 6. The data obtained from the experiments was analysed by two methods. First plotting analysis was used followed by a global curve fit analysis. All K_m and V_{max} values in this chapter are apparent values, unless otherwise is stated.

7.1 Substrate concentrations

As described in chapter 6 the method of Rudolph and Fromm consists of three sets of experiments. In each set one substrate is varied at different fixed concentrations of the other two, maintaining a constant ratio between these two [260]. The concentrations of the substrates and the ratios between the fixed substrates used are listed in table 7.1.

Table 7.1 Concentrations of the changing fixed substrates for the different experiment series.

Tryptophan variation		BH_4 variation		Oxygen variation	
$[O_2] = 3[BH_4]$		$[O_2]=13.33[Trp]$		$[BH_4]=4.286[Trp]$	
BH_4 (µM)	O_2 (µM)	Trp (µM)	O_2 (µM)	Trp (µM)	BH_4 (µM)
20	60	6.7	90	7	30
30	90	8.2	109.3	14	60
40	120	10	133	23.3	100
60	180	15	200	35	150
100	300	22.5	300	70	300
150	450	33.8	450		
300	900	52.5	700		
		75	1000		

The decisions made on concentrations and the ratios between the fixed substrates were based on the approximate K_m values for the three substrates obtained from some initial test experiments. Practical considerations were also taken into account, as for example the fact that high tryptophan concentrations will give high background fluorescence level and high concentrations of BH_4 will significantly attenuate the incoming light. Substrate concentrations should usually be varied in the range of K_m values [260]. The

initial estimates of the K_m values for tryptophan, BH_4 and O_2 are 14 µM, 50 µM and 170 µM, respectively.
In the following an experiment series is defined as the measurements of initial rates when one substrate concentration is varied and the other two are fixed. Varied tryptophan concentration at 30 µM BH_4 and 90 µM O_2 will for instance be one series.
For each experiment series the initial rate was measured at minimum 4 different concentrations of the varied substrate, and each different concentration was measured in triplicate. In some cases a large spread was observed in the initial rates and more than 3 measurements were done for each substrate concentration.

7.2 Enzyme concentration in the measurements

To eliminate small variations in enzyme activity, caused by differences in specific activity of each enzyme sample, a fixed amount of units of enzyme was used in each set of measurements. 0.254 units was used in the experiments with varied tryptophan while 0.256 units was used when BH_4 and O_2 were varied (1 unit is the amount of enzyme that produces 1 µmole product/min). c*h*TPH2 from two purification batches was used in these experiments. The activity of each enzyme sample was determined as the average activity from 4 measurements with 60 µM tryptophan, 300 µM BH_4 and 300 µM O_2. 0.256 units of c*h*TPH2 was in average equal to 0.50±0.05 µM.

7.3 Data analysis using the plotting methods

7.3.1 Analysis of the primary data

In one experiment series only one substrate concentration is changed. The reaction can therefore be treated as a mono substrate reaction and should follow the Michaelis-Menten equation (equation 5.1). The K_m and V_{max} values were obtained by non-linear regression using the program OriginPro 7.5. The data will be presented in a double reciprocal plot (Lineweaver-Burk plot, see equation 5.2) with the straight line constructed from the determined K_m and V_{max} values. The data will also be presented in V_i versus the substrate concentration plots in section 7.5.1.

7.3.2 Generation and analysis of replots

The K_m and V_{max} values obtained are used to construct replots. In the double reciprocal plot the slope is equal to K_m/V_{max} and the intercept equal to $1/V_{max}$. K_m/V_{max} and $1/V_{max}$ are plotted against the different reciprocal concentration of one of the fixed substrates. The replots should be either linear or parabolic upwards as described in section 5.5.1. Statistics can be used to determine whether the points follow a straight line or a parabolic curve. This is done using an F-test [269].

7.4 Results presented in double reciprocal plots and corresponding replots

The initial rates measured at varied tryptophan concentration at fixed levels of BH_4 and O_2 are presented in a double reciprocal plot in figure 7.1A. The replots of K_m/V_{max} and $1/V_{max}$ are presented in figure 7.1B and C. Similarly the initial rates at varied concentration of BH_4 and O_2 and corresponding replots are presented in figure 7.2 and 7.3, respectively.

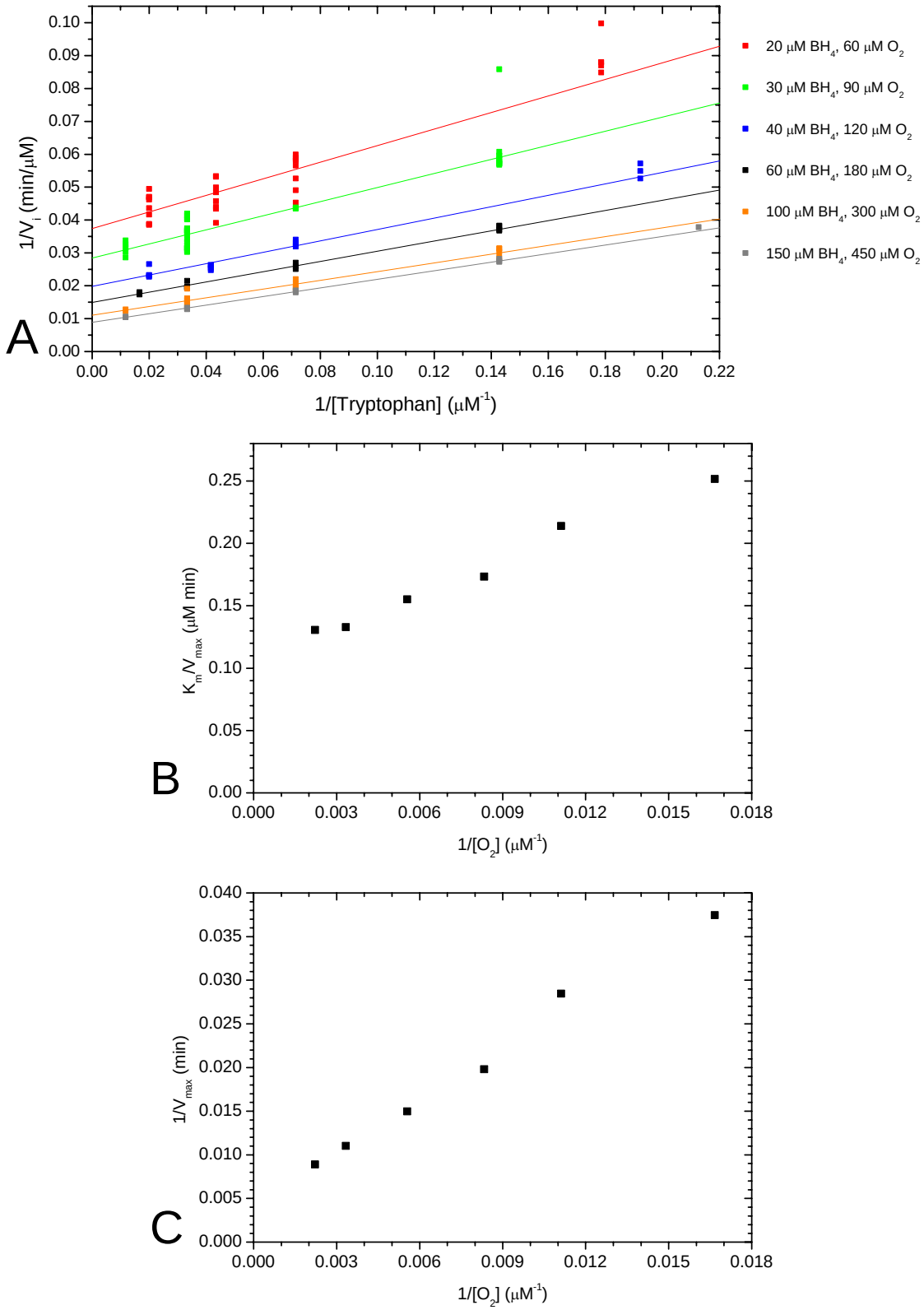

Figure 7.1 Results from the varied tryptophan concentration. **(A)** The double reciprocal plot. **(B)** K_m/V_{max} (the slopes of the lines in A) plotted against the reciprocal concentration of O_2. **(C)** $1/V_{max}$ (the intercepts of the lines in A) plotted against the reciprocal concentration of O_2.

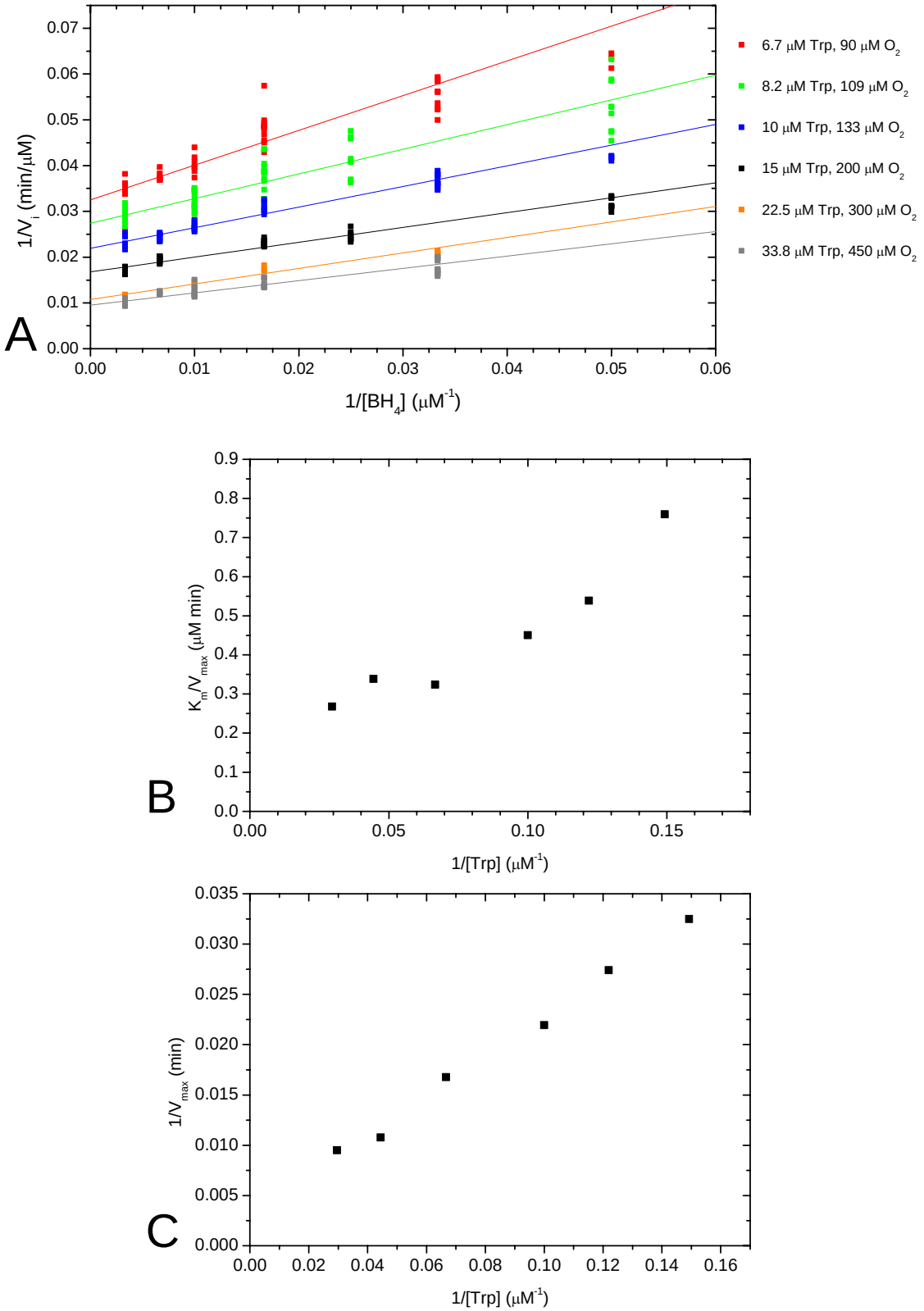

Figure 7.2 Results from the varied BH_4 concentration. **(A)** The double reciprocal plot $1/V_i$ versus $1/[BH_4]$. **(B)** K_m/V_{max} (the slopes of the lines in A) plotted against the reciprocal concentration of tryptophan. **(C)** $1/V_{max}$ (the intercepts of the lines in A) plotted against the reciprocal concentration of tryptophan.

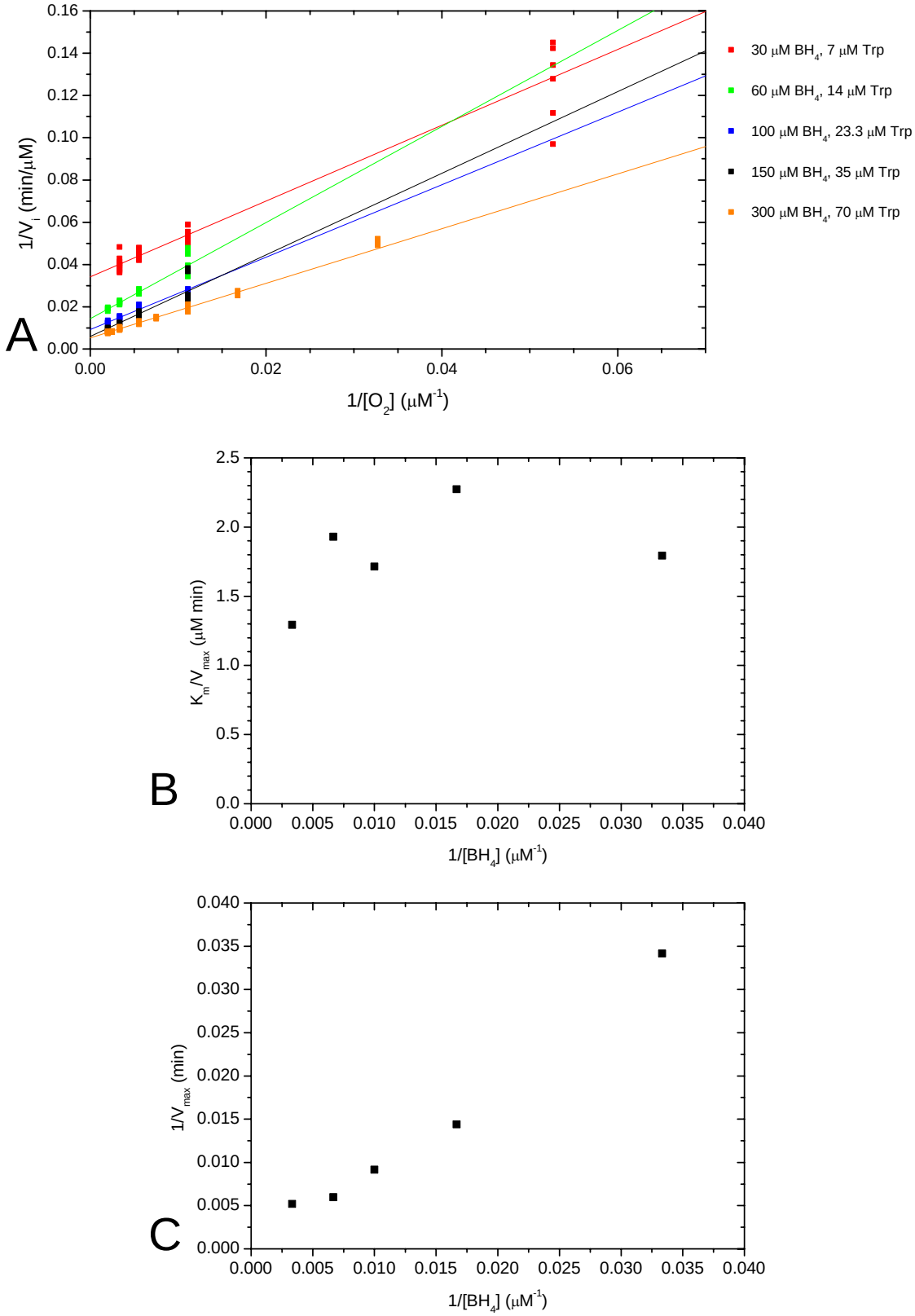

Figure 7.3 Results from the varied O_2 concentration. **(A)** The double reciprocal plot $1/V_i$ versus $1/[O_2]$. **(B)** K_m/V_{max} (the slopes of the lines in A) plotted against the reciprocal concentration of BH_4. **(C)** $1/V_{max}$ (the intercepts of the lines in A) plotted against the reciprocal concentration of BH_4.

7.4.1 Analysis of the plots

From the line patterns in the double reciprocal plots in figure 7.1A, 7.2A and 7.3A one should be able to determine whether the mechanism is a ping pong or a sequential mechanism. If the lines in all three double reciprocal plots intersect, the mechanism is sequential. The mechanism is a ping pong mechanism if parallel lines are observed in at least one of the replots. The lines in figure 7.1A and 7.2A intersect far to the left. The general trend for these lines in figure 7.1A and 7.2A is that the slopes (K_m/V_{max}) decrease as the concentrations of the substrates kept in a constant ratio are increased. This trend is not observed for the lines in figure 7.3A. Here lines intersect to the right of the y-axis, which is not in agreement with the theory (see section 5.5.1). Three lines, the 60, 100 and 300 µM BH_4, seem to follow the trend of a decreasing slope (see table 7.2) when the BH_4 and tryptophan concentrations are increased. While the other two lines, 30 and 150 µM BH_4 do not fit into this trend.
From the mixed pattern in figure 7.3A, it is difficult to confidently conclude that the lines intersect. This again makes it difficult to conclude whether the mechanism is a ping pong or a sequential mechanism.

Table 7.2 The K_m and V_{max} parameters obtained from the experiments with varied O_2 concentration.

Trp (µM)	BH_4 (µM)	K_m (µM)	V_{max} (min^{-1})	K_m/V_{max}	$1/V_{max}$
7	30	52.5	29.3	1.79	0.0342
14	60	157.9	69.5	2.27	0.0144
23.3	100	187.3	109.2	1.71	0.00916
35	150	323.9	167.8	1.93	0.00596
70	300	248.5	192.1	1.29	0.00521

The different possible patterns of the replots for the different mechanisms are shown in table 5.1. The replots can be linear, intersecting the y-axis at the origin or above. The replots can also be parabolic upwards with or without intersecting the origin.
The replots were treated statistically. Both replots of the varied tryptophan concentration experiments are linear. For varied BH_4 concentration the K_m/V_{max} replot is parabolic upwards ($p = 0.037$) while the $1/V_{max}$ is linear. In the case of varied O_2 concentration $1/V_{max}$ is parabolic upwards ($p = 0.036$), while the K_m/V_{max} replot is neither linear nor parabolic upwards.
All together this replot pattern does not fit with the possible patterns in table 5.1. Since it could not be concluded that any of the replots fit a certain mechanism, no conclusion could be drawn on the type of mechanism by analysing the data this way.

7.5 Analysis using global curve fitting

As analysing the data by the plotting method was inconclusive, the more robust method of global curve fitting was applied. In this method one may fit the full rate equation (equation 5.5-5.10) for different possible mechanisms to the data points (see section 5.5.2)[261,263] using OriginPro 7.5. The different rate equations can be entered in the software programme. The directly measured concentrations of the substrates [A], [B] and [C] are defined as independent variables while V_i is defined as a dependent variable. V_{max} and the different K parameters are entered as parameters, with the possibility of constraining these. Usually only one constraint being $K>0$ was

enforced on the parameters, which is reasonable since all the K parameters are ratios of rate constants k which can not be negative.
When the different rate equations have been fitted to the data, one may compare how well the different rate equations fit the data. Since it is easier to fit a complicated model (more parameters) than a simpler model (fewer parameters), one should always choose the simpler model unless the more complicated model is significantly better as determined by the F-test [269]. When the numbers of fitted parameters in the two rate equations are the same, the sum of squares of deviations of the data points from the model (SS) can be compared directly. If one rate equation has fewer fitted parameters than the other rate equation, the complexities of the rate equations have to be quantified with the degrees of freedom (DF). The degree of freedom is the number of data points minus the number of fitted parameters. If the simpler rate equation (null hypothesis) is correct, the relative increase in the sum of squares should be approximately equal to the relative increase in degrees of freedom. This is calculated in the F ratio (equation 7.1).

$$F = \frac{(SS_{null} - SS_{alt})/SS_{alt}}{(DF_{null} - DF_{alt})/DF_{alt}} \tag{7.1}$$

If the more complicated rate equation (alternative) is correct, one expect the relative increase in SS to be greater than the relative increase in degrees of freedom [269].
In the global curve fitting all 534 data points were used. The initial rates measured with varied tryptophan concentration were corrected for the small difference in the amount of enzyme used in the measurements.

7.5.1 Results from global curve fitting

The different rate equations were fit to all the data points with all combinations of tryptophan, BH_4 and O_2 as A, B and C. The lowest sum of squares for each rate equation is listed in table 7.3.

Table 7.3 Sum of squares for the fitting of rate equations to the initial rates. SS is the sum of squares and DF is the degrees of freedom.

Mechanism (equation number)	SS	DF	Substrate (A,B,C)	F ratio
Rapid equilibrium ordered (5.6)	21605	530	(BH_4, O_2, Trp)	
Bi uni uni uni ping pong (5.7)	9773	529	(Trp/BH_4, O_2)	10.5
Random A-B ordered C (5.8)	9583	528	(BH_4, Trp/O_2)	
Rapid equilibrium random (5.10)	9560	527	(-,-,-)	1.3
Ordered (5.5)	9515	528	(Trp/O_2, BH_4, Trp/O_2)	
Ordered A random B-C (5.9)	9478	528	(Trp, BH_4/O_2)	

The rapid equilibrium ordered rate equation does not fit data very well as the sum of squares is much higher than for any of the other rate equations. The ping pong rate equation has a higher sum of squares than the random A-B ordered C but they have different degrees of freedom. When comparing the random A-B ordered C fit with the ping pong fit, the calculated F ratio is 10.5. This says that the random A-B ordered C rate equation fits significantly better than the ping pong mechanism. The rapid equilibrium random rate equation has a lower sum of squares than the random A-B ordered C, but the F ratio of 1.3 ($p = 0.0013$) tells that the rapid equilibrium random

rate equation fit is better. The fit of the remaining rate equations (5.5, 5.8 and 5.9) can be compared directly since the degrees of freedom are the same for all three. The lowest sum of squares of 9478 is obtained when fitting the rate equation for the ordered A random B-C mechanism, where substrate A is tryptophan. The sum of squares of 9515 for the ordered mechanism with BH_4 as substrate B is close to that of the ordered A random B-C, while the sum of squares of the random A-B ordered C equation fit is somewhat worse.
Data points for each series of data are presented in figures 7.5-7.10, with the fitted curves for both the ordered A (A = tryptophan), random B-C rate equation (dashed blue curve) and the ordered rate equation with substrate B being BH_4 (red curve). Parameter values for these two best fits are listed in table 7.4.
Initially some of the series were done with O_2 concentrations up to 1000 µM. When O_2 concentrations above 500 µM were used a deviations from the Michaelis-Menten equation were observed which was similar to substrate inhibition. Examples of this observation are shown in figure 7.4 with the globally fit rate equations for the ordered A random B-C mechanism. This deviation might be caused by O_2 inactivation of the enzyme in different ways than ordinary substrate inhibition. All measurements done with O_2 concentrations above 500 µM have therefore not been used in the data analysis.

Table 7.4 Kinetic parameters obtained from the global curve fitting of the rate equations for the ordered A random B-C and ordered mechanism.

Ordered A random B-C		Ordered	
A= tryptophan		A = tryptophan, B = BH_4, C = O_2	
V_{max}	379±19 min^{-1}	V_{max}	358±17 min^{-1}
$K_{m,tryptophan}$	43.7±2.7 µM	$K_{m,tryptophan}$	40.1±2.7 µM
$K_{m,BH4}$	114±10 µM	$K_{m,BH4}$	90.2±8.4 µM
$K_{m,O2}$	497±37 µM	$K_{m,O2}$	467±33 µM
$K_{i,tryptophan}$	80±137 µM	$K_{i,tryptophan}$	4.52±1.20 µM
$K_{i,BH4}$, (BH_4 = C) $K_{i,O2}$, (O_2 = C)	1.6±2.5 µM 7.0±11.3 µM	$K_{i,BH4}$	6.3±2.0 µM

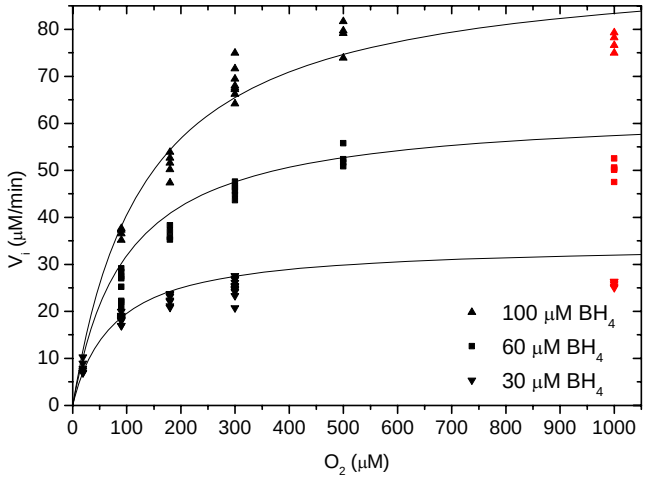

Figure 7.4 Initial rates measured at different O_2 concentrations. From the top the data is of 100 µM BH_4/23.3 µM tryptophan, 60 µM BH_4/14 µM tryptophan and 30 µM BH_4/7 µM tryptophan. The data points measured at 1000 µM are shown in red and these data points were not used in the fitting of the rate equation. The curves are the rate equations for the ordered A random B-C mechanism fitted to the data shown in figures 7.5-7.10.

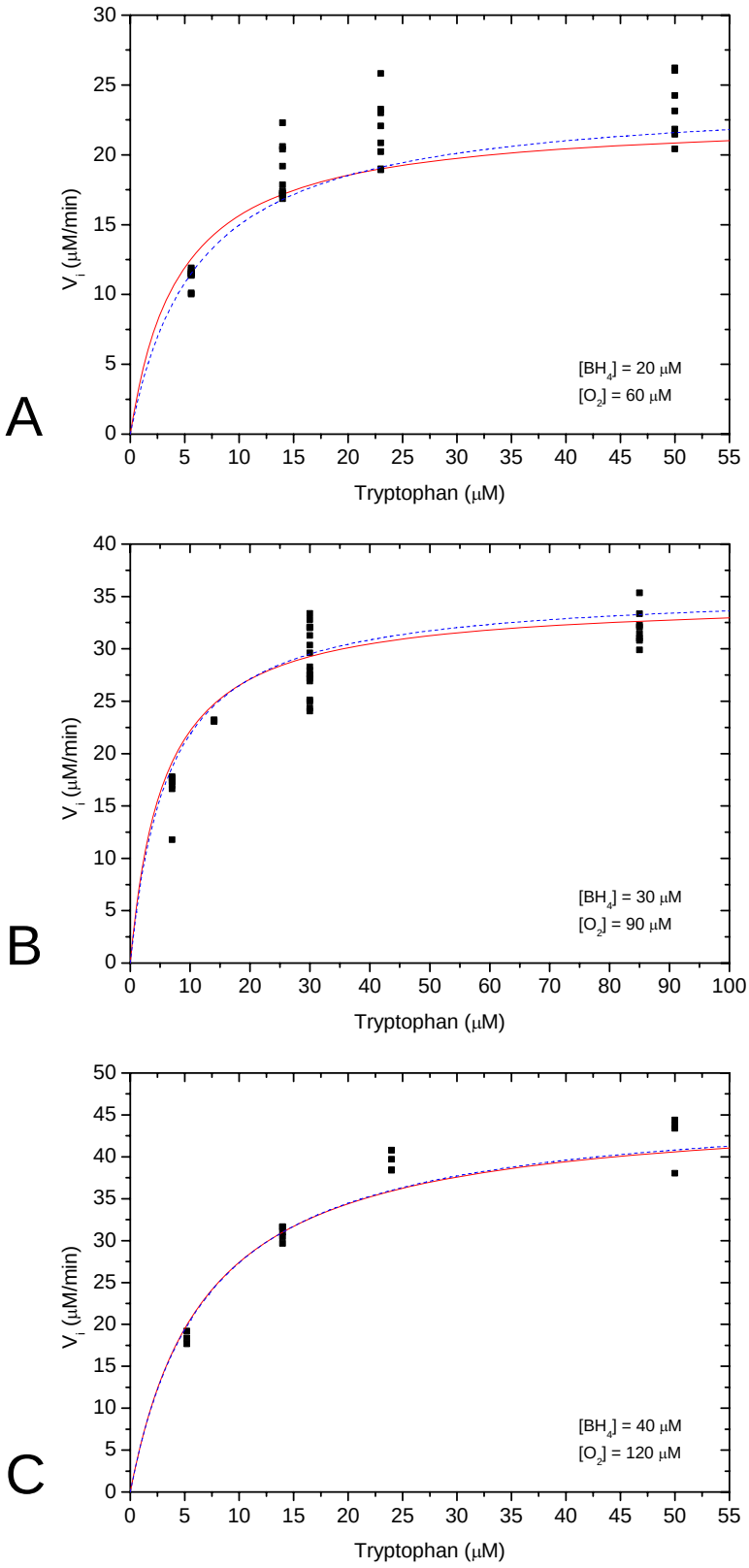

Figure 7.5 Initial rates measured at varied tryptophan concentration with the concentrations of BH_4 and O_2 in: **(A)** 20 μM and 60 μM, **(B)** 30 μM and 90 μM, **(C)** 40 μM and 120 μM. The red curve is the fitted ordered rate equation with BH_4 as substrate B. The dashed blue curve is the fitted ordered A random B-C rate equation with tryptophan as substrate A.

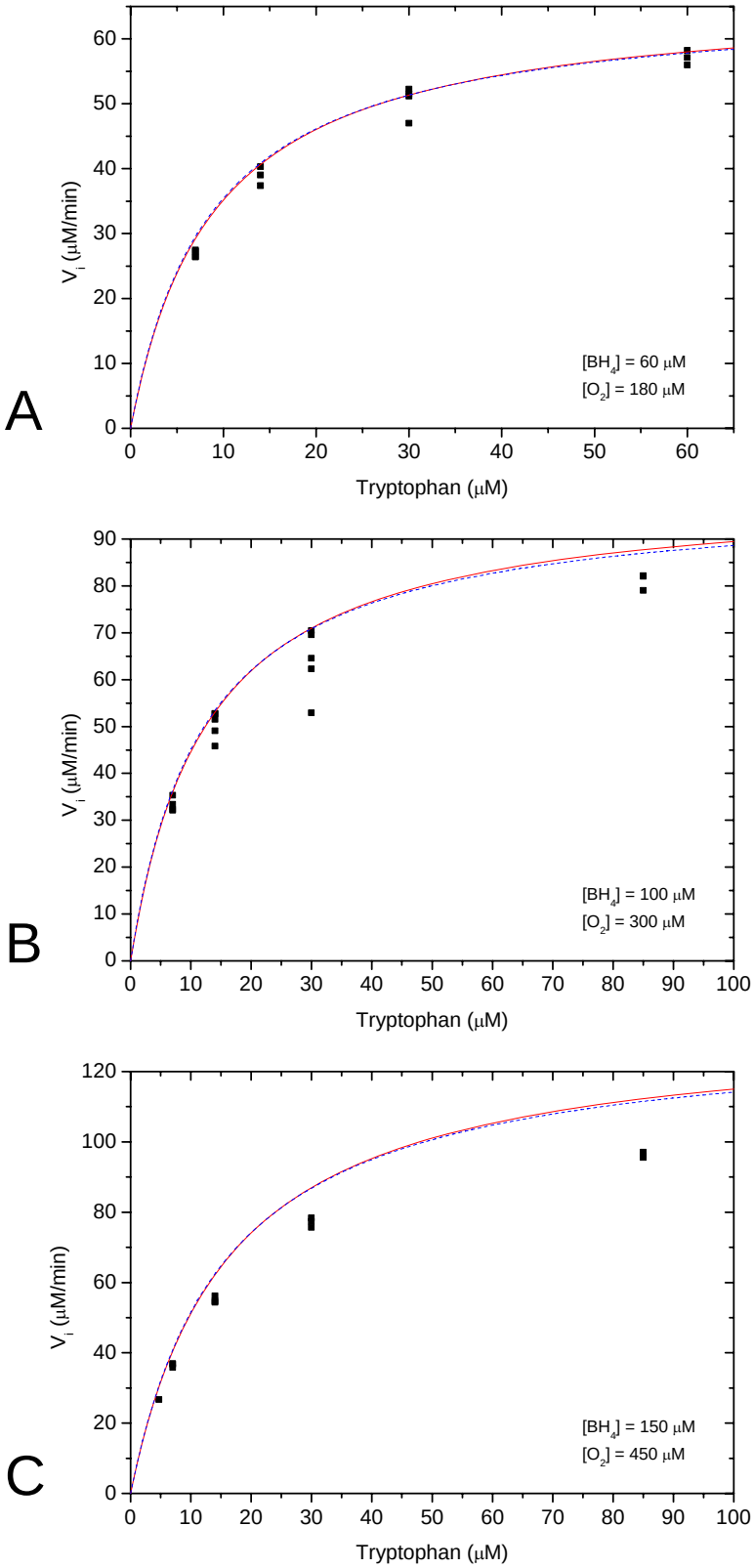

Figure 7.6 Initial rates measured at varied tryptophan concentration with the concentrations of BH_4 and O_2 in: **(A)** 60 µM and 180 µM, **(B)** 100 µM and 300 µM, **(C)** 150 µM and 450 µM. The red curve is the fitted ordered rate equation with BH_4 as substrate B. The dashed blue curve is the fitted ordered A, random B-C rate equation with tryptophan as substrate A.

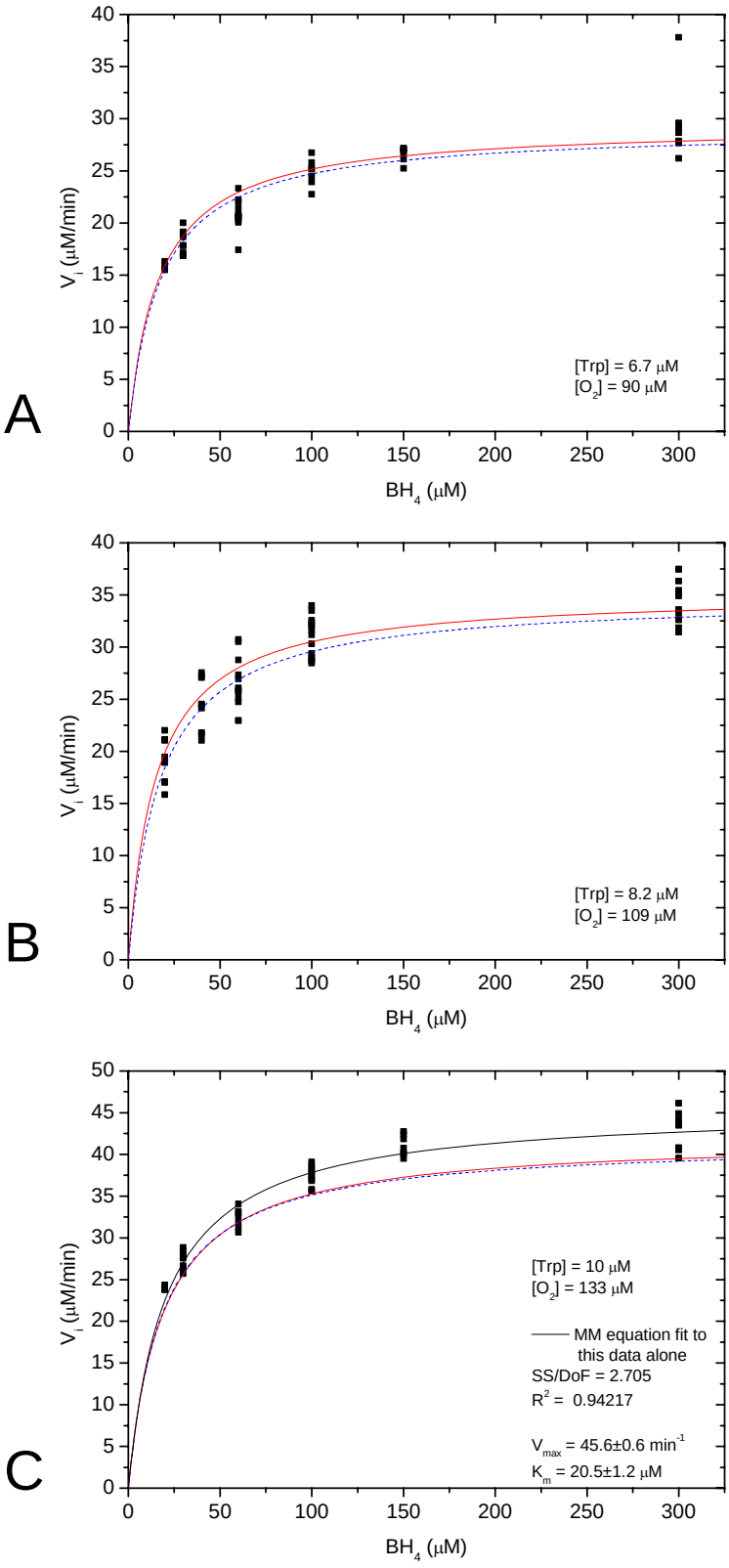

Figure 7.7 Initial rates measured at varied BH_4 concentration with the concentrations of tryptophan and O_2 in: **(A)** 6.7 µM and 90 µM, **(B)** 8.2 µM and 109 µM, **(C)** 10 µM and 133 µM. The red curve is the fitted ordered rate equation with BH_4 as substrate B. The dashed blue curve is the fitted ordered A, random B-C rate equation with tryptophan as substrate A. Equation 5.1 has been fitted (black) to this data alone for comparison with the *cg*TPH1 data in figure 6.4.

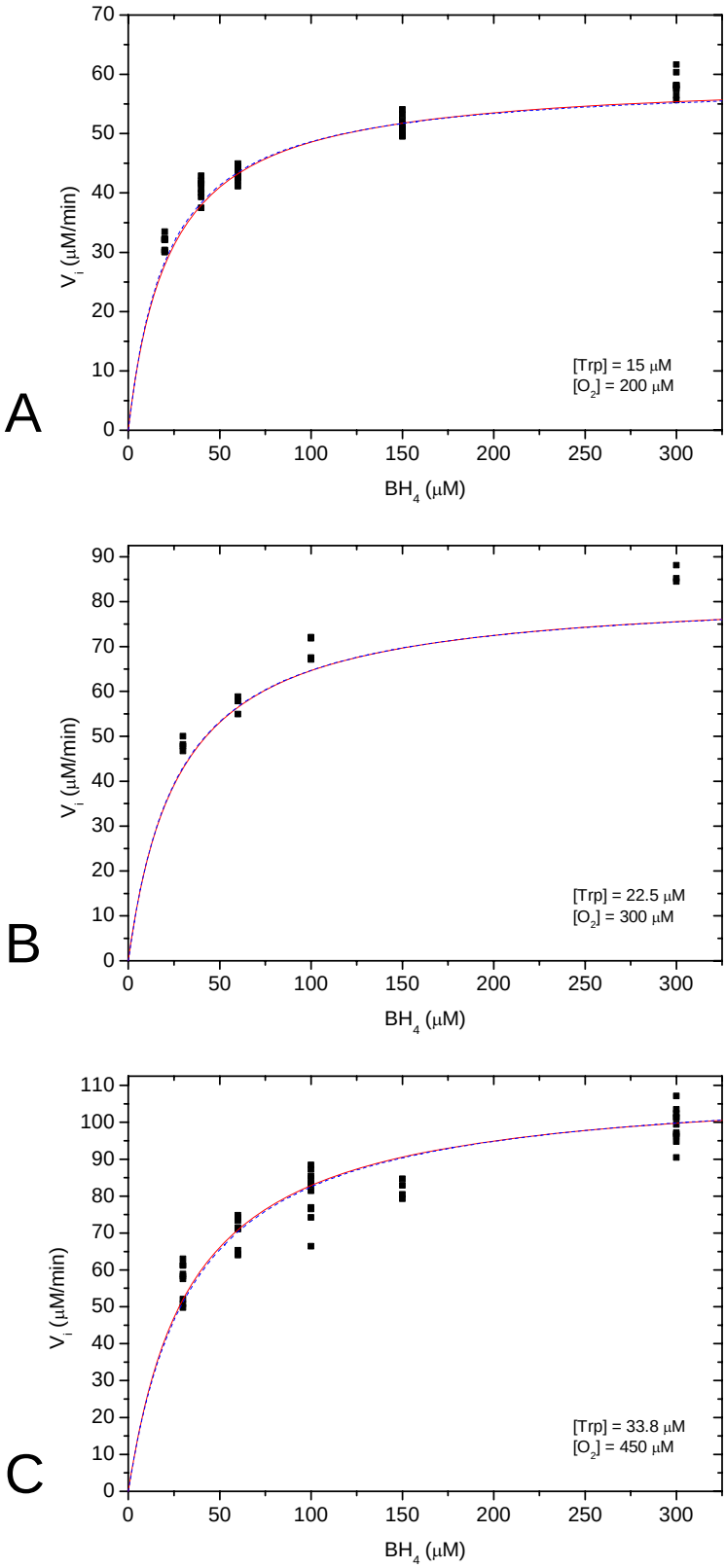

Figure 7.8 Initial rates measured at different BH_4 concentration. The tryptophan and O_2 concentrations are in: **(A)** 15 µM and 200 µM, **(B)** 22.5 µM and 300 µM, **(C)** 33.8 µM and 450 µM. The red curve is the fitted ordered rate equation with BH_4 as substrate B. The dashed blue curve is the fitted ordered A random B-C rate equation with tryptophan as substrate A.

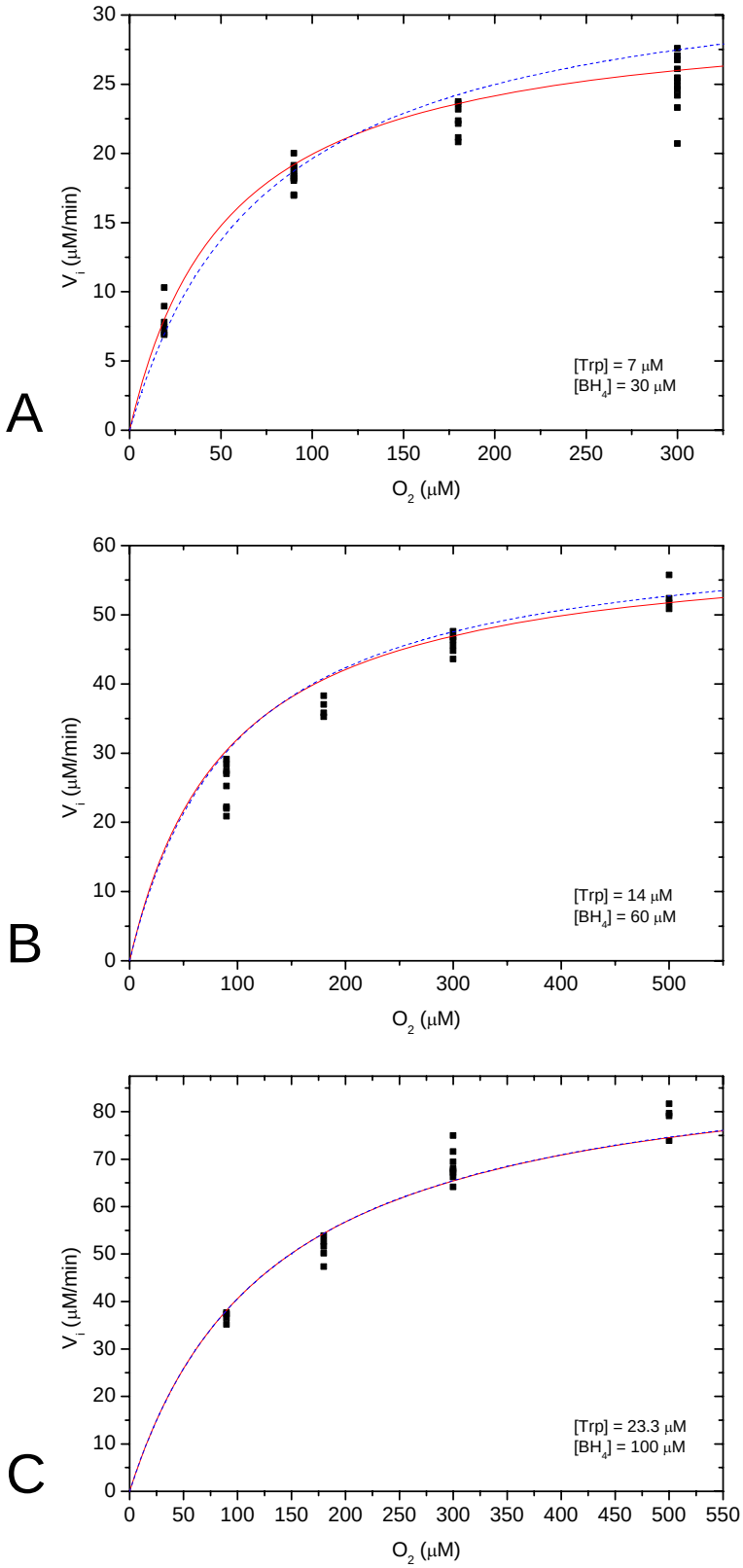

Figure 7.9 Initial rates measured at varied O_2 concentration. The concentrations of tryptophan and BH_4 are in: **(A)** 7 µM and 30 µM, **(B)** 14 µM and 60 µM, **(C)** 23.3 µM and 100 µM. The red curve is the fitted ordered rate equation with BH_4 as substrate B. The dashed blue curve is the fitted ordered A random B-C rate equation with tryptophan as substrate A.

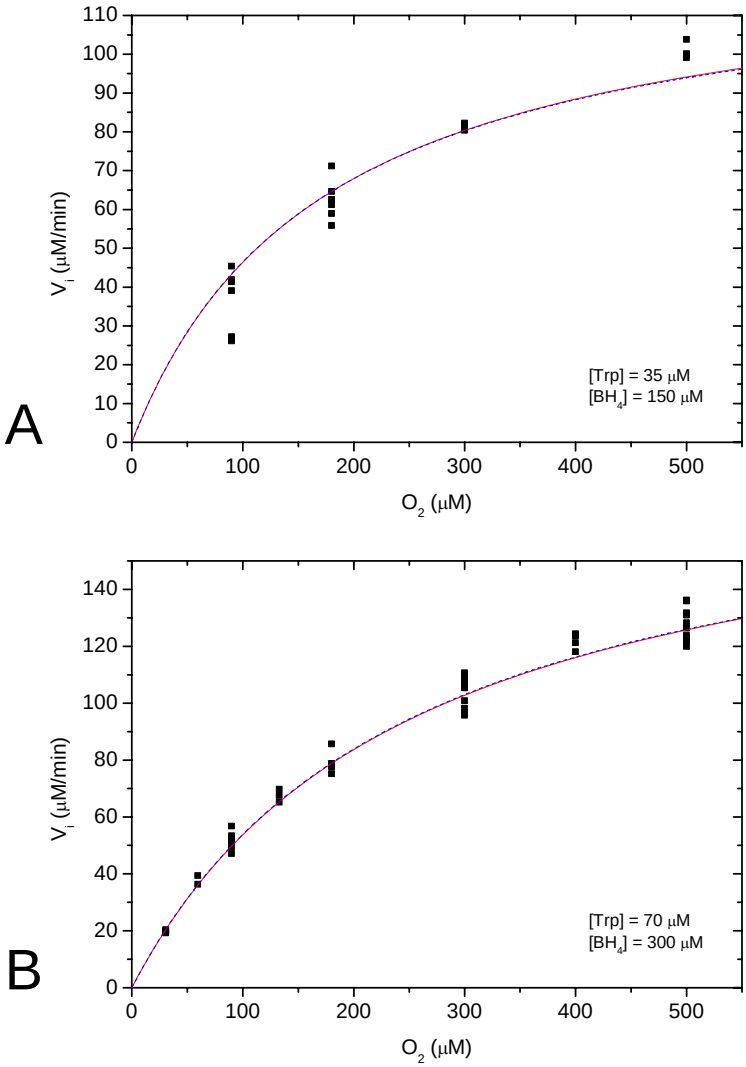

Figure 7.10 Initial rates measured at varied O_2 concentrations. The concentrations of tryptophan and BH_4 are in: **(A)** 35 µM and 150 µM, **(B)** 70 µM and 300 µM. The red curve is the fitted ordered rate equation with BH_4 as substrate B. The dashed blue curve is the fitted ordered A random B-C rate equation with tryptophan as substrate A.

7.5.2 Discussion of the results of the global curve fitting

Since the four rate equations (equations 5.5, 5.8, 5.9 and 5.10) that fit the data the best are all sequential mechanisms it can be concluded that *ch*TPH2 follows a sequential mechanism.

As can be seen in figures 7.5-7.10 the curves of the two rate equations fitting best to the data are quite similar, but since the sum of squares is lower for the ordered A, random B-C equation fit, this is the best fit. This means that the *ch*TPH2 mechanism probably follows an ordered binding of tryptophan as the first substrate followed by a random binding of BH_4 or O_2 either in the rapid equilibrium or in the steady-state fashion (scheme 5.6). The reaction then proceeds when all three substrates are bound in *ch*TPH2.

7.6 Overall discussion

In the literature there are no reports of steady-state mechanism analysis of TPH, but comparable studies have been made on rat TH [95] and *Cv*PAH [96,97]. Fitzpatrick used the same method with rat TH as used in this study and concludes that the mechanism is ordered with $6MePH_4$ binding as the first substrate (based on inhibitions studies), O_2 binding as the second (binding in a rapid equilibrium fashion) and tryptophan as the last substrate [95]. Volner *et al.* uses the method for *Cv*PAH used in this study. Additionally Volner *et al.* also uses the method where one of the substrates is held at a saturating level, and inhibition studies. Volner *et al.* concludes that the mechanism is ordered with $DMPH_4$ binding first, followed by phenylalanine and O_2 as the last substrate [97]. Pember *et al.* also used the method use here with *Cv*PAH and also concluded an ordered A random B-C mechanism but with O_2 as substrate A [96]. As mentioned in section 2.7 Pember *et al.* at the time thought that *Cv*PAH was a Cu protein [98]. As seen, several different steady-state mechanisms have been reported and the results here support the mechanism determined by Pember *et al.* but with tryptophan as substrate A instead of O_2. These examples show that there is no general consensus on the binding order of the substrates, but the mechanism is a sequential mechanism in all cases.

The inhibition by O_2 has also been reported for bovine TH by Oka *et al.* [101]. Oxygen inhibition of bovine TH was observed already at 40 - 90 µM being dependent on the BH_4 concentration [101]. The inhibition observed in this study is at much higher O_2 concentrations and the mechanism of inhibition in bovine TH and c*h*TPH2 might not be the same. The O_2 inhibition in bovine TH observed by Oka *et al.* could not be confirmed by Fitzpatrick using rat TH [95]. The O_2 inhibition observed in this study could be caused by O_2 binding in the reactive site preventing the other substrates in binding correctly. It might also bind directly to the iron, probably oxidising Fe^{2+} to Fe^{3+}. The oxidation of iron is a possible explanation for the inhibition, since the iron then has to be reduced to Fe^{2+} to be in the catalytic active state.

Further investigations will be needed to determine whether the kinetic mechanism in c*g*TPH1 and c*h*TPH2 is the same or not. If the substrate inhibition by tryptophan in c*g*TPH1 is uncompetitive, which is typical for a sequential mechanism [252], this indicates that tryptophan is the second substrate to bind in c*g*TPH1 (see section 5.3 and 6.4.2). This would then imply a different kinetic mechanism for c*g*TPH1 than the one proposed in this study for c*h*TPH2 where tryptophan binds as the first substrate.

7.6.1 Further kinetic analyses of c*h*TPH2

The results from the enzyme kinetic measurements above indicate that the kinetic mechanism is an ordered A random B-C mechanism with tryptophan as substrate A. This result should be supported by inhibition studies [252,259], which unfortunately could not be done within the time limit of this project. The inhibition studies could for example be performed with BH_2 which is a non-reactive BH_4 analogue, and should be a competitive inhibitor towards BH_4. Phenylalanine or 5-fluorotryptophan should be a competitive inhibitor towards tryptophan and should also be tested.

The measurements with varied tryptophan should also be extended to higher concentrations of tryptophan to explore if substrate inhibition is observed. In case of observed substrate inhibition, the type of substrate inhibition should be identified (see section 5.3).

Product inhibition by 5-hydroxytryptophan should also be studied in order to determine which product leaves the enzyme as the first.

7.7 Conclusion

Since it could not be concluded that any of the replots fit a certain mechanism, no conclusion could be drawn on the type of mechanism by analysing the data this way.
From the global curve analysis it can be concluded that the c*h*TPH2 kinetic mechanism is a sequential mechanism. It can also be concluded that the ordered A random B-C mechanism with tryptophan as substrate A fits the data best. The fit of ordered mechanism with BH_4 as substrate B is close to the fit for the ordered A random B-C. None of these mechanisms have BH_4 as the substrate bound first.

CHAPTER EIGHT

8 Crystallisation of proteins

Determination of the three-dimensional structure of a protein by X-ray crystallography requires growth of suitable crystals. This is the major obstacle in protein X-ray crystallography. This chapter will serve as a short introduction to some aspects of protein crystallisation and crystal annealing, which will be useful when proceeding to the next chapter.

8.1 Nucleation and growth of protein crystals

Protein crystals grow from a supersaturated solution of the protein [271]. Before a crystal can grow, stable nuclei have to be formed. Stable nuclei are small more or less ordered aggregations of protein molecules with a size large enough not to spontaneously dissolve [272]. Different degrees of protein supersaturation can be obtained as illustrated in the phase diagram in Figure 8.1. The degree of supersaturation necessary for nucleation is higher than that for crystal growth. The probability of nucleation is dependent on the degree of supersaturation, so if a high degree of supersaturation is reached a large number of nucleations might occur [272].
When stable protein nuclei have formed in the supersaturated state, protein molecules will start to order themselves in a crystal lattice. Because of the interactions formed in the crystal lattice, the crystal form is an energetically more favourable state than the supersaturated state of the protein. The crystals will grow until the protein concentration is decreased to the point of saturation [272]. The growth rate is dependent on the degree of supersaturation. Since the risk of crystal growth defects tends to be higher at higher growth rate, the desired degree of supersaturation should be just high enough for nucleation to occur. In this way fewer and better crystals should be obtained [272].
If the degree of supersaturation becomes too high the protein may form spherulites or phase separations, but more commonly the protein will form non-specific aggregates seen as amorphous precipitation (see Figure 8.1). If the supersaturation is too high the rate of precipitate formation is higher than that of crystal formation. The crystal form is still a lower energy state than the precipitate and this is why protein crystals sometimes grow concomitantly with the dissolution of precipitate [272].
The solubility of a protein in solution is dependent on various factors such as pH, temperature and the concentration of different precipitants (see section 8.3). Many other factors can also influence the crystallisation of a protein. Some examples are: purity of the protein, organism source of the protein, substrates, co-factors, reducing or oxidising environment, surfaces of the crystallisation vessel, vibration and sound and many more [272,273].

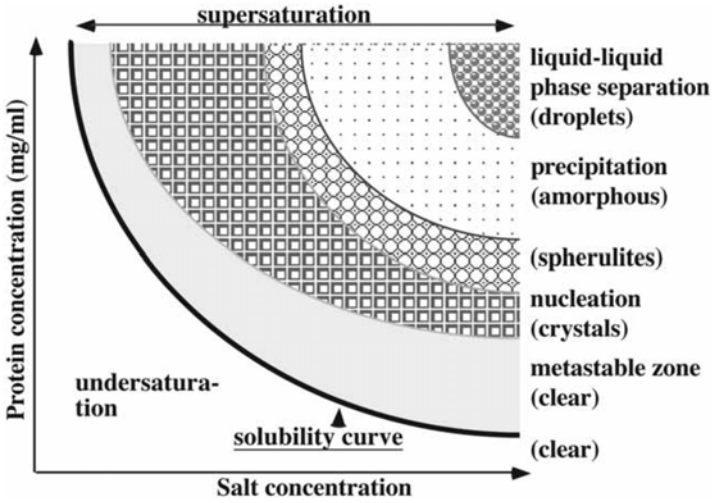

Figure 8.1 A phase diagram showing the different states of the protein phases [274]. This is an example phase diagram and all the states might not exist for a given protein and the sizes of the phases might vary greatly.

The interactions formed between the protein molecules in a crystal are essential for crystal growth. Proteins are sensitive and dynamic macromolecules that might easily loose their native structure. Therefore, it is generally accepted that the solution (the mother liquor) optimal for crystal growth supports the most structurally homogeneous state of the protein, which at the same time optimises the possible intermolecular interactions [272]. To determine the optimal conditions for crystal growth of a given protein is not an easy task. Currently, the conditions for crystallisation can not be predicted and are usually determined by screening a large number of possible conditions.

8.2 Crystallisation screens

The process of screening for crystallisation conditions is commonly done by using sparse matrix screens. Sparse matrix screens contain different solutions that have proven successful in the crystallisation of numerous proteins. The first sparse matrix screen was described by Jancarik and Kim [275]. Several companies sell this screen and small variations may exist, for example in whether the buffer pH is reached by using HCl or acetic acid [276].
Another sparse matrix screen is the commercially available JCSG+ screen, which is developed through experience gained from a structural genomics project [277].
More systematic (grid) screens are also used in the initial screening [277,278,279]. Some of these are the PEG/Ion screens or the PACT screen [277], while the Index screen from Hampton Research is a combination of sparse matrix and grid screening [280].

8.3 Precipitants

Precipitants are compounds that decrease the protein solubility. The supersaturation necessary for nucleation and crystal growth is usually obtained by increasing the precipitant concentration in the protein solution. This can be done momentarily using batch crystallisation or in a more gradual manner using dialysis or the vapour diffusion method [281]. In the vapour diffusion method the initial precipitant

concentration in the non-equilibrated drop is typically half of that in the reservoir. This causes water vapour to diffuse from the drop to the reservoir until equilibrium is reached. In the vapour diffusion method the precipitant serves to increase the protein concentration and to decrease the protein solubility [272].
Different types of precipitants are used in protein crystallisation and these are usually categorised in four groups: salts, organic solvents, long-chain polymers and low-molecular-mass polymers/non-volatile organic compounds [272]. Examples of organic solvents used as precipitants are ethanol, propanol and dioxane, while examples of low-molecular-mass polymers are polyethylene glycol (PEG) with a molecular weight of 200 or 400 g/mol. A typical non-volatile organic compound would be 2-methyl-2,4-pentanediol [272]. Salts and PEGs are the most successful precipitants used in protein crystallisation and a short description will be given in the following sections.

8.3.1 Salts as precipitants

The ionic strength of a solution greatly affects the solubility of proteins [272]. At very low ionic strength no ions are available to satisfy the electrostatic requirements of the protein molecules. The protein molecules will then seek to balance the electrostatic requirements with themselves which leads to aggregation or to crystals if it happens in an order fashion. This process is called salting-in [272].
As the ionic strength is increased the electrostatic requirements are satisfied and the solubility of the protein is increased. If the concentration of salts with strongly hydrated ions is further increased the protein solubility is decreased by the process called salting-out. The salting-out process is more complicated and can be explained in two ways whether one looks at the polar or non-polar surface of a protein [271,282,283,284]. For a typical protein 50-60% of the surface is non-polar [285]. The surface tension of the solvent is increased by strongly hydrated anions such as sulphate. The increased surface tension strongly affects the non-polar surface and will force the protein to decrease its surface accessible area by either crystallisation or aggregation [284]. For the polar surface of a protein, the solubility is highly dependent on the effectiveness of the hydration layers. The second hydration layer is disturbed by strongly hydrated anions making the bulk solution a less good solvent for the protein. The protein will therefore try to decrease the solvent accessible surface [284]. The effect of different ions on the solubility and of salting-out proteins was observed already in 1888 by F. Hofmeister and the order of the ions are therefore called the Hofmeister series [284]. Some of the ions are listed here in their efficiency in lowering the solubility of a negatively charged protein. For anions: $HPO_4^{2-}/H_2PO_4^- > SO_4^{2-} > CH_3COO^- >> Cl^- > NO_3^-$ and for cations: $Li^+ > Na^+ \approx K^+ > NH_4^+ > Cs^+$[284].
For a positively charged protein this order is reversed [283]. Both inorganic and organic salts are used extensively in crystallising proteins [272,286]. Some specific ions, for example different divalent cations may have essential roles in the stabilisation of the protein structure or in crystal lattice and are often tested as additives in a concentration of a few mM [287].

8.3.2 Polyethylene glycols as precipitants

PEGs with molecular weights ranging from 400 Da to 20 kDa have been used successfully in the crystallisation of many proteins [271,288,289]. PEGs have a random and flexible structure which occupies a large volume. The addition of PEGs to a protein solution reduces the solvent volume available for the protein resulting in favoured

attraction between the protein molecules [271,290]. The solubility of a protein decreases exponentially with the increasing concentration (%w/v) of the PEG and the typical concentration range used for crystallisation is 4-25% (w/v) [289]. An advantage of using PEG is that the PEG concentration interval yielding crystals is larger for a given protein, than that typically observed for salts [271]. This is valuable both in the screening and optimisation process, since crystals may form even though the PEG concentration differs a bit from the optimal concentration opposed to salts where the concentration often has to be spot-on for crystal formation. Polypropylene glycol and polyethylene glycol monomethyl ether (MPEG) are also used for crystallisation, but in a lesser extent than PEGs [291].

8.4 Additives used in crystallising proteins

Addition of certain ions or small organic molecules to the mother liquor may in some cases be necessary to establish the stabilising contacts between protein molecules in a crystal [287,292,293,294]. Typical additives would be substrates or substrate analogues, co-factors, linker molecules and osmolytes. Reports by McPherson *et al.* and Larson *et al.* suggest that screening additives may be a successful alternative to the more common buffer/precipitant screening [293,294]. Neutral detergents are usually used in the crystallisation of membrane proteins, but have also been reported to improve the crystallisation for some soluble proteins [295].

8.5 Annealing of protein crystals

Protein crystals are very seldom perfect crystals, but are instead made of mosaic blocks of ordered molecules. The mosaic blocks are generally well aligned but upon flash-freezing the mosaic blocks might rearrange relative to each other. If the mosaic blocks are not well aligned the crystal is said to have a high mosaicity.
Annealing of protein crystals is done to decrease the mosaicity. The term annealing is borrowed from metallurgy. Protein crystal annealing refers to a flash-frozen protein crystal being transferred from liquid nitrogen to a small drop of mother liquor with added cryo-protectant typically at 4˚C or room temperature [296]. After 3 minutes in the cryo-protectant buffer the crystal is remounted in the loop and flash-frozen in liquid nitrogen or cold nitrogen gas stream. This process may be repeated several times. It is essential that a suitable cryo-protectant is found so that the crystal is stable in the cryo-protectant buffer [296]. The purpose of the cryo-protectant is to prevent the formation of ice crystals in the mother liquor when the protein crystal is flash-frozen. Examples of typical cryo-proctectants are glycerol, ethylene glycol and PEG 400 [297].
It is believed that the annealing heal dislocation defects from the flash-freezing by recrystallisation at the dislocations [296]. This will decrease the mosaicity of the crystal. Resolution improvement is sometimes also observed upon annealing and this is believed to be caused by diffraction peak sharpening allowing detection of peaks that prior to annealing were too diffuse. Annealing is recommended for all flash-frozen crystals that do not diffract satisfactorily [296].

CHAPTER NINE

9 Crystallisation of TPH variants

As described in chapter 4 it is possible to obtain c*g*TPH1, c*h*TPH2 and ct*h*TPH2 in purities and amounts suitable for crystallographic characterisation. In this chapter I will describe the crystallisation experiments done with these three variants. The results from the crystallisation as well as collected diffraction data and structure solution will be presented. The crystallisation conditions of c*g*TPH1 were found by Charlotte R. Petersen in her M.Sc. project, in which I was a co-supervisor [15].

9.1 Crystallisation of c*g*TPH1

9.1.1 The initial crystallisation of c*g*TPH1

Initial screenings were done with Stura Footprint Screens (appendix 2.1), Index Screen from Hampton Research (appendix 2.2), JCSG+ screen from Qiagen (appendix 2.3) and PACT screen from Qiagen (appendix 2.4). The results from Index, JCSG+ and PACT screens will be described first.

9.1.1.1 Crystallisation trials using Index, JCSG+ and PACT screens

The c*g*TPH1 for the crystallisation experiments was purified as described in section 4.1.2.1. A c*g*TPH1 sample of 100 µL was mixed with 50 µL of ice cold 20 mM Tris/NaOH, 100 mM $(NH_4)_2SO_4$, pH 8.5. The solution was filtered through a 0.22 µm Ultrafree-MC durapore membrane centrifugal filter from Millipore at 8000 × g and 4˚C for 4 min. The protein concentration was determined using ε_{280} = 37820 M^{-1} cm^{-1}. The c*g*TPH1 solution was further diluted to the desired concentration with 20 mM Tris/NaOH, 100 mM $(NH_4)_2SO_4$, pH 8.5.
The Index, JCSG+ and PACT screens were set up at the Department of Chemistry at University of Copenhagen using an Oryx 8 robot from Douglas Instruments. The screens were set up with three drops per well. The c*g*TPH1 concentrations in the non-equilibrated drops were 4.2 mg/mL with 8 times molar excess of BH_4, 6.2 mg/mL with 8 times excess of BH_4 and 4.3 mg/mL without any BH_4, respectively. The trays were stored at 6˚C.
Precipitation was observed in most drops. Crystals were observed in several drops, but most of these drops contained calcium which could form $CaSO_4$ crystals with the sulphate from the c*g*TPH1 buffer (see section 4.1.2.1). The conditions containing calcium were tested with the sulphate containing buffer. Crystals appeared in all these drops and we concluded that these were most likely $CaSO_4$ crystals. The crystals from drops without calcium did not diffract and could furthermore not be reproduced.

9.1.1.2 Crystallisation trials using Stura Footprint screens

The Stura Footprint screens 1 and 2 were set up as sitting drop experiments. The trays were placed on ice during addition of 500 µL crystallisation solutions to the wells and during drop set up. The drops were set up with 2 µL crystallisation solution + 2 µL protein solution. The concentration of c*g*TPH1 in the protein solution was 3.5 mg/mL. The trays were sealed with clear sealing tape and stored at 4˚C.

9.1.2 The initial crystals of c*g*TPH1 and data collection

Semi crystalline assemblies were observed in the drop containing 1.32 M NaH_2PO_4/K_2HPO_4 pH 7.0. Trials to optimise these conditions were unsuccessful [15].
Protein crystals were observed after 40 days in the drop containing 0.2 M imidazole malate pH 8.5, 22.5 % PEG 10000. The larger crystals were flash-frozen in the mother liquor for testing at a synchrotron. The smaller crystals left in the drop were stained with methylene blue (Izit) (see figure 9.1). The crystals were brought to MAX-lab in Lund, Sweden, beamline 911-5. The crystals flash-frozen in the mother liquor diffracted to 8 Å and ice rings from the mother liquor were observed. At the synchrotron, cryo-protectant solutions were tested on the remaining crystals in the drop. Some crystals were successfully flash-frozen in a cryo-protectant solution with PEG 400 added to approximately 20% (v/v). Unfortunately these did not diffract. At this point it was unclear whether it was because of deterioration from storage in the drop for several weeks or if they were destroyed by cryo-protectant.

Figure 9.1 Crystals of c*g*TPH1 stained with methylene blue, crystallised with 0.2 M imidazole malate pH 8.5, 22.5% PEG 10000, c*g*TPH1 concentration was 3.5 mg/mL and the drops were stored at 4˚C [15].

Reproducing the crystallisation was successful only with the solution 0.2 M imidazole malate pH 8.5, 22.5% PEG 10000 from Molecular Dimensions. Drops setup with this solution in the sitting drop manner yielded new crystals after 70 days. Few crystals were present and we were afraid that the crystals would be destroyed in testing cryo-protectant solutions. These crystals were therefore flash-frozen in the mother liquor, and stored in liquid nitrogen. A data set was collected to 3.0 Å at the European Synchrotron Radiation Facility (ESRF), beam line ID 14-3. Ice rings were observed in the diffraction pattern.
After data collection several crystals were annealed in a cryo-solution of 20%(v/v) PEG 400, 0.2 M imidazole malate pH 8.5, 22.5% PEG 10000. Two crystals dissolved in the cryo-solution while one crystal was successfully transferred and flash-frozen. Through this annealing, the mosaicity of the crystal decreased and the diffraction limit improved from 5 Å to 3.5 Å. Diffraction patterns from the crystal, before and after transfer to the cryo-solution are shown in figure 9.2.

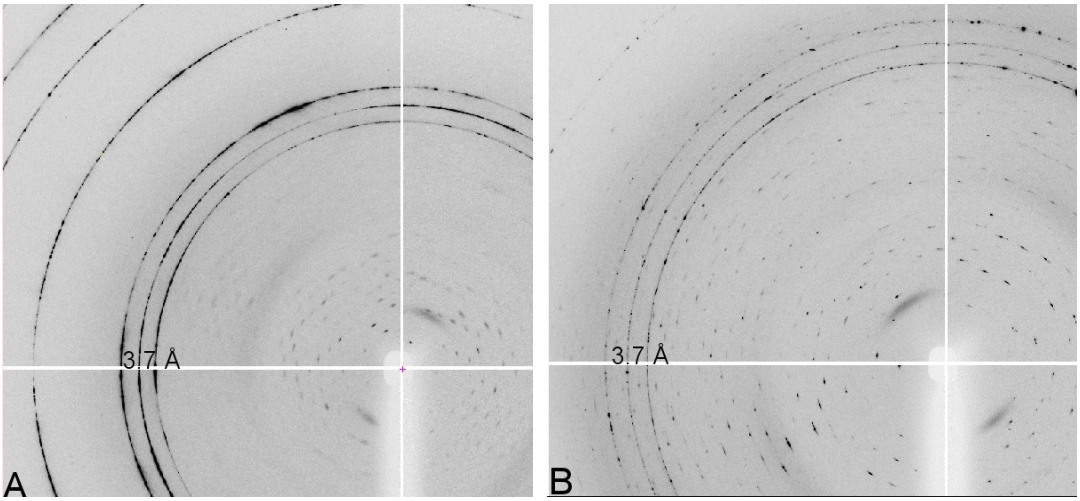

Figure 9.2 The diffraction patterns of the same crystal. **(A)** Before annealing. **(B)** After annealing. The middle ring of the three ice rings indicates 3.7 Å.

Data processing, structure solution and refinement were done by Associate Professor Pernille Harris. The reflections could be indexed to a lattice with the dimensions 61.5 Å, 79.2 Å, 86.8 Å and 62.9˚, 89.9˚and 89.9˚. The ice rings were cut out of the data, giving a reduced completeness of data. The data statistics for the possible space groups are listed in table 9.1.

Table 9.1 Data collection and processing statistics for the possible space groups for the c*g*TPH1 crystal.

Space group	P1	$P2_1$	C2	$C222_1$
Crystallisation conditions	0.2 M imidazole malate pH 8.5, 22.5% PEG 10000 Hanging drop, 4˚C			
X-ray source	ID14-3, ESRF			
Detector	ADSC Quantum CCD			
Wavelength (Å)	0.931			
Data collection temp. (K)	100			
Resolution limit (Å)	20- 3.0 (3.2-3.0)			
No. reflections	48427(9318)	48342 (9311)	48371 (9331)	46441 (9291)
Unique reflections	24728(4759)	13344 (2528)	13470 (2566)	6833 (1291)
Redundancy	1.96 (1.96)	3.62 (3.68)	3.59 (3.64)	6.80 (7.20)
Completeness (%)	84.3 (91.5)	87.8 (94.9)	89.6 (97.0)	90.4 (99.9)
R_{merge}	11.4 (30.5)	14.7 (38.4)	15.3 (38.4)	16.4 (39.9)
$\langle I/\sigma(I)\rangle$	5.67 (2.37)	7.08 (3.06)	6.98 (2.97)	9.55 (4.24)
Unit cell parameters				
a (Å)	61.5	79.2	154.5	78.1
b (Å)	79.2	61.5	79.2	152.4
c (Å)	86.8	86.9	61.5	60.6
α (˚)	62.9	90.0	90.0	90.0
β (˚)	89.9	117.2	90.1	90.0
γ (˚)	89.9	90.0	90.0	90.0
Solvent content (%)	52.8			
Matthews coef. ($Å^3\ Da^{-1}$)	2.61			

[a] Values in parentheses are for the outermost resolution shell.

[b] $R_{merge} = \sum_i |I_i - \langle I_i \rangle| / \sum_i I_i$, where $\langle I_i \rangle$ is the average of I_i over all symmetry equivalents.

The structure could be solved by molecular replacement in space group P1 with four molecules in the asymmetric unit using the structure of the catalytic domain of phenylalanine hydroxylase (PDB entry 1J8U) [84]. The structure could be refined to an R_{free} = 32.7%. Even though the model is not of superior quality, differences in the overall structure compared to the structure of c*h*TPH1 are observed and will be presented and discussed in section 9.4.

9.1.3 Further crystallisation of c*g*TPH1

To optimise the crystallisation of c*g*TPH1 a 0.2 M imidazole malate pH 8.5, 22.5 % PEG 10000 solution, a 50 % PEG 10000 solution and a 2 M imidazole malate pH 8.5 solution were bought from Molecular Dimensions.

9.1.3.1 Trials to optimise crystallisation of c*g*TPH1

Several conditions were tested in trials to optimise the crystallisation of c*g*TPH1. A full list of tested conditions is presented in appendix 3. In summary the c*g*TPH1 concentration was varied between 0.94 – 6.1 mg/mL. c*g*TPH1 from a new purification batch was tested. The PEG 10000 concentration was varied between 5 - 29%. A 0.2 M malonate imidazole borate (MIB) buffer [298] pH 7.0, 7.5, 8.0, 8.5 was tried instead of imidazole malate buffer. Addition of BH_4 or BH_2 to the drops was tested. DTT, β-mercaptoethanol and EDTA added to the reservoir solution of 0.2 M imidazole malate pH 8.5 and 22.5% PEG 10000 were tested. In addition to this the non-volatile additives from (the old version) Hampton's additive screens 1, 2 and 3 (appendix 2.5) and Hampton's detergent screens 1-3 (appendix 2.6) were tested with the condition 0.2 M imidazole malate, 22.5% PEG 10000. All trays were stored at 4˚C.

9.1.4 Results of optimisation trials and data collection

9.1.4.1 Crystals from the optimisation trials

The crystals proved difficult to reproduce and very few were observed. In a few drops with 17-22.5% PEG 10000 very small stacks of needles appeared. In one drop with 0.2 M imidazole malate pH 8.5, 18% PEG 10000 three crystals appeared after 3 months. These crystals were flash-frozen in the cryo-protectant solution determined earlier (section 9.1.2) [15] and stored in liquid nitrogen. These crystals were tested at the ESRF synchrotron (see section 9.1.4.2).
Crystals (see figure 9.3) also appeared after 3 weeks, in drops set up with 0.2 M MIB buffer pH 8.5, 22.5% PEG 10000 with a protein concentration of 3.5 mg/mL. These were flash-frozen in the mother liquor, thawed in 0.2 M MIB buffer pH 8.5, 20% PEG 400, 22.5% PEG 10000 and flash-frozen again, and stored in liquid nitrogen. These crystals appeared close to the end of this project and the crystals could not be tested before the deadline.

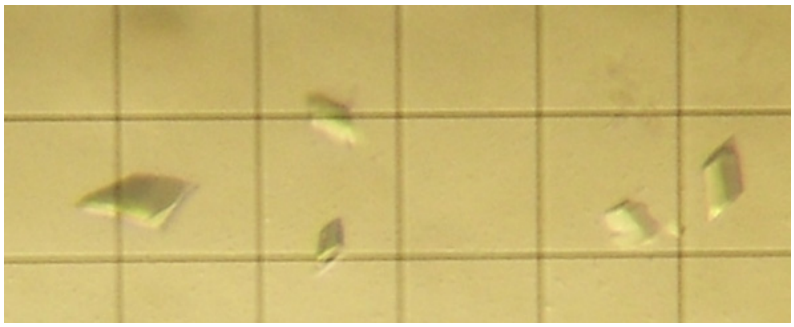

Figure 9.3 Crystals of c*g*TPH1 grown in 0.2 M MIB buffer pH 8.5, 22.5% PEG 10000, c*g*TPH1 concentration 3.5 mg/mL. One square in the mesh is 90 × 90 µm.

9.1.4.2 Data collection on crystals from optimisation trials

Three crystals grown in 0.2 M imidazole malate pH 8.5, 18% PEG 10000 (see section 9.1.4.1) were brought to ESRF, beamline ID-14.1. The diffraction quality of the three crystals was tested. The best crystal diffracted to approximately 6 Å. It was determined earlier that annealing in the cryo-protectant solution decreased the mosaicity of the crystals (section 9.1.2). Therefore each crystal was annealed 1-3 times. The crystals were tested again and the annealing significantly improved the diffraction quality. A data set was collected on the best crystal diffracting to approximately 4 Å. Examples of the diffraction patterns are shown in figure 9.4.

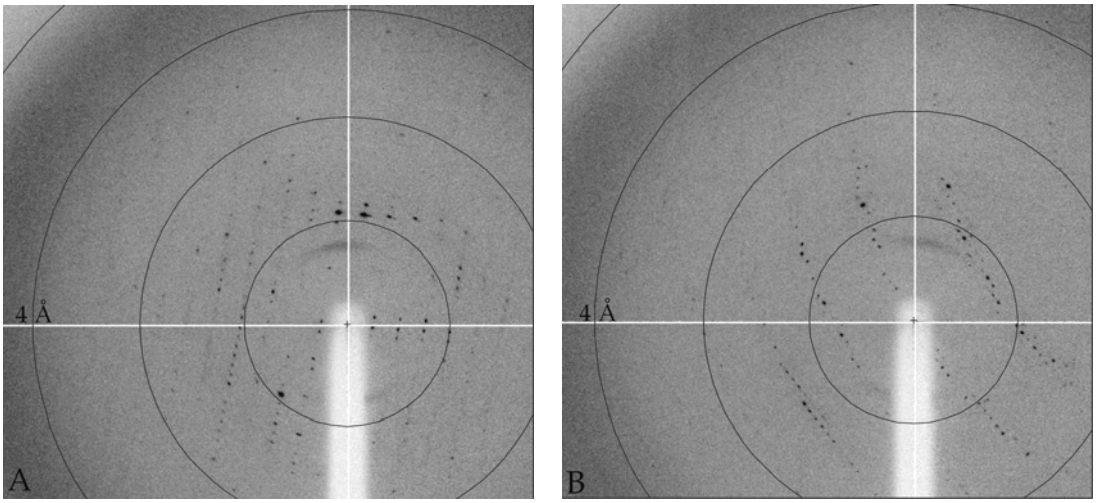

Figure 9.4 Diffraction patterns of the c*g*TPH1 crystal described in section 9.1.4 and 9.1.5 collected on ID 14-1 at ESRF. **(A)** Rotation angle 0˚. **(B)** Rotation angle 90˚. The third ring from the centre is 4 Å.

The data could be processed in space group $P2_1$ with the cell dimensions 185.8 Å, 49.9 Å, 139.6 Å and β = 110.9˚. The structure was attempted solved by molecular replacement using either the structure of c*h*TPH1 (PDB entry 1MLW) or the catalytic domain of PAH as a search model. For unknown reasons the crystal packing in all solutions were unrealistic with approximately half of the expected molecules missing. It was not possible to do any refinement of these structure solutions. Similar problems were observed for a data set collected the same day on a crystal of another protein. This crystal diffracted to 2 Å and had low mosaicity but the structure could not be refined. This indicates that some settings might have been wrong on the beam-line.

Many problems were encountered with automatic sample changer that day but this should not interfere with the data collection.

9.1.5 Discussion of the crystallisation of c*g*TPH1

It has proven difficult to optimise and even reproduce crystals of c*g*TPH1. The crystal formation usually takes from 40 to 120 days. This slow crystal growth is likely to involve the concomitant dissolution of precipitated c*g*TPH1 (see section 8.1).
A new batch of purified c*g*TPH1 should be prepared, and purity should be checked by SDS-PAGE and Western blot analysis. The structural homogeneity should be verified by dynamic light scattering [299].
Many conditions were tested in the initial screenings and none except the 0.2 M imidazole malate pH 8.5, 22.5% PEG 10000 proved successful. In the further experiments (section 9.1.4.1) crystals were formed in similar conditions (0.2 M imidazole malate pH 8.5, 18% PEG 10000 and in 0.2 M MIB, 22.5% PEG 10000). Therefore new grid screens should be set up testing the conditions around the initial conditions. More crystals combined with an optimised cryo-protectant solution will likely result in better data leading to a high resolution structure of c*g*TPH1.

9.2 Crystallisation experiments of c*h*TPH2

Initial crystallisation experiments were done with c*h*TPH2 purified and stored in a Tris buffer with pH 8.2. The pH 8.2 of this buffer proved not to be optimal for the stability and crystallisation of c*h*TPH2 and will not be described here. c*h*TPH2 purified in buffers with pH 7.2 proved more stable and suitable for crystallisation experiments. A few crystallisation experiments described in the following were done with c*h*TPH2 from a purification where the gel filtration was done in 20 mM MES/NaOH, 100 mM $(NH_4)_2SO_4$, 5% glycerol, pH 6.5. Also one crystallisation test was done to test if there was any difference in the tendency to precipitate between purified c*h*TPH2 from expression at 20˚C and 30˚C respectively. If nothing is noted the c*h*TPH2 used was from 20˚C expression in 20 mM HEPES/NaOH, 100 mM $(NH_4)_2SO_4$, 5% glycerol, pH 7.2.

9.2.1 Experimental

9.2.1.1 Preparation of trays and the c*h*TPH2 sample

The first screens showed that c*h*TPH2 had a very high tendency to precipitate even at very low protein concentrations. It was also observed that c*h*TPH2 is sensitive to temperature. Crystallisation experiments were set up with c*h*TPH2 (25 mg/mL), with 20 mM HEPES/NaOH, 100 mM $(NH_4)_2SO_4$, 5%(w/v) glycerol, pH 7.2, as the crystallisation solution. This crystallisation solution is the same as the gel filtration buffer (see section 4.1.2.2). If this experiment was set up at room temperature and kept at room temperature, precipitation was observed after one hour. When the same experiment was set up on ice and the tray moved to 4˚C immediately after, no precipitation was observed. Consequently, trays containing the crystallisation solutions were cooled at 4˚C prior to set up and the following set up were done on ice. Sitting drops were also used instead of hanging drops, since these are faster to set up and the drop is closer to the ice.

When thawed a sample of 100 µL c*h*TPH2 was centrifuged at 15000 x g for 8 min at 4˚C. The supernatant was transferred to a sterile eppendorf tube. The c*h*TPH2 concentration was determined using ε_{280} = 39310 M^{-1} cm^{-1}. The c*h*TPH2 was further diluted to the desired concentration using 20 mM HEPES, 100 mM $(NH_4)_2SO_4$, pH 7.2. Buffer without glycerol was used for dilution to decrease the glycerol concentration in the protein sample.

9.2.1.2 The c*h*TPH2 crystallisation experiments

The crystallisation experiments done with c*h*TPH2 are listed in table 9.2. Composition of the Stura Footprint 1 and 2 screens can be seen in appendix 2.1. Composition of Crystal Screen from Hampton Research is seen in appendix 2.7. Sigma's Crystallisation Basic Kit for Proteins contains the same solutions as Hampton's Crystal Screen and is therefore not listed in the appendix. Composition of Sigma's Crystallisation Extension Kit for Proteins is listed in appendix 2.8. The composition of the TPH screen which was designed for c*h*TPH2 can be seen in appendix 2.9.
Several additives have been tested in the crystallisation experiments. The function or role of some of the additives might need an explanation. BH_4, tryptophan and 5-hydroxytryptophan are substrates and product respectively. BH_2 is a substrate analogue and inhibitor. DL-4-chlorophenylalanine is an inhibitor. Hexaethylene glycol monododecylether ($C_{12}E_6$), octaethylene glycol monododecylether ($C_{12}E_8$) and dodecyl β-D-maltoside are detergents. Different metal ions are added to possibly stabilise the structure or crystal packing. Glycine, 1,3-diaminopropane and 1,4-diaminobutane are added to function as linkers.
BH_4 and BH_2 were dissolved in 10 mM HCl. Tryptophan, 5-hydroxytryptophan, DL-4-chlorophenylalanine, $C_{12}E_6$, $C_{12}E_8$ and dodecyl β-D-maltoside were dissolved in 20 mM HEPES, 100 mM $(NH_4)_2SO_4$, pH 7.2. $NiCl_2$, $CoCl_2$, $[Ru(NH_3)_6]Cl_3$, $[Co(NH_3)_6]Cl_3$ and CsCl were dissolved in water. Glycine, 1,3-diaminopropane and 1,4-diaminobutane were dissolved in water and pH adjusted to pH 7. In the experiments, the additives were added in one of three different ways. Some additives were added to the c*h*TPH2 solution prior to set up, other additives were added to the mixed drop while others again were added to the reservoir solution prior to set up. When an additive was added to the reservoir solution in the TPH screen a concentrated stock solution was used so that the dilution of the other components was minimised. The method used for adding the additive is also listed in table 9.2.

9.2.2 Results of the crystallisation experiments of c*h*TPH2

No crystals of c*h*TPH2 were observed in any of the drops. The following description and discussion will be on the properties observed from the crystallisation experiments and an explanation for the composition of the TPH screen. The first screens showed that c*h*TPH2 had a very high tendency to precipitate even at very low protein concentrations. For example precipitation was observed in all drops of the Crystal Screen with a c*h*TPH2 concentration of 1.2 mg/mL.
For a protein to crystallise it has to be supersaturated. If the degree of supersaturation is too high precipitation occurs. If precipitation occurs in the majority of the drops in a screen one would usually decrease the protein concentration. In the case of c*h*TPH2 it could be concentrated to 32 mg/mL without any sign of precipitation (at 4˚C) indicating that it can be stored in high concentrations. A protein concentration below 1 mg/mL is usually not recommended for crystallisation.

Table 9.2 List of crystallisation experiments with *ch*TPH2. Most of the screens were designed for the experiment, while Stura, Crystal Screen, Sigma Extension Kit are commercial screens with compositions found in appendix 2. +/- means with and without the following additive. "In *ch*TPH2" means that the additive was added to the protein solution prior to drop set up. "In reservoir" means that a small volume of concentrated additive was added to the crystallisation solution.

Screen	*ch*TPH2 conc. (mg/mL)	Additive
Stura Footprint 1+2	1.5	+/- BH_4, 0.7 mM in *ch*TPH2
Crystal Screen	1.2	+/- Trp, 0.13 mM in *ch*TPH2
Crystal Screen	8, MES pH 6.5	none
Sigma screen	4	BH_2, 1 mM in *ch*TPH2
Sigma Extension Kit	4	BH_2, 1 mM in *ch*TPH2
5-18% glycerol; 0.1 M $(NH_4)_2SO_4$; HEPES pH 7.2	3, 25 4	None +/- BH_2, 8 µM in *ch*TPH2
0.2-1.2 M $(NH_4)_2SO_4$; HEPES pH 7.0	1.3, 3 4	None +/- BH_2, 8 µM in *ch*TPH2
2-8% PEG 400, 4000, MPEG 5000; 0.1 M $(NH_4)_2SO_4$; MES pH 6.5, HEPES 7.5	1.5	+/- BH_4, 0.7 mM in *ch*TPH2
3-5% PEG 400, 1500, 4000, MPEG 550, 5000; 0.15 M $(NH_4)_2SO_4$; MES pH 6.0, 6.5, HEPES pH 7.0, 7.5	1.2	+/- Trp, 0.13 mM in *ch*TPH2
3-7% PEG 400, 1500, 4000, 8000; 0.15 M $(NH_4)_2SO_4$; MES pH 6.5	1.3 3	+/- BH_4, 0.36 mM in *ch*TPH2 None
3-7% PEG 400, 1500, 4000, 8000; 0.15 M $(NH_4)_2SO_4$; MES pH 6.5	4, MES pH 6.5	+/- BH_2, 8 µM in *ch*TPH2
10, 12, 14% MPEG 5000; HEPES, MIB pH 7.5	1.2, 4	$C_{12}E_8$, 0.1 mM in *ch*TPH2
TPH screen	4, 20˚C/30˚C expression	None
TPH screen	4	None
TPH screen	4	$NiCl_2$, 9.5 mM in reservoir
TPH screen	4	$CoCl_2$, 9.5 mM in reservoir
TPH screen	4	$[Ru(NH_3)_6]Cl_3$, 0.3 µL added to the drop
TPH screen	4	CsCl, 38 mM in reservoir
TPH screen	4	Trp, 0.8 mM in reservoir
TPH screen	4	$[Co(NH_3)_6]Cl_3$, 0.3 µL 0.1 M added to the drop
TPH screen	4	$C_{12}E_6$, 0.16 mM in *ch*TPH2
TPH screen	4	$C_{12}E_8$, 0.22 mM in *ch*TPH2
TPH screen	4	Dodecyl-m., 0.34 mM in *ch*TPH2
TPH screen	4	5-OH-Trp, 1.1 mM in *ch*TPH2
TPH screen	4	BH_4, 1 mM in *ch*TPH2
TPH screen	4	BH_2, 1 mM in *ch*TPH2
TPH screen	4	Glycine (pH 7), 0.1 M in reservoir
TPH screen	4	Diaminopropane, diaminobutane both 50 mM, pH 7, in reservoir
TPH screen	4	DL-4-Cl-Phe, 1 mM in *ch*TPH2
TPH screen	5	BH_2, 1 mM, in *ch*TPH2 $C_{12}E_8$, 0.22 mM, in *ch*TPH2

Therefore I decided to decrease the concentration of the precipitation agent instead of the protein in order to obtain a more appropriate degree of supersaturation. In most commercial screens the concentration of the precipitation agent was too high for c*h*TPH2 and dilution of the screen to a desired precipitant concentration would lead to an undesired low buffer capacity. Consequently I made my own TPH screen containing 24 conditions. The TPH screen spans a pH from 5.5 - 8.5 using different buffers. Several different PEGs in low concentrations were used. Prior to the final screen composition different PEG concentrations were tested with a c*h*TPH2 concentration of 4 mg/mL and the concentration giving only light precipitation was selected. The selected salts are the ones that seemed to stabilise c*h*TPH2 and which are also used in commercial screens. One condition with 2-methyl-2,4-pentanediol (MPD) and one with dioxane are included. Most conditions contain both a buffer and a salt. The composition of the TPH screen can be seen in appendix 2.9. The screen contains 24 conditions which made it possible to test several different additives in combination with the screen. Many drops have been set up and unfortunately none of the experiments yielded crystals or any crystalline precipitate that could be optimised to crystals. This does not mean that the protein can not crystallise, just that the right conditions have not yet been found. In the following section I will discuss new strategies for the crystallisation of c*h*TPH2.

9.2.3 New strategies for the crystallisation of c*h*TPH2

High purity of the protein sample used for crystallisation experiments is very important and when a protein will not crystallise one of the first things to check is the protein purity. The c*h*TPH2 used for crystallisation is very pure as judged from SDS-PAGE (see figure 4.4, lane 10) but there are small amounts of impurities. It might be necessary to optimise the purification to yield even purer protein. As mentioned in section 4.2.2 this is possible by collecting fractions in a narrower interval in the anion exchange. If this is not enough incorporating a third purification step is necessary. This could for example be hydrophobic interaction chromatography [300] or affinity chromatography using $DMPH_4$ adsorbent [155]. The latter method has been used successfully by several research groups [143,156,158]. Some of the impurities are also likely to be degradation products and including protease inhibitors in the lysis buffer might also improve homogeneity of the purified sample.
Judging from the elution profile of c*h*TPH2 from gel filtration (see figure 4.6) purified c*h*TPH2 is structurally homogeneous, but it has not been tested if this changes upon freezing and thawing. Therefore the structural homogeneity of c*h*TPH2 should be tested with dynamic light scattering [299].
Optimising the storage buffer of the protein to optimal solubility has been reported to significantly increase the likelihood of obtaining crystals [301,302,303]. That c*h*TPH2 is stable in 20 mM HEPES/NaOH, 100 mM $(NH_4)_2SO_4$, 5% glycerol, pH 7.2 does not necessarily mean that it is the optimal condition of c*h*TPH2. Maybe the purification should be done at a slightly different pH or the $(NH_4)_2SO_4$ and glycerol concentration in the gel filtration should be increased to 200 mM and 10%, respectively.
When the purity and homogeneity of the c*h*TPH2 sample have been optimised or checked, new crystallisation experiments should be done with various screens for example JCSG+ and PACT screens, maybe with different degrees of dilution of the screens (even though it might change the buffer capacity). The drops should be set up in a cold room (4-6˚C) and stored at this temperature. Glycerol is known to stabilise

protein structures but it is commonly believed that glycerol hinders crystallisation or reduces crystalline order. This might be true in some cases but for some proteins addition of glycerol (10-30% v/v) has proven necessary in the crystallisation [304]. It might very well be that the structure of c*h*TPH2 needs to be stabilised by for example glycerol in order to form crystals instead of precipitate. Addition of glycerol to the crystallisation solutions should therefore be tested.

9.3 Crystallisation experiments of ct*h*TPH2

9.3.1 Experimental

9.3.1.1 Preparation of the ct*h*TPH2 sample

A sample of 100 µL ct*h*TPH2 was centrifuged at 15000 x g for 8 min at 4˚C when thawed. The concentration was determined using ε_{280} = 40800 M^{-1} cm^{-1}. Dilution to the desired protein concentration was done with 20 mM Tris/HCl, 150 mM $(NH_4)_2SO_4$, pH 8.2.

9.3.1.2 Crystallisation experiments done with ct*h*TPH2

Initial screening was done with Stura Footprint screen 1 and 2 (see appendix 2.1) set up as hanging drops with and without BH_4. These screens showed that ct*h*TPH2 also had a high tendency to precipitate. Extensive screening was done using the Index, JCSG+ and PACT screens (see appendix 2.2-2.4). These were set up with an Oryx 8 robot at the Department of Chemistry, University of Copenhagen. The drop size was 150 nL+150 nL with three sitting drops per well. The ct*h*TPH2 concentrations in the solution used for drop 1, 2 and 3 were 1.3, 10 and 20 mg/mL respectively. The drops were set up at room temperature and subsequently stored at 6˚C.
When these experiments had been evaluated, follow-up experiments were done to test conditions where possible crystals or promising precipitates were observed. The test was set up as 2+2 µL sitting drops. For each original condition three experiments were done. One was identical to the original condition. In another experiment the precipitant concentration was lower than the original and in the third experiment it was higher than in the original condition. In addition to the above mentioned screens Hampton's Crystal Screen, Sigma's Crystallisation Extension Kit and the TPH screen were set up as 2+2 µL sitting drops as listed in table 9.3. All the trays except for the Index, JCSG+ and PACT were set up on ice and stored at 4˚C.

9.3.2 Results and discussion of the crystallisation experiments with ct*h*TPH2

In general ct*h*TPH2 behaved similar to c*h*TPH2. It was temperature sensitive and had a high tendency to precipitate even at low ct*h*TPH2 concentrations.
Many conditions for crystallisation of ct*h*TPH2 were tested and unfortunately no ct*h*TPH2 crystals were obtained. The drops of the Index, JCSG+ and PACT screens are very small and it can be difficult to determine whether things that look like small crystals really are crystals. Possible crystals were observed in some conditions in the Index, JCSG+ and PACT screens. I tried to reproduce these. Unfortunately no crystals could be reproduced.

Table 9.3 List of crystallisation experiments with ct*h*TPH2. The composition of Stura, Crystal, Sigma Extension, Index, PACT, JCSG+ and TPH screens is listed in appendix 2. +/- means with and without the following additive. The additives were added to the protein solution prior to drop set up.

Screen	ct*h*TPH2 concentration	Additives
Stura screen 1 + 2	7 and 20 mg/mL	None
Stura screen 1 + 2	5 mg/mL	+/- BH_4, 1 mM
Stura 1, (partial)	1, 2 mg/mL	None
Crystal screen	4 mg/mL	+/- BH_4, 1 mM
Sigma extension	4 mg/mL	None
Index	1.3, 10 and 20 mg/mL	None
PACT	1.3, 10 and 20 mg/mL	None
JCSG+	1.3, 10 and 20 mg/mL	None
Follow up on Index, PACT and JCSG+ screens	2, 5, 10, 15 and 20 mg/mL	None
TPH screen	4 mg/mL	None, $C_{12}E_6$, 0.16 mM $C_{12}E_8$, 0.22 mM Dodecyl maltoside, 0.34 mM

9.3.3 Future experiments with ct*h*TPH2

The ideas suggested for c*h*TPH2 are applicable to ct*h*TPH2. Especially experiments to find the optimal storage buffer. It was seen during the purification that some enzyme activity was lost when stored at pH 8.2 but not in buffers with pH 7. Unfortunately this was observed at the end of the project and the crystallisation experiments above had been performed. Performing the purification at pH 7-7.2 would be the first things to try in improving the crystallisation of ct*h*TPH2.

9.4 Presentation of the overall structure of c*g*TPH1

The structure of c*g*TPH1 determined from data described in section 9.1.2 could be refined to an R_{free} = 32.7%. The model contains residues 109-125, 134-345, 357-392 and 400-412. The overall structure is shown in figure 9.5 and structurally aligned with the catalytic domain of PAH (PDB entry 1PAH)[69] and c*h*TPH1 with bound BH_2 (PDB entry 1MLW)[64] in figure 9.6. Electron density is observed for the iron coordinated by His273, His279 and Glu318 (see figure 9.7A).

The largest differences between the structures of c*g*TPH1 and c*h*TPH1 are observed in the β-sheet of Phe319-Gly332 (see figure 9.6 and enlarged in 9.7B) and in the BH_4/BH_2 binding region (see figure 9.6 and enlarged in 9.8).

In c*g*TPH1 the BH_4 binding loop (Arg231-Leu243) has moved into the space where BH_4 would be positioned. The loop would have to move back if BH_4 was to bind as in the c*h*TPH1 structure. The aligned structure of PAH (shown in green in figure 9.6 and 9.8) does not contain BH_2/BH_4 and here the BH_4 binding loop moves away from the BH_4 position. When comparing different structures of PAH with and without bound BH_4 (PDB entries 1J8T, 1J8U and 1PAH) one also observes differences in the position of this loop.

The position of the BH_4 binding loop also affects the structure of the neighbouring N-terminal part of c*g*TPH1 having quite different structures in c*h*TPH1 and PAH (see figure 9.6). This part is not visible in the c*g*TPH1 structure but can not be positioned as

in *ch*TPH1 and PAH because it then would crash with the N-terminal of the neighbouring molecule. In PAH this N-terminal part is known to be flexible as illustrated in figure 2.8 where large movement of Tyr138 is observed upon binding of thienylalanine and BH_4 (see section 2.5.1).

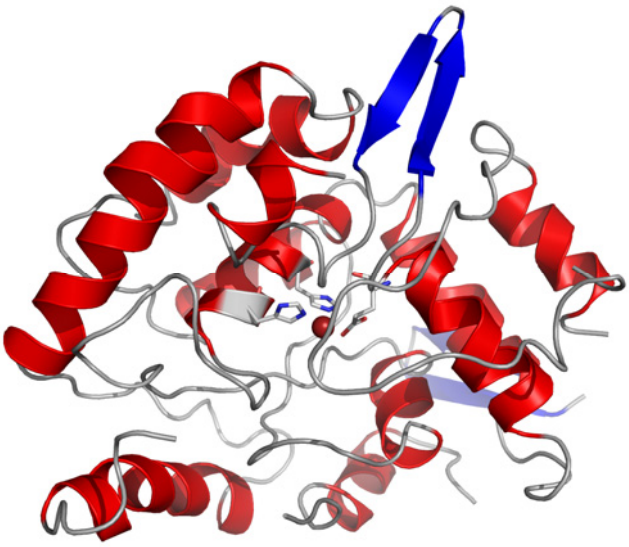

Figure 9.5 Overall structure of *cg*TPH1 determined at 3 Å resolution. His273 and His279 and Glu318 are shown with sticks and the iron as a brick red sphere. The figure was made using Pymol [72].

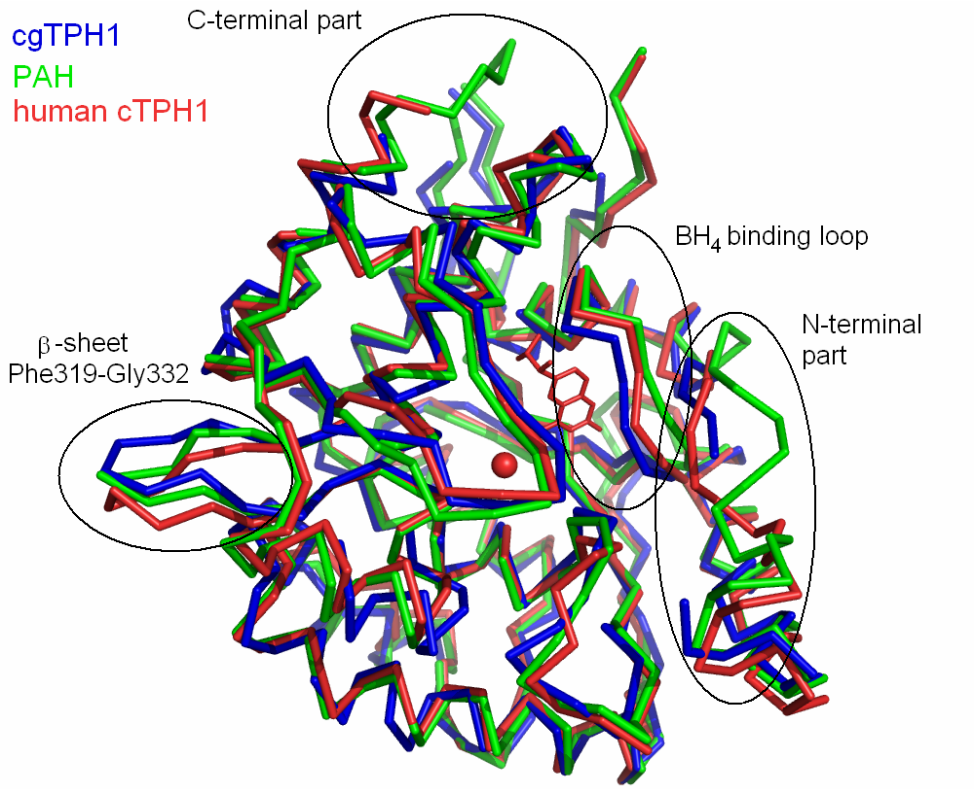

Figure 9.6 Structural alignment of *cg*TPH1 shown in blue, *ch*TPH1 (PDB entry 1MLW) shown in red and the catalytic domain of human PAH (PDB entry 1PAH) shown in green. The structural alignment was done using Coot 0.1 [94]. The figure was made using Pymol [72].

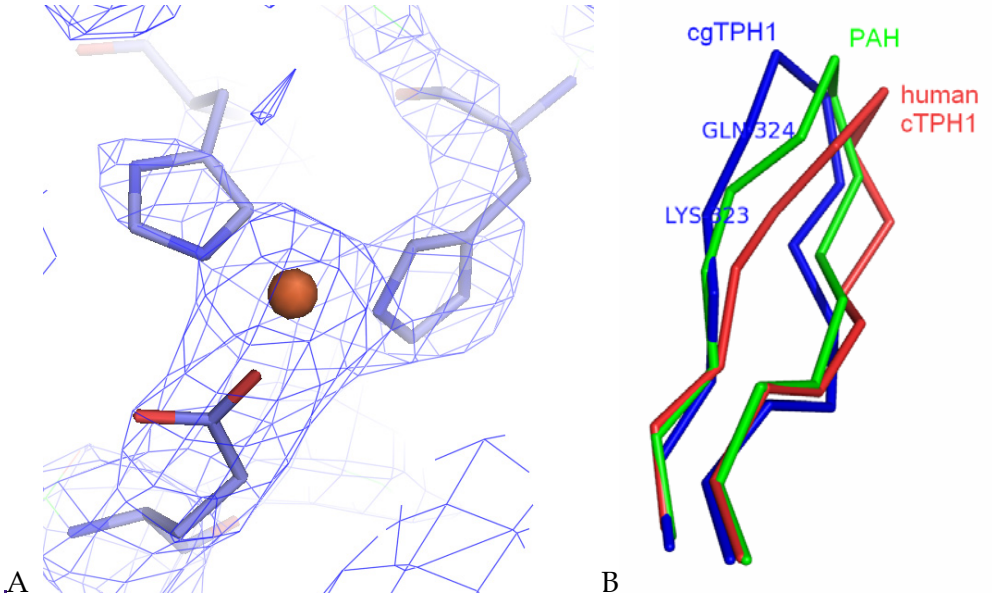

Figure 9.7 **(A)** Electron density of the iron coordination by His273 and His278 and Glu318. **(B)** Alignment of the β-sheet of Phe319-Gly332 of *cg*TPH1 (blue) with PAH (1PAH, green) and *ch*TPH1 (1MLW, red). The structural alignment was done using Coot 0.1 [94]. The figure was made using Pymol [72].

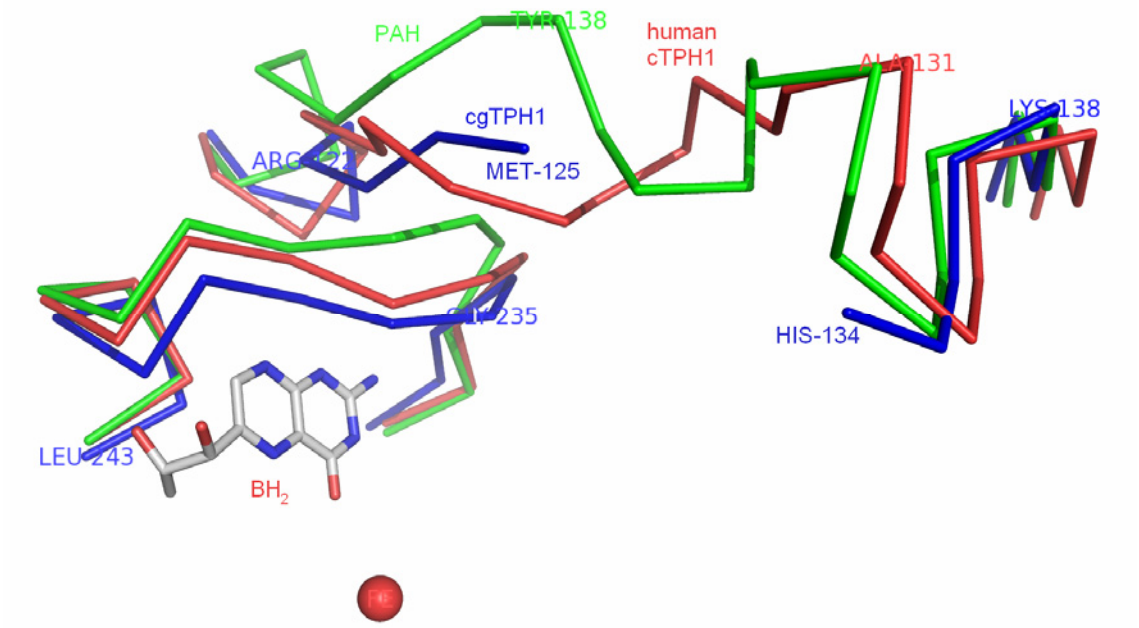

Figure 9.8 Structural alignment of *cg*TPH1 (blue) *ch*TPH1 (1MLW, red) and PAH (1PAH, green) zoomed on the BH_4 binding area with the BH_4 binding loop and the neighbouring N-terminal part. The iron (red sphere) and BH_2 is part of the *ch*TPH1 structure (red). The loop in *cg*TPH1, which would bind BH_4, has moved into the space where BH_4 would be positioned. The PAH structure does not contain BH_4/BH_2 and the BH_4 binding loop has moved further away. The position of the BH_4 binding loop affects the structure of the protein chains equivalent to Lys118-Lys138 in *cg*TPH1. In this region the structures of *ch*TPH1 and catalytic domain of PAH (1PAH) are quite different while the structure of *cg*TPH1 is disordered from Tyr126-Asp133. The structural alignment was done using Coot 0.1 [94]. The figure was made using Pymol [72].

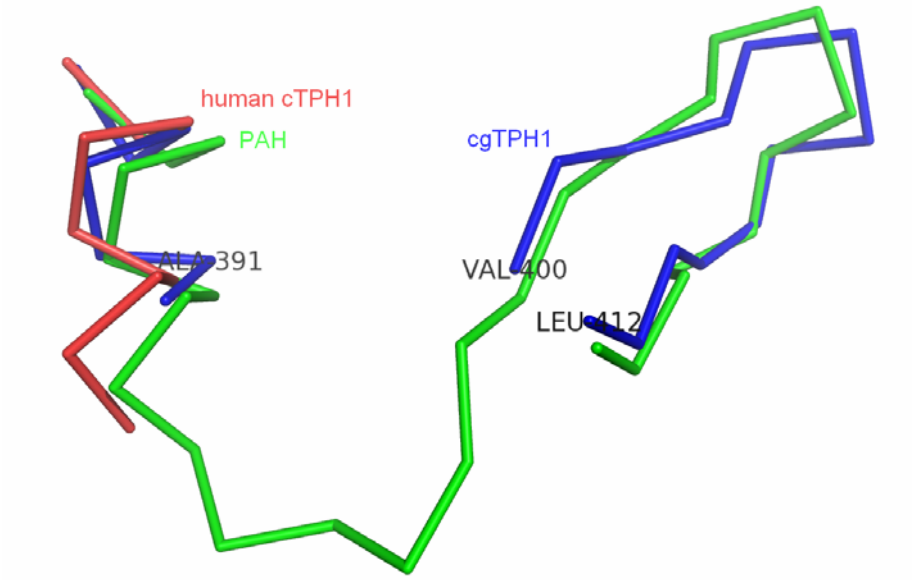

Figure 9.9 Alignment of the C-terminals of c*g*TPH1 (blue) with catalytic domain of PAH (1PAH, green) and c*h*TPH1 (1MLW, red). The last visible residue in the c*h*TPH1 structure is Thr392. Residues Thr393-Gly399 were not visible in the c*g*TPH1 structure, but Val400 -Leu412 shows β-sheet formation as seen in the structures of PAH and TH. The structural alignment was done using Coot 0.1 [94]. The figure was made using Pymol [72].

The last residue visible in the c*h*TPH1 structure is Thr392. In the c*g*TPH1 structure Thr393-Gly399 are not visible, but residues Val400-Leu412 are visible forming a β-sheet, which aligns well with the C-terminal of the catalytic domain of PAH (1PAH) as illustrated in figure 9.9. In the tetrameric TH and PAH (see figure 2.6) this β-sheet is followed by the helix responsible for the coiled-coiled interactions. In c*h*TPH2 the residues equivalent to the β-sheet were removed giving the xc*h*TPH2 and yc*h*TPH2 variants discussed in section 3.5.3-3.5.5. This β-sheet was removed in c*h*TPH2 because I feared that it was very dynamic and interfered with the crystallisation. The results from c*g*TPH1 indicate that this is not the case.

9.5 Conclusion

Crystals of c*g*TPH1 were produced and data was collected on the best diffracting to 3 Å. The data could be indexed in several space groups and the structure could be solved in space group P1 using molecular replacement. The structure was refined to an R_{free} of 32.7%. It was possible to build most of the protein chain and some overall structural differences are observed compared to the structures of the catalytic domains of *h*TPH1 and human PAH.
It was not possible to crystallise c*h*TPH2 and ct*h*TPH2, but suggestions for further experiments are given.

10 Concluding remarks

This project started shortly after the identification of the second gene for TPH. Since then, a few reports have since been published on the characterisation of TPH2 [22,141,144]. It may be concluded that TPH2 is as difficult to express in *E. coli* as TPH1 and also that the characterisation is hampered by the instability of TPH2. In this study two variants of TPH2 (c*h*TPH2 and ct*h*TPH2) and one variant of TPH1 (c*g*TPH1) have successfully been expressed and purified. All three enzymes were purified with a high yield and high specific activity (chapter 4). The yield of 60 mg purified c*h*TPH2 per L culture allows the production of this enzyme in amounts necessary for mechanistic studies.

The K_m and V_{max} parameters of c*g*TPH1, c*h*TPH2 and ct*h*TPH2 have been determined for all three substrates (chapter 6). This is the first report on $K_{m,O2}$ determination on purified TPH. Substrate inhibition by tryptophan is observed for c*g*TPH1 at concentrations above 15 µM. Substrate inhibition was not observed for c*h*TPH2 at concentrations up to 100 µM. Large differences are observed between K_m values of c*g*TPH1 and c*h*TPH2. These differences may to some extent be influenced by the tryptophan inhibition. The specific activity of c*h*TPH2 is also 10 times higher than the one of c*g*TPH1. Additionally, it was observed that c*h*TPH2 and ct*h*TPH2 have a yellowish colour, while c*g*TPH1 appears to be colourless.

The kinetic mechanism of c*h*TPH2 was studied (chapter 7) using the method of Rudolph and Fromm (chapter 5). The data were furthermore analysed using global curve fitting. Rate equations for different kinetic mechanisms were fitted to the data. From the fitted models, it can be concluded that c*h*TPH2 follows a sequential mechanism. The best model corresponds to the mechanism with ordered addition of tryptophan as the first substrate, followed by random addition of BH_4 and O_2. To my knowledge this is the first report of the kinetic mechanism of TPH.

Screenings for crystallisation conditions have been done for c*g*TPH1, c*h*TPH2 and ct*h*TPH2. Crystallisation conditions were found for c*g*TPH1 and several crystals were grown. The best crystal diffracted to 3 Å and a data set was collected on this crystal. The structure was solved by molecular replacement and could be refined to an R_{free} of 32.8%. The structure has been presented and structural differences are observed when compared to the structure of c*h*TPH1. The structure of c*h*TPH1 by Wang *et al.* from 2002 [64] is still the only published structure of TPH.

Further research on TPH1 and TPH2 is necessary to get a full understanding of these enzymes. Knowledge on TPH1 and TPH2 will aid the understanding of the biochemical roles of serotonin. Further research on TPH1 and TPH2 may also lead to the development of drugs that can regulate the function of TPH1 and TPH2 which might be useful in the treatment of neuropsychiatric disorders.

Bibliography

1 Lovenberg, W., Jequier, E., and Sjoerdsma, A., Tryptophan hydroxylation: Measurement in pineal gland, brainstem and carcinoid tumor, (1967) *Science 155*, 217-219.

2 Boadle-Biber, M. C., Regulation of serotonin synthesis, (1993) *Prog. Biophys. Mol. Biol. 60*, 1-15.

3 Ganguly, S., Coon, S. L., and Klein, D. C., Control of melatonin synthesis in the mammalian pineal gland: the critical role of serotonin acetylation, (2002) *Cell Tissue Res. 309*, 127-137.

4 Rapport, M. M., Green, A. A., and Page, I. H., Partial purification of the vasoconstrictor in beef serum, (1948) *J. Biol. Chem. 174*, 735-741.

5 Rapport, M. M., Green, A. A., and Page, I. H., Serum vasocontrictor (serotonin), isolation and characterization, (1948) *J. Biol. Chem. 176*, 1243-1251.

6 Udenfriend, S., Titus, E., Weissback and Peterson, R. E., Biogenesis and metabolism of 5-hydroxyindole compounds, (1956) *J. Biol. Chem. 219*, 335-344.

7 Lucki, I., The spectrum of behaviors influenced by serotonin, (1998) *Biol. Psychiatry 44*, 151-162.

8 Fisher, K. M., and Nielsen, P. G., Cloning and expression of tryptophan hydroxylase, B. Sc. project, Department of Chemistry, Technical University of Denmark, Kgs. Lyngby, 2002.

9 Nielsen, P. G., Tryptophan hydroxylase, expression and purification of the catalytic domain, Special course project, Department of Chemistry, Technical University of Denmark, Kgs. Lyngby, 2002.

10 Nielsen, M. S., Purification of tryptophan hydroxylase variants and the crystal structure of *Pyrococcus furiosus* [Fe_3S_4]-ferredoxin, M.Sc. thesis, Department of Chemistry, Technical University of Denmark, Kgs. Lyngby, 2004.

11 Petersen, C. R., and Rasmussen, T. V., Purification and stabilisation of the catalytic domain of tryptophan hydroxylase, B. Sc. project, Department of Chemistry, Technical University of Denmark, Kgs. Lyngby, 2004.

12 Boesen, J., and Klitgaard, M. K., Cloning and Chromatographic purification of full length tryptophan hydroxylase, B. Sc. project, Department of Chemistry, Technical University of Denmark, Kgs. Lyngby, 2004.

13 Munch, A., Chromatographic purification and stability studies of the catalytic domain of tryptophan hydroxylase isoform 1, M.Sc. thesis, Department of Chemistry, Technical University of Denmark, Kgs. Lyngby, 2006.

14 Walther, D. J., Peter, J.-U., Bashammakh, S., Hörtnagl, H., Voits, M., Fink, H., and Bader, M., Synthesis of serotonin by a second tryptophan hydroxylase isoform, (2003) *Science 299*, 76.

15 Petersen, C. R., Production, chromatographic purification and crystallization of the catalytic domain from *Gallus gallus* tryptophan hydroxylase isoform 1, M.Sc. thesis, Department of Chemistry, Technical University of Denmark, Kgs. Lyngby, 2006.

16 Levine, R. J., Lovenberg, W., and Sjoerdsma, A., Hydroxylation of tryptophan and phenylalanine in neoplastic mast cells of the mouse, (1964) *Biochem. Pharmacol. 13*, 1283-1290.

17 Grahame-Smith, D. G., Tryptophan hydroxylation in brain, (1964) *Biochem. Biophys. Res. Commun. 16*, 586-592.

18 Fitzpatrick, P. F., The aromatic amino acid hydroxylases, in: Advances in enzymology and related areas of molecular biology, Vol. 74, Editor Purich, D. L., John Wiley & Sons, Inc. New York, 2000, pp. 235-294.

19 Fisher, D. B., Kirkwood, R., and Kaufman, S., Rat liver phenylalanine hydroxylase, an iron enzyme, (1972) *J. Biol. Chem. 247*, 5161-5167.

20 Hoeldtke, R., and Kaufman, S., Bovine adrenal tyrosine hydroxylase, purification and properties, (1977) *J. Biol. Chem. 252*, 3160-3169.

21 Grenett, H. E., Ledley, F. D., Reed, L. L., and Woo, S. L. C., Full-length cDNA for rabbit tryptophan hydroxylase: functional domains and evolution of aromatic amino acid hydroxylases, (1987) *Proc. Nat. Acad. Sci. USA 84*, 5530-5534.

22 Carkaci-Salli, N., Flanagan, J. M., Martz, M. K., Salli, U., Walther, D. J., Bader, M., and Vrana, K. E., Functional domains of human tryptophan hydroxylase 2 (hTPH2), (2006) *J. Biol. Chem. 281*, 28105-28112.

23 Vrana, K. E., Walker, S. J., Rucker, P. J., and Liu, X., A carboxyl terminal leucine zipper is required for tyrosine hydroxylase tetramer formation, (1994) *J. Neurochem. 63*, 2014-2020.

24 Kappock, T. J., Harkins, P. C., Friendenberg, S., and Caradonna, J. P., Spectroscopic and kinetic properties of unphosphorylalted rat hepatic phenylalanine hydroxylase expressed in *Escherichia coli*, (1995) *J. Biol. Chem. 270*, 30532-30544.

25 Kaufman, S., The enzymatic conversion of phenylalanine to tyrosine, (1957) *J. Biol. Chem. 226*, 511-524.

26 Kaufman, S., Tetrahydrobiopterin, basic biochemistry and role in human disease, Chapter 3 and 7, The John Hopkins University Press, Baltimore, 1997.

27 Nakata, H., T. Yamauchi, and H. Fujisawa, Phenylalanine hydroxylase from *Chromobacterium violaceum*. Purification and characterization, (1979) *J. Biol. Chem. 254*, 1829-1833.

28 Chen, D., and Frey, P. A., Phenylalanine hydroxylase from *Chromobacterium violaceum*, (1998) *J. Biol. Chem. 273*, 25594-25601.

29 Leiros, H. S., Pey, A. L., Innselset, M., Moe, E., Leiros, I., Steen, I. H., and Martinez, A., Structure of phenylalanine hydroxylase from *Colwellia psychrerythraea* 34H; a monomeric cold active enzyme with local flexibility around the active site and high overall stability, (2007) *J. Biol. Chem. 282*, 21973-21986.

30 Nagatsu, T., Levitt, M., and Udenfriend, S., Tyrosine hydroxylase, the first step in the norephiphrine biosynthesis, (1964) *J. Biol. Chem. 239*, 2910-2917.

31 Flatmark, T., and Stevens, R. C., Structural insight into the aromatic amino acid hydroxylases and their disease-related mutant forms, (1999) *Chem. Rev. 99*, 2137-2160.

32 Rang, H. P., Dale, M. M., Ritter, J. M., and Moore, P. K., Noradrenergic transmission, Chapter 11 in Pharmacology, 5th edition, Churchill Livingstone, London 2003.

33 Kuhn, D. M., Rosenberg, R. C., and Lovenberg, W., Determination of some molecular parameters of tryptophan hydroxylase from rat midbrain and murine mast cells, (1979) *J. Neurochem. 33*, 15-21.

34 Kuhn, D. M., Meyer, M. A., and Lovenberg, W., Comparisons of tryptophan hydroxylase from a malignant murine mast cell tumor and rat mesencephalic tegmentum, (1980) *Arch. Biochem. Biophys. 190*, 355-361.

35 Nakata, H., and Fujisawa, H., Purification and properties of tryptophan 5-hydroxylase from rat brain-stem, (1982) *Eur. J. Biochem. 122*, 41-47.

36 Nakata, H., and Fujisawa, H., Tryptophan 5-monooxygenase from mouse mastocytoma P815, a simple purification and general properties, (1982) *Eur. J. Biochem. 124*, 595-601.

37 Cash, C. D., Vayer, P., Mandel, P., and Maitre, M., Tryptophan 5-hydroxylase, Rapid purification from whole rat brain and production of a specific antiserum, (1985) *Eur. J. Biochem 149*, 239-245.

38 Boularand, S., Darmon, M. C., Ganem, Y., Launay, J.-M., and Mallet, J., Complete coding sequence of human tryptophan hydroxylase, (1990) *Nucl. Acids Res. 18*, 4257.

39 Craig, S. P., Boularand, S., Darmon, M. C., Mallet, J., and Craig, I. W., Localization of human tryptophan hydroxylase (TPH) to chromosome 11p15.3-p14 by in situ hybridization, (1991) *Cytogenet. Cell Genet. 56*, 157-159.

40 Patel, P. D., Pontrello, C., and Burke, S., Robust and tissue-specific expresion of TPH2 versus TPH1 in rat raphe and pineal gland, (2004) *Biol. Psychiatry 55*, 428-433.

41 Gershon, M. D., Dreyfus, C. F., Pickel, V. M., Joh, T. H., and Reis, D. J., Serotonergic neurons in the peripheral nervous system: Identification in gut by immunohistochemical localization of tryptophan hydroxylase, (1977) *Proc. Natl. Acad. Sci. USA 74*, 3086-3089.

42 Zhang, X., Beaulieu, J., Sotnikova, T. D., Gainetdinov, R. R., and Caron, M. G., Tryptophan hydroxylase-2 controls brain serotonin synthesis, (2004) *Science 305*, 217.

43 Coates, M. D., Mahoney, C. R., Linden, D. R., Sampson, J. E., Chen, J., Blaszyk, H., Crowell, M. D., Sharkey, K. A., Gershon, M. D., Mawe, G. M., and Moses, P. L., Molecular defects in muscosal serotonin content and decreased serotonin reuptake transporter in ulcerative colitis and irritable bowel syndrome, (2004) *Gastroenterology 126*, 1657-1664.

44 Slominski, A., Pisarchik, A., Johansson, O., Jing, C., Semak, I., Slugocki, G., and Wortsman, J.,Tryptophan hydroxylase expression in human skin cells, (2003) *Biochim. Biophys. Acta 1639*, 80-86.

45 Hasegawa, H., Yanagisawa, M., Inoue, F., Yanaihara, N., and Ichiyama, A., Demonstration of non-neural tryptophan 5-mono-oxygenase in mouse intestinal mucosa, (1987) *Biochem. J. 248*, 501-509.

46 Grahame-Smith, D. G., Tryptophan hydroxylation in carcinoid tumors, (1964) *Biochim. Biophys. Acta 86*, 176-179.

47 Hosoda, S, Nakamura, W., and Takatsuki, K., Properties of tryptophan hydroxylase from human carcinoid tumor, (1977) *Biochim. Biophys. Acta 482*, 27-34.

48 Walther, D. J., and Bader, M., A unique central tryptophan hydroxylase isoform, (2003) *Biochem. Pharmacol. 66*, 1673-1680.

49 Lewis, D. A., Melchitzky, D. S., and Haycock, J. W., Four isoforms of tyrosine hydroxylase are expressed in human brain, (1993) *Neuroscience 54*, 477-492.

50 Florez, J. C., Seideman, K. J., Barrett, R. K., Sangoram, A. M., and Takahashi, J. S., Molecular cloning of chicken pineal tryptophan hydroxylase and circadian oscillation of its mRNA levels, (1996) *Mol. Brain Res. 42*, 25-30.

51 Kwok, S. C. M., Ledley, F. D., DiLella, A. G., Robson, K. J. H., and Woo, S. L. C., Nucleotide sequence of a full-length complementary DNA clone and amino acid sequence of human phenylalanine hydroxylase, (1985) *Biochemistry 24*, 556-561.

52 Grima, B., Lamouroux, A., Boni, C., Julien, J.-F., Javoy-Agid, F., and Mallet, J., A single human gene encoding multiple tyrosin hydroxylases with different predicted functional characteristics, (1987) *Nature 326*, 707-711.

53 Gasteiger E., Gattiker A., Hoogland C., Ivanyi I., Appel R. D., and Bairoch A., ExPASy: the proteomics server for in-depth protein knowledge and analysis, (2003) *Nucleic Acids Res. 31*, 3784-3788.

54 Chenna, R., Sugawara, H., Koike,T., Lopez, R., Gibson, T. J., Higgins, D. G., and Thompson, J. D., Multiple sequence alignment with the Clustal series of programs, (2003) *Nucleic Acids Res. 31*, 3497-3500. http://www.ebi.ac.uk/clustalw/ (August 9th 2007).

55 Pfleiderer, W., Chemistry of pterins, Chapter 2, Unconjugated pterins in neurobiology, Editors Lovenberg, W., and Levine, R. A., Taylor and Francis Ltd, London, 1987.

56 Almås, B., Toska, K., Teigen, K., Groehn, V., Pfleiderer, W., Martinez, A., Flatmark, T., and Haavik, J., A kinetic and conformational study on the interaction of tetrahydropteridines with tyrosine hydroxylase, (2000) *Biochemistry 39*, 13676-13686.

57 Kaufman, S., The structure or the phenylalanine-hydroxylation cofactor, (1963) *Proc. Natl. Acad. Sci. USA 50*, 1085-1093.

58 Taguchi, H., and Armarego, W. L. F., Glyceryl-ether monooxygenase [EC 1.14.16.5]. A microsomal enzyme of ether lipid metabolism, (1998) *Med. Res. Rev. 18*, 43-89.

59 Wei, C., Wang, Z., Meade, A. L., McDonald, J. F., and Stuehr, D. J., Why do nitric oxide synthases use tetrahydrobiopterin? (2002) *J. Inorg. Biochem. 91*, 618-624.

60 Kaufman, S., Metabolism of the phenylalanine hydroxylation cofactor, (1967) *J. Biol. Chem. 242*, 3934-3943.

61 Davis, M. D., Kaufman, S., and Milstein, S., The auto-oxidation of tetrahydrobiopterin, (1988) *Eur. J. Biochem. 173*, 345-351.

62 Kirsch, M., Korth, H., Stenert, V., Sustmann, R., and de Groot, H., The autooxidation of tetrahydrobiopterin revisited, proof of superoxide formation from reaction of tetrahydrobiopterin with molecular oxygen, (2003) *J. Biol. Chem. 278*, 24481-24490.

63 Thöny, B., Auerbach, G., and Blau, N., Tetrahydrobiopterin biosynthesis, regeneration and functions, (2000) *Biochem. J. 347*, 1-16.

64 Wang, L., Erlandsen, H., Haavik, J., Knappskog, P. M., and Stevens, R. C., Three-dimensional structure of human tryptophan hydroxylase and its implications for the biosynthesis of the neurotransmitters serotonin and melatonin, (2002) *Biochemistry 41*, 12569-12574.

65 Fitzpatrick, P. F., The metal requirement of rat tyrosine hydroxylase, (1989) *Biochem. Biophys Res. Com. 161*, 211-215.

66 Gibbs, B. S., Wojchowski, D., and Benkovic, S. J., Expression of rat liver phenylalanine hydroxylase in insect cells and site-directed mutagenesis of putative non-heme iron-binding sites, (1993) *J. Biol. Chem. 268*, 8046-8052.

67 Ramsey, A. J., Daubner, S. C., Ehrlich, J. I., and Fitzpatrick, P. F., Identification of iron ligands in tyrosine hydroxylase by mutagenesis of conserved histidyl residues, (1995) *Protein Sci. 4*, 2082-2086.

68 Goodwill, K. E., Sabatier, C., Marks, C., Raag, R., Fitzpatrick, P. F., and Stevens, R. C., Crystal structure of tyrosine hydroxylase at 2.3 Å and its implications for inherited neurodegenerative diseases, (1997) *Nat. Struct. Biol. 4*, 578-585.

69 Erlandsen, H., Fusetti, F., Martinez, A., Hough, E., Flatmark, T., and Stevens, R. C., Crystal structure of the catalytic domain of human phenylalanine hydroxylase reveals the structural basis for phenylketonuria, (1997) *Nat. Struct. Biol. 4*, 995-1000.

70 Costas, M., Mehn, M. P., Jensen, M. P., and Que, L., Jr., Dioxygen activation at mononuclear nonheme iron active sites: enzymes, models and intermediates, (2004) *Chem. Rev. 104*, 939-986.

71 Hausinger, R. P., Fe(II)-/α-Ketoglutarate-dependent hydroxylase and related enzymes, (2004) *Crit. Rev. Biochem Mol. Biol. 39*, 21-68.

72 The programme can be obtained at http://pymol.sourceforge.net (August 9th 2007).

73 Martinez, A., Knappskog, P. M., and Haavik, J., A structural approach into human tryptophan hydroxylase and its implications for the regulation of serotonin biosynthesis, (2001) *Curr. Med. Chem. 8*, 1077-1091.

74 Kobe, B., Jennings, I. G., House, C. M., Michell, B. J., Goodwill, K. E., Santarsiero, B. D., Stevens, R. C., Cotton, R. G. H., and Kemp, B. E., Structural basis of autoregulation of phenylalanine hydroxylase, (1999) *Nat. Struct. Biol. 6*, 442-448.

75 Andersen, O. A., Stokka, A. J., Flatmark, T., and Hough, E., 2.0 Å resolution crystal structure of the ternary complex of human phenylalanine hydroxylase with tetrahydrobiopterin and 3-(2-thienyl)-L-alanine, or L-norleucine: substrate specificity and molecular motions related to substrate binding. (2003) *J. Mol. Biol. 333*, 747-757.

76 Daubner, S. C., McGinnis, J. T., Gardner, M., Kroboth, S. L., Morris, A. R., and Fitzpatrick, P. F., A flexible loop in tyrosine hydroxylase controls coupling of amino acids hydroxylation to tetrahydropterin oxidation, (2006) *J. Mol. Biol. 359*, 299-307.

77 Sura, G. R., Lasagna, M., Gawandi, V., Reinhart, G. D., and Fitzpatrick, P. F., Effects of ligands on the mobility of an active-site loop in tyrosine hydroxylase as monitored by fluorescence anisotropy, (2006) *Biochemistry 45*, 9632-9638.

78 Goodwill, K. E., Sabatier, C., and Stevens, R. C., Crystal structure of tyrosine hydroxylase with bound cofactor analogue and iron at 2.3 Å resolution: Self-hydroxylation of Phe300 and the pterin-binding site, (1998) *Biochemistry 37*, 13437-13445.

79 Erlandsen, H., Martinez, A., Knappskog, P. M., Haavik, J., Hough, E., and Flatmark, T., Crystallization and preliminary diffraction analysis of a truncated homodimer of human phenylalanine hydroxylase, (1997) *FEBS Letters 406*, 171-174.

80 Fusetti, F., Erlandsen, H., Flatmark, T., and Stevens, R. C., Structure of tetrameric human phenylalanine hydroxylase and its implications for phenylketonuria, (1998) *J. Biol. Chem. 273*, 16962-16967.

81 Erlandsen, H., Flatmark, T., Stevens, R. C., and Hough, E., Crystallographic analysis of the human phenylalanine hydroxylase catalytic domain with bound catechol inhibitors at 2.0 Å resolution, (1998) *Biochemistry 37*, 15638-15646.

82 Erlandsen, H., Bjørgo, E., Flatmark, T., and Stevens, R. C, Crystal structures and site-specific mutagenesis of pterin-bound human phenylalanine hydroxylase, (2000) *Biochemistry 39*, 2208-2217.

83 Andersen, O. A., Flatmark, T., and Hough, E., Crystal structure of the ternary complex of the catalytic domain of human phenylalanine hydroxylase with tetrahydrobiopterin and 3-(2-thienyl)-L-alanine, and its implications for the mechanism of catalysis and substrate activation, (2002) *J. Mol. Biol. 320*, 1095-1108.

84 Andersen, O. A., Flatmark, T., and Hough, E., High resolution crystal structures of the catalytic domain of human phenylalanine hydroxylase in its catalytically active Fe(II) form and binary complex with tetrahydrobiopterin, (2001) *J. Mol. Biol. 314*, 279-291.

85 Erlandsen, H., Pey, A. L., Gámez, A., Pérez, B., Desviat, L. R., Aguado, C., Koch, R., Surendran, S., Tyring, S., Matalon, R., Scriver, C. R., Ugarte, M., Martinez, A., and Stevens, R. C., Correction of kinetic and stability by tetrahydrobiopterin in phenylketonuria patients with certain phenylalanine hydroxylase mutations, (2004) *Proc. Natl. Acad. Sci. USA 101*, 16903-16908.

86 Erlandsen, H., Kim, J. Y., Patch, M. G., Han, A., Volner, A., Abu-Omar, M. M., and Stevens, R. C., Structural comparison of bacterial and human iron-dependent phenylalanine hydroxylase: similar fold, different stability and reaction rates, (2002) *J. Mol. Biol. 320*, 645-661

87 Moran, G. R., Daubner, S. C., and Fitzpatrick P. F., Expression and characterization of the catalytic core of tryptonphan hydroxylase, (1998) *J. Biol. Chem. 273*, 12259-12266.

88 Renson, J., Goodwin, F., Weissbach, H., and Undenfriend, S., Conversion of tryptophan to 5-hydroxytryptophan by phenylalanine hydroxylase, (1961) *Biochem. Biophys. Res. Commun. 6*, 20-23.

89 Daubner, S. C., Hillas, P. J., and Fitzpatrick, P. F., Characterization of chimeric pterin-dependent hydroxylases: contribution of the regulatory domains of tyrosine and phenylalanine hydroxylase to substrate specificity, (1997) *Biochemistry 36*, 11574-11582.

90 Fitzpatrick, P. F., Studies of the rate-limiting step in the tyrosine hydroxylase reaction: alternate substrates, solvent isotope effects and transition-state analogues, (1991) *Biochemistry 30*, 6386-6391.

91 Daubner, S. C., Moran, G. R., and Fitzpatrick, P. F., Role of tryptophan hydroxylase Phe313 in determining substrate specificity, (2002) *Biochem Biophys Res Commun. 292*, 639-641.

92 McKinney, J., Teigen, K., Frøystein, N. Å., Salaün, C., Knappskog, P. M., Haavik, J., and Martínez, A., Conformation of the substrate and pterin cofactor bound to human tryptophan hydroxylase. Important role of Phe313 in substrate specificity, (2001) *Biochemistry 40*, 15591-15601.

93 Daubner, S. C., Melendez, J., and Fitzpatrick, P. F., Reversing the substrate specificities of phenylalanine and tyrosine hydroxylase: Aspartate 425 of tyrosine hydroxylase is essential for L-DOPA formation, (2000) *Biochemistry 39*, 9652-9661.

94 Emsley, P., and Cowtan, K., Coot: model-building tools for molecular graphics, (2004) *Acta Cryst. D60*, 2126-2132.

95 Fitzpatrick, P. F., Steady-state kinetic mechanism of rat tyrosine hydroxylase, (1991) *Biochemistry 30*, 3658-3662.

96 Pember, S. O., Johnson, K. A., Villafranca, J. J., and Benkovic, S. J., Mechanistic studies on phenylalanine hydroxylase from *Chromobacterium violaceum*. Evidence for the formation of an enzyme-oxgygen complex, (1989) *Biochemistry 28*, 2124-2130.

97 Volner, A., Zoidakis, J., Abu-Omar, M. M., Order of substrate binding in bacterial phenyalanine hydroxylase and its mechanistic implication for pterin-dependent oxygenases, (2003) *J. Biol. Inorg. Chem. 8*, 121-128.

98 Pember, S. O., Villafranca, J. J., and Benkovic, S. J., Phenylalanine hydroxylase from *Chromobacterium violaceum* is a copper-containing monooxygenase. Kinetics of the reductive activation of the enzyme, (1986) *Biochemistry 25*, 6611 – 6619.

99 Carr, R. T., and Benkovic, S. J., An examination of the copper requirement of phenylalanine hydroxylase from *Chromobacterum violaceum*, (1993) *Biochemistry 32*, 14132-14138.

100 Nielsen, K. H., Rat liver phenylalanine hydroxylase, a method for the measurement of activity, with particular reference to the distinctive features of the enzyme and the pteridine cofactor, (1969) *Eur. J. Biochem. 7*, 360-369.

101 Oka, K., Kato, T., Sugimoto, T., Matsuura, S., and Nagatsu, T., Kinetic properties of tyrosine hydroxylase with natural tetrahydrobiopterin as cofactor, (1981) *Biochim. Biophys. Acta. 661*, 45-53.

102 Fitzpatrick, P. F., Mechanism of aromatic amino acid hydroxylation, (2003) *Biochemistry 42*, 14083-14091.

103 Pavon, J. A., and Fitzpatrick, P. F., Insights into the catalytic mechanisms of phenylalanine and tryptophan hydroxylase from kinetic isotope effects on aromatic hydroxylation, (2006) *Biochemistry 45*, 11030-11037.

104 Kaufman, S., Bridgers, W. F., Eisenberg, F., and Friedman, S., The source of oxygen in the phenylalanine hydroxylase and the dopamine-β-hydroxylase catalyzed reactions, (1962) *Biochem. Biophys. Res. Commun. 9*, 497-502.

105 Dix, T. A., Bollag, G. E., Domanico, P., and Benkovic, S. J., Phenylalanine hydroxylase: absolute configuration and source of oxygen of the 4a-hydroxytetrahydropterin species, (1985) *Biochemistry 24*, 2955 - 2958.

106 Jéquier, E., Robinson, D. S., Lovenberg, W., and Sjoerdsma, A., Further studies on tryptophan hydroxylase in rat brainstem and beef pineal, (1969) *Biochem. Pharmacol. 18*, 1071-1081.

107 Naoi, M., Maruyama, W., Takahashi, T., Ota, M., and Parvez, H., Inhibibition of tryptophan hydroxylase by dopamine and the precursor amino acids, (1994) *Biochem. Pharmacol. 48*, 207-212.

108 Andersson, K. K., Cox, D. D., Que, Jr., L., Flatmark, T., and Haavik, J., Resonance Raman studies on blue-green-colored bovine adrenal tyrosine 3-monooxygenase (tyrosine hydroxylase), (1988) *J. Biol. Chem. 263*, 18621-18626.

109 Wallick, D. E., Bloom, L. M., Gaffney, J., and Benkovic, S. J., Reductive activation of phenylalanine hydroxylase and its effect on the redox state of the non-heme iron, (1984) *Biochemistry 23*, 1295-1302.

110 Marota, J. J. A., and Shiman, R., Stoichiometric reduction of phenylalanine hydroxylase by its cofactor: a requirement for enzymatic activity, (1984) *Biochemistry 23*, 1303-1311.

111 Ramsey, A. J., Hillas, P., and Fitzpatrick, P. F., Characterization of the active site iron in tyrosine hydroxylase, (1996) *J. Biol. Chem. 271*, 24395-24400.

112 Dix, T. A., Kuhn, D. M., and Benkovic, S. J., Mechanism of oxygen activation by tyrosine hydroxylase, (1987) *Biochemistry 26*, 3354-3361.

113 Moran, G. R., Derecskei-Kovacs, A., Hillas, P. J., and Fitzpatrick, P. F., On the catalytic mechanism of tryptophan hydroxylase, (2000) *J. Am. Chem. Soc. 122*, 4535-4541.

114 Davis, M. D., and Kaufman, S., Evidence for the formation of the 4a-carbinolamine during the tyrosine- dependent oxidation of tetrahydrobiopterin by rat liver phenylalanine hydroxylase, (1989) *J. Biol. Chem. 264*, 8585-8596.

115 Davis, M. D., and Kaufman, S., Products of the tyrosine-dependent oxidation of tetrahydrobiopterin by rat liver phenylalanine hydroxylase, (1993) *Arch. Biochem. Biophys. 304*, 9-16.

116 Kaufman, S., and Mason, K., Specificity of amino acids as activators and substrates for phenylalanine hydroxylase, (1982) *J. Biol. Chem. 257*, 14667-14678.

117 Bassan, A., Blomberg, M. R. A., and Siegbahn, P. E. M., Mechanism of dioxygen cleavage in tetrahydrobiopterin-dependent amino acid hydroxylases, (2003) *Chem. Eur. J. 9*, 106-115.

118 Bassan, A., Borowski, T., and Siegbahn, P. E. M., Quantum chemical studies of dioxygen activation by mononuclear non-heme iron enzymes with the 2-His-1-carboxylate facial triad, (2004) *Dalton Trans. 20*, 3155-3162.

119 Price, J. C., Barr, E. W., Tirupati, B., Bollinger, J. M., Jr., and Krebs, C., The first direct characterization of a high-valent iron intermediate in the reaction of an α-ketogluarate-dependent dioxygenase: a high-spin Fe(IV) complex in taurine/α-ketoglutarate dioxygenase (TauD) from *Escherichia coli*, (2003) *Biochemistry 42*, 7497-7508.

120 Price, J. C., Barr, E. W., Glass, T. E., Krebs, C., and Bollinger., J. M., Jr., Evidence for hydrogen abstraction from C1 of taurine by the high-spin Fe(IV) intermediate detected during oxygen activation by taurine: α-ketoglutarate dioxygenase (TauD), (2003) *J. Am. Chem. Soc. 125*, 13008-13009.

121 Proshlyakov, D. A., Henshaw, T. F., Monterosso, G. R., Ryle, M. J., and Hausinger, R. P., Direct detection of oxygen intermediates in the non-heme Fe enzyme taurine/α-ketoglutarate dioxygenase, (2004) *J. Am. Chem. Soc. 126*, 1022-1023.

122 Riggs-Gelasco, P. J., Price, J. C., Guyer, R. B., Brehm, J. H., Barr, E. W., Bollinger, J. M., Jr., and Krebs, C., EXAFS spectroscopic evidence for an Fe=O unit in the Fe(IV) intermediate observed during oxygen activation by taurine: α-ketoglutarate dioxygenase, (2004) *J. Am. Chem. Soc. 126*, 8108-8109.

123 Hoffart, L. M., Barr, E. W., Guyer, R. B., Bollinger, J. M., Jr., and Krebs, C., Direct spectroscopic detection of a C-H-cleaving high-spin Fe(IV) complex in a prolyl-4-hydroxylase, (2006) *Proc. Natl. Acad. Sci. USA, 103*, 14738-14743.

124 Krebs, C., Fujimori, D. G., Walsh, C. T., and Bollinger, J. M., Jr., Non-heme Fe(IV)-oxo intermediates, (2007) *Acc. Chem. Res. 40*, 484-492.

125 Kovaleva, E. G., and Lipscomb, J. D., Crystal structures of Fe^{2+} dioxygenase superoxo, alkylperoxo and bound product intermediates, (2007) *Science 316*, 453-457.

126 Renson, J., Goodwin, F., Weissbach, H., and Udenfriend, S., Enzymatic conversion of 5-tritiotryptophan to 4-tritio-5-hydroxytryptophan, (1966) *Biochem. Biophys. Res. Commun. 25*, 504-513.

127 Guroff, G., and Daly, J., Quantitative studies on the hydroxylation induced migration of deuterium and tritium during phenylalanine hydroxylation, (1967) *Arch. Biochem. Biophys. 122*, 212-217.

128 Daly, J., Levitt, M., Guroff, G., and Udenfriend, S., Isotope studies on the mechanism of action of adrenal tyrosine hydroxylase, (1968) *Arch. Biochem. Biophys. 126*, 593-598.

129 Hillas, P. J., and Fitzpatrick, P. F., A mechanism for hydroxylation by tyrosine hydroxylase based on partitioning of substituted phenylalanines, (1996) *Biochemistry 35*, 6969-6975.

130 Bassan, A., Blomberg, M. R. A., and Siegbahn, P. E. M., Mechanism of aromatic hydroxylation by an activated Fe(IV) = O core in tetrahydrobiopterin-dependent hydroxylases, (2003) *Chem. Eur. J. 9*, 4055-4067.

131 Shiota, Y., and Yoshizawa, K., QM/MM study of the mononuclear non-heme iron active site of phenylalanine hydroxylase, (2004) *J. Phys. Chem. B. 108*, 17226-17237.

132 Moran, G. R., Phillips, R. S., and Fitzpatrick P. F., Influence of steric bulk and electrostatics on the hydroxylation regiospecificity of tryptophan hydroxylase: characterization of methyltryptophans and azatryptophans as substrates, (1999) *Biochemistry 38*, 16283-16289.

133 Francisco, W. A., Tian, G., Fitzpatrick, P. F., and Klinman, J. P., Oxygen-18 kinetic isotope effect studies of the tyrosine hydroxylase reaction: evidence of rate limiting oxygen activation, (1998) *J. Am. Chem. Soc. 120*, 4057-4062.

134 Abita, J.P., Parniak, M. and Kaufman, S., The activation of rat liver phenylalanine hydroxylase by limited proteolysis, lysolecithin, and tocopherol phosphate. Changes in conformation and catalytic properties, (1984) *J. Biol. Chem. 259*, 14560 – 14566.

135 Baneyx, F., Recombinant protein expression in *Esherichia coli*, (1999) *Curr. Opin. Biotechnol. 10*, 411-421.

136 Swartz, J. R., Advances in *Escherichia coli* production of therapeutic proteins, (2001) *Cur. Opin. Biotechnol. 12*, 195-201.

137 Carrió, M. M., and Villaverde, A., Construction and destruction of bacterial inclusion bodies, (2002) *J. Biotechnol. 96*, 3-12.

138 McKinney, J., Knappskog, P. M., Pereira, J., Ekern, T., Toska, K., Kuitert, B. B., Levine, D., Gronenborn, A. M., Martinez, A., and Haavik, J., Expression and purification of human tryptophan hydroxylase from *Escherichia coli* and *Pichia pastoris*, (2004) *Protein Expr. Purif. 33*, 185-194.

139 Yang, X-J., and Kaufman, S., High-level expression and deletion mutagenesis of human tryptophan hydroxylase, (1994) *Proc. Natl. Acad. Sci. USA 91*, 6659-6663.

140 Tipper, J. P., Citron, B. A., Ribeiro, P., and Kaufman, S., Cloning and expression of rabbit and human brain tryptophan hydroxylase cDNA in *Escherichia coli*, (1994) *Arch. Biochem. Biophys. 315*, 445-453.

141 McKinney, J., Knappskog, P. M., and Haavik, J., Different properties of the central and peripheral forms of human tryptophan hydroxylase, (2005) *J. Neurochem. 92*, 311-320.

142 Vrana, K. E., Rucker, P. J., and Kumer, S. C., Recombinant rabbit tryptophan hydroxylase is a substrate for cAMP-dependent protein kinase, (1994) *Life Sci. 55*, 1045-1052.

143 Kowlessur, D., and Kaufman, S., Cloning and expression of recombinant human pineal tryptophan hydroxylase in *Esherichia coli*: purification and characterization of the cloned enzyme, (1999) *Biochim. Biophys. Acta 1434*, 317-330.

144 Sakowski, S. A., Geddes, T. J., and Kuhn, D. M., Mouse tryptophan hydroxylase isoform 2 and the role of proline 447 in enzyme function, (2006) *J. Neurochem. 96*, 758-765.

145 Banik, U., Wang, G., Wagner, P. D., and Kaufman, S., Interaction of phosphorylated tryptophan hydroxylase with 14-3-3 proteins, (1997) *J. Biol. Chem. 272*, 26219-26225.

146 D´Sa, C., Arthur, R. E., Jr., and Kuhn, D. M., Expression and deletion mutagenesis of tryptophan hydroxylase fusion proteins: delineation of the enzyme catalytic core, (1996) *J. Neurochem. 67*, 917-926.

147 D´Sa, C., Arthur, R. E., Jr., States, C., and Kuhn, D. M., Tryptophan hydroxylase: cloning and expression of the rat brain enzyme in mammalian cells, (1996) *J. Neurochem. 67*, 900-906.

148 Park, D. H., Stone, D. M., Kim, K. S., and Joh, T. H., Characterization of recombinant mouse tryptophan hydroxylase expressed in *Escherichia coli*, (1994) *Mol. Cell. Neurosci. 5*, 87-93.

149 Hamdan, F. F., and Ribeiro, P., Characterization of a stable form of tryptophan hydroxylase from the human parasite *Schistosoma mansoni*, (1999) *J. Biol. Chem. 274*, 21746-21754.

150 Tenner, K., Walther, D., and Bader, M., Influence of human tryptophan hydroxylase 2 N- and C-terminus on enzymatic activity and oligomerization, (2007) *J. Neurochem.* Published online June 1st 2007.

151 Dyson, M. R., Shadbolt, S. P., Vincent, K. J., Perera, R. L., and McCarfferty, J., Production of soluble mammalian proteins in *Escherichia coli*: identification of protein freatures that correlate with successful expression, (2004) *BMC Biotechnology 4*, 32.

152 Banci, L., Bertini, I., Cusack, S., de Jong, R. N., Heinemann, U., Jones, E. Y., Kozielski, F., Maskos, K., Messerschmidt, A., Owens, R., Perrakis, A., Poterszman, A., Schneider, G., Siebold, C., Silman, I., Sixma, T., Stewart-Jones, G., Sussman, J. L., Thierry, J.-C., and Moras, D., First steps towards effective methods in exploiting high-througput technologies for the determination of human protein structures of high biomedical value, (2006) *Acta Cryst. D62*, 1208-1217.

153 Hosoda, S., Further studies on tryptophan hydroxylase from neoplastic murine mast cells, (1975) *Biochim. Biophys. Acta 397*, 58-68.

154 Nukiwa, T., Tohyama, C., Okita, C., Kataoka, T., and Ichiyama, A., Purification and some properties of bovine pineal tryptophan 5-monooxygenase, (1974) *Biochem. Biophys. Res. Commun. 60*, 1029-1035.

155 Cotton, R. G. H. and Jennings, I. G., Affinity chromatography of phenylalanine hydroxylase, the structure of a pteridine adsorbent, (1978) *Eur. J. Biochem. 85*, 357-363.

156 Nakata, H., and Fujisawa, H., Simple and rapid purification of tryptophan 5-monooxygenase from rabbit brain by affinity chromatography, (1981) *J. Biochem*. 90, 567-569.

157 Cash, C. D., Why tryptophan hydroxylase is difficult to purify: A reactive oxygen-derived species-mediated phenomenon that may be implicated in human pathology, (1998) *Gen. Pharmac. 30*, 569-574.

158 Hasegawa, H., and Ichiyama, A., Distinctive iron requirement of tryptophan 5-monooxygenase: TPH1 requires dissociable ferrous iron, (2005) *Biochem. Biophys. Res. Com. 338*, 277-284.

159 Shiman, R., Jones, S. H., and Gray, D. W., Mechanism of phenylalanine regulation of phenyalanine hydroxylase, (1990) *J. Biol. Chem. 265*, 11633-44642.

160 Stokka, A. J. and Flatmark, T., Substrate-induced conformational transition in human phenylalanine hydroxylase as studied by surface plasmon resonance analyses: the effect of terminal deletions, substrate analogues and phosphorylation, (2003) *Biochem. J. 369*, 509-518.

161 Fisher, D. B., and Kaufman, S., The stimulation of rat liver phenylalanine hydroxylase by phospholipids, (1972) *J. Biol. Chem. 247*, 2250-2252.

162 Parniak, M. A., and Kaufman, S., Rat liver phenylalanine hydroxylase. Activation by sulfhydryl modification, (1981) *J. Biol. Chem. 256*, 6876-6882.

163 Abita, J. P., Parniak, M. and Kaufman, S., The activation of rat liver phenylalanine hydroxylase by limited proteolysis, lysolecithin, and tocopherol phosphate. Changes in conformation and catalytic properties, (1984) *J. Biol. Chem. 259*, 14560 – 14566.

164 Jennings, I. G., Teh, T., and Kobe, B., Essential role of the N-terminal autoregulatory sequence in the regulation of phenylalanine hydroxylase, (2001) *FEBS Letters 488*, 196-200.

165 Fujisawa, H., and Okuno, S., Regulatory mechanism of tyrosine hydroxylase activity, (2005) *Biochem. Biophys. Res. Commun. 338*, 271-276.

166 Kuhn, D, M., Arthur, R. E. Jr., and States, C. J., Phosphorylation and activation of brain tryptophan hydroxylase: identification of serine 58 as a substrate site for protein kinase A, (1997) *J. Neurochem. 68*, 2220-2223.

167 Johansen, P. A., Jennings, I., Cotton, R. G. H., and Kuhn, D. M., Tryptophan hydroxylase is phosphorylated by protein kinase A, (1995) *J. Neurochem. 65*, 882-888.

168 Boadle-Biber, M. C. and Phan, T. Involvement of calmodulin-dependent phosphorylation in the activation of brainstem tryptophan hydroxylase induced by depolarization of slices or other treatments that raise intracellular free calcium levels, (1987) *Biochem. Pharmacol. 36*, 1174-1176.

169 Kuhn, D. M., O'Callaghan, J. P., Juskevich, J. and Lovenberg, W., Activation of brain tryptophan hydroxylase by ATP-Mg2+ dependence on calmodulin, (1980) *Proc. Natl. Acad. Sci. USA 77*, 4688-4691.

170 Yamauchi, T., Nakata, H., and Fujisawa, H., A new activator protein that activates tryptophan 5-monooxygenase and tyrosine 3-monooxygenase in the presence of Ca^{2+}, calmodulin-dependent protein kinase, (1981) *J. Biol. Chem. 256*, 5404-5409.

171 Ichimura, T., Isobe, T., Okuyama, T., Yamauchi, T., and Fujisawa, H., Brain 14-3-3 protein is an activator protein that activates tryptophan 5-monooxygenase and tyrosine 3-monooxygenase in the presence of Ca^{2+}, calmodulin-dependent protein kinase II, (1987) *FEBS Letters 219*, 71-82.

172 Furukawa, Y., Ikuta, N., Omata, S., Yamauchi, T., Isobe, T., and Ichimura, T., Demonstration of the phosphorylation-dependent interaction of tryptophan hydroxylase with the 14-3-3 protein, (1993) *Biochem. Biophys. Res. Commun. 194*, 144-149.

173 Yaffe, M. B., How do 14-3-3 proteins work? Gatekeeper phosphorylation and the molecular anvil hypothesis, (2002) *FEBS Lett. 513*, 53-57.

174 Yang, X, Lee, W. H., Sobott, F., Papagrigoiou, E., Robinson, C. V., Grossmann, J. G., Sundstöm, M., Doyle, D. A., and Elkins, J. M., Structural basis for protein-protein interactions in the 14-3-3 protein familily, (2006) *Proc. Natl. Acad. Sci. USA. 103*, 17237-17242.

175 Iida, Y., Sawabe, K., Koijima, M., Oguro, K., Nakanishi, N., and Hasegawa, H., Proteasome-driven turnover of tryptophan hydroxylase is triggered by phosphorylation in RBL2H3 cells, a serotonin producing mast cell line, (2002) *Eur. J. Biochem. 269*, 4780-4788.

176 Kojima, M., Oguro, K., Sawabe, K., Iida, Y., Ikeda, R., Yamashita, A., Nakanishi, N., and Hasegawa, H., Rapid turnover of tryptophan hydroxylase is driven by proteasomes in RBL2H3 cells, a serotonin producing mast cell line, (2000) *J. Biochem. 127*, 121-127.

177 Hasegawa, H., Kojima, M., Oguro, K., and Nakanishi, N., Rapid turnover of tryptophan hydroxylase in serotonin producing cells: demonstration of ATP-dependent proteolytic degradation, (1995) *FEBS Letters 368*, 151-154.

178 Patel, P. D., Bochar, D. A., Turner, D. L., Meng, F., Mueller, H. M., and Pontrello, C. G., Regulation of tryptophan hydroxylase-2 gene expression by a bipartite REST/NRSF binding motif, (2007) *J. Biol. Chem.* Online July 5th, 2007.

179 Veenstra-VanderWeele, J., Anderson, G. M., and Cook Jr., E. H., Pharmacogenetics and the serotonin system: initial studies and future directions, (2000) *Eur. J. Pharmacol. 410*, 165-181.

180 Lesurtel, M., Graf, R., Aleil, B., Walther, D. J., Tian, Y., Jochum, W., Gachet, C., Bader, M., and Clavien, P., Platelet-derived serotonin mediates liver regeneration, (2006) *Science 312*, 104-107.

181 Mössner, R., and Lesch, K., Role of serotonin in the immune system and in neuroimmune interactions, (1998) *Brain Behav. Immun. 12*, 249–271.

182 Gershon, M. D., Roles played by 5-hydroxytryptamine in the physiology of the bowel, (1999) *Alinment. Pharmacol. Ther. 13* (Suppl. 2) 15-30.

183 Cote, F., Thevenot, E., Fligny, C., Fromes, Y., Darmon, M., Ripoche, M.A., Bayard, E., Hanoun, N., Saurini, F., Lechat, P., Dandolo, L., Hamon, M., Mallet, J., and Vodjdani, G., Disruption of the nonneuronal tph1 gene demonstrates the importance of peripheral serotonin in cardiac function, (2003) *Proc Natl Acad Sci U S A. 100*, 13525-13530.

184 Obsil, T., Ghirlando, R., Klein, D. C., Ganguly, S., and Dyda, F., Crystal structure of the 14-3-3ζ:Serotonin N-acetyltransferase complex: a role for scaffolding in enzyme regulation, (2001) *Cell 105*, 257-267.

185 Walitza, S., Renner, T. J., Dempfle, A., Konrad, K., Wewetzer, C., Halbach, A., Herpertz-Dahlmann, B., Remschmidt, H., Smidt, J., Linder, M., Flierl, L., Knölker, U., Friedel, S., Schäfer, H., Gross, C., Hebebrand, J., Warnke, A., and Lesch, K. P., Transmission disequilibrium of polymorphic variants in the tryptophan hydroxylase-2 gene in attention-deficit/hyperactivity disorder, (2005) *Mol. Psychiatry 10*, 1126-1132.

186 Paterson, D. S., Trachtenberg, F. L., Thompson, E. G., Belliveau, R. A., Beggs, A. H., Darnall, R., Chadwick, A. E., Krous, H. F., and Kinney, H. C., Multiple serotonergic branstem abnormalities in sudden infant death syndrome, (2006) *JAMA 296*, 2124-2132.

187 Mann, J. J., Malone, K. M., Diehl, D. J., Perel, J., Cooper, T. B., and Mintun, M. A., Demonstration in vivo of reduced serotonin responsivity in the brain of untreated depressed patients, (1996) *Am. J. Psychiatry 153*, 174-182.

188 Wong, D. T., Bymaster, F. P., and Engleman, E. A., Prozac (fluoxetine, Lilly 110140), the first selective serotonin uptake inhibitor and an antidepressant drug: twenty years since its first publication, (1995) *Life Sci. 57*, 411-441.

189 Zhang, X., Beaulieu, J.M., Gainetdinov, R.R., and Caron, M. G., Functional polymorhphisms of the brain serotonin synthesising enzyme tryptophan hydroxylase-2, (2006) *Cell. Mol. Life. Sci 63*. 6-11.

190 Mann, J. J., Brent, D. A., and Arango, V., The neurobiology and genetics of suicide and attempted suicide: A focus on the serotonergic system, (2001) *Neuropsychopharmacology 24*, 467-477.

191 Nakamura, K., Sugawara, Y., K. Sawabe, A. Ohashi, H. Tsurui, Y. Xiu, M. Ohtsuji, Q. S. Lin, H. Nishimura, H. Hasegawa, and Hirose, S., Late developmental stage-specific role of tryptophan hydroxylase 1 in brain serotonin levels, (2006) *J. Neurosci 26*, 530-534.

192 Nakamura, K., and Hasegawa, H., Developmental role of tryptophan hydroxylase in the nervous system, (2007) *Mol. Neurobiol. 35*, 45-53.

193 Mössner, R., Walitza, S., Geller, F., Scherag, A., Gutknecht, L., Jacob, C., Bogusch, L., Remschmidt, H., Simons, M., Herpertz-Dahlmann, B., Fleischhaker, C., Schulz, E., Warnke, A., Hinney, A., Wewtzer, C., and Lesch, K., Transmission disequilibrium of polymorphic variants in the tryptophan hydroxylase-2 gene in children and adolescents with obsessive-compulsive disorder, (2006) *Int. J. Neuropsychopharmacol. 9,* 437-442.

194 Sheehan, K., Lowe, N., Kirley, A., Mullins, C., Fitzgerald, M., Gill, M., and Hawi, Z., Tryptophan hydroxylase 2 (TPH2) gene variants associated with ADHD, (2005) *Mol. Psychiatry 10*, 944-949.

195 Zill, P., Baghai, T. C., Zwanzger, P., Schüle, C., Eser, D., Rupprecht, R., Möller, H. J., Bondy, B., and Ackenheil, M., SNP and haplotype analysis of a novel tryptophan hydroxylase isoform (TPH2) gene provide evidence for association with major depression, (2004) *Mol. Psychiatry 9*,1030-1036.

196 Zhang, X., Gainetdinov, R.R., Beaulieu, J. M., Sotnikova, T. D., Burch, L. H., Williams, R. B., Schwartz, D. A., Krishnan, K. R., and Caron, M. G., Loss-of-function mutation in tryptophan hydroxylase-2 identified in unipolar major depression, (2005) *Neuron* 45, 11-16.

197 Winge, I., McKinney, J. A., Knappskog, P. M. and Haavik, J., Characterization of wild type and mutant forms of human tryptophan hydroxylase 2, (2007) *J. Neurochem. 100*, 1648-1657.

198 Guruprasad, K., Reddy, B. V. B., and Pandit, M. W., Correlation between stability of a protein and its dipeptide composition: a novel approach for predicting *in vivo* stability of a protein from its primary sequence, (1990) *Protein Engineering 4*, 155-161.

199 Wilkinson, D. L., and Harrison, R. G., Predicting the solubility of recombinant proteins in *Escherichia coli*, (1991) *Bio/Technol. 9*, 443-448.

200 Davis, G. D., Elisee, C., Newham, D. M., and Harrison, R. G., New fusion protein systems designed to give soluble expression in *Escherichia coli*, (1999) *Biotechnol. Bioeng. 65*, 382-288.

201 http://www.biotech.ou.edu/ (August 9th 2007).

202 Dunker, A. K., Lawson, J. D., Brown, C. J., Williams, R. M., Romero, P., Oh, J. S., Oldfield, C. J., Campen, A. M., Ratliff, C. M., Hipps, K. W., Ausio, J., Nissen, M. S., Reeves, R., Kang, C., Kissinger, C. R., Bailey, R. W., Griswold, M. D., Chiu, W., Garner, E. C., and Obradovic, Z., Intrinsically disordered protein, (2001) *J. Mol. Graph. Model. 19*, 26-59.

203 Quevillon-Cheruel, S., Leulliot, N., Gentils, L., van Tilbeurgh, and Poupon, A., Production and crystallization of protein domains: How useful are disorder predictions? (2007) *Curr. Prot. Pep. Sci. 8*, 151-160.

204 Ward, J. J., Sodhi, J. S., McGuffin, L. J., Buxton, B. F., and Jones, D. T., Prediction and functional analysis of native disorder in proteins from the three kingdoms of life, (2004) *J. Mol. Biol. 337*, 635-645.

205 Uversky, V. N., Gillespie, J. R., and Fink, A. L., Why are "natively unfolded" proteins unstructured under physiologic conditions? (2000) *Proteins 41*, 415-427.

206 Prilusky, J., Felder, C. E., Zeev-Ben-Mordehai, T., Rydberg, E. H., Man, O., Beckmann, J. S., Silman, I., and Sussman, J. L., FoldIndex: a simple tool to predict whether a given protein sequence is intrinsically unfolded. (2005) *Bioinformatics 21*, 3435-3438.

207 Galzitskaya, O. V., Garbuzynskiy, S. O., and Lobanov, M. Y., Prediction of natively unfolded regions in protein chain, (2006) *Mol Biol (Mosk). 40*, 341-348.

208 Linding, R., Russell, R. B., Neduva, V., and Gibson, T. J., GlobPlot: Exploring protein sequences for globularity and disorder, (2003) *Nucleic Acids Res. 31*, 3701-3708.

209 Dosztanyi, Z., Csizmok, V., Tompa, P., and Simon, I., IUPred: web server for the prediction of intrinsically unstructured regions of proteins based on estimated energy content, (2005) *Bioinformatics 21*, 3433-3434.

210 Obradovic, Z., Peng, K., Vucetic, S., Radivojac, P., Brown, C. J., and Dunker, A. K., Predicting intrinsic disorder from amino acid sequence, (2003) *Proteins 53*, Suppl 6, 566-572.

211 Coeytaux, K., and Poupon, A., Prediction of unfolded segments in a protein sequence based on amino acid composition, (2005) *Bioinformatics 21*, 1891-1900.

212 Yang, Z. R., Thomson, R., McNeil, P., and Esnouf, R. M., RONN: the bio-basis function neural network technique applied to the detection of natively disordered regions in proteins, (2005) *Bioinformatics 21*, 3369-3376.

213 Vucetic, S., Obradovic, Z., Vacic, V., Radivojac, P., Peng, K., Iakoucheva, L. M., Cortese, M.S., Lawson, J.D., Brown, C.J., Sikes, J. G., Newton, C. D., and Dunker, A. K., DisProt: a database of protein disorder, (2005) *Bioinformatics 21*, 137-140. http://www.disprot.org (August 9th 2007).

214 Ichimura, T., Uchiyama, J., Kunihiro, O., Ito, M., Horigome, T., Omata, S., Shinkai, F., Kaji, H., and Isobe, T., Identifcation of the site of interaction of the 14-3-3 protein with phosphorylated tryptophan hydroxylase, (1995) *J. Biol. Chem. 270*, 28515-28518.

215 http://www.ncbi.nlm.nih.gov/BLAST/Blast.cgi (August 9th 2007).

216 Lee, A. Y., Karplus, P. A., Ganem, B., and Clardy, J., Atomic structure of the buried catalytic pocket of *Eshcerichia coli* chorismate mutase, (1995) *J. Am. Chem. Soc. 117*, 3627-3628.

217 Zhang, S., Wilson, D. B., and Ganem, B., Probing the catalytic mechanism o prephenate dehydratase by site-directed mutagenesis of the *Escherichia coli* P-protein dehydratase domain, (2000) *Biochemistry 39*, 4722-4728.

218 Pohmert, G., Zhang, S., Husain, A., Wilson, D. B., and Ganem, B., Regulation of phenylalanine biosynthesis. Studies on the mechanism of phenylalanine binding and feedback inhibition in the *Escherichia coli* P-protein, (1999) *Biochemistry 38*, 12212-12217.

219 Aravind, L., and Koonin, E. V., Gleaning non-trivial structural, functional and evolutionary information about proteins by iterative database searches, (1999) *J. Mol. Biol. 287*, 1023-1040.

220 Liberles, J. S., Thórólfsson, M. and Martínez, A., Allosteric mechanisms in ACT domain containing enzymes involved in amino acid metabolism, (2005) *Amino Acids 28*, 1-12.

221 Chipman, D. M., and Shaanan, B., The ACT domain family, (2001) *Cur. Opin. Struct. Biol. 11*, 694-700.

222 Esposito, D., and Chatterjee, D. K., Enhancement of soluble protein expression through the use of fusion tags, (2006) *Curr. Opin. Biotechnol. 17*, 353-358.

223 Pilon, A. L., Yost, P., Chase, T. E., Lohnas, G. L., and Bentley, W. E., High-level expression and efficient recovery of ubiquitin fusion proteins from *Escherichia coli*, (1996) *Biotechnol. Prog. 12*, 331-337.

224 Marblestone, J. G., Edavettal, S. C., Lim, Y., Lim, P., Zuo, X., and Butt, T. R., Comparison of SUMO fusion technology with traditional gene fusion systems: Enhanced expression and solubility with SUMO, (2006) *Protein Sci. 15*, 182-189.

225 Zhang, Y., Howitt, J., McCorkle, S., Lawrence, P., Springer, K., and Freimuth, P., Protein aggregation during overexpression limited by peptide extensions with large net negative charge, (2004) *Prot. Expr. Purif. 36*, 207-216.

226 Welchman, R. L., Gordon, C., and Mayer, R. J., Ubiquitin and ubiquitin-like proteins as multifunctional signals, (2005) *Nature Rev. Mol. Cell Biol. 6*, 599-609.

227 Butt, T. R., Jonnalagadda, S., Monia, B. P., Sternberg, E. J., Marsh, J. A., Stadel, J. M., Ecker, D. J., and Crooke, S. T., Ubiquitin fusion augments the yield of cloned gene products in *Escherichia coli*, (1989) *Proc. Natl. Acad. Sci. USA 86*, 2540-2544.

228 Guzzo, C. M., and Yang, D. C. H., Systematic analysis of fusion and affinity tags using human aspartyl-tRNA synthetase expressed in *E. coli*, (2007) *Prot. Expr. Purif. 54*, 166-175.

229 Baker, R. T., Protein expression using ubiquitin fusion and cleavage, (1996) *Curr. Opin. Biotechnology 7*, 541-546.

230 Gohara, D. W., Ha, C. S., Ghosh, S. K. B., Arnold, J. J., Wisniewski, T. J., and Cameron, C. E., Production of authentic poliovirus RNA-dependent RNA polymerase ($3D^{pol}$) by ubiquitin-protease-mediated cleavage in *Esherichia coli*, (1999) *Protein Expr. Purif. 17*, 128-138.

231 Vendelboe, T. V., Cloning and expression of full-length and truncated dopamine-β-monooxygenase in *Escherichia coli* and initial purification of a tryptophan hydroxylase mutant, M. Sc. thesis, Department of Chemistry, Technical University of Denmark, Kgs. Lyngby, 2007.

232 Zhou, P., Lugovskoy, A. A., and Wagner, G., A solubility-enhancement tag (SET) for NMR studies of poorly behaving proteins, (2001) *J. Biomol. NMR 20*, 11-14.

233 http://www.stratagene.com/lit_items/PROEXP_BR59_Q204.pdf (August 9th 2007).

234 http://www.expasy.org/tools/protparam.html (August 9th 2007).

235 Moran, G. R., and Fitzpatrick P. F., A continuous fluorescence assay for tryptophan hydroxylase, (1999) *Anal. Biochem. 266*, 148-152.

236 Sachdev, D., and Chirgwin, J. M., Properties of soluble fusion between mammalian aspartic proteinases and bacterial maltose-binding protein, (1999) *J. Protein Chem. 18*, 127-136.

237 Nominé, Y., Ristriani, T., Laurent, C., Lefèvre, J., Weiss, É., and Travé, G., Formation of soluble inclusion bodies by HPV E6 oncoprotein fused to maltose-binding protein, (2001) *Protein Expr. Purif. 23*, 22-32.

238 Zanier, K., Nomine, Y., Charbonnier, S., Ruhlmann, C., Schultz, P., Schweizer, J., and Travé, G., Formation of well-defined soluble aggregates upon fusion to MBP is a generic property of E6 proteins from various human papillomavirus species, (2007) *Protein Expr. Purif.* 51, 59-70

239 Kane, J. F., and Hartley, D. L., Formation of recombinant inclusion bodies in *Escherichia coli*, (1988) *Trends Biotechnol. 6*, 95-101.

240 Rudolph, R., and Lilie, H., *In vitro* folding of inclusion body proteins, (1996) *FASEB J.* 10, 49-56.

241 Stevens, R. C., Design of high-throughput methods of protein production for structural biology, (2000) *Structure 8*, R177-R185.

242 Ding, H., Ren, H., Chen, Q., Fang, G., Li, L., Li, R., Wang, Z., Jia, X., Liang, Y., Hu, M., Li, Y., Luo, J., Gu, X., Su, X.-D., Luo, M., and Lu, S., Parallel cloning, expression, purification and crystallization of human proteins for structural genomics, (2002) *Acta Cryst. D58*, 2102-2108

243 Finley, J. B., Qiu, S.-H., Luan, C.-H., and Luo, M., Structural genomics for *Caenorhabditis elegans*: high throughput protein expression ananlysis, (2004) *Prot. Expr. Purif. 34*, 49-55.

244 Dyson, M. R., Shadbolt, S. P., Vincent, K. J., Perera, R. L., and McCarfferty, J., Production of soluble mammalian proteins in *Escherichia coli*: identification of protein freatures that correlate with successful expression, (2004) *BMC Biotechnology* 4, 32.

245 Pace, C. N., Vajdos, F., Fee, L., Grimsley, G., and Gray, T., How to measure and predict the molar absorption coefficient of a protein, (1995) *Protein Sci. 4*, 2411-2423.

246 http://www.bio-rad.com/LifeScience/pdf/Bulletin_9281.pdf (August 9th 2007)

247 Segel, I. H., Introduction – enzymes as biological catalysts, Chapter 1, Enzyme kinetics, behavior and analysis of rapid equilibrium and steady-state enzyme systems,. John Wiley and Son, Inc., New York, 1975.

248 Fersht, A., Detection of intermediates in enzymatic reactions, Chapter 7, Structure and mechanism in protein science, a guide to enzyme catalysis and protein folding, , W. H. Freemann and Comp. New York, 1999.

249 Cleland, W. W., The kinetics of enzyme-catalyzed reactions with two or more substrates or products, I. nomenclature and rate equations, (1963) *Biochim. Biophys. Acta 67*, 104-137.

250 Leskovac, V., Trisubstrate mechanism, Chapter 12, Comprehensive enzyme kinetics, Kluwer Academic/Plenum Press, New York, 2003.

251 Henderson, P. J., Statistical ananlysis of enzyme kinetic data, Chapter 10, Enzyme Assays, A practical approach, Editors Eisenthal, R., and Danson, M. J., Oxford University Press, Oxford, 1992.

252 Cleland, W. W., Steady state kinetics, Chapter 1, The enzymes, kinetics and mechanism, vol. 2, 3rd edition, Editor Boyer, P. D., Academic Press, New York, 1970.

253 King, E. L., and Altman, C., A schematric method of deriving the rate laws for enzyme catalyzed reactions, (1956) *J. Phys. Chem. 60*, 1375-1378.

254 Frieden, C., Glutamic dehydrogenase III. The order of substrate addition in the enzymatic reaction, (1959) *J. Biol. Chem. 234*, 2891-2896.

255 Viola, R. E., and Cleland, W. W., Initial velocity analysis for terreactant mechanisms, (1982) *Methods Enzymol. 87*, 353-366.

256 Segel, I. H., Steady-state kinetics of multireactant enzymes, Chapter 9, Enzyme kinetics, behavior and analysis of rapid equilibrium and steady-state enzyme systems,. John Wiley and Son, Inc., New York, 1975.

257 Segel, I. H., Rapid equilibrium bireactant and terreactant systems, Chapter 6, Enzyme kinetics, behavior and analysis of rapid equilibrium and steady-state enzyme systems,. John Wiley and Son, Inc., New York, 1975.

258 Dalziel, K., The interpretation of kinetic data for enzyme-catalysed reactions involving three substrates, (1969) *Biochem. J. 114*, 547-556.

259 Fromm, H. J., The use of competitive inhibitors in studying the mechanism of action of some enzyme systems utilizing three substrates, (1967) *Biochim. Biophys. Acta 139*, 221-230.

260 Rudolph, F. B., and Fromm, H. J., Plotting methods for analyzing enzyme rate data, (1979) *Methods Enzymol. 63*, 138-159.

261 Emanuele J. J., Jr., Jin, H., Yanchunas, J., and Villafranca, J. J., Evaluation of kinectic mechanism of *Escherichia coli* uridine diphosphate-N-acetylmuramate:L-alanine ligase, (1997) *Biochemistry 36*, 7264-7271.

262 Brekken, D. L., and Phillips, M. A., *Trypanosoma brucei* γ-glutamylcysteine synthetase, (1998) *J. Biol. Chem. 273*, 26317-26322.

263 Jez, J. M., and Cahoon, R. E., Kinetic mechanism of glutathione synthetase from *Arabidopsis thaliana*, (2004) *J. Biol. Chem. 279*, 42726-42731.

264 Xu, H., West, A. H., and Cook, P. F., Overall kinetic mechanism of saccharopine dehydrogenase from *Saccharomyces cerevisiae*, (2006) *Biochemistry 45*, 12156-12166.

265 Rudolph, F. B., and Fromm, H. J., Initial rate studies of adenylosuccinate synthetase with product and competitive inhibitors, (1969) *J. Biol. Chem. 244*, 3832-3839.

266 Friedman P. A., Kappelman A. H., and Kaufman S. Partial purification and characterization of tryptophan hydroxylase from rabbit hindbrain, (1972) *J. Biol. Chem. 247*, 4165-4173.

267 Battino, R., Editor, IUPAC Solubility data series, Vol. 7, Oxygen and Ozone, Pergamon Press, Oxford, 1981.

268 Cleland, W. W., Dithiothreitol, a new protective reagent for SH groups, (1964) *Biochemistry 3*, 480-482.

269 Motulsky, H., and Christopoulos, A., Fitting models to biological data using linear and nonlinear regression, a practical guide to curve fitting, Oxford University Press, Oxford, 2004.

270 Ndubuizu, O., and LaManna, J. C., Brain tissue oxygen concentration measurements, (2007) *Antioxid. Redox. Signal. 9*, 1207-1220.

271 McPherson, A., Introduction to protein crystallization, (2004) *Methods 34*, 254–265.

272 McPherson, A., Current approaches to macromolecular crystallization, (1990) *Eur. J. Biochem. 189*, 1-23.

273 Giegé, R., and Ducruix, A., An introduction to the crystallogenesis of biological macromolecules, Chapter 1 in Crystallization of nucleic acids and proteins, A practical approach, Editors Ducruix, A., and Giegé, R., 2nd edition, Oxford University Press, Oxford, 1999.

274 Carter, Jr., C. W. and Riés-Kautt, M., Improving marginal crystals, (2007) *Methods Mol. Biol. 363*, 153-174.

275 Jancarik, J., and Kim, S.-H., Sparse matrix sampling: a screening method for crystallization of proteins, (1991) *J. Appl. Crystallogr. 24*, 409-411.

276 Wooh, J. W., Kidd, T. D., Martin, J. L., and Kobe, B., Comparison of three commercial sparse-matrix crystallization screens, (2003) *Acta Cryst. D59*, 769-772.

277 Newman, J., Egan, D., Walter, T. S., Meged, R., Berry, I., Jelloul, M. B., Sussman, J. L., Stuart, D. I., and Perrakis, A., Towards rationalization of crystallization screening for small- to medium-sized academic laboratories: the PACT/JCSG+ strategy, (2005) *Acta Cryst D61*, 1426-1431.

278 Riés-Kautt, M., Strategy 2: An alternative to sparse matrix screens, in Protein crystallization, techniques, strategies and tips, A laboratory manual, Editor Bergfors, T. M., International University Line, La Jolla, 1999.

279 Haire, L. L., Strategy 4: Imperial College grid screen, in Protein crystallization, techniques, strategies and tips, A laboratory manual, Editor Bergfors, T. M., International University Line, La Jolla, 1999.

280 http://www.hamptonresearch.com/products/ProductDetails.aspx?cid=1&sid=24&pid=5 (August 9th 2007)

281 Weber, P. C., Overview of protein crystallization methods, (1997) *Methods Enzymol. 276*, 13-22.

282 Timasheff, S. N., and Arakawa, T., Mechanism of protein precipitation and stabilization by co-solvents, (1988) *J. Cryst. Growth 90*, 39-46.

283 Riés-Kautt, M., and Ducruix, A., Inferences drawn from physicochemical studies of crystallogenesis and precrystalline state, (1997) *Methods Enzymol. 276*, 23-59.

284 Collins, K. D., Ions from the Hofmeister series and osmolytes: effects on proteins in solution and in the crystallization process, (2004) *Methods 34*, 300-311.

285 Miller, S., Janin, J., Lesk, A. M., and Chothia, C., Interior and surface of monomeric proteins, (1987) *J. Mol. Biol. 196*, 641-636.

286 McPherson, A., A comparison of salts for the crystallization of macromolecule, (2001) *Protein Sci. 10*, 418-422.

287 Trakhanov, S., and Quiocho, F. A., Influence of divalent cations in protein crystallization, (1995) *Protein Sci. 4*, 1914-1919.

288 McPherson, Jr., A., Crystallization of proteins from polyethylene glycol, (1976) *J. Biol. Chem. 251*, 6300-6303.

289 Ingham, K. C., Precipitation of proteins with polyethylene glycol, (1990) *Methods Enzymol. 182*, 301-306.

290 Finet, S., Vivarés, D., Bonneté, F., and Tardieu, A., Controlling biomolecular crystallization by understanding the distinct effects of PEGs and salts on solubility, (2003) *Methods Enzymol. 368*, 105-129.

291 Patel, S., Cudney, B., and McPherson, A., Polymeric precipitants for the crystallization of macromolecules, (1995) *Biochem. Biophys. Res. Comm. 207*, 819-828.

292 Bolen, D. W., Effects of naturally occurring osmolytes on protein stability and solubility: issues important in protein crystallization, (2004) *Methods 34*, 312-322.

293 McPherson, A., and Cudney, B., Searching for silver bullets: An alternative strategy for crystallizing macromolecules, (2006) *J. Struct. Biol. 156*, 387-406.

294 Larson, S. B., Day, J. S., Cudney, R., and McPherson, A., A novel strategy for the crystallization of proteins: X-ray diffraction validation, (2007) *Acta Cryst. D63*, 310-318.

295 McPherson, A., Koszelak, S., Axelrod, H., Day, J., Robinson, L., McGrath, M., Williams, R., and Cascio, D., The effects of neutral detergents on the crystallization of soluble proteins, (1986) *J. Cryst. Growth 76*, 547-553.

296 Hanson, B. L., and Bunick, G. J., The well-tempered protein crystal: annealing macromolecular crystals, (2003) *Methods Enzymol. 368*, 217-235.

297 Garman, E., Crystallization for cryo-data collection, in Protein crystallization, Techniques, strategies, and tips, a laboratory manual, Editor Bergfors, T. M., International University Line, La Jolla, 1999.

298 Newman, J., Novel buffer systems for macromolecular crystallization, (2004) *Acta Cryst. D60*, 610-612.

299 Bergfors, T. M., Dynamic light scattering, Chapter 4 in Protein crystallization: techniques, strategies and tips, Editor Bergfors, T. M., International University Line, La Jolla, 1999.

300 Scopes, R. K., Chapter 6 in Protein purification, principles and practise, 3rd edition, Springer-Verlag, New York, 1994.

301 Jancarik, J., Pufan, R., Hong, C., Kim, S.-H., and Kim, R., Optimum solubility (OS) screening: an efficient method to optimize buffer conditions for homogeneity and crystallization of proteins, (2004) *Acta Cryst. D60*, 1670-1673.

302 Collins, B., Stevens, R. C., and Page, R., Crystallization optimum solubility screening: using crystallisation results to identify the optimal buffer for protein crystal formation, (2005) *Acta Cryst. D61*, 1035-1038.

303 Izaac, A., Schall, C. A., and Mueser, T. C., Assessment of a preliminary solubility screen to improve crystallization trials, uncoupling crystal condition searches, (2006) *Acta Cryst. D62*, 833-842.

304 Sousa, R., Using cosolvents to stabilize protein conformation for crystallisation, (1997) *Methods Enzymol. 276*, 131-143.

APPENDIX ONE

A.1 Standard curves of 5-hydroxytryptophan

The standard curves for 5-hydroxytryptophan at different concentrations of BH_4.

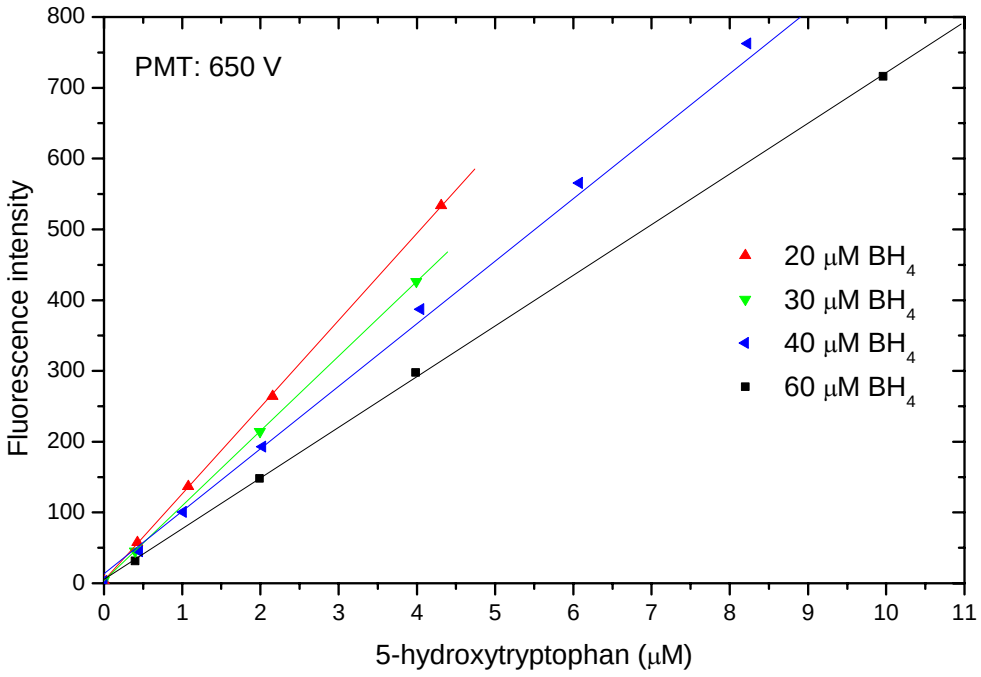

Slopes of the standard curves for 5-hydroxytryptophan at different concentrations of BH_4 with a PMT of 650 V.

BH_4 (μM)	Slope (f.i./ μM 5-hydroxytryptophan)	R^2
20	122.65±0.72	0.9999
30	105.81±0.23	0.9999
40	88.36±1.84	0.9987
60	71.625±0.567	0.9999
100	44.635±0.607	0.9996
150	27.552±0.453	0.9995
200	18.015±0.046	0.9999
300	7.7749±0.0835	0.9996
400	4.5998±0.0356	0.9999

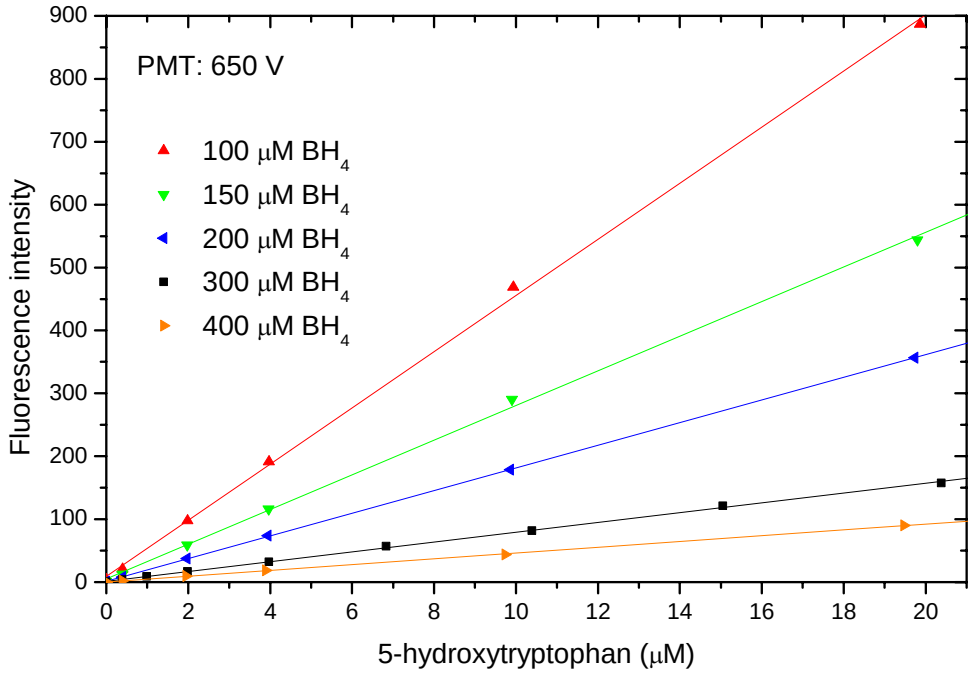

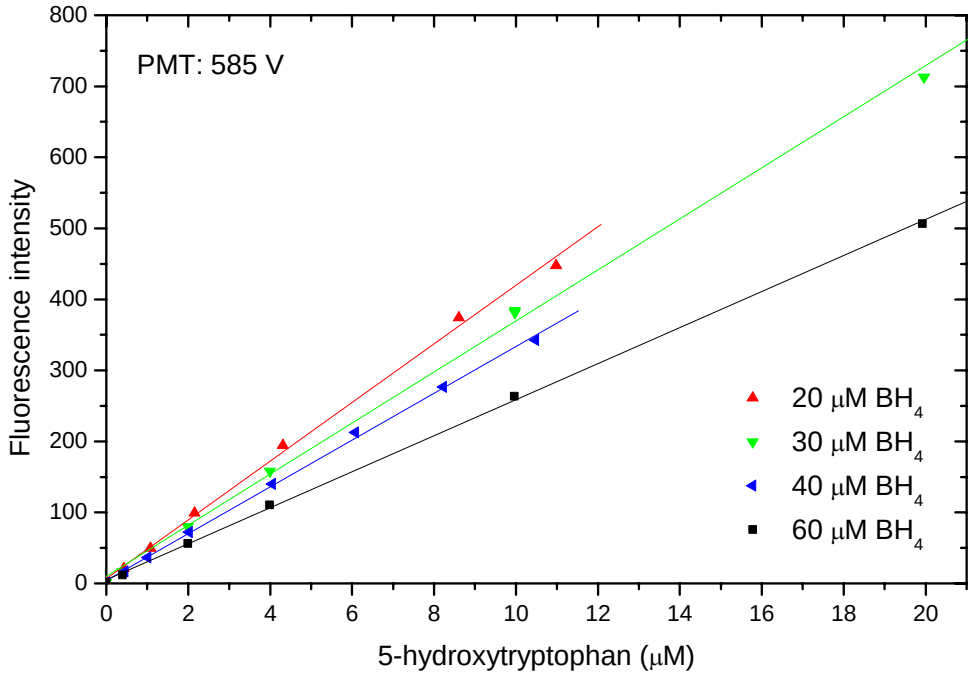

Slopes of the standard curves for 5-hydroxytryptophan at different concentrations of BH_4 with a PMT of 585 V.

BH_4 (μM)	Slope (f.i./ μM 5-hydroxytryptophan)	R^2
20	41.296±0.900	0.9988
30	35.950±0.703	0.9991
40	32.939±0.457	0.9994
60	25.374±0.278	0.9998

APPENDIX TWO

A.2 Composition of crystallisation screens

A.2.1 Stura Footprint

The Stura Footprint screens are from Molecular Dimensions.

A.2.1.1 Stura Footprint screen 1

#	Buffer	Salt	Other
A1	0.2 M imidazole malate pH 5.5		15% PEG 600
B1	0.2 M imidazole malate pH 5.5		24% PEG 600
C1	0.2 M imidazole malate pH 5.5		33% PEG 600
D1	0.2 M imidazole malate pH 5.5		42% PEG 600
A2	0.2 M imidazole malate pH 7.0		10% PEG 4000
B2	0.2 M imidazole malate pH 7.0		15% PEG 4000
C2	0.2 M imidazole malate pH 7.0		20% PEG 4000
D2	0.2 M imidazole malate pH 7.0		25% PEG 4000
A3	0.2 M imidazole malate pH 8.5		7.5% PEG 10000
B3	0.2 M imidazole malate pH 8.5		12.5% PEG 10000
C3	0.2 M imidazole malate pH 8.5		17.5% PEG 10000
D3	0.2 M imidazole malate pH 8.5		22.5% PEG 10000
A4	0.15 M sodium citrate pH 5.5	0.75 M $(NH_4)_2SO_4$	
B4	0.15 M sodium citrate pH 5.5	1.0 M $(NH_4)_2SO_4$	
C4	0.15 M sodium citrate pH 5.5	1.5 M $(NH_4)_2SO_4$	
D4	0.15 M sodium citrate pH 5.5	2.0 M $(NH_4)_2SO_4$	
A5	0.8 M NaH_2PO_4 /K_2HPO_4 pH 7.0		
B5	1.32 M NaH_2PO_4 /K_2HPO_4 pH 7.0		
C5	1.6 M NaH_2PO_4 /K_2HPO_4 pH 7.0		
D5	2.0 M NaH_2PO_4 /K_2HPO_4 pH 7.0		
A6	10 mM sodium borate pH 8.5	0.75 M Citrate	
B6	10 mM sodium borate pH 8.5	1.0 M Citrate	
C6	10 mM sodium borate pH 8.5	1.2 M Citrate	
D6	10 mM sodium borate pH 8.5	1.5 M Citrate	

A.2.1.2 Stura Footprint screen 2

#	Buffer	Salt	Other
A1	0.1 M HEPES pH 8.2		30% MPEG 550
B1	0.1 M HEPES pH 8.2		40% MPEG 550
C1	0.1 M HEPES pH 8.2		50% MPEG 550
D1	0.1 M HEPES pH 8.2		60% MPEG 550
A2	0.1 M HEPES pH 7.5		18% PEG 600
B2	0.1 M HEPES pH 7.5		27% PEG 600
C2	0.1 M HEPES pH 7.5		36% PEG 600

D2	0.1 M HEPES pH 7.5		45% PEG 600
A3	0.1 M sodium cacodylate pH 6.5		18% PEG 2000
B3	0.1 M sodium cacodylate pH 6.5		27% PEG 2000
C3	0.1 M sodium cacodylate pH 6.5		36% PEG 2000
D3	0.1 M sodium cacodylate pH 6.5		45% PEG 2000
A4	0.2 M imidazole malate pH 6.0		8% PEG 4000
B4	0.2 M imidazole malate pH 6.0		15% PEG 4000
C4	0.2 M imidazole malate pH 6.0		20% PEG 4000
D4	0.2 M imidazole malate pH 6.0		30% PEG 4000
A5	0.1 M sodium acetate pH 5.5		12% MPEG 5000
B5	0.1 M sodium acetate pH 5.5		18% MPEG 5000
C5	0.1 M sodium acetate pH 5.5		24% MPEG 5000
D5	0.1 M sodium acetate pH 5.5		36% MPEG 5000
A6	0.1 M ammonium acetate pH 4.5		9% PEG 10000
B6	0.1 M ammonium acetate pH 4.5		15% PEG 10000
C6	0.1 M ammonium acetate pH 4.5		22.5% PEG 10000
D6	0.1 M ammonium acetate pH 4.5		27% PEG 10000

A.2.2 Index screen

The Index screen is from Hampton Research

#	Buffer	Salt	Other
1	0.1 M Citric acid pH 3.5	2.0 M $(NH_4)_2SO_4$	
2	0.1 M Na-acetate pH 4.5	2.0 M $(NH_4)_2SO_4$	
3	0.1 M Bis-Tris pH 5.5	2.0 M $(NH_4)_2SO_4$	
4	0.1 M Bis-Tris pH 6.5	2.0 M $(NH_4)_2SO_4$	
5	0.1 M HEPES pH 7.5	2.0 M $(NH_4)_2SO_4$	
6	0.1 M Tris pH 8.5	2.0 M $(NH_4)_2SO_4$	
7	0.1 M Citric acid pH 3.5	3.0 M NaCl	
8	0.1 M Na-acetate pH 4.5	3.0 M NaCl	
9	0.1 M Bis-Tris pH 5.5	3.0 M NaCl	
10	0.1 M Bis-Tris pH 6.5	3.0 M NaCl	
11	0.1 M HEPES pH 7.5	3.0 M NaCl	
12	0.1 M Tris pH 8.5	3.0 M NaCl	
13	0.1 M Bis-Tris pH 5.5	0.3 M Mg-$(formate)_2$	
14	0.1 M Bis-Tris pH 6.5	0.5 M Mg-$(formate)_2$	
15	0.1 M HEPES pH 7.5	0.5 M Mg-$(formate)_2$	
16	0.1 M Tris pH 8.5	0.3 M Mg-$(formate)_2$	
17	None - pH 5.6	1.26 M NaH_2PO_4, 0.14 M K_2HPO_4	
18	None - pH 6.9	0.49 M NaH_2PO_4 0.91 M K_2HPO_4	
19	None - pH 8.2	0.056 M NaH_2PO_4 1.344 M K_2HPO_4	
20	0.1 M HEPES pH 7.5	1.4 M Na_3-citrate	
21	None	1.8 M $(NH_4)_3$-citrate pH 7.0	
22	None	0.8 M succinic acid pH 7.0	
23	None	2.1 M DL-malic acid pH 7.0	
24	None	2.8 M Na-acetate pH 7.0	
25	None	3.5 M Na-formate pH 7.0	
26	None	1.1 M $(NH_4)_2$-tartrate pH 7.0	
27	None	2.4 M Na-malonate pH 7.0	

28	None	35% v/v Tacsimate pH 7.0	
29	None	60% v/v Tacsimate pH 7.0	
30	0.1 M Bis-Tris pH 6.5	0.1 M NaCl	1.5 M $(NH_4)_2SO_4$
31	0.1 M Tris pH 8.5	0.8 M Na/K-tartrate	0.5% w/v M PEG 5000
32	0.1 M Bis-Tris pH 5.5	1.0 M $(NH_4)_2SO_4$	1% w/v PEG 3350
33	0.1 M HEPES pH 7.0	1.1 M Na-malonate pH 7.0	0.5% v/v Jeffamine ED-2001, reagent pH 7
34	0.1 M HEPES pH 7.0	1.0 M succinic acid pH 7.0	1% w/v MPEG 2000
35	0.1 M HEPES pH 7.0	1.0 M $(NH_4)_2SO_4$	0.5% w/v PEG 8000
36	0.1 M HEPES pH 7.0	15% v/v Tacsimate pH 7.0	2% w/v PEG 3350
37	None		25% w/v PEG 1500
38	0.1 M HEPES pH 7.0		30% v/v Jeffamine M-600 reagent pH 7.0
39	M HEPES pH 7.0		30% v/v Jeffamine ED-2001 reagent pH 7
40	0.1 M Citric Acid pH 3.5		25% w/v PEG 3350
41	0.1 M Na-acetate pH 4.5		25% w/v PEG 3350
42	0.1 M Bis-Tris pH 5.5		25% w/v PEG 3350
43	0.1 M Bis-Tris pH 6.5		25% w/v PEG 3350
44	0.1 M HEPES pH 7.5		25% w/v PEG 3350
45	0.1 M Tris pH 8.5		25% w/v PEG 3350
46	0.1 M Bis-Tris pH 6.5		20% w/v MPEG 5000
47	0.1 M Bis-Tris pH 6.5		28% w/v MPEG 2000
48	0.1 M Bis-Tris pH 5.5	0.2 M $CaCl_2$	45% v/v MPD
49	0.1 M Bis-Tris pH 6.5	0.2 M $CaCl_2$	45% v/v MPD
50	0.1 M Bis-Tris pH 5.5	0.2 M (NH_4)-acetate	45% v/v MPD
51	0.1 M Bis-Tris pH 6.5	0.2 M (NH_4)-acetate	45% v/v MPD
52	0.1 M HEPES pH 7.5	0.2 M (NH_4)-acetate	45% v/v MPD
53	0.1 M Tris pH 8.5	0.2 M (NH_4)-acetate	45% v/v MPD
54	0.1 M Bis-Tris pH 6.5	0.05 M $CaCl_2$	30% v/v MPEG 550
55	0.1 M HEPES pH 7.5	0.05 M $MgCl_2$	30% v/v MPEG 550
56	0.05 M HEPES pH 7.5	0.2 M KCl	35% v/v Penta-erythritol propoxylate
57	0.05 M Bis-Tris pH 6.5	0.05 M $(NH_4)_2SO_4$	30% v/v Penta-erythritol ethoxylate
58	0.1 M Bis-Tris pH 6.5	None	45% v/v PPG P 400
59	0.1 M HEPES pH 7.5	0.02 M $MgCl_2$	22% w/v Polyacrylic Acid 5100 Na-salt
60	0.1 M Tris pH 8.5	0.01 M $CoCl_2$	20% w/v Polyvinyl-pyrrolidone K15
61	0.1 M HEPES pH 7.5	0.2 M Proline	10% w/v PEG 3350
62	0.1 M Tris pH 8.5	0.2 M TMAO	20% w/v MPEG 2000
63	0.1 M HEPES pH 7.0	5% v/v Tacsimate pH 7.0	10% w/v MPEG 5000
64	0.1 M HEPES pH 7.5	0.005 M $CoCl_2$ 0.005 M $NiCl_2$ 0.005 M $CdCl_2$ 0.005 M $MgCl_2$	12% w/v PEG 3350
65	0.1 M Bis-Tris pH 5.5	0.1 M (NH_4)-acetate	17% w/v PEG 10000
66	0.1 M Bis-Tris pH 5.5	0.2 M $(NH_4)_2SO_4$	25% w/v PEG 3350
67	0.1 M Bis-Tris pH 6.5	0.2 M $(NH_4)_2SO_4$	25% w/v PEG 3350
68	0.1 M HEPES pH 7.5	0.2 M $(NH_4)_2SO_4$	25% w/v PEG 3350
69	0.1 M Tris pH 8.5	0.2 M $(NH_4)_2SO_4$	25% w/v PEG 3350

70	0.1 M Bis-Tris pH 5.5	0.2 M NaCl	25% w/v PEG 3350
71	0.1 M Bis-Tris pH 6.5	0.2 M NaCl	25% w/v PEG 3350
72	0.1 M HEPES pH 7.5	0.2 M NaCl	25% w/v PEG 3350
73	0.1 M Tris pH 8.5	0.2 M NaCl	25% w/v PEG 3350
74	0.1 M Bis-Tris pH 5.5	0.2 M Li_2SO_4	25% w/v PEG 3350
75	0.1 M Bis-Tris pH 6.5	0.2 M Li_2SO_4	25% w/v PEG 3350
76	0.1 M HEPES pH 7.5	0.2 M Li_2SO_4	25% w/v PEG 3350
77	0.1 M Tris pH 8.5	0.2 M Li_2SO_4	25% w/v PEG 3350
78	0.1 M Bis-Tris pH 5.5	0.2 M (NH_4)-acetate	25% w/v PEG 3350
79	0.1 M Bis-Tris pH 6.5	0.2 M (NH_4)-acetate	25% w/v PEG 3350
80	0.1 M HEPES pH 7.5	0.2 M (NH_4)-acetate	25% w/v PEG 3350
81	0.1 M Tris pH 8.5	0.2 M (NH_4)-acetate	25% w/v PEG 3350
82	0.1 M Bis-Tris pH 5.5	0.2 M $MgCl_2$	25% w/v PEG 3350
83	0.1 M Bis-Tris pH 6.5	0.2 M $MgCl_2$	25% w/v PEG 3350
84	0.1 M HEPES pH 7.5	0.2 M $MgCl_2$	25% w/v PEG 3350
85	0.1 M Tris HCl pH 8.5	0.2 M $MgCl_2$	25% w/v PEG 3350
86		0.2 M K/Na-tartrate	20% w/v PEG 3350
87		0.2 M Na-malonate pH 7.0	20% w/v PEG 3350
88		0.2 M $(NH_4)_3$-citrate pH 7.0	20% w/v PEG 3350
89		0.1 M Succinic acid pH 7.0	15% w/v PEG 3350
90		0.2 M Na-formate	20% w/v PEG 3350
91		0.15 M DL-malic acid pH 7.0	20% w/v PEG 3350
92		0.1 M Mg-$(formate)_2$	15% w/v PEG 3350
93		0.05 M Zn-$(acetate)_2$	20% w/v PEG 3350
94		0.2 M Na_3-citrate	20% w/v PEG 3350
95		0.1 M KSCN	30% w/v MPEG 2000
96		0.15 M KBr	30% w/v MPEG 2000

A.2.3 JCSG+ screen

The JCSG+ screen is from Qiagen.

	Buffer	Salt	Other
1	0.1 M Na-acetate pH 4.5	0.2 M Li_2SO_4	50% w/v PEG 400
2	0.1 M Na_3-citrate pH 5.5		20% w/v PEG 3000
3	0.2 M $(NH_4)_2$-citrate pH 5.0		20% w/v PEG 3350
4	0.1 M Na-acetate pH 4.6	0.02 M $CaCl_2$	30% v/v MPD
5	0.2 M $Mg(formate)_2$ pH 5.9		20% w/v PEG 3350
6	0.1 M Phosphate-citrate pH 4.2	0.2 M Li_2SO_4	20% w/v PEG 1000
7	0.1 M CHES pH 9.5		20% w/v PEG 8000
8	0.2 M NH_4-formate pH 6.6		20% w/v PEG 3350
9		0.2 M NH_4Cl pH 6.3	20% w/v PEG 3350
10	0.2 M K-formate pH 7.3		20% w/v PEG 3350
11	0.1 M Tris pH 8.5	0.2 M NH_4 H_2PO_4	50% v/v MPD
12		0.2 M KNO_3 pH 6.9	20% w/v PEG 3350
13	0.1 M Na_3-citrate pH 4	0.8 M $(NH_4)_2SO_4$	
14		0.2 M NaSCN pH 6.9	20% w/v PEG 3350
15	0.1 M BICINE pH 9		20% w/v PEG 6000
16	0.1 M HEPES pH 7.5		10% w/v PEG 8000 8% ethylene glycol
17	0.1 M Na-cacodylate pH 6.5		40% v/v MPD 5% w/v PEG 8000

18	0.1 M Phosphate-citrate pH 4.2		40% v/v ethanol 5% w/v PEG 1000
19	0.1 M Na-acetate pH 4.6		8% w/v PEG 4000
20	0.1 M Tris pH 7	0.2 M $MgCl_2$	10% w/v PEG 8000
21	0.1 M Na_3-citrate pH 5		20% w/v PEG 6000
22	0.1 M Na cacodylate pH 6.5	0.2 M $MgCl_2$	50% v/v PEG 200
23		1.6 M Na_3-citrate	
24		0.2 M K_3-citrate pH 8.3	20% w/v PEG 3350
25	0.1 M Phosphate-citrate pH 4.2	0.2 M NaCl	20% w/v PEG 8000
26	0.1 M Na_3-citrate pH 4	1 M LiCl	20% w/v PEG 6000
27		0.2 M NH_4NO_3 pH 6.3	20% w/v PEG 3350
28	0.1 M HEPES pH 7		10% w/v PEG 6000
29	0.1 M HEPES pH 7.5	0.8 M Na_3PO_4 0.8 M K_3PO_4	
30	0.1 M Phosphate-citrate pH 4.2		40% v/v PEG 300
31	0.1 M Na acetate pH 4.5	0.2 M $Zn(acetate)_2$	10% w/v PEG 3000
32	0.1 M Tris pH 8.5		20% v/v ethanol
33	0.1 M Na/K phosphate pH 6.2		25% v/v 1,2 propan-diol, 10% v/v glycerol
34	0.1 M BICINE pH 9		10% w/v PEG 20000, 2 %v/v dioxane
35	0.1 M Na acetate pH 4.6	2 M $(NH_4)_2SO_4$	
36			10% w/v PEG 1000, 10% w/v PEG 8000
37			24 %w/v PEG 1500, 20% w/v glycerol
38	0.1 M HEPES pH 7.5	0.2 M $MgCl_2$	30% v/v PEG 400
39	0.1 M Na/K phosphate pH 6.2	0.2 M NaCl	50% v/v PEG 200
40	0.1 M Na-acetate pH 4.5	0.2 M Li_2SO_4	30% w/v PEG 8000
41	0.1 M HEPES pH 7.5	0.2 M $MgCl_2$	70% v/v MPD
42	0.1 M Tris pH 8.5		20% w/v PEG 8000
43	0.1 M Tris pH 8.5	0.2 M Li_2SO_4	40% v/v PEG 400
44	0.1 M Tris pH 8		40% v/v MPD
45		0.17 M $(NH_4)_2SO_4$	25.5% w/v PEG 4000 15% v/v glycerol
46	0.1 M Na-cacodylate pH 6.5	0.2 M $Ca(acetate)_2$	40% v/v PEG 300
47	0.07 M Na-acetate pH 4.6	0.14 M $CaCl_2$	14% v/v isopropanol 30% v/v glycerol
48		0.04 M K_3-phosphate	16% w/v PEG 8000, 20% v/v glycerol
49	0.1 M Na-cacodylate pH 6.5	1 M Na_3-citrate	
50	0.1 M Na-cacodylate pH 6.5	0.2 M NaCl 2 M $(NH_4)_2SO_4$	
51	0.1 M HEPES pH 7.5	0.2 M NaCl	10% v/v isopropanol
52	0.1 M Tris pH 8.5	0.2 M Li_2SO_4 1.26 M $(NH_4)_2SO_4$	
53	0.1 M CAPS pH 10.5		40% v/v MPD
54	0.1 M Imidazole pH 8	0.2 M $Zn(acetate)_2$	20% w/v PEG 3000
55	0.1 M Na-cacodylate pH 6.5	0.2 M $Zn(acetate)_2$	10% v/v isopropanol
56	0.1 M Na-acetate pH 4.5	1 M $(NH_4)_2HPO_4$	
57	0.1 M MES pH 6.5	1.6 M $MgSO_4$	
58	0.1 M BICINE pH 9		10% w/v PEG 6000

59	0.08 M Na cacodylate pH 6.5	0.16 M Ca-(acetate)$_2$	14.4% w/v PEG 8000 20% v/v glycerol
60	0.1 M Imidazole pH 8		10% w/v PEG 8000
61	0.1 M MES pH 6.5	0.05 M CsCl	30% w/v Jeffamine M-600
62	0.1 M Na_3-citrate pH 5	3.15 M $(NH_4)_2SO_4$	
63	0.1 M Tris pH 8		20% v/v MPD
64	0.1 M HEPES pH 6.5		20% w/v Jeffamine M-600
65	0.1 M Tris pH 8.5	0.2 M $MgCl_2$	50% v/v ethylene glycol
66	0.1 M BICINE pH 9		10% v/v MPD
67	0.8 M Succinic acid pH 7.0		
68	2.1 M DL-malic acid pH 7.0		
69	2.4 M Na-malonate pH 7.0		
70	0.1 M HEPES pH 7.0	1.1 M Na-malonate pH 7	0.5 % v/v Jeffamine ED-2001 pH 7.0
71	0.1 M HEPES pH 7.0	1 M Succinic acid pH 7	1% w/v MPEG 2000
72	0.1 M HEPES pH 7.0		30% v/v Jeffamine M-600 pH 7.0
73	0.1 M HEPES pH 7.0		30% v/v Jeffamine ED-2001 pH 7.0
74	0.1 M HEPES pH 7.5	0.02 M $MgCl_2$	22% w/v Polyacrylic acid 5100 sodium salt
75	0.1 M Tris pH 8.5	0.1 M $CoCl_2$	20% w/v Polyvinyl-pyrrolidone K15
76	0.1 M Tris pH 8.5	0.2 M TMAO	20% w/v MPEG 2000
77	0.1 M HEPES pH 7.5	0.005 M $CoCl_2$ 0.005 M $CdCl_2$ 0.005 M $MgCl_2$ 0.005 M $NiCl_2$	12% w/v PEG 3350
78	0.2 M Na-malonate pH 7.0		20% w/v PEG 3350
79	0.1 M Succinic acid pH 7.0		15% w/v PEG 3350
80	0.15 M DL-Malic acid pH 7.0		20% w/v PEG 3350
81		0.1 M KSCN	30% w/v MPEG 2000
82		0.15 M KBr	30% w/v MPEG 2000
83	0.1 M bis-Tris pH 5.5	2 M $(NH_4)_2SO_4$	
84	0.1 M bis-Tris pH 5.5	3 M NaCl	
85	0.1 M bis-Tris pH 5.5	0.3 M Mg-(formate)$_2$	
86	0.1 M bis-Tris pH 5.5	1 M $(NH_4)_2SO_4$	1% w/v PEG 3350
87	0.1 M bis-Tris pH 5.5		25% w/v PEG 3350
88	0.1 M bis-Tris pH 5.5	0.2 M $CaCl_2$	45% v/v MPD
89	0.1 M bis-Tris pH 5.5	0.2 M NH_4-acetate	45% v/v MPD
90	0.1 M bis-Tris pH 5.5	0.1 M NH_4-acetate	17% w/v PEG 10000
91	0.1 M bis-Tris pH 5.5	0.2 M $(NH_4)_2SO_4$	25% w/v PEG 3350
92	0.1 M bis-Tris pH 5.5	0.2 M NaCl	25% w/v PEG 3350
93	0.1 M bis-Tris pH 5.5	0.2 M Li_2SO_4	25% w/v PEG 3350
94	0.1 M bis-Tris pH 5.5	0.2 M NH_4-acetate	25% w/v PEG 3350
95	0.1 M bis-Tris pH 5.5	0.2 M $MgCl_2$	25% w/v PEG 3350
96	0.1 M HEPES pH 7.5	0.2 M NH_4-acetate	45% v/v MPD

A.2.4 PACT screen

The JCSG+ screen is from Qiagen.

	Buffer	Salt	Other
1	0.1 M SPG buffer pH 4		25% w/v PEG 1500
2	0.1 M SPG buffer pH 5		25% w/v PEG 1500
3	0.1 M SPG buffer pH 6		25% w/v PEG 1500
4	0.1 M SPG buffer pH 7		25% w/v PEG 1500
5	0.1 M SPG buffer pH 8		25% w/v PEG 1500
6	0.1 M SPG buffer pH 9		25% w/v PEG 1500
7	0.1 M Na-acetate pH 5	0.2 M NaCl	20% w/v PEG 6000
8	0.1 M Na-acetate pH 5	0.2 M NH_4Cl	20% w/v PEG 6000
9	0.1 M Na-acetate pH 5	0.2 M $LiCl_2$	20% w/v PEG 6000
10	0.1 M Na-acetate pH 5	0.2 M $MgCl_2$	20% w/v PEG 6000
11	0.1 M Na-acetate pH 5	0.2 M $CaCl_2$	20% w/v PEG 6000
12	0.1 M Na-acetate pH 5	0.01 M ZnCl	20% w/v PEG 6000
13	0.1 M MIB buffer pH 4		25% w/v PEG 1500
14	0.1 M MIB buffer pH 5		25% w/v PEG 1500
15	0.1 M MIB buffer pH 6		25% w/v PEG 1500
16	0.1 M MIB buffer pH 7		25% w/v PEG 1500
17	0.1 M MIB buffer pH 8		25% w/v PEG 1500
18	0.1 M MIB buffer pH 9		25% w/v PEG 1500
19	0.1 M MES pH 6	0.2 M NaCl	20% w/v PEG 6000
20	0.1 M MES pH 6	0.2 M NH_4Cl	20% w/v PEG 6000
21	0.1 M MES pH 6	0.2 M LiCl	20% w/v PEG 6000
22	0.1 M MES pH 6	0.2 M MgCl	20% w/v PEG 6000
23	0.1 M MES pH 6	0.2 M $CaCl_2$	20% w/v PEG 6000
24	0.1 M MES pH 6	0.01 M $ZnCl_2$	20% w/v PEG 6000
25	0.1 M PCB buffer pH 4		25% w/v PEG 1500
26	0.1 M PCB buffer pH 5		25% w/v PEG 1500
27	0.1 M PCB buffer pH 6		25% w/v PEG 1500
28	0.1 M PCB buffer pH 7		25% w/v PEG 1500
29	0.1 M PCB buffer pH 8		25% w/v PEG 1500
30	0.1 M PCB buffer pH 9		25% w/v PEG 1500
31	0.1 M HEPES pH 7	0.2 M NaCl	20% w/v PEG 6000
32	0.1 M HEPES pH 7	0.2 M NH_4Cl	20% w/v PEG 6000
33	0.1 M HEPES pH 7	0.2 M LiCl	20% w/v PEG 6000
34	0.1 M HEPES pH 7	0.2 M $MgCl_2$	20% w/v PEG 6000
35	0.1 M HEPES pH 7	0.2 M $CaCl_2$	20% w/v PEG 6000
36	0.1 M HEPES pH 7	0.01 M $ZnCl_2$	20% w/v PEG 6000
37	0.1 M MMT buffer pH 4		25% w/v PEG 1500
38	0.1 M MMT buffer pH 5		25% w/v PEG 1500
39	0.1 M MMT buffer pH 6		25% w/v PEG 1500
40	0.1 M MMT buffer pH 7		25% w/v PEG 1500
41	0.1 M MMT buffer pH 8		25% w/v PEG 1500
42	0.1 M MMT buffer pH 9		25% w/v PEG 1500
43	0.1 M Tris pH 8	0.2 M NaCl	20% w/v PEG 6000
44	0.1 M Tris pH 8	0.2 M NH_4Cl	20% w/v PEG 6000
45	0.1 M Tris pH 8	0.2 M LiCl	20% w/v PEG 6000
46	0.1 M Tris pH 8	0.2 M $MgCl_2$	20% w/v PEG 6000
47	0.1 M Tris pH 8	0.2 M $CaCl_2$	20% w/v PEG 6000
48	0.1 M Tris pH 8	0.01 M $ZnCl_2$	20% w/v PEG 6000

49		0.2 M NaF	20% w/v PEG 3350
50		0.2 M NaBr	20% w/v PEG 3350
51		0.2 M NaI	20% w/v PEG 3350
52		0.2 M KSCN	20% w/v PEG 3350
53		0.2 M $NaNO_3$	20% w/v PEG 3350
54		0.2 M Na formate	20% w/v PEG 3350
55		0.2 M Na acetate	20% w/v PEG 3350
56		0.2 M Na_2SO_4	20% w/v PEG 3350
57		0.2 M K/Na tartrate	20% w/v PEG 3350
58		0.2 M Na/K phosphate	20% w/v PEG 3350
59		0.2 M Na citrate	20% w/v PEG 3350
60		0.2 M Na malonate	20% w/v PEG 3350
61	0.1 M Bis Tris propane pH 6.5	0.2 M NaF	20% w/v PEG 3350
62	0.1 M Bis Tris propane pH 6.5	0.2 M NaBr	20% w/v PEG 3350
63	0.1 M Bis Tris propane pH 6.5	0.2 M NaI	20% w/v PEG 3350
64	0.1 M Bis Tris propane pH 6.5	0.2 M KSCN	20% w/v PEG 3350
65	0.1 M Bis Tris propane pH 6.5	0.2 M $NaNO_3$	20% w/v PEG 3350
66	0.1 M Bis Tris propane pH 6.5	0.2 M Na formate	20% w/v PEG 3350
67	0.1 M Bis Tris propane pH 6.5	0.2 M Na acetate	20% w/v PEG 3350
68	0.1 M Bis Tris propane pH 6.5	0.2 M Na_2SO_4	20% w/v PEG 3350
69	0.1 M Bis Tris propane pH 6.5	0.2 M K/Na tartrate	20% w/v PEG 3350
70	0.1 M Bis Tris propane pH 6.5	0.2 M Na/K phosphate	20% w/v PEG 3350
71	0.1 M Bis Tris propane pH 6.5	0.2 M Na citrate	20% w/v PEG 3350
72	0.1 M Bis Tris propane pH 6.5	0.2 M Na malonate	20% w/v PEG 3350
73	0.1 M Bis Tris propane pH 7.5	0.2 M NaF	20% w/v PEG 3350
74	0.1 M Bis Tris propane pH 7.5	0.2 M NaBr	20% w/v PEG 3350
75	0.1 M Bis Tris propane pH 7.5	0.2 M NaI	20% w/v PEG 3350
76	0.1 M Bis Tris propane pH 7.5	0.2 M KSCN	20% w/v PEG 3350
77	0.1 M Bis Tris propane pH 7.5	0.2 M $NaNO_3$	20% w/v PEG 3350
78	0.1 M Bis Tris propane pH 7.5	0.2 M Na-formate	20% w/v PEG 3350
79	0.1 M Bis Tris propane pH 7.5	0.2 M Na-acetate	20% w/v PEG 3350
80	0.1 M Bis Tris propane pH 7.5	0.2 M Na_2SO_4	20% w/v PEG 3350
81	0.1 M Bis Tris propane pH 7.5	0.2 M K/Na-tartarte	20% w/v PEG 3350
82	0.1 M Bis Tris propane pH 7.5	0.2 M Na/K phosphate	20% w/v PEG 3350
83	0.1 M Bis Tris propane pH 7.5	0.2 M Na citrate	20% w/v PEG 3350
84	0.1 M Bis Tris propane pH 7.5	0.2 M Na-malonate	20% w/v PEG 3350
85	0.1 M Bis Tris propane pH 8.5	0.2 M NaF	20% w/v PEG 3350
86	0.1 M Bis Tris propane pH 8.5	0.2 M NaBr	20% w/v PEG 3350
87	0.1 M Bis Tris propane pH 8.5	0.2 M NaI	20% w/v PEG 3350
88	0.1 M Bis Tris propane pH 8.5	0.2 M KSCN	20% w/v PEG 3350
89	0.1 M Bis Tris propane pH 8.5	0.2 M $NaNO_3$	20% w/v PEG 3350
90	0.1 M Bis Tris propane pH 8.5	0.2 M Na formate	20% w/v PEG 3350
91	0.1 M Bis Tris propane pH 8.5	0.2 M Na acetate	20% w/v PEG 3350
92	0.1 M Bis Tris propane pH 8.5	0.2 M Na_2SO_4	20% w/v PEG 3350
93	0.1 M Bis Tris propane pH 8.5	0.2 M K/Na tartrate	20% w/v PEG 3350
94	0.1 M Bis Tris propane pH 8.5	0.2 M Na/K phosphate	20% w/v PEG 3350
95	0.1 M Bis Tris propane pH 8.5	0.2 M Na citrate	20% w/v PEG 3350
96	0.1 M Bis Tris propane pH 8.5	0.2 M Na malonate	20% w/v PEG 3350

A.2.5 Additive screens

These screens are from Hampton Research.

A.2.5.1 Additive screen 1

#	Concentration		Additive	Class
1	0.1	M	barium chloride	Divalent cation
2	0.1	M	cadmium chloride	Divalent cation
3	0.2	M	calcium chloride	Divalent cation
4	0.1	M	cobaltous chloride	Divalent cation
5	0.1	M	cupric chloride	Divalent cation
6	0.1	M	magnesium chloride	Divalent cation
7	0.1	M	manganese (II) chloride	Divalent cation
8	0.1	M	strontium chloride	Divalent cation
9	0.1	M	yttrium chloride	Trivalent cation
10	0.1	M	zinc chloride	Divalent cation
11	30	% v/v	ethylene glycol	Organic
12	30	% v/v	Glycerol anhydrous	Organic
13	30	% w/v	1,6 hexanediol	Organic
14	30	% v/v	MPD	Organic
15	50	% v/v	polyethylene glycol 400	Organic
16	0.1	M	trimethylamine HCl	Chaotrope
17	1.0	M	guanidine HCl	Chaotrope
18	0.1	M	urea	Chaotrope
19	15	% w/v	1,2,3-heptanetriol	Amphiphile, micelle manipulator
20	20	% w/v	benzamidine HCl	Amphiphile, micelle manipulator
21	30	% v/v	dioxane	Organic, volatile
22	30	% v/v	ethanol	Organic, volatile
23	30	% v/v	iso-propanol	Organic, volatile
24	30	% v/v	methanol	Organic, volatile

A.2.5.2 Additive screen 2

#	Concentration		Additive	Class
1	1.0	M	NaI	Ion
2	0.1	M	L-cysteine	Reducing agent
3	0.1	M	EDTA sodium salt	Chelator
4	0.1	M	NAD	Co-factor
5	0.1	M	ATP disodium salt	Co-factor
6	30	% w/v	D(+)-glucose monohydrate	Carbohydrate
7	30	% w/v	D(+)-sucrose	Carbohydrate
8	30	% w/v	xylitol	Carbohydrate
9	0.1	M	spermidine	Polyamine
10	0.1	M	spermine tetra-HCl	Polyamine
11	30	% v/v	6-aminocaproic acid	Linker
12	30	% v/v	1,5-diaminopentane di-HCl	Linker
13	30	% w/v	1,6-diaminohexane	Linker
14	30	% v/v	1,8-diaminooctane	Linker
15	1.0	M	glycine	Linker
16	0.3	M	glycyl-glycyl-glycine	Organic
17	0.1	M	hexaminecobalt trichloride	Polyamine

18	0.1	M	taurine	Linker
19	0.1	M	betaine monohydrate	Linker
20	5	% w/v	polyvinylpyrrolidone K15	Polymer
21	3.0	M	non-detergent sulfo-betaine 195	Non-detergent solubilizing agent
22	2	% v/v	non-detergent sulfo-betaine 201	Non detergent solubilizing agent
23	0.1	M	phenol	Chaotrope
24	30	% v/v	Dimethyl sulfoxide	Dissociating agent, volatile

A.2.5.3 Additive screen 3

#	Concentration		Additive	Class
1	1.0	M	ammonium sulfate	Salt
2	1.0	M	cesium chloride	Salt
3	1.0	M	potassium chloride	Salt
4	1.0	M	lithium chloride	Salt
5	2.0	M	sodium chloride	Salt
6	0.5	M	sodium fluoride	Salt
7	2.0	M	sodium thiocyanate	Salt
8	30	% w/v	dextran sulfate sodium salt	Polymer
9	50	% v/v	jeffamine M-600	Organic, non-volatile
10	40	% v/v	2,5 Hexanediol	Organic, non-volatile
11	40	% v/v	(+/-)-1,3 butanediol	Organic, non-volatile
12	40	% v/v	polypropylene glycol P400	Organic, non-volatile
13	40	% v/v	1,4 butanediol	Organic, non-volatile
14	40	% v/v	tert-butanol	Organic, volatile
15	40	% v/v	1,3 propanediol	Organic, volatile
16	40	% v/v	acetonitrile	Organic, volatile
17	40	% v/v	gamma butyrolactone	Organic, volatile
18	40	% v/v	propanol	Organic, volatile
19	5	% w/v	ethyl acetate	Organic, volatile
20	40	% v/v	acetone	Organic, volatile
21	0.3	% v/v	dichloromethane	Organic, volatile
22	7	% v/v	n-butanol	Organic, volatile
23	40	% v/v	2,2,2 trifluoroethanol	Organic, volatile
24	0.1	M	1,4-Dithio-DL-threitol (DTT)	Reducing agent, volatile

A.2.6 Detergent screens

These screens are from Hampton Research.

A.2.6.1 Detergent screen 1

#	Detergent	Classification
1	C12E9	Polyoxyethylene(9)dodecyl ether
2	C12E8	Octaethyleneglycol Mono-n-dodecyl Ether
3	n-Dodecyl-ß-D-maltoside	n-Dodecyl-β-D-maltopyranoside
4	Sucrose monolaurate	β-D-Fructopyranosyl-α-D-glucopyranoside monododecanoate
5	CYMAL®-6	6-Cyclohexyl-1-hexyl-β-D-maltoside
6	TRITON® X-100	Octylphenoxypolyethoxyethanol
7	CTAB	Hexadecyltrimethylammonium bromide
8	Deoxy BigChap	N,N-bis-(3-D-Gluconamidopropyl)deoxycholamide

9	n-Decyl-ß-D-maltoside	n-Decyl-β-D-maltopyranoside
10	LDAO	Lauryldimethylamine-N-oxide
11	CYMAL®-5	5-Cyclohexyl-1-pentyl-β-D-maltoside
12	ZWITTERGENT® 3-12	n-Dodecyl-N,N-dimethyl-3-ammonio-1-propanesulfonate
13	Nonyl-ß-D-glucoside	n-Nonyl-β-D-glucopyranoside
14	1-s-Octyl-ß-D-thioglucoside	n-Octyl-β-D-thioglucopyranoside
15	DDAO	N,N-Dimethyldecylamine-N-oxide
16	HECAMEG	Methyl-6-O-(N-heptylcarbamoyl)-α-D-glucopyranoside
17	n-Octanoylsucrose	Sucrose monocaproylate
18	Heptyl-ß-D-thioglucoside	Heptyl-β-D-thioglucoside
19	n-Octyl-ß-D-glucoside	n-Octyl-β-D-glucopyranoside
20	CYMAL®-3	3-Cyclohexyl-1-propyl-β-D-maltoside
21	C-HEGA-10	Cyclohexylbutanoyl-N-hydroxyethylglucamide
22	ZWITTERGENT® 3-10	n-Decyl-N,N-dimethyl-3-ammonio-1-propanesulfonate
23	MEGA-8	Octanoyl-N-methylglucamide
24	n-Hexyl-ß-D-glucoside	n-Hexyl-β-D-glucoside

A.2.6.2 Detergent screen 2

#	Detergent	Classification
1	Pluronic® F-68	Polyoxyethylene-polyoxypropylene Block Copolymer
2	Anapoe® 35	Polyethylene glycol (23) monododecyl ether
3	n-Dodecyl-ß-D-maltotrioside	n-Dodecyl-β-D-maltopyranoside
4	Anapoe® 58	Polyethylene glycol (20) monohexadecyl ether
5	Anapoe® X-114	α-[(1,1,3,3-Tetramethylbutyl)phenyl]-w-hydroxy-poly(oxy-1,2-ethanediyl)
6	Anapoe® X-305	α-[4-(1,1,3,3-Tetramethylbutyl)phenyl]-w-hydroxy-poly(oxy-1,2-ethanediyl)
7	Anapoe® X-405	α-[4-(1,1,3,3-Tetramethylbutyl)phenyl]-w-hydroxy-poly(oxy-1,2-ethanediyl)
8	Anapoe® 20	Polyoxyethylene(20)sorbitan monolaurate
9	Anapoe® 80	Polyoxyethylene(80)sorbitan monolaurate
10	Anapoe® C10E6	Polyoxyethylene(6)decyl ether
11	Anapoe® C10E9	Polyoxyethylene(9)decyl ether
12	Anapoe® C12E10	Polyoxyethylene(10)dodecyl ether
13	Anapoe® C13E8	Polyoxyethylene(8)tridecyl ether
14	IPTG	Isopropyl-β-D-thiogalactopyranoside,
15	n-Dodecyl-N,N-dimethylglycine	None
16	HEGA-10	Decanoyl-N-hydroxyethylglucamide
17	C8E5	Pentaethylene glycol monooctyl ether,
18	CHAPS	3-[(3-Cholamidopropyl)-dimethylammonio]-1-propane sulfonate
19	CHAPSO	3-[(3-Cholamidopropyl)dimethylammonio]-2-hydroxy-1-propanesulfonate
20	C-HEGA-11	Cyclohexylpentanoyl-N-hydroxyethylglucamide
21	HEGA-9	Nonanoyl-N-hydroxyethylglucamide
22	C-HEGA-9	Cyclohexylpropanoyl-N-hydroxyethylglucamide
23	HEGA-8	Octanoyl-N-hydroxyethylglucamide
24	CYPFOS-3	Cyclohexylethanoyl-N-hydroxyethylglucamide

A.2.6.3 Detergent screen 3

#	Detergent	Classification
1	BAM	Benzyldimethyldodecylammonium bromide
2	n-Hexadecyl-ß-D-maltoside	n-Hexadecyl-β-D-maltopyranoside
3	n-Tetradecyl-ß-D-maltoside	n-Tetradecyl-β-D-maltopyranoside
4	n-Tridecyl-ß-D-maltoside	n-Tridecyl-β-D-maltopyranoside
5	Thesit®	Dodecylpoly(ethyleneglycolether)n
6	Zwittergent® 3-14	n-Tetradecyl-N,N-dimethyl-3-ammonio-1-propanesulfonate
7	n-Undecyl-ß-D-maltoside	n-Undecyl-β-D-maltopyranoside
8	n-Decyl-ß-D-thiomaltoside	n-Decyl-β-D-thiomaltopyranoside
9	FOS-Choline®-12	n-Dodecylphosphocholine
10	n-Decanoylsucrose	α-D-Glucopyranoside
11	1-s-Nonyl-ß-D-thioglucoside	1-s-Nonyl-β-D-thioglucopyranoside
12	n-Nonyl-ß-D-maltoside	n-Nonyl-β-D-thiomaltopyranoside
13	DDMAB	N-Dodecyl-N,N-(dimethlammonio)butyrate
14	n-Nonyl-ß-D-maltoside	n-Nonyl-β-D-maltopyranoside
15	Cymal®-4	4-Cyclohexyl-1-butyl-β-D-maltoside
16	n-Octyl-ß-D-thiomaltoside	n-Octyl-β-D-thiomaltopyranoside
17	FOS-Choline®-10	n-Decylphosphocholine
18	FOS-Choline®-9	n-Nonylphosphocholine
19	MEGA-9	Nonanoyl-N-methylglucamide
20	1-s-Heptyl-ß-D-thioglucoside	n-Heptyl-β-D-thioglucopyranoside
21	FOS-Choline®-8	n-Octylphosphocholine
22	Cymal®-2	2-Cyclohexyl-1-ethyl-β-D-maltoside
23	Zwittergent®-3-08	n-Octyl-N,N-dimethyl-3-ammonio-1-propanesulfonate
24	Cymal®-1	Cyclohexyl-methyl-β-D-maltoside

A.2.7 Crystal screen

This screen is from Hampton Research.

#	Buffer	Salt	Other
1	0.1 M Na-acetate pH 4.6	0.02 M $CaCl_2$	30% v/v MPD
2		0.4 M K/Na-tartrate	
3		0.4 M $NH_4H_2PO_4$	
4	0.1 M Tris pH 8.5	2 M $(NH_4)_2SO_4$	
5	0.1 M HEPES pH 7.5	0.2 M Na_3-citrate	30% v/v MPD
6	0.1 M Tris pH 8.5	0.2M $MgCl_2$	30% w/v PEG 4000
7	0.1 M Cacodylate pH 6.5	1.4 M Na-acetate	
8	0.1 M Cacodylate pH 6.5	0.2 M Na_3-citrate	30%v/v isopropanol
9	0.1 M Na_3-citrate pH 5.6	0.2 M (NH_4)-acetate	30% w/v PEG 4000
10	0.1 M Na-acetate pH 4.6	0.2 M (NH_4)-acetate	30 % w/v PEG 4000
11	0.1 M Na_3-citrate pH 5.6	1 M $NH_4H_2PO_4$	
12	0.1 M HEPES pH 7.5	0.2 M $MgCl_2$	30%v/v isopropanol
13	0.1 M Tris pH 8.5	0.2 M Na_3-citrate	30%v/v PEG 400
14	0.1 M HEPES pH 7.5	0.2 M $CaCl_2$	28%v/v PEG 400
15	0.1 M Cacodylate pH 6.5	0.2 M $(NH_4)_2SO_4$	30%w/v PEG 8000
16	0.1 M HEPES pH 7.5	1.5 M Li_2SO_4	
17	0.1 M Tris pH 8.5	0.2 M Li_2SO_4	30%w/v PEG 4000
18	0.1 M Cacodylate pH 6.5	0.2 M Mg-$(acetate)_2$	20%w/v PEG 8000
19	0.1 M Tris pH 8.5	0.2M (NH_4)-acetate	30%v/v isopropanol

20	0.1 M Na-acetate pH 4.6	0.2 M $(NH_4)_2SO_4$	25%w/v PEG 4000
21	0.1 M Cacodylate pH 6.5	0.2 M Mg-acetate	30%v/v MPD
22	0.1 M Tris pH 8.5	0.2 M Na-acetate	30%w/v PEG 4000
23	0.1 M HEPES pH 7.5	0.2 M $MgCl_2$	30%v/v PEG 400
24	0.1 M Na-acetate pH 4.6	0.2 M $CaCl_2$	20%v/v isopropanol
25	0.1 M Imidazole pH 6.5	1 M Na-acetate	
26	0.1 M Na_3-citrate pH 5.6	0.2 M (NH_4)-acetate	30%v/v MPD
27	0.1 M HEPES pH 7.5	0.2 M Na_3-citrate	20%v/v isopropanol
28	0.1 M Cacodylate pH 6.5	0.2 M Na-acetate	30%w/v PEG 8000
29	0.1 M HEPES pH 7.5	0.8 M K/Na-tartrate	
30		0.2 M $(NH_4)_2SO_4$	30%w/v PEG 8000
31		0.2 M $(NH_4)_2SO_4$	30%w/v PEG 4000
32		2 M $(NH_4)_2SO_4$	
33		4 M Na-formate	
34	0.1 M Na-acetate pH 4.6	2 M Na-formate	
35	0.1 M HEPES pH 7.5	0.8 M KH_2PO_4	
36	0.1 M Tris pH 8.5		8%w/v PEG 8000
37	0.1 M Na-acetate pH 4.6		8%w/v PEG 4000
38	0.1 M HEPES pH 7.5	1.4 M Na_3-citrate	
39	0.1 M HEPES pH 7.5	2 M $(NH_4)_2SO_4$	2%v/v PEG 400
40	0.1 M Na_3-citrate pH 5.6		20%v/v isopropanol 20%w/v PEG 4000
41	0.1 M HEPES pH 7.5		10%v/v isopropanol 20%w/v PEG 4000
42		0.05 M KH_2PO_4	20%w/v PEG 8000
43			30%w/v PEG 1500
44		0.2 M Mg(formate)$_2$	
45	0.1 M Cacodylate pH 6.5	0.2 M Zn-(acetate)$_2$	18%w/v PEG 8000
46	0.1 M Cacodylate pH 6.5	0.2 M Ca-(acetate)$_2$	18%w/v PEG 8000
47	0.1 M Na-acetate pH 4.6	2 M $(NH_4)_2SO_4$	
48	0.1 M Tris pH 8.5	2 M $(NH_4)H_2PO_4$	
49		1 M Li_2SO_4	2%w/v PEG 8000
50		0.5 M Li_2SO_4	15%w/v PEG 8000

A.2.8 Crystallization extension kit for protein

This screen is from Sigma.

#	Buffer	Salt	Other
1		2 M NaCl	10% PEG 6000
2		0.5 M NaCl, 0.01 M $MgCl_2$	0.01 M CTAB
3			25% Ethylene glycol
4			35% Dioxane
5		2 M $(NH_4)_2SO_4$	5% 2-Propanol
6	1 M Imidazole pH 7.0		
7			10% PEG 1000 10% PEG 8000
8		1.5 M NaCl	10% Ethanol
9	0.1 M Na-acetate pH 4.6	2 M NaCl	
10	0.1 M Na-acetate pH 4.6	0.2 M NaCl	30% MPD
11	0.1 M Na-acetate pH 4.6	0.01 M $CoCl_2$	1 M 1,6-Hexanediol
12	0.1 M Na-acetate pH 4.6	0.1 M $CdCl_2$	30% PEG 400
13	0.1 M Na-acetate pH 4.6	0.2 M $(NH_4)_2SO_4$	30% PEG MME 2000

14	0.1 M Na-citrate pH 5.6	0.2 M K/Na-tartrate, 2 M $(NH_4)_2SO_4$	
15	0.1 M Na-citrate pH 5.6	1 M Li_2SO_4, 0.5 M $(NH_4)_2SO_4$	
16	0.1 M Na-citrate pH 5.6	0.5 M NaCl	2% Polyethylenimin
17	0.1 M Na-citrate pH 5.6		35% tert.-Butanol
18	0.1 M Na-citrate pH 5.6	0.01 M $FeCl_3$	10% Jeffamine M-600
19	0.1 M Na-citrate pH 5.6		2.5 M 1,6-Hexanediol
20	0.1 M MES pH 6.5	1.6 M $MgSO_4$,	
21	0.1 M MES pH 6.5	2 M NaCl, 0.1 M Ka H_2PO_4	0.1 M NaH_2PO_4
22	0.1 M MES pH 6.5		12% PEG 20'000
23	0.1 M MES pH 6.5	1.6 M $(NH_4)_2SO_4$	10% Dioxane
24	0.1 M MES pH 6.5	0.05 M CsCl	30% Jeffamine M-600
25	0.1 M MES pH 6.5	0.01 M $CoCl_2$, 1.8 M $(NH_4)_2SO_4$	
26	0.1 M MES pH 6.5	0.2 M $(NH_4)_2SO_4$	30% PEG MME 5000
27	0.1 M MES pH 6.5	0.01 M $ZnSO_4$	25% PEG MME 550
28	1.6 M Na-citrate pH 6.5		
29	0.1 M HEPES pH 7.5	0.5 M $(NH_4)_2SO_4$	30% MPD
30	0.1 M HEPES pH 7.5		5% MPD, 10% PEG 6000
31	0.1 M HEPES pH 7.5		20% Jeffamine M-600
32	0.1 M HEPES pH 7.5	1.6 M $(NH_4)_2SO_4$, 0.1 M NaCl	
33	0.1 M HEPES pH 7.5	2.0 M NH_4 -formate	
34	0.1 M HEPES pH 7.5	1.0 M Na-acetate, 0.05 M $CdSO_4$	
35	0.1 M HEPES pH 7.5		70% MPD
36	0.1 M HEPES pH 7.5	4.3 M NaCl	
37	0.1 M HEPES pH 7.5		8% Ethylene glycol 10% PEG 8000
38	0.1 M HEPES pH 7.5		20% PEG 10000
39	0.1 M Tris-HCl pH 8.5	0.2 M $MgCl_2$	3.4 M 1,6-Hexanediol
40	0.1 M Tris-HCl pH 8.5		25% tert.-Butanol
41	0.1 M Tris-HCl pH 8.5	1 M Li_2SO_4, 0.01 M $NiCl_2$,	
42	0.1 M Tris-HCl pH 8.5	1.5 M $(NH_4)_2SO_4$	12% Glycerol
43	0.1 M Tris-HCl pH 8.5	0.2M $(NH_4)_3PO_4$	50% MPD
44	0.1 M Tris-HCl pH 8.5		20% Ethanol
45	0.1 M Tris-HCl pH 8.5	0.01 M $NiCl_2$	20% PEG MME 2000
46	0.1 M Bicine pH 9.0	0.1M NaCl	20% PEG MME 550
47	0.1 M Bicine pH 7.5	2 M $MgCl_2$	
48	0.1 M Bicine pH 9.0		2% Dioxane 10% PEG 20000
49	0.1 M Tris-HCl pH 8.5	0.1 M $MgCl_2$	15% PEG 20000
50			20 % PEG 20000

A.2.9 TPH screen

This screen was designed for c*h*TPH2.

#	Buffer	Salt	Other
1	100 mM HEPES pH 7.0	0.2 M $(NH_4)_2SO_4$	7% PEG 400
2	100 mM HEPES pH 7.5	1.0 M $(NH_4)_2SO_4$	
3	100 mM HEPES pH 7.5	0.6 M Li_2SO_4	
4	100 mM HEPES pH 7.0	1.0 M $(NH_4)_2SO_4$	
5	100 mM HEPES pH 7.0	1.2 M $(NH_4)_2SO_4$	
6	100 mM HEPES pH 7.0	1.4 M $(NH_4)_2SO_4$	
7	100 mM Bis Tris pH 5.5	0.2 M $(NH_4)_2SO_4$	3% PEG 4000
8	100 mM Citrate pH 5.6		3% PEG 10000
9	100 mM MES pH 6.0	0.2 M K/Na tatrate	3% PEG 6000
10	100 mM MES pH 6.0	0.2 M Na_3-Citrate	6% PEG 1500
11	100 mM MES pH 6.5	0.2 M Malonate pH 7.2	6% PEG 400
12	100 mM MES pH 6.5	0.2 M $(NH_4)_2SO_4$	10% MPD
13	100 mM Bis Tris pH 6.5	0.2 M Na_3-citrate	4% MPEG 550
14	100 mM PIPES pH 7.0	0.2 M $MgCl_2$	4% PEG 3350
15	100 mM HEPES pH 7.0	0.2 M Malonate pH 7.2	3% PEG 10000
16	100 mM HEPES pH 7.0	0.2 M $(NH_4)_2SO_4$	5% Dioxane
17	100 mM HEPES pH 7.5	1 M Malonate pH 7.2	
18	100 mM HEPES pH 7.5	0.2 M Na_3-Citrate	3% MPEG 5000
19	100 mM MIB pH 7.5	0.2 M $(NH_4)_2SO_4$	4%PEG 3350
20	100 mM Bis Tris Propane pH 8.0	0.2 M Malonate pH 7.2	3% PEG 10000
21	100 mM Tris pH 8	0.2 M $(NH_4)_2SO_4$	5% MPEG 550
22	100 mM Imidazol malate pH 8	0.1 M $(NH_4)_2SO_4$	3% MPEG 5000, 10% glycerol
23	100 mM Tris pH 8.5	0.2 M K/Na tatrate	5% PEG 1500
24	100 mM Tris pH 8.5	0.2 M NaCl	3% PEG 8000

APPENDIX THREE

A.3 *cg*TPH1 crystallisation experiments

In all the experiments the trays were stored at 4˚C. The drops were 2+2 µL unless otherwise stated. Imidazole malate is abbreviated IM and malonate imidazole borate is abbreviated MIB.

Experiment 1. Set up as both sitting and hanging drops.

Drop	*cg*TPH1 conc. (mg/mL)	Buffer	Precipitant
1+2	3.5, with and without 1 mM BH_2	0.2 M IM pH 8.5	18 % PEG 10000
3+4	3.5, with and without 1 mM BH_2	0.2 M IM pH 8.5	19 % PEG 10000
5+6	3.5, with and without 1 mM BH_2	0.2 M IM pH 8.5	20 % PEG 10000
7+8	3.5, with and without 1 mM BH_2	0.2 M IM pH 8.5	21 % PEG 10000
9+10	3.5, with and without 1 mM BH_2	0.2 M IM pH 8.5	22 % PEG 10000
11+12	3.5, with and without 1 mM BH_2	0.2 M IM pH 8.5	23 % PEG 10000
13+14	3.5, with and without 1 mM BH_2	0.2 M IM pH 8.5	24 % PEG 10000
15+16	3.5, with and without 1 mM BH_2	0.2 M IM pH 8.5	25 % PEG 10000
17+18	3.5, with and without 1 mM BH_2	0.2 M IM pH 8.5	26 % PEG 10000
19+20	3.5, with and without 1 mM BH_2	0.2 M IM pH 8.5	27 % PEG 10000
21+22	3.5, with and without 1 mM BH_2	0.2 M IM pH 8.5	28 % PEG 10000
23+24	3.5, with and without 1 mM BH_2	0.2 M IM pH 8.5	29 % PEG 10000

Experiment 2. Set up as both sitting and hanging drops.

Drop	*cg*TPH1 conc. (mg/mL)	Buffer	Precipitant
1-4	2.8	0.2 M IM pH 8.5	22.5 % PEG 10000
5-8	3.5	0.2 M IM pH 8.5	22.5 % PEG 10000
9-12	4.2	0.2 M IM pH 8.5	22.5 % PEG 10000
13-16	5.2	0.2 M IM pH 8.5	22.5 % PEG 10000
17-20	3.5, with 1 mM BH_2	0.2 M IM pH 8.5	22.5 % PEG 10000
21-24	3.5, with 1 mM BH_4	0.2 M IM pH 8.5	22.5 % PEG 10000

Experiment 3. Set up as hanging drops.

Drop	*cg*TPH1 conc. (mg/mL)	Buffer	Precipitant
1-4	2.8	0.2 M IM pH 8.5	22.5 % PEG 10000
5-8	3.5	0.2 M IM pH 8.5	22.5 % PEG 10000
9-12	4.2	0.2 M IM pH 8.5	22.5 % PEG 10000
13-16	5.2	0.2 M IM pH 8.5	22.5 % PEG 10000
17-20	6.5	0.2 M IM pH 8.5	22.5 % PEG 10000
21-24	3.7, with 1 mM BH_2	0.2 M IM pH 8.5	22.5 % PEG 10000

Experiment 4. Set up as sitting drops. 0.3 µL 0.1 M $[Co(NH_3)_6]Cl_3$ were added to the 2+2 µL drop.

Drop	c*g*TPH1 conc. (mg/mL)	Buffer	Precipitant
1-4	2.8	0.2 M IM pH 8.5	22.5 % PEG 10000
5-8	3.5	0.2 M IM pH 8.5	22.5 % PEG 10000
9-12	4.2	0.2 M IM pH 8.5	22.5 % PEG 10000
13-16	5.2	0.2 M IM pH 8.5	22.5 % PEG 10000
17-20	6.1	0.2 M IM pH 8.5	22.5 % PEG 10000
21-24	3.5, with $[Co(NH_3)_6]^{3+}$	0.2 M IM pH 8.5	22.5 % PEG 10000

Experiment 5. Set up as sitting drops. Well 1-12 were 2+2 µL and 13-24 were 4+4 µL drops.

Drop	c*g*TPH1 conc. (mg/mL)	Buffer	Precipitant
1-4	2.8	0.2 M IM pH 8.5	22.5 % PEG 10000
5-8	3.5	0.2 M IM pH 8.5	22.5 % PEG 10000
9-12	4.2	0.2 M IM pH 8.5	22.5 % PEG 10000
13-16	5.2	0.2 M IM pH 8.5	22.5 % PEG 10000
17-20	6.1	0.2 M IM pH 8.5	22.5 % PEG 10000
21-24	3.5, with $[Co(NH_3)_6]^{3+}$	0.2 M IM pH 8.5	22.5 % PEG 10000

Experiment 6. Set up as sitting 4+4 µL drops. The c*g*TPH1 had been purified the same day as the set up.

Drop	c*g*TPH1 conc. (mg/mL)	Buffer	Precipitant
1-6	2.5	0.2 M IM pH 8.5	22.5 % PEG 10000

Experiment 7. Set up as sitting drops. The c*g*TPH1 was from the new purification batch used in experiment 6.

Drop	c*g*TPH1 conc. (mg/mL)	Buffer	Precipitant
1-6	3.5	0.2 M IM pH 8.5	22.5% PEG 10000
7	3.5	0.2 M IM pH 8.5	5% PEG 10000
8	3.5	0.2 M IM pH 8.5	6% PEG 10000
9	3.5	0.2 M IM pH 8.5	7% PEG 10000
10	3.5	0.2 M IM pH 8.5	8% PEG 10000
11	3.5	0.2 M IM pH 8.5	9% PEG 10000
12	3.5	0.2 M IM pH 8.5	10% PEG 10000
13	3.5	0.2 M IM pH 8.5	11% PEG 10000
14	3.5	0.2 M IM pH 8.5	12% PEG 10000
15	3.5	0.2 M IM pH 8.5	13% PEG 10000
16	3.5	0.2 M IM pH 8.5	14% PEG 10000
17	3.5	0.2 M IM pH 8.5	15% PEG 10000
18	3.5	0.2 M IM pH 8.5	16% PEG 10000
19	3.5	0.2 M IM pH 8.5	17% PEG 10000
20	3.5	0.2 M IM pH 8.5	18% PEG 10000
21	3.5	0.2 M IM pH 8.5	19% PEG 10000
22	3.5	0.2 M IM pH 8.5	20% PEG 10000
23	3.5	0.2 M IM pH 8.5	21% PEG 10000
24	3.5	0.2 M IM pH 8.5	22% PEG 10000

Experiment 8. Additive screen 1 (1-20). Set up as sitting drops. The c*g*TPH1 concentration was 3.5 mg/mL in the protein solution.

Drop	Additive 0.4 µL to a 2+2 µL drop	Buffer	Precipitant
1	barium chloride	0.2 M IM pH 8.5	22.5 % PEG 10000
2	cadmium chloride dihydrate	0.2 M IM pH 8.5	22.5 % PEG 10000
3	calcium chloride dihydrate	0.2 M IM pH 8.5	22.5 % PEG 10000
4	cobaltous chloride dihydrate	0.2 M IM pH 8.5	22.5 % PEG 10000
5	cupric chloride dihydrate	0.2 M IM pH 8.5	22.5 % PEG 10000
6	magnesium chloride hexahydrate	0.2 M IM pH 8.5	22.5 % PEG 10000
7	manganese (II) chloride	0.2 M IM pH 8.5	22.5 % PEG 10000
8	strontium chloride hexahydrate	0.2 M IM pH 8.5	22.5 % PEG 10000
9	yttrium chloride hexahydrate	0.2 M IM pH 8.5	22.5 % PEG 10000
10	zinc chloride	0.2 M IM pH 8.5	22.5 % PEG 10000
11	ethylene glycol	0.2 M IM pH 8.5	22.5 % PEG 10000
12	Glycerol anhydrous	0.2 M IM pH 8.5	22.5 % PEG 10000
13	1,6 hexanediol	0.2 M IM pH 8.5	22.5 % PEG 10000
14	MPD	0.2 M IM pH 8.5	22.5 % PEG 10000
15	polyethylene glycol 400	0.2 M IM pH 8.5	22.5 % PEG 10000
16	trimethylamine HCl	0.2 M IM pH 8.5	22.5 % PEG 10000
17	guanidine HCl	0.2 M IM pH 8.5	22.5 % PEG 10000
18	urea	0.2 M IM pH 8.5	22.5 % PEG 10000
19	1,2,3-heptanetriol	0.2 M IM pH 8.5	22.5 % PEG 10000
20	benzamidine HCl	0.2 M IM pH 8.5	22.5 % PEG 10000

Experiment 9. Additive screen 2 (1-23). The c*g*TPH1 concentration was 3.5 mg/mL in the protein solution.

Drop	Additive 0.4 µL to a 2+2 µL drop	Buffer	Precipitant
1	NaI	0.2 M IM pH 8.5	22.5 % PEG 10000
2	L-cysteine	0.2 M IM pH 8.5	22.5 % PEG 10000
3	EDTA sodium salt	0.2 M IM pH 8.5	22.5 % PEG 10000
4	NAD	0.2 M IM pH 8.5	22.5 % PEG 10000
5	ATP disodium salt	0.2 M IM pH 8.5	22.5 % PEG 10000
6	D(+)-glucose monohydrate	0.2 M IM pH 8.5	22.5 % PEG 10000
7	D(+)-sucrose	0.2 M IM pH 8.5	22.5 % PEG 10000
8	xylitol	0.2 M IM pH 8.5	22.5 % PEG 10000
9	spermidine	0.2 M IM pH 8.5	22.5 % PEG 10000
10	spermine tetra-HCl	0.2 M IM pH 8.5	22.5 % PEG 10000
11	6-aminocaproic acid	0.2 M IM pH 8.5	22.5 % PEG 10000
12	1,5-diaminopentane di-HCl	0.2 M IM pH 8.5	22.5 % PEG 10000
13	1,6-diaminohexane	0.2 M IM pH 8.5	22.5 % PEG 10000
14	1,8-diaminooctane	0.2 M IM pH 8.5	22.5 % PEG 10000
15	glycine	0.2 M IM pH 8.5	22.5 % PEG 10000
16	glycyl-glycyl-glycine	0.2 M IM pH 8.5	22.5 % PEG 10000
17	hexaminecobalt trichloride	0.2 M IM pH 8.5	22.5 % PEG 10000
18	taurine	0.2 M IM pH 8.5	22.5 % PEG 10000
19	betaine monohydrate	0.2 M IM pH 8.5	22.5 % PEG 10000
20	polyvinylpyrrolidone K15	0.2 M IM pH 8.5	22.5 % PEG 10000
21	non-detergent sulfo-betaine 195	0.2 M IM pH 8.5	22.5 % PEG 10000
22	non-detergent sulfo-betaine 201	0.2 M IM pH 8.5	22.5 % PEG 10000
23	phenol	0.2 M IM pH 8.5	22.5 % PEG 10000

Experiment 10. Additive screen 3 (1-13) was tested with sitting drops. The c*g*TPH1 concentration was 3.5 mg/mL in the protein solution.

Drop	Additive 0.4 µL to a 2+2 µL drop	Buffer	Precipitant
1	ammonium sulfate	0.2 M IM pH 8.5	22.5 % PEG 10000
2	cesium chloride	0.2 M IM pH 8.5	22.5 % PEG 10000
3	potassium chloride	0.2 M IM pH 8.5	22.5 % PEG 10000
4	lithium chloride	0.2 M IM pH 8.5	22.5 % PEG 10000
5	sodium chloride	0.2 M IM pH 8.5	22.5 % PEG 10000
6	sodium fluoride	0.2 M IM pH 8.5	22.5 % PEG 10000
7	sodium thiocyanate	0.2 M IM pH 8.5	22.5 % PEG 10000
8	dextran sulfate sodium salt	0.2 M IM pH 8.5	22.5 % PEG 10000
9	jeffamine M-600	0.2 M IM pH 8.5	22.5 % PEG 10000
10	2,5 Hexanediol	0.2 M IM pH 8.5	22.5 % PEG 10000
11	(+/-)-1,3 butanediol	0.2 M IM pH 8.5	22.5 % PEG 10000
12	polypropylene glycol P400	0.2 M IM pH 8.5	22.5 % PEG 10000
13	1,4 butanediol	0.2 M IM pH 8.5	22.5 % PEG 10000

Experiment 11. Detergent screen 1 was tested with sitting drops. The c*g*TPH1 concentration was 3.5 mg/mL in the solution used for all drops.

Drop	Additive 0.4 µL to a 2+2 µL drop	Buffer	Precipitant
1	C12E9	0.2 M IM pH 8.5	22.5 % PEG 10000
2	C12E8	0.2 M IM pH 8.5	22.5 % PEG 10000
3	n-Dodecyl-ß-D-maltoside	0.2 M IM pH 8.5	22.5 % PEG 10000
4	Sucrose monolaurate	0.2 M IM pH 8.5	22.5 % PEG 10000
5	CYMAL®-6	0.2 M IM pH 8.5	22.5 % PEG 10000
6	TRITON® X-100	0.2 M IM pH 8.5	22.5 % PEG 10000
7	CTAB	0.2 M IM pH 8.5	22.5 % PEG 10000
8	Deoxy BigChap	0.2 M IM pH 8.5	22.5 % PEG 10000
9	n-Decyl-ß-D-maltoside	0.2 M IM pH 8.5	22.5 % PEG 10000
10	LDAO	0.2 M IM pH 8.5	22.5 % PEG 10000
11	CYMAL®-5	0.2 M IM pH 8.5	22.5 % PEG 10000
12	ZWITTERGENT® 3-12	0.2 M IM pH 8.5	22.5 % PEG 10000
13	Nonyl-ß-D-glucoside	0.2 M IM pH 8.5	22.5 % PEG 10000
14	1-s-Octyl-ß-D-thioglucoside	0.2 M IM pH 8.5	22.5 % PEG 10000
15	DDAO	0.2 M IM pH 8.5	22.5 % PEG 10000
16	HECAMEG	0.2 M IM pH 8.5	22.5 % PEG 10000
17	n-Octanoylsucrose	0.2 M IM pH 8.5	22.5 % PEG 10000
18	Heptyl-ß-D-thioglucoside	0.2 M IM pH 8.5	22.5 % PEG 10000
19	n-Octyl-ß-D-glucoside	0.2 M IM pH 8.5	22.5 % PEG 10000
20	CYMAL®-3	0.2 M IM pH 8.5	22.5 % PEG 10000
21	C-HEGA-10	0.2 M IM pH 8.5	22.5 % PEG 10000
22	ZWITTERGENT® 3-10	0.2 M IM pH 8.5	22.5 % PEG 10000
23	MEGA-8	0.2 M IM pH 8.5	22.5 % PEG 10000
24	n-Hexyl-ß-D-glucoside	0.2 M IM pH 8.5	22.5 % PEG 10000

Experiment 12. Detergent screen 2. Sitting drops. The c*g*TPH1 concentration was 3.5 mg/mL in the solution used for all drops.

Drop	Additive 0.4 µL to a 2+2 µL drop	Buffer	Precipitant
1	Pluronic® F-68	0.2 M IM pH 8.5	22.5 % PEG 10000
2	Anapoe® 35	0.2 M IM pH 8.5	22.5 % PEG 10000

3	n-Dodecyl-ß-D-maltotrioside	0.2 M IM pH 8.5	22.5 % PEG 10000
4	Anapoe® 58	0.2 M IM pH 8.5	22.5 % PEG 10000
5	Anapoe® X-114	0.2 M IM pH 8.5	22.5 % PEG 10000
6	Anapoe® X-305	0.2 M IM pH 8.5	22.5 % PEG 10000
7	Anapoe® X-405	0.2 M IM pH 8.5	22.5 % PEG 10000
8	Anapoe® 20	0.2 M IM pH 8.5	22.5 % PEG 10000
9	Anapoe® 80	0.2 M IM pH 8.5	22.5 % PEG 10000
10	Anapoe® C10E6	0.2 M IM pH 8.5	22.5 % PEG 10000
11	Anapoe® C10E9	0.2 M IM pH 8.5	22.5 % PEG 10000
12	Anapoe® C12E10	0.2 M IM pH 8.5	22.5 % PEG 10000
13	Anapoe® C13E8	0.2 M IM pH 8.5	22.5 % PEG 10000
14	IPTG	0.2 M IM pH 8.5	22.5 % PEG 10000
15	n-Dodecyl-N,N-dimethylglycine	0.2 M IM pH 8.5	22.5 % PEG 10000
16	HEGA-10	0.2 M IM pH 8.5	22.5 % PEG 10000
17	C8E5	0.2 M IM pH 8.5	22.5 % PEG 10000
18	CHAPS	0.2 M IM pH 8.5	22.5 % PEG 10000
19	CHAPSO	0.2 M IM pH 8.5	22.5 % PEG 10000
20	C-HEGA-11	0.2 M IM pH 8.5	22.5 % PEG 10000
21	HEGA-9	0.2 M IM pH 8.5	22.5 % PEG 10000
22	C-HEGA-9	0.2 M IM pH 8.5	22.5 % PEG 10000
23	HEGA-8	0.2 M IM pH 8.5	22.5 % PEG 10000
24	CYPFOS-3	0.2 M IM pH 8.5	22.5 % PEG 10000

Experiment 13. Detergent screen 3. Sitting drops. The *cg*TPH1 concentration was 3.5 mg/mL in the solution used for all drops.

Drop	Additive 0.4 µL to a 2+2 µL drop	Buffer	Precipitant
1	BAM	0.2 M IM pH 8.5	22.5 % PEG 10000
2	n-Hexadecyl-ß-D-maltoside	0.2 M IM pH 8.5	22.5 % PEG 10000
3	n-Tetradecyl-ß-D-maltoside	0.2 M IM pH 8.5	22.5 % PEG 10000
4	n-Tridecyl-ß-D-maltoside	0.2 M IM pH 8.5	22.5 % PEG 10000
5	Thesit®	0.2 M IM pH 8.5	22.5 % PEG 10000
6	Zwittergent® 3-14	0.2 M IM pH 8.5	22.5 % PEG 10000
7	n-Undecyl-ß-D-maltoside	0.2 M IM pH 8.5	22.5 % PEG 10000
8	n-Decyl-ß-D-thiomaltoside	0.2 M IM pH 8.5	22.5 % PEG 10000
9	FOS-Choline®-12	0.2 M IM pH 8.5	22.5 % PEG 10000
10	n-Decanoylsucrose	0.2 M IM pH 8.5	22.5 % PEG 10000
11	1-s-Nonyl-ß-D-thioglucoside	0.2 M IM pH 8.5	22.5 % PEG 10000
12	n-Nonyl-ß-D-maltoside	0.2 M IM pH 8.5	22.5 % PEG 10000
13	DDMAB	0.2 M IM pH 8.5	22.5 % PEG 10000
14	n-Nonyl-ß-D-maltoside	0.2 M IM pH 8.5	22.5 % PEG 10000
15	Cymal®-4	0.2 M IM pH 8.5	22.5 % PEG 10000
16	n-Octyl-ß-D-thiomaltoside	0.2 M IM pH 8.5	22.5 % PEG 10000
17	FOS-Choline®-10	0.2 M IM pH 8.5	22.5 % PEG 10000
18	FOS-Choline®-9	0.2 M IM pH 8.5	22.5 % PEG 10000
19	MEGA-9	0.2 M IM pH 8.5	22.5 % PEG 10000
20	1-s-Heptyl-ß-D-thioglucoside	0.2 M IM pH 8.5	22.5 % PEG 10000
21	FOS-Choline®-8	0.2 M IM pH 8.5	22.5 % PEG 10000
22	Cymal®-2	0.2 M IM pH 8.5	22.5 % PEG 10000
23	Zwittergent®-3-08	0.2 M IM pH 8.5	22.5 % PEG 10000
24	Cymal®-1	0.2 M IM pH 8.5	22.5 % PEG 10000

Experiment 14. 0.4 µL 0.1 M cysteine or 0.1 M DTT were added to 2 + 2 µL sitting drops. c*g*TPH1 from a new purification batch was used (new) and older batch when noted (old).

Drop	c*g*TPH1 conc. (mg/mL)	Buffer	Precipitant
1-2	3.5 (new), cysteine	0.2 M IM pH 8.5	22.5 % PEG 10000
3	3.5 (new), DTT	0.2 M IM pH 8.5	22.5 % PEG 10000
4	3.5 (new)	0.2 M IM pH 8.5	22.5 % PEG 10000
5-6	3.5 (new), cysteine	0.2 M IM pH 8.5	22.5 % PEG 10000
7	3.5 (new), DTT	0.2 M IM pH 8.5	22.5 % PEG 10000
8	3.5 (new)	0.2 M IM pH 8.5	22.5 % PEG 10000
9-10	3.5 (old), cysteine	0.2 M IM pH 8.5	22.5 % PEG 10000
11	3.5 (old), DTT	0.2 M IM pH 8.5	22.5 % PEG 10000
12	3.5 (old)	0.2 M IM pH 8.5	22.5 % PEG 10000
13-14	3.5 (old), cysteine	0.2 M IM pH 8.5	22.5 % PEG 10000
15	3.5 (old), DTT	0.2 M IM pH 8.5	22.5 % PEG 10000
16	3.5 (old)	0.2 M IM pH 8.5	22.5 % PEG 10000

Experiment 15. Sitting drops. c*g*TPH1 from a new purification batch was used (new) and older batch when noted (old).

Drop	c*g*TPH1 conc. (mg/mL)	Buffer	Precipitant
1	3.5 (old)	0.2 M IM pH 8.5	12 % PEG 10000
2	0.9 (old)	0.2 M IM pH 8.5	12 % PEG 10000
3	3.5 (new)	0.2 M IM pH 8.5	12 % PEG 10000
4	0.9 (new)	0.2 M IM pH 8.5	12 % PEG 10000
5	3.5 (old)	0.2 M IM pH 8.5	14% PEG 10000
6	0.9 (old)	0.2 M IM pH 8.5	14% PEG 10000
7	3.5 (new)	0.2 M IM pH 8.5	14% PEG 10000
8	0.9 (new)	0.2 M IM pH 8.5	14% PEG 10000
9	3.5 (old)	0.2 M IM pH 8.5	16% PEG 10000
10	0.9 (old)	0.2 M IM pH 8.5	16% PEG 10000
11	3.5 (new)	0.2 M IM pH 8.5	16% PEG 10000
12	0.9 (new)	0.2 M IM pH 8.5	16% PEG 10000
13	3.5 (old)	0.2 M IM pH 8.5	18% PEG 10000
14	0.9 (old)	0.2 M IM pH 8.5	18% PEG 10000
15	3.5 (new)	0.2 M IM pH 8.5	18% PEG 10000
16	0.9 (new)	0.2 M IM pH 8.5	18% PEG 10000
17	3.5 (old)	0.2 M IM pH 8.5	20% PEG 10000
18	0.9 (old)	0.2 M IM pH 8.5	20% PEG 10000
19	3.5 (new)	0.2 M IM pH 8.5	20% PEG 10000
20	0.9 (new)	0.2 M IM pH 8.5	20% PEG 10000
21	3.5 (old)	0.2 M IM pH 8.5	22% PEG 10000
22	0.9 (old)	0.2 M IM pH 8.5	22% PEG 10000
23	3.5 (new)	0.2 M IM pH 8.5	22% PEG 10000
24	0.9 (new)	0.2 M IM pH 8.5	22% PEG 10000

Experiment 16. Sitting drops. c*g*TPH1 from a new purification batch was used (new) and older batch when noted (old).

Drop	c*g*TPH1 conc. (mg/mL)	Buffer	Precipitant
1	3.5 (old)	0.2 M MIB pH 8.7	22.5 % PEG 10000
2	0.9 (old)	0.2 M MIB pH 8.7	22.5 % PEG 10000
3	3.5 (new)	0.2 M MIB pH 8.7	22.5 % PEG 10000
4	0.9 (new)	0.2 M MIB pH 8.7	22.5 % PEG 10000
5	3.5 (old)	0.2 M MIB pH 8.5	22.5 % PEG 10000
6	0.9 (old)	0.2 M MIB pH 8.5	22.5 % PEG 10000
7	3.5 (new)	0.2 M MIB pH 8.5	22.5 % PEG 10000
8	0.9 (new)	0.2 M MIB pH 8.5	22.5 % PEG 10000
9	3.5 (old)	0.2 M MIB pH 8.25	22.5 % PEG 10000
10	0.9 (old)	0.2 M MIB pH 8.25	22.5 % PEG 10000
11	3.5 (new)	0.2 M MIB pH 8.25	22.5 % PEG 10000
12	0.9 (new)	0.2 M MIB pH 8.25	22.5 % PEG 10000
13	3.5 (old)	0.2 M MIB pH 8.0	22.5 % PEG 10000
14	0.9 (old)	0.2 M MIB pH 8.0	22.5 % PEG 10000
15	3.5 (new)	0.2 M MIB pH 8.0	22.5 % PEG 10000
16	0.9 (new)	0.2 M MIB pH 8.0	22.5 % PEG 10000
17	3.5 (old)	0.2 M MIB pH 7.5	22.5 % PEG 10000
18	0.9 (old)	0.2 M MIB pH 7.5	22.5 % PEG 10000
19	3.5 (new)	0.2 M MIB pH 7.5	22.5 % PEG 10000
20	0.9 (new)	0.2 M MIB pH 7.5	22.5 % PEG 10000
21	3.5 (old)	0.2 M MIB pH 7.0	22.5 % PEG 10000
22	0.9 (old)	0.2 M MIB pH 7.0	22.5 % PEG 10000
23	3.5 (new)	0.2 M MIB pH 7.0	22.5 % PEG 10000
24	0.9 (new)	0.2 M MIB pH 7.0	22.5 % PEG 10000

Experiment 17. Sitting drops. c*g*TPH1 from a new purification batch was used (new) and older batch when noted (old).

Drop	c*g*TPH1 conc. (mg/mL)	Buffer	additive	Precipitant
1+2	3.5 (old)	0.2 M IM pH 8.5	4 mM DTT	12 % PEG 10000
3+4	3.5 (new)	0.2 M IM pH 8.5	4 mM DTT	12 % PEG 10000
5+6	3.5 (old)	0.2 M IM pH 8.5	4 mM DTT	16% PEG 10000
7+8	3.5 (new)	0.2 M IM pH 8.5	4 mM DTT	16% PEG 10000
9+10	3.5 (old)	0.2 M IM pH 8.5	4 mM DTT	18% PEG 10000
11+12	3.5 (new)	0.2 M IM pH 8.5	4 mM DTT	18% PEG 10000
13+14	3.5 (old)	0.2 M IM pH 8.5	4 mM DTT	20% PEG 10000
15+16	3.5 (new)	0.2 M IM pH 8.5	4 mM DTT	20% PEG 10000
17+18	3.5 (old)	0.2 M IM pH 8.5	4 mM DTT	22% PEG 10000
19+20	3.5 (new)	0.2 M IM pH 8.5	4 mM DTT	22% PEG 10000
21+22	3.5 (old)	0.2 M IM pH 8.5	4 mM DTT	24% PEG 10000
23+24	3.5 (new)	0.2 M IM pH 8.5	4 mM DTT	24% PEG 10000

Experiment 18. Sitting drops. c*g*TPH1 from a new purification batch was used (new) and older batch when noted (old).

Drop	c*g*TPH1 conc. (mg/mL)	Buffer	β-mercaptoethanol	Precipitant
1+2	3.5 (old)	0.2 M IM pH 8.5	1%(v/v)	12 % PEG 10000
3+4	3.5 (new)	0.2 M IM pH 8.5	1%(v/v)	12 % PEG 10000
5+6	3.5 (old)	0.2 M IM pH 8.5	1%(v/v)	16% PEG 10000
7+8	3.5 (new)	0.2 M IM pH 8.5	1%(v/v)	16% PEG 10000
9+10	3.5 (old)	0.2 M IM pH 8.5	1%(v/v)	18% PEG 10000
11+12	3.5 (new)	0.2 M IM pH 8.5	1%(v/v)	18% PEG 10000
13+14	3.5 (old)	0.2 M IM pH 8.5	1%(v/v)	20% PEG 10000
15+16	3.5 (new)	0.2 M IM pH 8.5	1%(v/v)	20% PEG 10000
17+18	3.5 (old)	0.2 M IM pH 8.5	1%(v/v)	22% PEG 10000
19+20	3.5 (new)	0.2 M IM pH 8.5	1%(v/v)	22% PEG 10000
21+22	3.5 (old)	0.2 M IM pH 8.5	1%(v/v)	24% PEG 10000
23+24	3.5 (new)	0.2 M IM pH 8.5	1%(v/v)	24% PEG 10000

Experiment 19. Testing EDTA. Sitting 2+2 µL drops. c*g*TPH1 from a new purification batch was used (new) and older batch when noted (old).

Drop	c*g*TPH1 conc. (mg/mL)	Buffer	EDTA	Precipitant
1+2	3.5 (old)	0.2 M IM pH 8.5	4 mM	12 % PEG 10000
3+4	3.5 (new)	0.2 M IM pH 8.5	4 mM	12 % PEG 10000
5+6	3.5 (old)	0.2 M IM pH 8.5	4 mM	16% PEG 10000
7+8	3.5 (new)	0.2 M IM pH 8.5	4 mM	16% PEG 10000
9+10	3.5 (old)	0.2 M IM pH 8.5	4 mM	18% PEG 10000
11+12	3.5 (new)	0.2 M IM pH 8.5	4 mM	18% PEG 10000
13+14	3.5 (old)	0.2 M IM pH 8.5	4 mM	20% PEG 10000
15+16	3.5 (new)	0.2 M IM pH 8.5	4 mM	20% PEG 10000
17+18	3.5 (old)	0.2 M IM pH 8.5	4 mM	22% PEG 10000
19+20	3.5 (new)	0.2 M IM pH 8.5	4 mM	22% PEG 10000
21+22	3.5 (old)	0.2 M IM pH 8.5	4 mM	24% PEG 10000
23+24	3.5 (new)	0.2 M IM pH 8.5	4 mM	24% PEG 10000

Experiment 20. Sitting drops. c*g*TPH1 from a new purification batch was used (new) and older batch when noted (old).

Drop	c*g*TPH1 conc. (mg/mL)	Buffer	Precipitant
1+2	3.5 (old)	0.2 M IM pH 8.5	22.5% PEG 10000
3+4	3.5 (new)	0.2 M IM pH 8.5	22.5% PEG 10000
5+6	3.5 (old)	0.2 M IM pH 8.5	22.5% PEG 10000
7+8	3.5 (new)	0.2 M IM pH 8.5	22.5% PEG 10000
9+10	3.5 (old)	0.2 M MIB pH 7.0	22.5% PEG 10000
11+12	3.5 (new)	0.2 M MIB pH 7.0	22.5% PEG 10000
13+14	3.5 (old)	0.2 M MIB pH 7.5	22.5% PEG 10000
15+16	3.5 (new)	0.2 M MIB pH 7.5	22.5% PEG 10000
17+18	3.5 (old)	0.2 M MIB pH 8.0	22.5% PEG 10000
19+20	3.5 (new)	0.2 M MIB pH 8.0	22.5% PEG 10000
21+22	3.5 (old)	0.2 M MIB pH 8.5	22.5% PEG 10000
23+24	3.5 (new)	0.2 M MIB pH 8.5	22.5% PEG 10000